

AN INVESTIGATION INTO THE EFFECTS OF PRESSURE OSCILLATIONS ON AIRWAY SMOOTH MUSCLE IN CHRONIC ASTHMA.

Kevin Lamar Turepu Roos

**A thesis submitted to Auckland University of Technology
in fulfilment of the degree of
Doctor of Philosophy (PhD)**

AUT
UNIVERSITY

NEW ZEALAND

2018

Institute of Biomedical Technologies

Primary Supervisor: Professor Ahmed Al-Jumaily

Acknowledgments

There are many people without whom this work would have not been possible. First and foremost, I would like to express my gratitude and thanks to God for blessing me with this opportunity, and for the sustenance to complete it. To my primary supervisor Prof. Ahmed Al-Jumaily for welcoming me into his research and life's work, I am forever grateful. He has been a steady, guiding, older brother. The tuakana/teina relationship that we have is one that I value and appreciate for all the support I receive, and the lessons I learn. I will pass on the knowledge. Ahmed's oversight, expertise and vision relative to the aspects most pertinent to the work's completion are invaluable facets that define the success of this project. I would also like to thank my second and third supervisors, Associate Professor Jun Lu and Associate Professor Simeon Cairns. Their involvement with physiological applications and insights, as well as with protocol development, was essential for the basis of modelling the animals in healthy and sensitized states. To Dr Miguel Jo-Avila, there will always be thanks and admiration. His guidance through the ethical applications, animal-related orders, equipment training, and establishment of the chronic model was critical, and almost as invaluable as his friendship.

My daily interactions with students and staff at AUT have been the foundation for furthering this project's success. Tinuoluwa Odeleye, surely you have a special place in heaven for dealing so well with this adventure named me. To my friends and colleagues at WN and WD buildings, particularly Associate Professor Andrew Lowe, Ali Ali, Dr Gautam Anand, Riya Biswas, Piyush Bugde, Dr Anubha Kalra, Bhawana Prakash, Andries Meintjes, and Dr Kelvin Wang, thank you for your comradery and humour through our daily efforts to perform meaningful science in our electrically-challenged

building. Additionally, to all the past and present IBTec team (notably, Yasmitha Manilal, Prachi Redey, Dr Lulu Wang, Dr Sherif Ashaat), to the KODE Biotech staff, and to the Auckland AEC and VJU staff: thank you thank you and thank you again.

Jo Stone (Administrative and Research Assistant at IBTec) and Liz Chandy (School Manager), Liline Vailea (Service Centre Administrator at Estates), The AUT Scholarships Office (particularly Eva Ihaia, Stefania Patrone, and Trish Richardson), the incomparable Josephine Prasad (Postgraduate Coordinator), AUT Security, Electricians, and Custodial staff members: to each of you I give special thanks for your efforts that affect so many of us each day, and that specifically have aided my progress through this programme.

Finally, this work would not have happened without the generous IBTec, Vice-Chancellor, and Mature Student Doctoral Scholarships' financial support of my tuitions and fees. To Rosser Johnson and Tony Clear, I specifically recognise the impact of your oversight in awarding me key funding to complete my studies. To my whanau, my 'anau, my family, I acknowledge your patience and understanding as I have sought to achieve this goal for us. Through every easy and difficult choice along this path, I have considered (and tried to make) a better future for us all.

Abstract

The hyperconstriction of airway smooth muscle (ASM) is the main driving mechanism during an asthmatic attack. The airway lumen is reduced, resistance to airflow increases, and normal breathing becomes more difficult. The tissue contraction can be temporarily relieved by using bronchodilator drugs which induce relaxation of the constricted airways. With one of the highest prevalence rates in the world, New Zealand's costs for asthma treatments total an estimated NZD\$825 million per year.

While widely used in asthma therapies, pharmacological treatments vary in their effectiveness from one subject to another, as do the side effects of long-term usage. Studies have shown that application of mechanical oscillations which are equivalent to the physiological patterns of normal breathing and deep inspirations in healthy airways can induce airway relaxation. This type of relaxation response is not observed in asthmatics.

Utilizing length oscillations (arising from positive pressure) in association with breathing patterns provides non-pharmacological options for augmenting treatment of the ASM hyperconstriction which is present in many respiratory diseases such as asthma. There is currently little known about the effects of applying superimposed pressure oscillations in combination with breathing patterns to healthy and asthmatic airways during an asthmatic attack.

Results from *in vivo* studies of a chronic murine asthmatic model indicate that the use of superimposed pressure oscillations (SIPO) over normal breathing patterns facilitates relaxation during an induced asthmatic attack in healthy and asthmatic subjects. Oscillation patterns, physiological pressure equivalents, and their effects on key

respiratory parameters are presented. Comparisons of healthy and asthmatic lung resistance (R_L) and dynamic compliance (C_{dyn}) values are used as assessments of the changes in airway responses to applied mechanical pressure oscillations. Additionally, a standard respiratory constant is used to normalize acute and chronic asthmatic models' data. Use of the constant assists in modeling the effects of SIPO by transforming R_L and C_{dyn} data into Work and Power equivalents for use in interpreting ASM mechanics.

Keywords: mechanical oscillations, superimposed pressure oscillations, airway smooth muscle, breathing, contraction, relaxation, resistance, compliance

TABLE OF CONTENTS

<i>List of figures</i>	8
<i>List of tables</i>	10
<i>List of Terms and abbreviations</i>	13
Chapter I	14
Background	14
1.1. Introduction	14
1.2. Respiratory physiology.....	16
1.3. Airway smooth muscle.....	18
1.4. Structure of the contractile apparatus.....	22
1.5. Mouse anatomy	32
1.6. Thesis structure.....	34
1.7. Summary	35
Chapter II	36
Asthma, ASM and mechanical response	36
2.1. Introduction	36
2.2. Asthma.....	36
2.3. Asthma Treatments	37
2.4. Airway remodeling in asthma.....	41
2.5. ASM and asthma.....	42
2.6. Asthma assessment techniques	47
2.7. Mechanical oscillations.....	54
2.8. Pressure oscillations	57
2.9. Purpose of the Study.....	58
2.10. Summary.....	59
Chapter III	61
Murine model for long-term chronic asthma	61
3.1. Introduction	61
3.2. Animal models	62
3.3. Selection of criteria	63
3.4. Asthmatic models.....	65
3.5. Sensitization for a chronic asthmatic mouse model	67
3.6. Selected techniques to evaluate the model	72
3.7. Assessment of long-exposure chronic asthma sensitization	78
3.8. Summary.....	81
Chapter IV	82
Experimental investigation of the asthmatic model	82
4.1. Introduction.....	82
4.2. Experimental layout	83
4.3. Animal positioning	84
4.4. Measurement components	85

4.5. Drugs and allergen-mix delivery system	94
4.6. Calibration of pressure transducers and oscillation setup.....	99
4.7. Testing superimposed pressure oscillations in vivo	102
4.8. Summary.....	104
Chapter V.....	106
Lung resistance in healthy and chronic, sensitized mice	106
5.1. Introduction.....	106
5.2. Method.....	106
5.3. Statistical analysis.....	107
5.4. Results	109
5.5. Discussion	119
5.6. Summary.....	127
Chapter VI.....	129
Dynamic compliance in healthy and chronic sensitized mice	129
6.1. Introduction.....	129
6.2. Method.....	129
6.3. Statistical analysis.....	130
6.4. Results	131
6.5. Discussion	141
6.6. Summary.....	150
Chapter VII.....	152
SIPO effects on asthmatic ASM.....	152
7.1. Introduction.....	152
7.2. Length and pressure oscillations.....	153
7.3. \check{R}_L in two asthmatic models	156
7.4. \check{C}_{dyn} in two asthmatic models.....	167
7.5. Discussion	177
7.6. Future work	179
7.7. Conclusions	180
References	182
Appendix.....	197
Appendix A. Ethical approval.....	197
Appendix B. Institutional Drug Administration Order (IDAO)	198
Appendix C. Protocols for imposed treatments.....	199
Appendix D. Acute asthma sensitization protocol	202
Appendix E. GraphPad Prism 7.0™ screenshot.....	203
Appendix F: Normalization of R_L and C_{dyn} values.....	204
Appendix G: Summary data tables.....	208

LIST OF FIGURES

Figure 1.1: Respiratory system.....	20
Figure 1.2: Components of cytoskeleton and myofilaments on smooth muscle.....	24
Figure 1.3: ASM components of contractile apparatus.....	26
Figure 1.4: Myosin structure.....	26
Figure 1.5: Smooth muscle contraction process.....	32
Figure 1.6: Four state model of Hai and Murphy (1988).....	33
Figure 1.7: Mice upper airways anatomy.....	34
Figure 1.8: Mice lower airways.....	36
Figure 2.1: Invasive plethysmograph.....	50
Figure 2.2: Non-invasive whole-body plethysmography.....	52
Figure 2.3: Lung volumes occurring during breathing cycles.....	54
Figure 2.4: Bronchodilation and bronchoconstriction in response to deep inspiration.....	57
Figure 3.1: Control protocol for healthy mice.....	71
Figure 3.2: Sensitization protocol for chronic asthmatic mice.....	73
Figure 3.3: Positioning of mouse for tracheotomy and insertion of tracheal cannula.....	75
Figure 3.4: Insertions of the tracheal cannula and oesophageal catheter.....	76
Figure 3.5: Representation of system carrying aerosol drug from nebulizer to mouse.....	77
Figure 3.6: Lung resistance in response to aerosolised ACh.....	80
Figure 3.7: Lung resistance in response to aerosolised ISO following treatment with ACh (10^{-4} M).....	81
Figure 3.8: Standard curve for total IgE.....	81
Figure 4.1: The experimental layout for respiratory parameter protocols in this study.....	85
Figure 4.2: Data collection surface and thermo-regulated blanket.....	87
Figure 4.3: Representative map of respiratory parameter measurements.....	88
Figure 4.4: HSE-Pneumotachometer PTM Type 378/0.9 for mice and rats.....	89
Figure 4.5: Differential Low Pressure Transducer DLP 2.5.....	90
Figure 4.6: TAM-A transducer amplifier module and its PLUGSYS Minicase.....	91
Figure 4.7: Oesophageal catheter.....	92
Figure 4.8: Sensor technics model 26PC0050D6A.....	93
Figure 4.9: ADInstruments PowerLab 16/30.....	94
Figure 4.10: Screenshot of ADInstruments LabChart.....	95
Figure 4.11: Harvard Apparatus aerosol jet nebulizer particle size chart.....	96
Figure 4.12: Harvard Apparatus aerosol jet nebulizer protocol setup.....	97
Figure 4.13: Generation of the positive pressure oscillations is accomplished by IBTec's waveform oscillator.....	99
Figure 4.14: Pressure oscillation setup: a) Shaker, b) Chamber, c) Piston and d) base.....	99
Figure 4.15: Representative diagram of the water manometer setup used for the calibration curve of the DLP 2.5 low pressure transducer.	100
Figure 4.16: Calibration curve for the DLP 2.5 low pressure transducer.....	101
Figure 4.17: Calibration curve for the Honeywell (oesophageal) low pressure transducer.....	102

Figure 4.18: Oscillation device pressures (cmH ₂ O) measured by the calibrated DLP 2.5 transducer.....	105
Figure 5.1: Treatment values of R_L (expressed as [(cmH ₂ O·ml)/s] ⁻¹) from applications of 5 Hz-generated SIPO waveform set with amplitudes in the range of 100 – 400 mV (0.8 – 3.6 cmH ₂ O).....	123
Figure 5.2: Treatment values of R_L (expressed as [(cmH ₂ O·ml)/s] ⁻¹) from applications of 10 Hz-generated SIPO waveform set with amplitudes in the range of 100 – 400 mV (0.7 – 3.3 cmH ₂ O).....	124
Figure 5.3: Treatment values of R_L (expressed as [(cmH ₂ O·ml)/s] ⁻¹) from applications of 15 Hz-generated SIPO waveform set with amplitudes in the range of 100 – 400 mV (0.4 – 2.4 cmH ₂ O).....	125
Figure 5.4: Treatment values of R_L (expressed as [(cmH ₂ O·ml)/s] ⁻¹) from applications of 20 Hz-generated SIPO waveform set with amplitudes in the range of 100 – 400 mV (0.4 – 2.3 cmH ₂ O).....	127
Figure 6.1: Treatment values of C_{dyn} (expressed as μl/mmH ₂ O) from applications of 5 Hz-generated SIPO waveform set with amplitudes in the range of 100 – 400 mV (0.8 – 3.6 cmH ₂ O).....	145
Figure 6.2: Treatment values of C_{dyn} (expressed as μl/mmH ₂ O) from applications of 10 Hz-generated SIPO waveform set with amplitudes in the range of 100 – 400 mV (0.7 – 3.3 cmH ₂ O).....	147
Figure 6.3: Treatment values of C_{dyn} (expressed as μl/mmH ₂ O) from applications of 15 Hz-generated SIPO waveform set with amplitudes in the range of 100 – 400 mV (0.4 – 2.4 cmH ₂ O).....	148
Figure 6.4: Treatment values of C_{dyn} (expressed as μl/mmH ₂ O) from applications of 20 Hz-generated SIPO waveform set with amplitudes in the range of 100 – 400 mV (0.4 – 2.3 cmH ₂ O).....	149
Figure 7.1a-d: Transformations of 5 Hz R_L values to \check{R}_L	160
Figure 7.2a-d: Transformations of 10 Hz R_L values to \check{R}_L	162
Figure 7.3a-d: Transformations of 15 Hz R_L values to \check{R}_L	165
Figure 7.4a-d: Transformations of 20 Hz R_L values to \check{R}_L	167
Figure 7.5a-d: Transformations of 5 Hz C_{dyn} values to \check{C}_{dyn}	170
Figure 7.6a-d: Transformations of 10 Hz C_{dyn} values to \check{C}_{dyn}	172
Figure 7.7a-d: Transformations of 15 Hz C_{dyn} values to \check{C}_{dyn}	175
Figure 7.8a-d: Transformations of 20 Hz C_{dyn} values to \check{C}_{dyn}	177

LIST OF TABLES

<i>Table 3.1: Details of sensitization protocol for control group</i>	70
<i>Table 3.2: Details of sensitization protocol for asthmatic group</i>	72
<i>Table 4.1: Specifications for HSE-Pneumotachometer PTM Type 378/0.9, P/N 73-0981, for mice and rats</i>	89
<i>Table 4.2: Specifications for the Differential Low Pressure Transducer DLP 2.5, P/N 73-3882 from Hugo Sachs (Germany)</i>	90
<i>Table 4.3: Specifications for the TAM-A transducer amplifier module (P/N 73-0065) from Hugo Sachs (Germany)</i>	91
<i>Table 4.4: Sensor technics pressure transducer specifications. Honeywell S&C (P/N HSCSAAN001PDAA5)</i>	93
<i>Table 4.5: Calibration measurements of the DLP 2.5 low pressure transducer</i>	101
<i>Table 4.6: Calibration measurements of the Honeywell (oesophageal) low pressure transducer</i>	102
<i>Table 4.7: Table of pressures (cmH₂O) generated by frequency (Hz) and amplitude (mV) combinations.</i>	104
<i>Table 5.1: Summary table of Healthy and Sensitized Groups' tracheal pressure (Tp), Flow, and respiratory rate (rr) responses from applied pressure oscillations in the 5 Hz-generated set</i>	111
<i>Table 5.2: Summary table of Healthy and Sensitized Groups' tracheal pressure (Tp), Flow, and respiratory rate (rr) responses from applied pressure oscillations in the 10 Hz-generated set</i>	112
<i>Table 5.3: Summary table of Healthy and Sensitized Groups' tracheal pressure (Tp), Flow, and respiratory rate (rr) responses from applied pressure oscillations in the 15 Hz-generated set</i>	113
<i>Table 5.4: Summary table of Healthy and Sensitized Groups' tracheal pressure (Tp), Flow, and respiratory rate (rr) responses from applied pressure oscillations, 20 Hz-generated set</i>	114
<i>Table 5.5: 5 Hz experimental data set for R_L evaluation of sensitized and healthy subjects. 5 Hz-generated waveforms combined with indicated amplitudes produce the applied SIPO treatment (cmH₂O)</i>	116
<i>Table 5.6: 10 Hz experimental data set for R_L evaluation of sensitized and healthy subjects. 10 Hz-generated waveforms combined with indicated amplitudes produce the applied SIPO treatment (cmH₂O)</i>	117
<i>Table 5.7: 15 Hz experimental data set for R_L evaluation of sensitized and healthy subjects. 15 Hz-generated waveforms combined with indicated amplitudes produce the applied SIPO treatment (cmH₂O)</i>	118
<i>Table 5.8: 20 Hz experimental data set for R_L evaluation of sensitized and healthy subjects. 20 Hz-generated waveforms combined with indicated amplitudes produce the applied SIPO treatment (cmH₂O)</i>	119
<i>Table 6.1: Summary table of Healthy Group Tv, (PIP-PEEP) and rr responses from applied pressure oscillations, 5 Hz-generated set</i>	133
<i>Table 6.2: Summary table of Healthy Group Tp, Flow, Tv, (PIP-PEEP) and rr responses from applied pressure oscillations, 10 Hz-generated set</i>	134
<i>Table 6.3: Summary table of Healthy Group Tp, Flow, Tv, (PIP-PEEP) and rr responses from applied pressure oscillations, 15 Hz-generated set</i>	135

Table 6.4: Summary table of Healthy Group T_v , (PIP-PEEP) and rr responses from applied pressure oscillations, 20 Hz-generated set.....	136
Table 6.5: 5 Hz experimental data set for C_{dyn} evaluation of sensitized and healthy subjects. 5 Hz-generated waveforms combined with indicated amplitudes produce the applied SIPO treatment (cmH_2O).....	138
Table 6.6: 10 Hz experimental data set for C_{dyn} evaluation of sensitized and healthy subjects. 10 Hz-generated waveforms combined with indicated amplitudes produce the applied SIPO treatment (cmH_2O).....	139
Table 6.7: 15 Hz experimental data set for C_{dyn} evaluation of sensitized and healthy subjects.....	140
Table 6.8: 20 Hz experimental data set for C_{dyn} evaluation of sensitized and healthy subjects.....	141
Table 7.1: Sensitized \check{R}_L from the 5 Hz-derived pressure set. 5 Hz-generated waveforms combined with indicated amplitudes produce the applied SIPO treatment (cmH_2O).....	159
Table 7.2: Sensitized \check{R}_L from the 10 Hz-derived pressure set. 10 Hz-generated waveforms combined with indicated amplitudes produce the applied SIPO treatment (cmH_2O).....	161
Table 7.3: Sensitized \check{R}_L data from the 15 Hz-derived pressure set. 15 Hz-generated waveforms combined with indicated amplitudes produce the applied SIPO treatment (cmH_2O).....	163
Table 7.4: Sensitized \check{R}_L and data from the 20 Hz-derived pressure set. 20 Hz-generated waveforms combined with indicated amplitudes produce the applied SIPO treatment (cmH_2O).....	166
Table 7.5: Sensitized \check{C}_{dyn} from the 5 Hz-derived pressure set. 5 Hz-generated waveforms combined with indicated amplitudes produce the applied SIPO treatment (cmH_2O).....	169
Table 7.6: Sensitized \check{C}_{dyn} from the 10 Hz-derived pressure set. 10 Hz-generated waveforms combined with indicated amplitudes produce the applied SIPO treatment (cmH_2O).....	171
Table 7.7: Sensitized \check{C}_{dyn} from the 15 Hz-derived pressure set. 15 Hz-generated waveforms combined with indicated amplitudes produce the applied SIPO treatment (cmH_2O).....	173
Table 7.8: Sensitized \check{C}_{dyn} from the 20 Hz-derived pressure set. 20 Hz-generated waveforms combined with indicated amplitudes produce the applied SIPO treatment (cmH_2O).....	176
Table A.D.1: Details of sensitization protocol for (acute) control group.....	203
Table A.D.2: Details of sensitization protocol for (acute) asthmatic group.....	203
Table A.G.1. Sensitized \check{R}_L from the 5 Hz-derived pressure set.....	207
Table A.G.2. Sensitized \check{R}_L from the 10 Hz-derived pressure set.....	207
Table A.G.3. Sensitized \check{R}_L from the 15 Hz-derived pressure set.....	208
Table A.G.4. Sensitized \check{R}_L from the 20 Hz-derived pressure set.....	208
Table A.G.5. Sensitized \check{C}_{dyn} from the 5 Hz-derived pressure set.....	209
Table A.G.6. Sensitized \check{C}_{dyn} from the 10 Hz-derived pressure set.....	209
Table A.G.7. Sensitized \check{C}_{dyn} from the 15 Hz-derived pressure set.....	210
Table A.G.8. Sensitized \check{C}_{dyn} from the 20 Hz-derived pressure set.....	210

Attestation of Authorship

“I hereby declare that this submission is my own work and that to the best of my knowledge and belief, it contains no material previously published or written by another person (except where explicitly defined in the acknowledgments), no material which to a substantial extent has been submitted for the award of any other degree or diploma of a university or other institution or higher learning.”

(Signed)

11/05/2018

..... (Date)

LIST OF TERMS AND ABBREVIATIONS

ASM	Airway Smooth Muscle
ACh	Acetylcholine
AHR	Airway hyperresponsiveness
ATP	Adenosine triphosphate
C_{dyn}	Dynamic compliance
DI	Deep inspiration
DRA	Allergen mix for chronic sensitization
IP	Intraperitoneal
ISO	Isoproterenol
OVA	Ovalbumin, used for acute sensitization
PSS	Physiological salt solution
Ptp	Transpulmonary pressure
R_L	Pulmonary resistance
SILO	Super imposed length oscillations
SIPO	Super imposed pressure oscillations
SM	Smooth muscle
Tp	Tracheal pressure
TO	Tidal oscillations
Tv	Tidal volume
WBP	Whole body plethysmograph

CHAPTER I

Background

1.1. Introduction

Asthma is a misunderstood disease. Despite years of research which continue to refine the details of asthma's interference with the breathing process, it remains an enigma. On one hand, it is a collaborative disease, utilising the body's immunological and physiological responses to environmental challenges. On the other, its mechanisms of action remain aloof from effective management and elimination tactics. It is increasing in prevalence around the world, and unfortunately is suffered by an alarmingly high number of New Zealanders [1, 2]. In New Zealand, Maori and Pasifika rates of diagnosed asthma are inordinately high compared to European, Asian and other ethnicity's diagnosis rates. Of particular concern, low-income individuals are more likely to suffer the disease than higher-income individuals [1-3]. Efforts to treat the symptoms of asthma have not attenuated the progression of the disease at a population level. In fact, treatments as they are currently administered do not even cure the disease on an individual level. At best, treatment offers relief, and at times there are unfortunate side effects [4-7].

Asthma is a chronic respiratory disease, characterized by inflammation, airway hyperresponsiveness and obstruction of the airways. During an asthma attack, the contraction of ASM in combination with an increased mucus production reduces the bronchial diameter, and increases the resistance to airflow into the lungs. Some of the most recurrent symptoms of asthma are wheezing, shortness of breath, chest tightness and coughing. Cellular signals determine the activities of tissues within the respiratory system, with the resultant healthy or diseased response providing immunological, biochemical, and mechanical parameters as defining characteristics [4, 8, 9]. The tissue

within the respiratory system which is responsible for active constriction of the airways is ASM. Mechanical behaviours of ASM are therefore of intense interest in order to relate their contraction and relaxation to a diseased or disease-free state.

For almost two decades, the Institute of Biomedical Technologies (IBTec) has studied tracheal ASM response to mechanical oscillations in order to investigate greater therapeutic value for asthma treatments. Current research within IBTec's Theme for Respiratory Therapies is focusing on building both acute and chronic models of asthma in mammals. By ascertaining the response of tracheal ASM to pharmacological treatments and mechanical oscillations under healthy and acute/chronic asthma conditions, IBTec is leading the way in researching the impact of interfering with actin and myosin binding in asthmatic models [10-13]. Results from IBTec studies will further elucidate the role of medicinal and mechanical targeting of the actinomyosin crossbridges as the site of action for ASM relaxation in a chronic asthma model.

Use of data gained from studying breathing dynamics and tissue functions from healthy and asthmatic individuals is of value in understanding the mechanical properties inherent to building effective models and treatment schemes. The response of ASM in healthy and asthmatic airways seems to be influenced by breathing patterns such as tidal breathing and deep inspiration, with strong differences between healthy and asthmatic airways [14, 15]. Given that mechanical oscillations act directly in perturbing the binding between actin and myosin [16-18], further understanding of airway mechanics and the dynamic response of ASM *in vivo* seems to be an essential component in the search for a new alternative in the treatment of asthma.

An estimated 300 million people suffer from asthma [1-3, 19, 20], with the number of sufferers expected to rise another 100 million by 2025 [20]. The prevalence of asthma in New Zealand is one of the highest in the world, and the burden of this disease to government, health care systems, families, and patients continues to increase [21].

The purpose of the current study is to model chronic asthma in an animal model using mice as healthy and asthmatic subjects. As a result of the studies, and comparisons with an acute model of asthma, an understanding of the roles of mechanical oscillations in improving therapeutic outcomes will be presented. This chapter summarizes the respiratory system, physiology and the ASM role in the contraction process.

1.2. Respiratory physiology

The respiratory system is the general site of action for asthmatic attacks. In order to understand the context of asthma research therefore, it is necessary to present an appropriate overview of the respiratory system.

The purpose of the respiratory system is to provide oxygen for the body's tissues, and to remove carbon dioxide [22]. This is accomplished by preparing air for transport, providing a conduit system to move air in and out of the system, and exchanging applicable gases between the external and internal environments at specific sites.

Air is first prepared to enter the respiratory system by temperature regulation and filtration. As air moves through the nasal passage and sinus cavities it is brought closer to the body's own temperature by either warming or cooling to the environment. Filtration and removal of the majority of debris and/or dust also occurs in the nasal passage and sinus cavities [22]. Specialised cells throughout the respiratory system

produce mucus, which is responsible for trapping particles that need to be removed from the system. Epithelial cells with ciliated borders line the airways, and mucus is expelled as cilia beats to move unwanted materials away from the smaller diameter branches of the respiratory system. Immune system screening of the trapped particles also assists in detecting challenges to the body.

The means by which air is moved towards and away from the gas exchange sites is through the tube-like passageways of the respiratory system. Initially the mouth, nasal passage and sinus cavities create variable routes of access to the remainder of the system. The pharynx unites airflow pathways from the mouth and sinus cavities, and integrates with the larynx. From the larynx to the trachea there is a change in tissue characteristics. Cartilaginous rings reinforce the structure of the trachea, and smooth muscle cells provide a circular format for contracting and expanding the diameter of the airway. Epithelial cells in the trachea are composed mostly of ciliated populations, but there are also goblet cells for mucus production [23].

The trachea branches into two bronchi: One bronchus each for the right and left lungs respectively. The right lung is built of three lobes of tissue, and the left lung of two lobes. The first two bronchi that split from the trachea are termed primary bronchi. These will each split to smaller and smaller diameter bronchi and then even smaller bronchioles, until terminal bronchioles are realised. The primary bronchi split into secondary bronchi and secondary bronchi split into tertiary bronchi. Tertiary bronchi give rise to primary bronchioles and finally to terminal bronchioles. Terminal bronchioles transition to respiratory bronchioles and then alveolar ducts. The alveolar ducts are the last stage of the airway before the alveolar sacs. Alveolar sacs are the site of gas exchange, where

individual alveoli provide a means for passing oxygen into the body, and removing carbon dioxide from it (Fig. 1.1) [23].

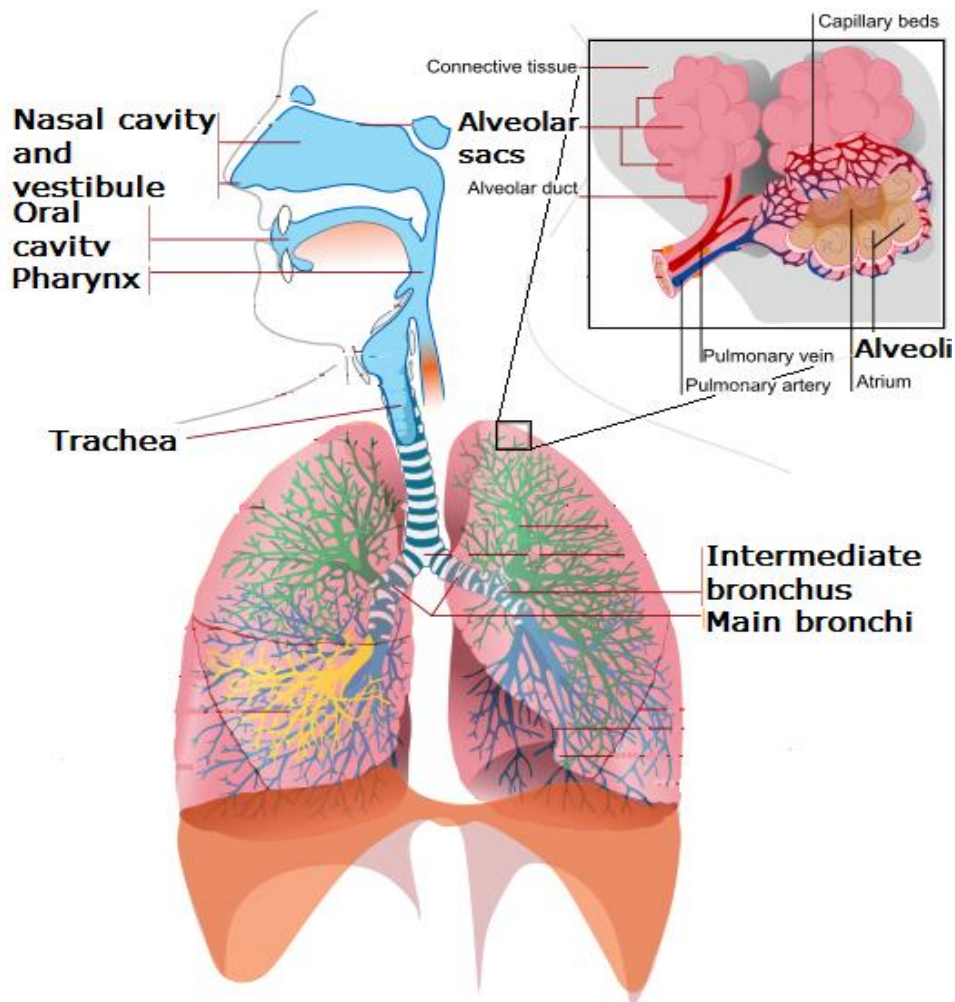


Figure 1.1. Respiratory system [24]. The human respiratory system with its various functional regions are highlighted. Of particular interest for this study are applications germane to the trachea and its ASM.

1.3. Airway smooth muscle

Airway smooth muscle is a tissue of great interest in asthma research. It is the tissue responsible for the mechanical effects of an asthmatic attack. The machinery of the ASM cell is responsible for the contractions that decrease the diameter of airways as actinomyosin crossbridges exert their forces.

Although airway smooth muscle is of specific concern in addressing therapeutic resolutions for asthma, it is initially appropriate to review smooth muscle in general terms. Smooth muscle is found throughout the body [25]. It is most prominent in the vascular system, associated mainly with arterial walls and their functions [25-28]. The gastrointestinal system also utilises smooth muscle in the walls of its organ systems in order to assist digestion and transport of foodstuffs. Smooth muscle in the bladder assists meeting demands encountered as it changes shape, contracts, and expands [28]. Of particular interest, smooth muscle is located within the airways, notably the walls of the trachea and bronchi.

Smooth muscle works in tandem with the surrounding tissues to carry out its role in the respiratory system. Within the extracellular matrix of tissue are proteins such as elastin and collagen. These elements assist in maintaining and changing the overall shape of the environment around the airways throughout the breathing cycle. During the breathing cycle, smooth muscle involvement around the trachea and bronchi is responsible for decreasing and increasing the diameter of the airways, thereby modulating the movement of air to and from the functional tissues of the alveolar sacs.

Airway smooth muscle contraction is the primary method of regulating the dynamics of the airway. It is effective at governing as it establishes an effective equilibrium of contraction and relaxation relative to the requirements of the system's demands. An advantage in utilising smooth muscle within the airways is that ASM utilises less energy for sustained contractions as opposed to the more expensive use of energy found in skeletal muscle contraction [29-31]. This characteristic proves useful in our further considerations of the mechanism of asthmatic attacks. ASM contraction during an asthmatic attack is not offset by subsequent relaxation. Instead, with a lower demand for

energy needs, contractions can be maintained for longer periods of time in exacerbating the disease state.

Muscular forces utilised by the respiratory system are both passive and active. The passive forces are characteristic of a resting state, while active forces are associated with the contraction of tissues. There are several elements involved in the forces in the respiratory system. Both the ASM immediately associated with system structures (trachea and bronchi) and skeletal musculature which drive the breathing process (diaphragm and intercostals) can be described by these terms. Resting forces describe the resting state, when muscle tone is maintained, and energy use is low relative to the active state. Active forces are associated with the contraction of muscle tissue, and the increased use of energy for this purpose. It is possible to model such forces in order to describe the contractions and relaxations of muscle tissue.

Models to describe the actions of skeletal and smooth muscle are constantly evolving to describe nuances of new discoveries and conditions of studies in the tissues [29, 30, 32]. The various models maintain a common theme of portraying the conversion of chemical energy into mechanical energy, and endeavour to address the differences of cellular mechanics and observed physiological phenomena [32].

The seminal work of Huxley in coordination with other specialists resulted in the presentation of skeletal muscle's inner workings [33, 34]. Huxley's work with skeletal muscle is the basis upon which all smooth muscle contraction models are based. Huxley's early description of filaments sliding past each other as forces are transferred, combined with the proposal that there are two states of actin and myosin interaction – attached and detached – initiated the basis set for further details elucidated in later studies [33]. Hai

and Murphy adapted Huxley's model to fit with their work with smooth muscle tissue [35, 36]. Where Huxley details the regulation of skeletal muscle contraction by actin activation, Hai and Murphy present the importance of myosin phosphorylation as the regulator of smooth muscle contraction. This leads to the addition of a slower cycling of actin and myosin as alternate energy-utility states are considered in modelling the contractile system [35-38].

Actin and myosin are the molecular mechanics of force generation in models used to describe contraction and relaxation. The chemical energy utilised by the mechanical levers is predominantly adenosine triphosphate, commonly referred to as ATP [36]. Use of the energy-rich molecule is possible due to the availability of its terminal phosphate group. This phosphate is transferred between substrates as a means of exchanging energy through a system. Energy in the form of ATP is used in essentially the same way in the different muscle types, but there are variations at the molecular level which distinguish the tissues from each other [23, 25]. For example, in skeletal muscle ATP is used in the contraction process in two main steps. It is hydrolysed by the myosin head to adenosine diphosphate and inorganic phosphate prior to the myosin head binding to actin. ATP also binds to the myosin light chain in order to release it from actin [39]. If ATP is unavailable for this step, myosin remains bound to actin and is unavailable for subsequent contraction activity. In smooth muscle contraction, ATP is used to phosphorylate the enzyme myosin light chain kinase (MLCK). This step precedes phosphorylation of the myosin light chain, which is necessary for myosin to bind actin. Once myosin is bound to actin, the myosin head is also able to hydrolyse ATP to ADP and Pi, and release myosin from actin [25]. It is the formation of the actinomyosin interaction, the crossbridge, which is of greatest interest in understanding the effective treatment of asthmatic attacks. The following

sections present a detailed explanation of the molecular mechanisms of force development as a result of the actinomyosin cross-bridges' cyclic interactions.

1.4. Structure of the contractile apparatus

The mechanical features of smooth muscle are responsible for the contractions and relaxations of the cells. The contractile apparatus is built up of active and passive components which are associated with energy-use and providing structural support respectively [32, 40]. Smooth muscle contraction is an active process accomplished using actin and myosin components. Actin appears as thin filaments in the ASM cells, and myosin as thick filaments. There are also intermediate filaments, dense bodies, and plaques within the cellular structure which add to the contractile continuum. Plaques are conglomerates of proteins that act as attachment points for thin filaments (actin) [40, 41]. Intermediate filaments link dense bodies to the cytoskeleton, and the cytoskeleton is the basis for the rigidity of the cell when there is no contraction [42, 43] (Fig. 1.2.).

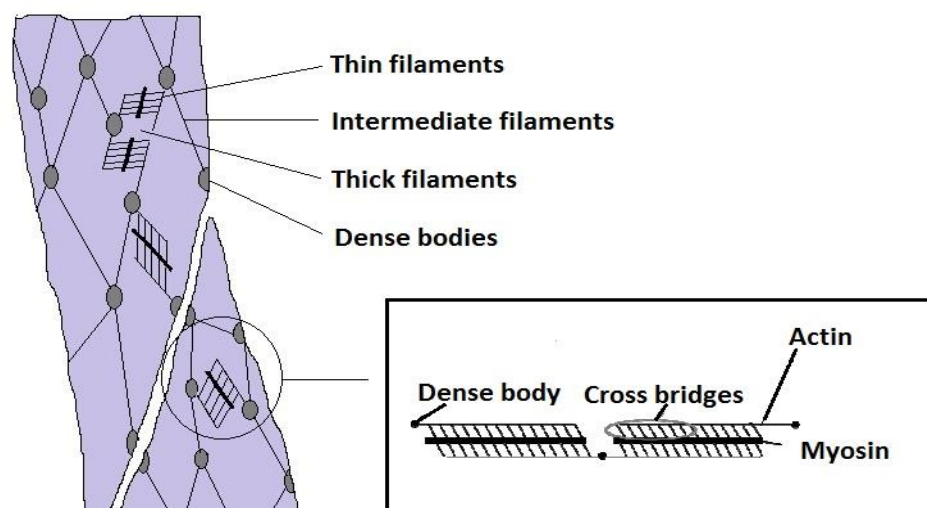


Figure 1.2. Components of cytoskeleton and myofilaments on smooth muscle [26]. Dense bodies are characterised as anchoring points for actin-rich thin filaments of the contractile machinery.

a. Thin filaments

Thin filaments in ASM cells are functionally critical to the activities of contraction and relaxation. Thin filaments are primarily composed of actin, with additional proteins and inorganic factors supporting their function [43-46]. There are two forms of actin, G- and F-actin, named according to their chemical state [44]. Actin can be found in the cell as either a monomer (G-actin) or as a polymerised filamentous strand (F-actin) (Fig. 1.3). The F-actin state is necessary and required for interaction with myosin in the contractile process [39, 47]. A result of this fact is that the ratio of (F-actin/G-actin) can be used to identify the character of the cell's contractile state. A generic assumption is that higher contractile states have more F-actin relative to G-actin.

Important actin-associated proteins in the thin filaments include tropomyosin, caldesmon, and calponin. Tropomyosin is primarily known for its role in regulating skeletal muscle contraction but plays a somewhat different role in smooth muscle cells [39]. Tropomyosin in smooth muscle cells acts in concert with the actinomyosin contractile structure to enhance the functionality of the unit. Tropomyosin is regulated by caldesmon and calponin [41, 48]. Caldesmon is a smooth muscle-specific protein involved in regulatory pathways of contraction. It is Ca^{2+} -regulated when involved in enhancing the actin-tropomyosin interaction, and can also be phosphorylated as part of its regulatory pathway [41, 47]. Caldesmon activity is carried out in conjunction with another protein, calponin, and functions to interfere with tropomyosin's affinity for thin strands in order to present myosin binding sites on polymerised actin strands [39].

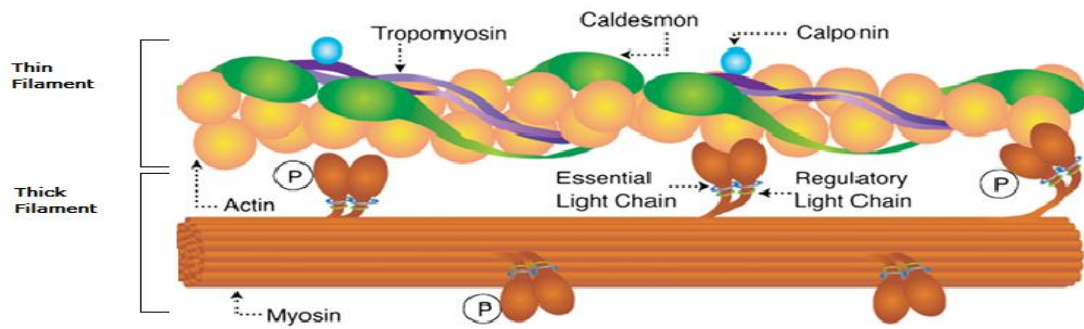


Figure 1.3. ASM components of the contractile apparatus [39]. Myosin thick filaments slide along the predominantly-actin thin filaments of the contractile machinery.

b. Thick Filaments

The thick filaments of ASM cells are composed of polymerised myosin arranged into chains of differing functional characteristics. Six myosin chains (4 heavy chains and 2 light chains) are involved in forming a thick filament [39]. The four heavy chains are formed into 2 dimers, each containing 2 heavy chains (~205 kDa each). Each dimer is characterised by 4 regional domains: the main body, the neck, and 2 terminal globular heads [48]. The heavy chain dimer consists of a main body and two terminal globular heads (Fig. 1.4 and Fig. 1.5). The light chains are classified as “regulatory” (~20 kDa) and “essential” (~17 kDa) ([48]), based on their respective functions, and are located in the neck region of each dimer (Fig. 1.4).

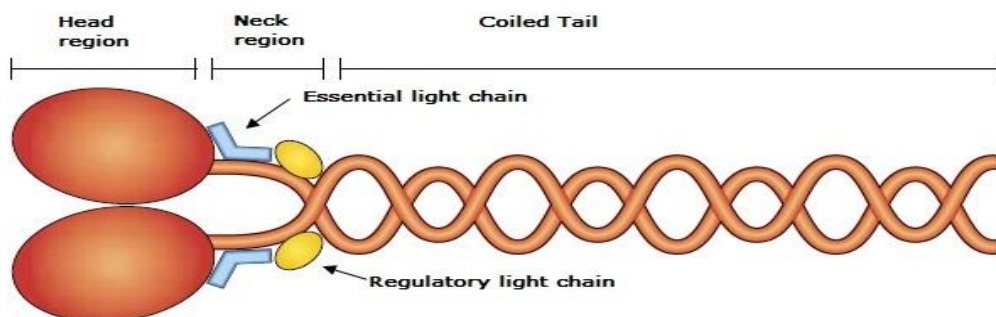


Figure 1.4. Myosin structure (Adapted from reference [45]). The head region of the molecule interacts with the actin components of the contractile apparatus in smooth muscle cells.

c. Intermediate filaments

Intermediate filaments are protein complexes responsible for cellular structure and continuity, often associated with other proteins in various capacities. Intermediate filaments link dense bodies into the cytoskeletal network and give rigidity to the cell and cellular structures, while associated proteins augment the processes [42]. Intermediate filaments are located along the inner surface of the cell membrane and with cytosolic and nuclear structures [44]. Six types of intermediate filaments are described, based on grouping similar protein structures of over 70 different IF gene products.

Four proteins are classified as Type III IFs, of which two are relevant to our discussion. Desmin and vimentin are both associated with structural support and networking within the cell [43]. Desmin is associated with sarcomere structures and their support in the cytosol [43]. Vimentin is also characterised as supporting cellular membranes in the cytoskeletal network [22]. Notably, phosphorylation of the head region of vimentin is a regulatory mechanism for filament stability. This stability may also be affected by a vimentin-associated protein, plectin.

Plectin is a protein which facilitates interactions between actin and microtubules, intermediate filaments (such as vimentin – vimentin), and thick filaments. The role of plectin in ASM contraction and relaxation is of interest in that plectin-vimentin association is seen to play a role in length adaptability of ASM [45-50]. Together with phosphorylation cascades, the intermediate filaments and their associated proteins can be seen to carry out important functions in the contractile state.

d. Membrane-associated dense plaques

In addition to the intermediate filaments that accommodate structural stability along their membranes, cells also utilise dense plaques as anchoring points in their cellular networks. Dense plaques are so named because they are observed as darkened bands of localised proteins along the inner cell membrane [50-52]. They are also referred to as focal adhesion plaques. These plaques are centralised association regions for such proteins as intermediate filaments, F-actin polymers, and transmembrane integrins. The plaques are a connection point between extracellular matrix proteins and proteins of the cytoskeleton [53]. In ASM the protein interactions at dense plaques also include localised proteins such as vinculin, talin, alpha-actinin and paxillin [42, 54]. The specific roles of these associated proteins are functionally relevant to structural stability and malleability of the filaments and polymers as they interact with the cell membrane. In the context of ASM cells, this region assists in polymerisation of F-actin, and the cytoskeletal mechanics involved in cell shape during contraction and relaxation.

e. Cytosolic dense bodies

Dense bodies are not associated with membranes alone. Their function is of such importance that they are also localised throughout the cytoplasm. Dense bodies in ASM cell cytoplasm share similar characteristics with those associated with membranes, and actin filaments are almost always identified with them as well. The cytosolic locations are attachment sites for proteins involved in the processes of the cell's contractile states [42-45, 55]. In that sense, cytosolic dense bodies correspond to the Z-disks of striated/skeletal muscle cells [45, 48]. Because the dense bodies are associated with thin and intermediate filaments, they will move through the cytoplasm towards other dense bodies as contraction occurs. From a mechanical standpoint, cytosolic dense bodies are

responsible for coupling the extracellular matrix and cell surface proteins to the intracellular cytoskeleton and contractile apparatus.

f. Dynamic relation of structural components

Smooth muscle fibres are key participants in active processes throughout the body. It follows that the structural components of smooth muscle are also active. They are not static. Smooth muscle changes its shape and size, its width and length during contraction and relaxation. The dynamics of the cell are a reflection of these processes, and must respond/adapt according to the external stimuli that direct them in order to achieve optimal mechanical functions. Stimulation of smooth muscle contraction requires length changes in cytoskeletal structures. In ASM, these length changes are primarily due to the polymerisation/depolymerisation of actin and the interactions of associated proteins in order to ensure that a maximal force is generated and maintained over time across different lengths of tissue [51-56].

Actin and myosin filaments must interact for contraction to occur. To achieve optimal function, the ratios of thin and thick filaments are regulated via a multitude of biochemical pathways within the cell. G-actin monomers combine to form F-actin polymers, and myosin polymers assemble into thick dimers and thin filaments. The myosin dimers and filaments arrange into chains preparatory to mature contractile structures and operational ASM length adaptations. Canine trachea ASM studies indicate that prior to contraction, 40% of total cellular actin is G-actin, a G- to F-actin ratio of 2:3 [47,48]. This ratio decreases to 3:7 after contraction (30% G-actin) indicating ASM cellular increases in thin filaments [47]. Porcine trachea ASM contraction studies further elucidate the relationship between contractile filaments [55]. The increase of both F-actin and polymerised myosin support the demands placed on the cells to facilitate greater numbers of functional

contractile units for ASM contraction. Additional proteins involved in the dynamics of this polymerisation process include vinculin, gelsolin, and profilin [56-58].

The machinery of smooth muscle tissue contracts to generate maximal force across variable lengths of tissue. In order to accomplish this, the various filamentous and aggregate components coordinate their actions and utilize available cellular energy resources. Thin, thick and intermediate filaments, dense plaques and bodies, all interact and optimize activities to match the regulatory stimulations and inhibitions that constitute the resting and contractile processes. Energy requirements (and availability of energy) vary according to the demands of relaxations and contractions [56]. The smooth muscle cell accommodates the varying demands with effective and unique management of energy resources.

The primary unit of energy for cellular processes, and particularly in our discussion of muscle contractions is ATP, a mainstay of the body's biochemical processes [23, 35-37]. ATP is composed of a nucleoside base (adenosine) attached to the C-1 carbon of ribose, a five-membered (pentose) sugar ring, which is in turn joined to a series of three phosphate groups via phosphoanhydride ("high-energy") bonds [22, 23]. Moving outward as a linear appendage from the C-5 carbon of the pentose sugar, each phosphate is designated as α -, β -, and γ -phosphates. The terminal γ -group's bond to the β -group is broken and formed in cyclic fashion by enzymatic activity in order to transfer and store energy respectively. Cleavage/hydrolysis of the terminal phosphoanhydride bond results in the conversion of ATP to ADP and an inorganic phosphate group, with the inorganic group being transferred to a new substrate. The substrate may be a protein, enzyme, or other phosphate-compatible molecule. As a result of this transfer, an additional function

beyond energy-use arises: a signaling cascade is carried out based on movement of the phosphate group.

Smooth muscle functionality can be assigned two specific states: A resting state which is preparatory to contractions, and the contractile state [32, 33]. Each of the states has key metabolic events involving ATP and the interactions of actin and myosin filaments. The resting state of smooth muscle is characterized by the lack of force being generated between actin and myosin. This is commonly generalized by stating that actin and myosin are detached from each other, but effectively covers the sequence of events that proceed from actin-myosin separation to myosin's reattachment, a force-free period [35, 36]. In the case of myosin detachment from actin, this is due to the biochemical environment and inaccessibility of the myosin binding site on the actin strand [35].

Various stimuli act on the cell and signal for myosin-binding-site accessibility in order to overcome this mechanical pause. Signals for phosphorylation of the myosin light chain, and ATP binding to the myosin head precede myosin's reorientation and the interaction of a new actinomyosin cross bridge [42-44]. Phosphorylation of the myosin regulatory light chain is the result of an upstream calcium (Ca^{2+})-calmodulin complex activation of MLCK. MLCK then phosphorylates myosin regulatory light chain. Smooth muscle actinomyosin crossbridge formation requires this phosphorylation to take place [45]. Accounting for energy, a molecule of ATP is used as a phosphate group is transferred by MLCK to the light chain of myosin, and another molecule of ATP is bound to the ATPase site on one of the myosin chain's two heads (Fig. 1.5(a)).

Contraction of smooth muscle efficiently utilizes energy in order to maintain mechanical force at low cost to ATP stores [51]. Contraction is generally explained in the following

stepwise manner (illustrated for further reference in Fig. 1.5): Following ATP hydrolysis on the myosin head (Fig. 1.5(b)), crossbridge formation takes place. The myosin head attaches to the myosin binding site on actin and P_i is released from the ATP binding site (Fig. 1.5(c)), completing the steps described as the resting state. Activity from this point is the contraction's power stroke. The power stroke is the mechanical force of contraction as it shortens the muscle tissue (Fig. 1.5(d)). This occurs as the thin filament is displaced along the thick filament due to each actinomyosin crossbridge generating force. The actinomyosin crossbridge disassembles at the completion of the power stroke. This is due to de novo binding of ATP to myosin, thereby destabilizing the crossbridge. The myosin head detaches from actin, and the resting state is recovered (Fig. 1.5(e)).

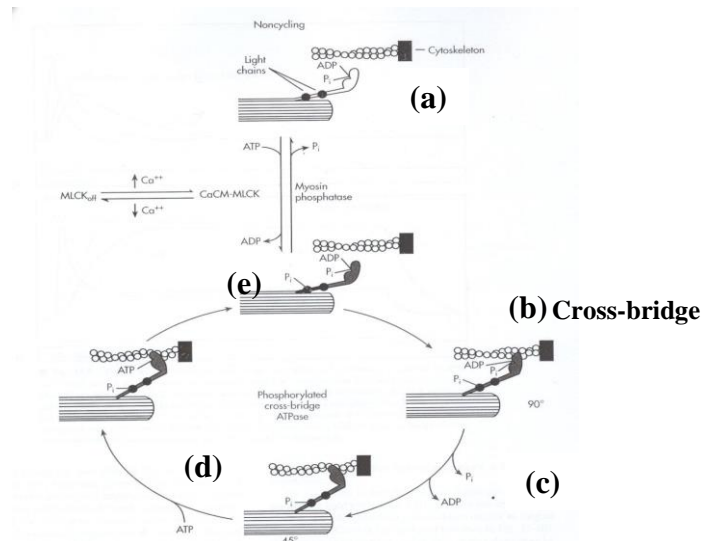


Figure 1.5. Smooth muscle contraction process [54]. The cross-bridge modeling of smooth muscle contractile units is established by actin and myosin interactions. Transfer of P_i through the interacting contractile elements provides necessary energy resources.

Hai and Murphy have proposed further refinements (illustrated in Fig. 1.6) [35, 36] to this generalization. Two states of myosin interaction with actin are presented (phosphorylated and dephosphorylated), and each relates to stability of the crossbridge. This in turn affects the rate of detachment of actin from myosin; it is not always uniform for all crossbridges. A slower cycle is proposed based on actinomyosin formation, and then dephosphorylation of myosin by myosin light chain phosphatase (MLCP) with the crossbridge still intact. A

dephosphorylated crossbridge is more stable, so slower cycling results. Interpretation of this proposal is extended to an association of initial fast cycling of the crossbridges with variable length changes of the muscle cell, and then slower cycling more prevalent when muscle cell length is stable.

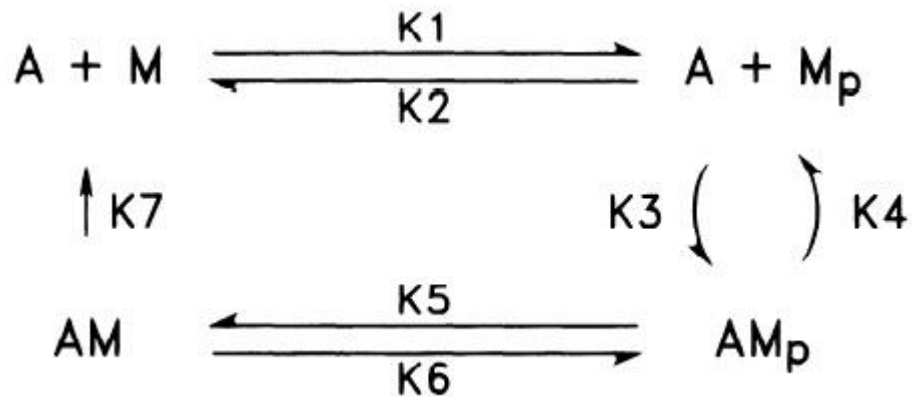


Figure 1.6: Four state model of Hai and Murphy (1988) [35]. Abbreviations for the model are as follows: A, actin (thin filament); M myosin (detached, unphosphorylated); Mp (detached, phosphorylated); AMp (attached, phosphorylated); AM (attached, unphosphorylated); K1-K7 are forward and reverse rate constants between the various states of the model. The crossbridge is modelled to vary constantly between the states indicated, and cycling speeds are dependent on phosphorylation, with the detachment rate of AM to A+M being lower than AMp to A+Mp.

Appropriately, crossbridge cycling can be related to physiological manifestations. Smooth muscle dysfunction is associated with a number of diseases, such as erectile and bladder dysfunctions, as well as vascular and, notably, respiratory disorders [8, 27, 28]. Smooth muscle diseases such as chronic obstructive pulmonary disease and asthma are prime candidates for investigations in the context of actinomyosin crossbridge disruption. It is impossible however, to carry out this type of research on humans, and so other suitable animal models must be investigated. For our purposes, the use of mouse models is preferable to other options, with the reasoning for this choice discussed in further detail (Chapt. II).

1.5. Mouse anatomy

Mouse anatomy and physiology associated with the respiratory system are relevant to this chronic asthma study as a means of investigating actinomyosin crossbridge disruption of ASM. A brief discussion of pertinent murine airway components is presented in this section, with Fig. 1.7 illustrating the mouse upper airway anatomy as an initial reference point.

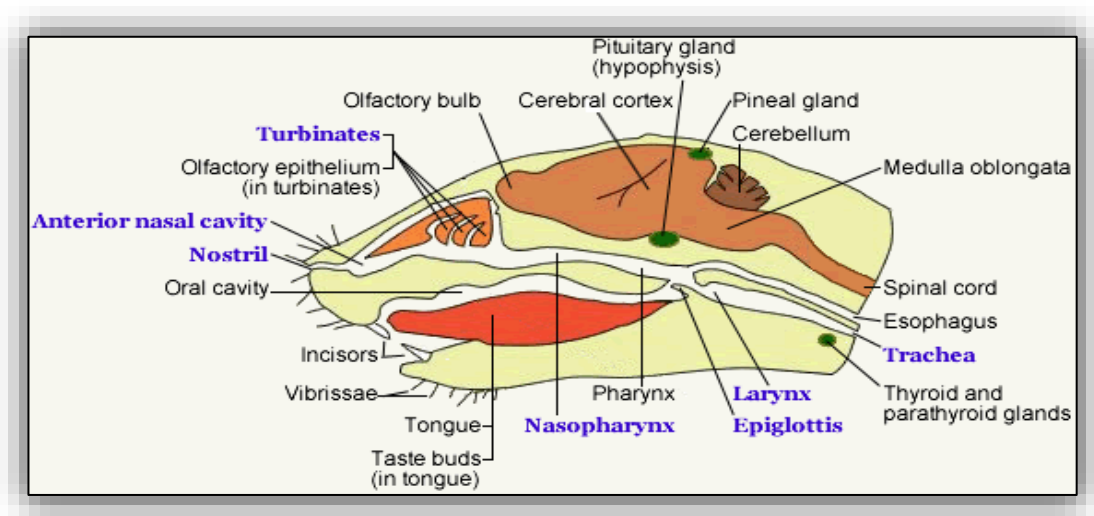


Figure 1.7. Mice upper airways anatomy [118]. Of particular interest to this study are the nasal and oral cavities as well as the oesophagus and trachea.

a) Pharynx and Epiglottis

Mice are nasal breathers. All inhaled air and substances pass initially through the nostrils to the nasal cavity and then to the nasopharynx prior to reaching the pharynx. The pharynx is continuous with both the nasal and oral cavities. The epiglottis covers the opening to the larynx when food is swallowed, preventing food from entering the trachea and respiratory tract.

b) Larynx

The larynx is separated from the pharynx by the epiglottis and extends to the trachea. The tissue character of the larynx consists of respiratory epithelium, with elastic fibres, glands, cartilage and vocal cords.

c) Trachea

The trachea connects the larynx and primary bronchi. The tissue of the trachea contains multiple incomplete hyaline cartilage rings which support an open lumen for air movement, and are spaced along its length. The ends of the cartilage are connected by airway smooth muscle which contracts and relaxes to influence the diameter of the trachea. A tracheotomy cuts a small hole in the connective tissue between adjacent cartilage rings, and a cannula is inserted into the lumen of the trachea. The cannula is secured with surgical silk, closing the tracheotomy's hole, allowing the mouse to maintain spontaneous breathing patterns.

d) Lungs

The right lung of the mouse is divided into four lobes and the left lung is a single lobe, as shown in Fig. 1.8. The lungs receive air that is passed from the trachea through the bronchial tree to the site of gas exchange in the alveoli. The trachea divides into the primary bronchi, which still contain cartilage and respiratory epithelium. The primary bronchi then branch into bronchioli and the terminal bronchioli with their alveoli. (Unlike humans, mice do not have respiratory bronchioli between terminal bronchioli and alveoli.) As the airways decrease in size, their walls become thinner, containing less connective tissue and smooth muscle. The associated epithelium also becomes more simplified, allowing for gas and drug exchange with pulmonary vasculature. Not all air

that is inhaled participates in gas exchange, either because it does not reach the alveoli, or the alveoli are unable to transport the molecules.

e) Ventilation

The normal breathing rate for a mouse is approximately 150 breaths/min, with a tidal volume of air between 0.15 and 0.2 ml [13]. As mentioned, not all inhaled air perfuses the alveoli. This residual volume of air constitutes the dead space within the respiratory system. Using the percentage of human dead space [25] as an approximation, 30 percent of the mouse tidal volume is equivalent to ~50 μ l of dead space.

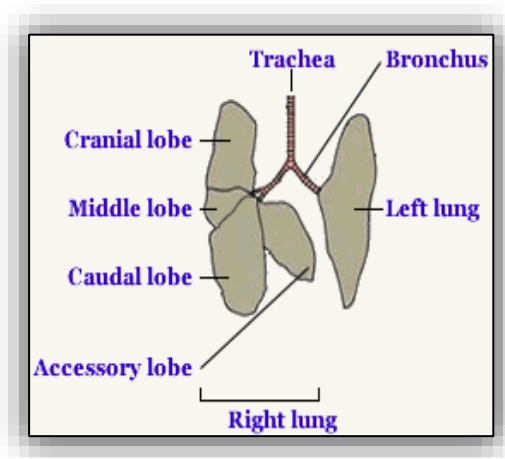


Figure 1.8. Mice lower airways [118]. Notably in mice, the number of lobes in the right lung is four times greater than the single left lobe. By comparison, human lungs have three and two lobes respectively.

1.6 Thesis structure

This thesis covers information in the following chapters: Current knowledge on asthma and its therapies (Chapt. II); Animal models and sensitization protocols for a chronic asthma model (Chapt. III); Experimental investigation methods used with the chronic asthma model (Chapt. IV); Results and evaluation of lung resistance, R_L , respiratory functions in chronic asthmatic models (Chapt. V); Results and evaluation of dynamic compliance, C_{dyn} , respiratory functions in chronic asthmatic models (Chapt. VI);

Comparison of acute and chronic asthmatic subjects in the presence of SIPO *in vivo* and finally, discussion points and conclusions gained from the results of the studies (Chapt. VII).

1.7 Summary

This chapter presented respiratory system and airway smooth muscle components in humans and mice, whose functions are relevant to this asthma study. To understand how these components interact and change during asthma, further details on how asthma alters the basic structure of the airways will be presented. The next chapter will discuss these topics and provide information relative to (mechanically-generated) applied physiological oscillations and their impact on the airways.

CHAPTER II

Asthma, ASM and mechanical response

2.1. Introduction

This chapter discusses asthma, available asthma treatments, as well as airway remodelling and the effects of different breathing patterns on asthmatic systems. Relevant literature is presented, cited and discussed, and the main objectives of this chronic asthmatic model research are provided in the conclusion of this chapter.

2.2. Asthma

Asthma is increasing in prevalence around the world, and particularly in New Zealand. Studies indicate that the past two decades have seen a marked rise in cases of diagnosed asthma [1-3]. In New Zealand there is particular concern over the incursion of this disease amongst Maori and Pasifika [1]. Asthma is identified by both acute and chronic states. The disease manifests as intermittent events of shortness of breath, coughing, tightness of the chest, and wheezing, with additional persistent bouts of breathlessness [3]. These symptoms can vary in frequency and severity from individual to individual. Heightened physical activity may also play a role in their manifestation and intensity. Symptoms may even be localised in time to either day- or night-time attacks leading to sleeplessness and over-all fatigue throughout the night and day.

Asthma attacks involve more than outward symptoms. Physiologically the airways narrow as a result of multiple factors. Inflammatory responses, bronchospasm, and airway hyperreactivity combine to create a life-threatening condition in worst-case scenarios. (Airway hyperresponsiveness, AHR, is an applicable term which combines the descriptors hyperreactivity, the heightened response of the airway, and hypersensitivity,

high sensitivity to low amounts of allergen [56].) Production of mucus from specialised airway cells further exacerbates the condition, as the airway narrows and normal breathing is challenged [57]. Constriction of the airway smooth muscle compounds the severity of the deficient bronchial channels.

Healthy individuals do not respond to allergen challenges in the same way as those who suffer from asthma. Healthy airways do not collapse in a manner indicative of inflammatory, bronchospastic, or hyperreactive tissues of asthmatics. Unfortunately there is a marked difference between healthy and asthmatic airways, yet the fact will aid in differentiating results from across study groups. Asthmatics' airways constant efforts to overcome the disease indicators eventually remodel their constituent tissue identities. This airway remodelling is seen as a distinct structural change to the tissue [57], with proliferation of epithelial cells, a thickening of the reticular basement membranes, and subepithelial fibrosis combining to decrease the compliance of the airway. The increases in vascular flow to support this proliferation also aid in the accumulation of smooth muscle mass surrounding the airways.

2.3. Asthma Treatments

Asthma treatments can be classified as either Medicinal (Pharmaceutical) or Non-medicinal (Alternative). The traditional approach to treating asthma is with pharmaceuticals responsible for either anti-inflammatory or bronchodilatory functions. Alternative methods of treatment are aimed at decreasing the amounts of drugs used in suppressing symptoms. Medicinal and non-medicinal treatments are discussed in the following sections.

2.3.1. Medicinal Treatments

As mentioned, there is no cure for asthma. Consequently, medications used in the treatment of asthma are potentially, and most-often, a life-long habit. The two types of medications used in asthma therapies are anti-inflammatories and bronchodilators. Anti-inflammatory therapy is used to target the pathways in ASM that are responsible for the narrowing of the airway lumen as a result of inflammatory responses [4, 5]. Corticosteroids are the class of drug used in this respect. Bronchodilators are used to stimulate relaxation of ASM tissue [6]. Beta (β)-2 adrenergic receptor agonists are used for this purpose. There are always risks for side effects from drug use, and in the case of both approaches for asthma therapies, this is also the case [6]. Inefficiency of drug delivery, tolerance, and development of side-effects over time are facts of the medicinal approach to asthma treatments.

a. Beta-2 adrenergic receptor agonists

β -2 adrenoceptor agonists relax ASM via pathways responsible for stimulating the cellular messenger cyclic-AMP, abbreviated as cAMP. The class of drug is used for pulmonary diseases including asthma [7]. The pathways affected by cAMP stimulation are utilised to relax ASM components used in contraction. These agonists have both short- and long-term actions depending on the specific drug being used. Short-term acting agonists are useful for treating mild-to-acute asthma attacks over the space of a few hours, and include drugs such as isoproterenol (ISO), salbutamol, and terbutaline [58, 59]. Long-term acting agonists are not as quick to act against the symptoms of asthma, but over time maintain therapeutic objectives [60]. Salmeterol and formoterol are two such drugs. The targets of both short- and long-term agonists are the different subtypes of adrenoceptors along the surface of cells. Some agonists are non-specific and stimulate multiple subtypes, with notably different outcomes. This is exemplified by ISO which targets β -1 and β -2 receptors [58, 60], though in ASM only β -2 receptors are available.

b. Corticosteroids

Corticosteroids naturally arise from the adrenal cortex. They are also synthesized commercially as pharmaceutical-grade therapeutic agents. Corticosteroids have subclassifications based on initial identifications of their physiological influences, mineralocorticosteroids for their effects on minerals, and glucocorticosteroids for their role in glucose metabolism [25]. Glucocorticosteroids are the subclass of corticosteroids used in asthma therapies, targeting inflammatory processes to inhibit them.

The mechanism of action of corticosteroids with respect to ASM is to inhibit the phospholipase A2 pathway inside the cell. This pathway is responsible for producing and regulating inflammatory molecules. Prostaglandins and leukotrienes are molecular participants in physiological pathways which (in this context) ultimately constrict ASM, increase goblet cell production of mucus, and upregulate the number of inflammatory cells in the matrices around the airways [57].

2.3.2. Alternative treatments

Alternative treatments of asthma have been developed in order to decrease the amounts of pharmaceuticals used as therapeutics. Buteyko breathing, continuous positive airways pressure (CPAP), and bronchial thermoplasty are three main areas of consideration for finding benefits away from total-dependence on drug therapies.

Buteyko breathing is a method intent on implementing changes to breathing patterns as a way to offset asthmatic symptoms. Buteyko is characterized by high-volume, low frequency nasal breathing. Its aim to achieve a decrease in therapeutic drug use has been documented in studies [61]. Use of this technique is not associated with improvements to lung functionality [62].

CPAP is primarily used to treat sleep apnea. The positive pressure of CPAP helps to offset observed negative pressures which are present in airways of sleep apnea sufferers [63]. This negative pressure reduces the size of the airway lumen and presents additional challenges to asthma sufferers who also suffer from sleep apnea. Use of CPAP in studies of a population of dual-sufferers indicated a reduction in key biochemical markers for asthma [63-65].

Bronchial thermoplasty is a costly, invasive technique which removes ASM mass from the airway wall. Introduction of a flexible bronchoscope through either the nose or mouth to the lungs allows for delivery of radio frequency energy to targeted tissue. Thermal destruction of the airway tissue is aimed at decreasing total contraction force during an asthmatic attack. There are overall benefits to the procedure, particularly a reduction in respiratory attacks, emergency room visits, and hospital stays, though cost and case-by-case assessment/qualification limit its widespread utility [66-68]. The benefits are also associated with maintained dosage of medications, so the decrease of drug-use is not achieved in this respect [68].

Current knowledge and research indicates that a definitive physical treatment for asthma is still a future (necessary) accomplishment. Current therapies are largely centred on the chemical pathways involved in the asthmatic response, with a smaller percentage of efforts focusing on alternative treatments. Application of mechanically-generated physiological pressure oscillations are a potential area of research which looks to address effective physical treatment of asthma sufferers.

2.4. Airway remodeling in asthma

Acute and chronic asthma are different stages of the same disease. Acute asthma is not affected by tissue remodeling, but chronic asthma, with its consistent inflammatory insult over time, is characterized by the resultant airway remodeling which takes place [69]. It is the inflammatory response which is responsible for driving the escalating cycle of chronic asthma's airway remodeling. Inflammation causes tissue damage and structural changes within the airway [70]. It is also an accessory to the bronchospasms which are symptomatic of the disease. The efficiency of a healthy airway is compromised as the tissues further change from their ideal composition. Although corticosteroid therapies are applied to counter the inflammation, the treatment does not address the tissue and extracellular matrix remodeling which occurs over time [71]. In vivo analysis of relevant tissue samples has revealed the extent to which pathology is evident in chronic asthmatic airways [71-73].

Airway remodeling is detailed by an increase in smooth muscle mass, a change in the characteristics of extracellular matrix constituents, and pathological markers at the molecular level. Remodeling of the smooth muscle is described with two main terms, hypertrophy and hyperplasia. Hypertrophy is an increase in size of the tissue, and hyperplasia refers to the increase in number of cells in the tissue [73]. The extracellular matrix surrounding the airways is rich in tissue components and molecular products which add to the structural stability of the system. The airway's epithelial cells are supported by a basement membrane, which is composed of two layers (the basal and reticular laminae). The reticular membrane is thickened in chronic asthma pathology [72]. The collagen and fibronectin deposits in this layer accompany immunoglobulin increases as well as increased vascularity and stiffening of the tissues [69]. In additional studies, goblet cell pathology and mucus increase are also noted [73].

2.5. ASM and asthma

Mechanical oscillations and biochemical processes are ubiquitous within and around our physiologies. Breathing is a primary example of a biological process generating oscillations within the airways. The biochemical signalling pathways within cells are also of prime importance to sustaining functional efficiency and effectiveness. Within the context of ASM, both oscillations and cellular signalling are of interest in our research. Breathing naturally changes the luminal diameter of the airway wall as volumes of air transit in and out of the system. Contractions and expansions of the airway result in constant changes (oscillations) to the lengths of the ASM [15, 56, 74-79]. Tidal oscillations (TO) occur during normal breathing, and deep inspirations (DI), as the name implies, are the result of deeper breathing beyond normal oscillations. External application of oscillations to ASM is also possible and controlling the length change in order to elicit a bronchoprotective response [10-13] is a focus of our work. In response to length change demands as well as administered pharmaceuticals, the biochemical machinery likewise carries out its activities to support or inhibit contractile oscillations [44-46].

Volumetric measures for both TO and DI have yielded percentage values which describe the intrinsic variance of ASM length changes. These length changes during normal breathing are calculated at 4% for TO, and 25-30% during deep inspiration [13, 80]. The utility of these numbers allows for mechanical application of similar oscillations back into physiological systems, and specifically into ASM. Mechanical TO (4% amplitude, 0.33 Hz) [10-13, 76] or volumetric oscillations [77, 78] applied to regions of healthy airways results in relaxation of the tissue. TO applications also relax ASM when applied before a contractile stimulation, providing a bronchoprotective effect. Similarly, the

observed relaxation of precontracted ASM by TO treatment indicates a bronchodilatory effect [76-80]. When comparing the bronchodilatory effect of TO application to the benefits of current pharmaceutical bronchodilators (Isoproterenol for example), there are comparable levels of relaxation [78, 80-84].

Similar benefits are seen in applications of oscillations which imitate DI: Chemically-constricted healthy airways are dilated by DI oscillations [15, 32, 85-88]. Further, DI oscillation applications prior to contraction of ASM as a result of allergen challenge provide a bronchoprotective effect [15, 88]. In the case of DI therapy, the mechanism of action is thought to be associated with cytoskeletal reorganization [48-51] since the length changes in the tissue are nearly 7 times greater than those in tidal oscillations. Unfortunately, deep inspirations are largely absent in asthmatics. Application of DI oscillations to asthmatics yields variable results. In severe cases there is an increase in ASM constriction, and in non-severe cases there is only a mild dilation of the airways [84]. The severity of the disease likely determines the physiological response to DI applications, indicating that cytoskeletal or mechanical remodelling (as well as changes in biochemical regulation) likely occurs within the tissues as the disease progresses.

Asthmatic airways respond differently to TO and DI therapies administered to healthy subjects. The wave types and frequencies used in in vitro studies discussed thus far are ineffective as treatment for precontracted asthmatic ASM. However, studies using alternative oscillation patterns identify more-effective conditions for asthmatic therapies. Inhibition of active force and stiffness by imposing parameters that differ from traditional TO and DI values has been shown [16, 48, 80, 83, 84]. Importantly, alternative oscillation specifications applied to allergen-challenged ASM resulted in long-term (greater than 30 minutes) reduction in force after the oscillations were concluded [14]. Identifying force

as the measure of contraction and noting that the reference length is the length that ASM generates the highest contractile force in the presence of bronchoconstrictors [8, 80, 85], additional literature supports the impact of oscillations on ASM contractions.

IBTec in vitro studies on porcine tracheal smooth muscle (frequency range 0.2-80 Hz, amplitude range 2-8% of reference length) have shown up to 40% reduction in ASM constrictive force [12]. Furthermore, refining the parameters of frequency and amplitude has shown that force reductions in ASM are dependent on oscillation amplitude and to a lesser degree on frequency [13]. In addition to TO- and DI-related methods, IBTec is also pioneering the study of combining breathing patterns with superimposed length oscillations (SILO). Pre-contracted healthy and acute airways treated with 5-20Hz, and a range of amplitudes have been completed. The hypothesis that TO and DI oscillations have the ability to disrupt the cross-bridge cycle within ASM cells [10-13] intimates a direct relationship between application of oscillations and subsequent perturbation of the mechanical force generated by the actinomyosin (biochemical) infrastructure of ASM cells and will be further tested by application of SILO in our research. It is also appropriate to consider that the contractile apparatus is not only perturbed, but possibly rearranged in a temporal fashion thereby reducing the generated contractile force.

It is useful to briefly review the context of how pharmacology and the mechanics of contraction and relaxation are related to each other in this research. The biochemical infrastructure of the ASM cell is intricately tied to its functions. For this reason, it is believed that the use of pharmacology in the research may assist in providing critical insights into the mechanisms of action which facilitate contraction and relaxation in response to mechanical oscillations of ASM. ASM cells contain receptors in their membranes which bind with agonists, initiating signalling cascades associated with either

relaxation or contraction [96-100]. β -2 adrenergic receptors are one of several G-protein coupled receptors responsible for key smooth muscle responses to chemical signals. These receptors are associated with different types of G-proteins which carry out intracellular signalling to the various networks that maintain cellular activities. β -2 receptors are sensitive to ISO, activating a relaxation signal pathway, and are therefore of interest in asthma therapeutic research [6, 10-13, 17, 101, 102]. Muscarinic acetylcholine receptors are also G-protein coupled receptors in ASM and respond to ACh. ACh is another key chemical used in asthma studies because it activates signal cascades which favour ASM contraction [58, 60, 96-98]. Muscarinic acetylcholine receptors in ASM are the targets of ACh treatment in asthma studies that may, for example, endeavour to measure the tissue's contractile force.

Isoproterenol is important in asthma research because it activates β -2 receptors in smooth muscle tissue. The resulting muscle relaxation is due to activation of vital biochemical signalling pathways. The primary signal from the ISO-bound receptor involves movement of the G_s protein to a membrane-bound enzyme, adenylyl cyclase. Binding of the G-protein to adenylyl cyclase activates the enzyme, resulting in increased conversion of ATP to cyclic AMP [102-104]. Cyclic AMP is a critical secondary messenger in the cell because it is ultimately responsible for ASM relaxation via signalling through pathways which inhibit phospholipase C [104]. Inhibition of this phospholipase interferes with signals that support contraction of the cell [98]. Ultimately, phospholipase C inhibition destabilises actinomyosin crossbridges (the contractile machinery) of ASM cells.

Phospholipase C is also of interest in research which utilises ACh as a means to stimulate ASM contraction. Phospholipase C activity increases cellular levels of phospholipid-

derived Inositol trisphosphate and diacylglycerol, two important signalling molecules derived from cell membranes [98]. Inositol trisphosphate binds to its receptor in the sarcoplasmic reticulum of ASM cells, releasing calcium through membrane channels into the cytoplasm. As a result, calcium binds to another prominent messenger protein, Calmodulin [102], and the complex activates an enzyme, Myosin Light Chain Kinase. This kinase phosphorylates the Myosin Light Chain within the ASM cell's contractile machinery, and the actinomyosin crossbridge cycle is engaged for contraction [98, 100-106]. Diacylglycerol participates in activation of an enzyme which inhibits Myosin Light Chain Phosphatase. (The primary role of this phosphatase is to dephosphorylate the Myosin Light Chains of actinomyosin crossbridges, and with the loss of phosphate groups from the machinery, elicits ASM relaxation.) The inhibition of Myosin Light Chain Phosphatase however counteracts relaxation by allowing for kinase phosphorylation of myosin light chains to proceed relatively unchecked, and therefore drive ASM contraction.

As mentioned, there are three main factors responsible for the narrowing of the airways during an asthmatic attack: AHR, inflammation and bronchospasms, the intermittent airway constrictions. Even though these three factors have been the focus of many studies in the past, airway smooth muscle is considered the main effector of the narrowing of the airways. Narrowing has been observed to occur either in the presence or absence of inflammation showing how important ASM is during an asthma attack [1, 107-113]. ASM has shown an exceptional capacity to shorten its initial length by 80-90% when stimulated *in vitro*. Reduction of length at this level could easily result in complete closure of the airways *in vivo* [2], but complete airways closure does not appear to occur normally in healthy subjects.

Experimental data obtained by Martin et al. and other groups [2, 3] suggested that alterations in the mass of ASM or changes in its contractile force may explain the excessive narrowing in asthma. Even though ASM is the main effector of airways narrowing, the interaction with other structures such as constituents of the airway wall and lung parenchyma could also be important. Notably, it must be considered that cyclical stress applied to ASM by physiological phenomena such as tidal breathing or deep inspiration help to maintain the airways' dilated state. Biochemical changes and alterations in the dynamic properties of ASM occurring during the development of the disease seem to increase the ASM resistance to the dilating influence of breathing and deep inspiration.

2.6. Asthma assessment techniques

In order to assess asthmatic respiratory parameters that result from the disease, several techniques are available. Evaluation of the modelled asthmatic state can thereby be achieved following the sensitization protocol. Invasive and non-invasive testing of pulmonary functionality in mice will be discussed within the context of relevant mechanical, chemical, and physiological methods. The primary pulmonary parameters which are derived from these methods will also be explained, along with their use in defining respiratory markers of bronchoconstriction, dynamic compliance and lung resistance.

2.6.1. Mechanical testing of pulmonary functions in mice

Mechanical testing of pulmonary functions in mice can be achieved by invasive and non-invasive techniques. Invasive techniques such as intubation and tracheotomy are used in anaesthetized animals to measure primary parameters of bronchoconstriction. Non-invasive plethysmography techniques also measure these parameters, but with less

accuracy. Accurate determination of primary parameters is necessary in order to ascertain the effect of the study on bronchoconstriction.

Invasive measurement of bronchoconstriction is assessed by determining two pulmonary parameters: lung resistance and dynamic compliance [119-122]. The values of R_L and C_{dyn} are calculated from measuring the primary measurements of tidal air volume (T_v), tidal flow (V), and transpulmonary pressure (P_{tp}). Measurements of T_v and V can be carried out by intubating tracheotomized mice, at the expense of one procedure per animal, or by orotracheal intubation, which can be performed multiple times [119, 120]. P_{tp} is measured by intubating to the lower third of the oesophagus (mid-thorax), and can also be performed multiple times over a relatively short time period. The method of invasive plethysmography developed by Glaab, et al. [119, 120] is presented in Fig. 2.1. An additional technique for estimating pulmonary function is through the use of low-frequency forced oscillations. This method was developed in humans and larger animals, and estimates lung impedance, offering arguably the most accurate assessment of pulmonary function [120].

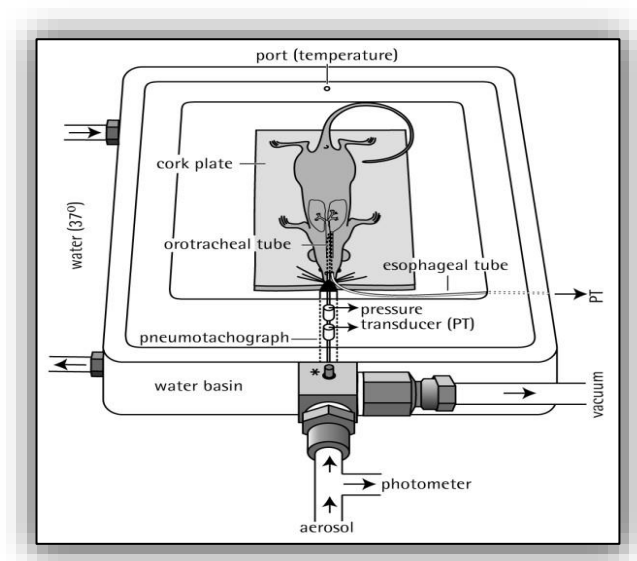


Figure 2.1. Invasive plethysmograph [120]. The unconscious animal is placed in the device; parameters for bronchoconstriction such as tidal flow, tidal volume, and respiratory rate are measured, and lung resistance and dynamic compliance are calculated.

Non-invasive partial measurements of bronchoconstriction are assessed by determining lung capacity values using plethysmographic methods. The plethysmograph detects changes in lung volumes, which are in turn used to calculate both functional residual capacity and total lung capacity. Mice are conscious during the testing, and the technique allows for long-term study of animals. The application of this technology to murine respiratory studies allows for mass screening of candidate animals prior to final tidal volume, tidal flow, respiratory rate and enhanced-pause parameter data. Values for resistance are not gained from this technique, and so care must be taken not to over-interpret the data gained from this technology.

Whole-body plethysmography and head-out body plethysmography are two methods which utilize a closed chamber and pressure fluctuations to record breathing cycle data. The former technique encloses the entire animal (Fig. 2.2), and the latter, as its name describes, maintains the animal's head outside of the measurement device. Mice are able to remain awake during the protocols, which is an advantage over the anaesthesia required for invasive techniques. Additionally, plethysmography allows for repetitive measures from the same animal. A critical distinguishing feature of plethysmography is the loss of accuracy (relative to invasive methods) in the bronchoconstriction parameters that are measured. Unfortunately, neither of the invasive or non-invasive *in vivo* technologies discussed measures the delivery of allergens to targeted tissue in the airways, but they do allow for relative comparisons of bronchoconstriction based on the allergen delivery method within their given contexts.

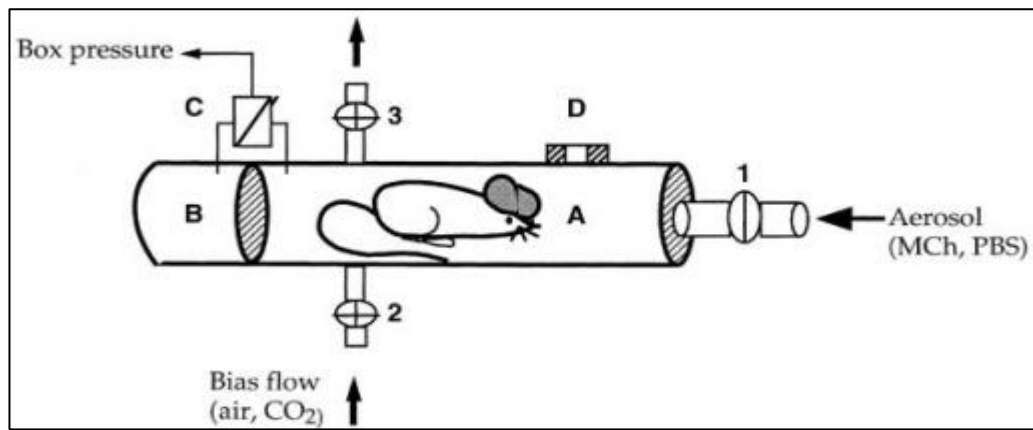


Figure 2.2. Non-invasive whole-body plethysmography [119, 120]. The conscious animal is placed in the device; parameters for bronchoconstriction such as tidal flow, tidal volume, and respiratory rate are measured. This image indicates the use of methacholine (MCh) to initiate breathing challenges; acetylcholine (ACh) is also used as a bronchoconstrictor in this regard.

Present asthma studies require careful consideration of the available technologies and their ability to garner data which best evaluates bronchoconstriction parameters of interest. Whole-body plethysmography is appropriate for screening large animal populations and long-term, multiple-use protocols which measure volumetric and flow parameters. The animals are conscious during the allergen challenge and subsequent measurements. Given that asthmatic attacks occur in conscious individuals with different frequencies over a period of time, this technology can replicate elements of interest in an asthmatic study. However, the importance of understanding airway resistance in the context of a chronic asthmatic model's bronchoconstriction is of great importance. For this reason, an invasive approach to gathering data for R_L and C_{dyn} values is required. Although less practical, the accuracy of data points and additional resistance parameters that arise from invasive procedures must be measured.

2.6.2. Pulmonary parameters required for calculations of R_L and C_{dyn}

The invasive technology and methodologies selected for this study collect data for determining values of R_L and C_{dyn} as indicators of bronchoconstriction. In order to calculate these indicators, pulmonary parameters of V , T_v , and P_{tp} are required. This

section discusses the parameters measured and calculations performed for R_L and C_{dyn} variables in order to interpret bronchoconstriction responses in a chronic asthmatic state. Details of the measurement devices which are beyond the scope of this chapter are provided in Chapter IV.

a) *Tidal air flow*

Tidal airflow is measured in mice using a pneumotachometer. Flow restriction and pressure differences are evaluated across two detector ports. The analogue signals generated from the differentials are proportional to the velocity of air and are integrated by a low pressure transducer for measurement as V in the raw data of the murine breathing cycle.

b) *Tidal volume*

Tidal volume is measured by integrating the tidal flow over a known period of breathing cycles. Figure 2.3 depicts murine breathing cycles and the classification of volumes that occur during breathing. Tidal volume is determined by the difference in the amount of air present at the completion of each inspiration and expiration in the breathing cycle and does not describe the total lung volume. Software is used in the study to monitor and record continuous values of T_v as changes in V are detected.

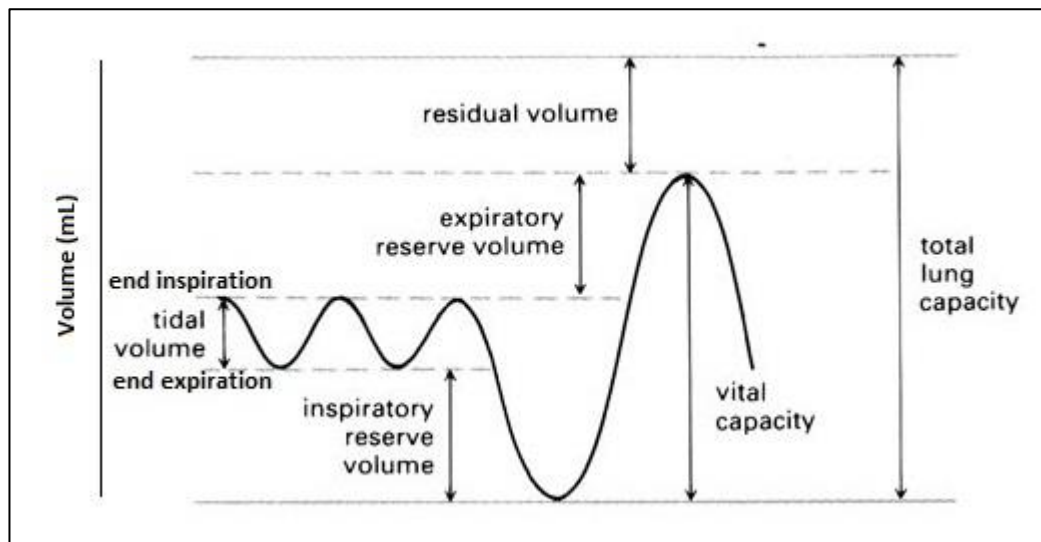


Figure 2.3. Lung volumes occurring during breathing cycles [120]. Total lung capacity is the sum of several volumetric classifications. Tidal volume is the smallest volumetric unit illustrated here and is the difference between end inspiration and end expiration volumes. Inspiratory and expiratory reserve volumes, as well as residual lung volume also add to the total lung capacity.

c) *Transpulmonary pressure*

Transpulmonary pressure is the differential measured between the pleural and alveolar pressures. P_{tp} is the positive pressure which prevents the lungs from collapsing and is difficult to acquire as a measurement. It is determined by the pressures (physically monitored at the level of the lungs) before inspiration but also at the end of expiration. Measurement of P_{tp} is accomplished by using a fluid-filled catheter that is inserted into the oesophagus of the mouse, with the terminal end of the tube positioned at the level of the mid-thorax [120]. The catheter is connected to a pressure transducer which sends data to a computer for incorporation into parametric values. The fluid in the catheter is displaced as the lungs expand and contract, causing a volumetric change which is converted by the transducer into a transpulmonary pressure reading. Critical to this method is the placement of the catheter in the oesophagus and maintaining a close proximity to the neighbouring trachea and bronchi. Slight adjustments of the catheter's placement are then able to yield maximum values of P_{tp} for use in subsequent analyses.

d) Pulmonary Resistance

Pulmonary resistance is a measurement of the respiratory system's opposition to air flow. Pleural pressure values, measured with the oesophageal catheter, are compared against the airflow measured by the pneumotachometer. In the airways, resistance is lower with a larger lumen diameter, and resistance increases with the narrowing of the airway lumen. Applied to an asthmatic model, the narrowing of the airway lumen results in larger resistance values, or a greater opposition to airflow in the lungs. Using measured parameters of T_p and Flow, the R_L (Eqn. 2.2) can be found for conditions before and after aerosol challenges of control or bronchoconstricting agents. Pulmonary flow resistance is important to assess in murine asthma studies as it indicates the effectiveness of a treatment's ability to decrease the opposition to air flow, and thereby increase the flow of air available for respiratory functions:

$$R_L = T_p / \text{Flow} \quad (\text{Eqn. 2.1})$$

Further, the overall resistance of the lungs can be addressed beyond the flow resistance within the lumen of the airway by utilizing the parameters which are affected by pressures across and within the airways.

Given that the transpulmonary pressure and remaining pressures across the trachea and inflating the lungs are in equilibrium, these relationships allow for calculation of the lung resistance based on measured parameters in the study. Use of tidal volume (TV) and flow values in collaboration with the software's calculated dynamic compliance, combine to render the resistance of the system. Presenting this relationship as pressures yields Eqn. 2.2.

$$P_{tp} = R_L * \text{Flow} + (TV/C_{dyn}) \quad (\text{Eqn. 2.2})$$

Written another way, the equation isolates R_L :

$$R_L = (P_{tp} - [TV/C_{dyn}]) / \text{Flow} \quad (\text{Eqn. 2.3})$$

e) Dynamic compliance

Dynamic compliance is calculated from specific parameters measured during respiratory cycles. In this calculation of C_{dyn} , tidal volume and transpulmonary pressure values, measured from the end of a preceding cycle to the end of a current respiratory cycle, are defined as the dividend and the divisor, respectively [14]. Computer software and programmes can then determine C_{dyn} from these two known pulmonary parameters. Dynamic compliance is interpreted physiologically as the total (elastic and airway) pulmonary resistance and is important in murine asthma studies to assess how of treatments affect the volume of air that is taken into the airways.

$$C_{dyn} = Tv / Ptp \quad (\text{Eqn. 2.2})$$

2.7. Mechanical oscillations

Different oscillations are constantly present affecting our body, some of them coming from external sources and others produced by different physiological phenomena. Among the oscillations resulting from physiological phenomena, include the oscillations generated by the breathing process which affect the thoracic box. Volume changes associated with breathing have been shown to result in changing airway diameters [4]; and thus generate length changes in the ASM [1, 5]. Length oscillations for the purpose of this project will be defined as the application of external sinusoidal length change on ASM. Several studies have shown that a control over this length change can induce “bronchoprotective response” and “bronchodilation response” in contracted airways from healthy subjects [5-8].

2.7.1. Oscillations and ASM

During breathing the lungs contract and expand, which results in changes of the airway wall diameter. Consequently the ASM in the airway is exposed to continuous length changes. Assuming that airway compliance is similar to total lung compliance, then ASM length oscillation can be derived from the cube root of the lung volume changes ($\sqrt[3]{\Delta V}$) as suggested by Hughes et al. and Fredberg et al. [4, 9]. Values have been calculated to be about 4% for normal breathing and about 25-30% for deep inspiration [13, 80]. It has been hypothesized that these oscillations have the ability to disrupt the crossbridge cycle [9]. Alternatively, temporal rearrangement of the contractile apparatus may occur, which may also result in force reduction during the contraction (relaxation).

a) Tidal oscillations

Several studies have shown that the application of TO (4% amplitude) either mechanically [9, 11, 12], or as volume oscillations in different portions of airways [13, 14] result in some form of relaxation in healthy subjects. TO is capable of reducing constriction when applied before stimulation (a bronchoprotective response), and also relaxing muscle when applied during contraction (a bronchodilation response). Also tidal oscillations have been shown to induce similar levels of relaxation in pre-contracted ASM compared to medicinal bronchodilators such as Isoproterenol [10, 13].

b) Deep Inspiration

Length oscillations that mimic DI have the ability to dilate airways [80] previously constricted by chemical stimulation [29-32]. The application of DI oscillations applied before a contraction reduces the subsequent response (contraction) of the ASM with allergen challenge [18, 21] (Fig. 2.4). These mechanisms seem to be related with

cytoskeletal reorganization [7]. However, in asthmatic subjects the beneficial effect of deep inspiration is absent [1, 92, 93]. When DI oscillations are applied in asthmatic patients, the response of their airways varies according to the severity of the asthma, resulting in an increase in constriction in severe cases of asthma and only a mild dilation in less severe cases [1, 8].

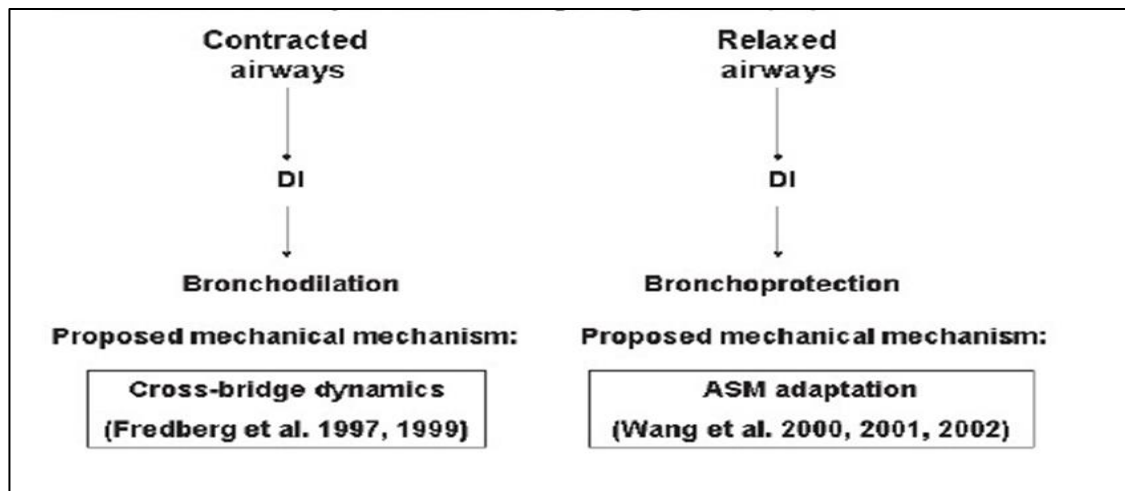


Figure 2.4. Bronchodilation and bronchoconstriction in response to deep inspiration [44]. Deep inspirations are modelled to dilate airways that have contracted, and also to prevent contraction of airways that are relaxed.

Even if DI and TO have shown utility treating pre-contracted smooth muscle *in vitro* from healthy subjects, the response of the asthmatic airways under these dynamic condition seems to be altered and ineffective [1]. However other frequencies or wave types may give better results in asthma [10, 84, 89-91].

c) Other oscillation patterns

It has been established that imposition of periodic load fluctuations on smooth muscle inhibits development of active force and stiffness [81], and that length oscillations cause long term (>30 min) reductions in isometric force when ASM is allergen challenged after the cessation of oscillations [85]. IBTec has conducted several *in vitro* tests on porcine tracheal smooth muscle, subjecting them to frequencies of 0.2-80 Hz and amplitude of 2-

8 % of reference length [11, 12]. This specific length corresponds to the length in which the smooth muscle generates the higher contraction in the presence of bronchoconstrictors, after several stretches and induced contractions [12, 80]. In this proposal, the amplitudes of oscillations are expressed as percentage of the reference length. Muscle contractile force reduction has been observed up to 40 % at frequencies above 20 Hz and amplitudes of 6 % [12, 13]. It has also been shown that the force reduction observed in ASM has a strong dependence on oscillation amplitude and a weak dependence on oscillation frequency [13].

d) Superimposed oscillations

Several groups have studied the responses of ASM in the presence of oscillations that mimic breathing and deep inspiration [1, 6, 8-10, 13, 15, 22, 23, 27, 29], but little is known yet about the effects of superimposition of length oscillations on breathing patterns. Superimposed oscillations on isolated pre-contracted healthy porcine airways with frequencies in the range of 10-30 Hz and an amplitude of 1 %, have been tested previously by our group [11], showing improvement of the relaxation observed. Additionally, a murine acute asthmatic model has tested *in vitro* and *in vivo* tissue conditions with frequencies in the range of 5-20 Hz across several amplitudes, also indicating ASM relaxation effects [13].

2.8. Pressure oscillations

In the last couple of decades, research groups focussing on airway smooth muscle and asthma have studied the mechanical properties of ASM and the effects of breathing oscillations on the tissue [5, 12, 30, 114-116]. Studies have shown that the application of oscillations mimicking physiological processes such as breathing and deep inspiration can induce relaxation in contracted airway smooth muscle [8, 10, 60, 75]. These findings

suggest that these oscillations could be acting directly on the dynamic process of the contraction and more specifically on the cross-bridge cycle [1, 8, 10, 31, 117]. However, more evidence is needed. Some issues with the existing studies regarding the effect of oscillations on ASM are:

- (1) It is assumed that the relaxation of contracted airways is due to the direct effect on the crossbridge cycle, when it could be more related to an adaptive response of the tissue [7]
- (2) Most of the studies have been carried out in isolated smooth muscle, which ignores other structures which may play a role during asthma attacks such as cartilage, parenchyma, etc.
- (3) Most of the experiments have been done in tissues obtained from healthy animals, even though it has been proven that these oscillation patterns act differently in asthmatic smooth muscle [1, 8, 75]
- (4) Most studies have focussed only on physiological oscillation patterns of deep inspiration and breathing [8, 13, 28, 62]
- (5) Not many studies have been conducted in the presence of bronchodilator medication.

2.9 Purpose of the Study

With regards to the aforementioned points, this study is the first of its kind to take into consideration the effect of non-physiological mechanically-generated pressure oscillations on long-term chronically sensitized airways. The novelty of this research is that it develops a long-term asthmatic model and combines traditional oscillations on these types of airways in combination with superimposed pressure oscillations. Use of

the combined applications gives a more realistic scenario of how these oscillations affect ASM, thereby working to reduce assumptions held in current asthmatic models.

This project is investigating the effects of a range of superimposed pressure oscillations in contracted airway smooth muscle in order to demonstrate their relaxant effects. The aims of the study are expected to be fulfilled through the following objectives:

1. Generation of a chronic asthmatic model in order to observe and compare the effects of SIPO on healthy and sensitized airways (Chapters III and IV).
2. Testing a relevant range of SIPO values on intact airways from healthy and asthmatic subjects in dynamic, spontaneously breathing, (*in vivo*) conditions (Chapters V and VI).
3. Assessing the effects of SIPO in the established chronic model alongside a previous [13] short-term asthmatic murine model (Chapt. VII).

2.10. Summary

The understanding of pressure oscillations' effects on asthmatic airways *in vivo* is important to further elucidate the dynamic response of airway smooth muscle as a means for developing new therapies for asthma. The application of oscillations (at specific frequencies and amplitudes) *in vitro* has relaxed pre-contracted smooth muscle from healthy subjects [6, 9-11, 13, 29, 32, 33]. However studies carried out on asthmatic subjects using physiological oscillations have not been as effective inducing the same relaxation as is observed in healthy airways [1, 34]. This study builds on the hypothesis that oscillations are capable of disrupting the interaction between myosin and actin during contractions similar to those occurring in contracting asthmatic airways. The effective oscillations are most likely different from those tested during healthy breathing due to remodelling and adaptation of the airways during the development of the disease [3, 19,

34-45]. Superimposed oscillations are an interesting alternative therapy because they do not completely change the breathing, rather they modulate the breathing waves. It is believed that this modulation further influences the physiological conditions which are measured as resistance and compliance in the pulmonary system. This study requires that testing needs to be carried out in an established asthmatic model (described, with sensitization results in Chapt. III). Investigations relative to breathing parameters are then carried out in the established chronic model (Chapt. IV), and results are gathered (Chapters V and VI). A comparison of the trends in the chronic asthmatic model is made with the acute asthmatic model (Chapt. VII) as a means of elucidating addition insight into the effects of SIPO treatment on asthmatic ASM.

CHAPTER III

Murine model for long-term chronic asthma

3.1. Introduction

Animal models are the basis for understanding the pathophysiology of asthma in a research setting [119]. Such models maintain the key components of asthma: linking intact immune and respiratory systems as the disease progresses. Animal models of asthma are notable for identifying elements of the allergic response as well as prospective drug targets within the response pathways. The most popular animal model for asthma research is the murine model, though other rodents such as rats and guinea pigs are also used along with rabbits, dogs and sheep. The rodent models are useful in terms of both cost effectiveness and ease of handling during treatments [124, 125].

Murine physiological characteristics are advantageous when addressing specific traits of diseases and for better understand of their pathophysiology. A good pathology model must fulfil requirements that elucidate the important concepts of the study and apply them to a wider research context. In moving from an earlier short-term asthmatic model [13] established in our lab, the long-term model of this study is designed to maintain asthmatic characteristics over (and beyond) the course of sensitization, while eliminating the long-term OVA-associated loss of asthmatic characters. This chapter will present 1) animal models and their application to respiratory studies, 2) the reasoning for animals chosen for this chronic asthma study, 3) the requirements/characteristics under study that determine the model under investigation, 4) preliminary functional evaluations of the murine respiratory system, and 5) results and summary of the asthma sensitization evaluations.

3.2. *Animal models*

The amount of work performed in animal models has created a wealth of existing data to compare studies against or base new studies on. The most popular animal models are those that use rodents, particularly inbred mice, rats and guinea-pigs. Advantages with any rodent model are found in the facts that the animals are easy to handle, and the cost is relatively low compared to other selected animals [119, 124, 125]. Mice are particularly advantageous to use in an asthmatic model for these reasons, and additionally offer short breeding cycles as a way to provide adequate animal numbers for the research to proceed at a manageable pace. The amount of existing data in mouse studies, generally, also presents a resource for pathophysiological understanding and the planning of specific asthma studies in mouse models.

The use of mice in animal models is further supported by the sheer volume of mouse-specific technologies, ranging from transgenic strains on the large scale to molecular probes on the microscopic [121, 122]. While larger-sized animal models are useful, they are costly. Sheep and dog models, for example, have been developed, but do not have the range of transgenic strains or molecular probes available to researchers. In particular, there are far fewer methods and materials available to characterize the allergic and airway responses of these larger animals compared to the resources available for murine-based asthma studies [124-128].

The technology available for animal models, and asthmatic mouse models in particular, is not without limitations. Unfortunately, the efforts to draw conclusions for humans from tests on mice have to consider important differences between the two mammals before determining the overall understanding that is gained. Anatomy is a clear point of consideration, and differences in immunology are also important in building applicable

understanding of an asthmatic model. In some cases, mouse models for asthma require more than just the allergen to stimulate immunological and allergic responses, and adjuvants, as added variables are used to accomplish this.

It is not possible for an animal model to display all features of human wellness or disease. No mouse model will perfectly mimic human asthma. For this reason, certain criteria are established as points to study in order to increase the understanding of specific features of asthma. The respiratory and immunological responses of mice in asthmatic models is of greatest interest. Indeed, research in mouse models of asthma focusses on these two areas rather than on all of the human features of asthma. Sensitization of mice to an asthmatic state by using allergens, and adjuvants if necessary, has allowed researchers to emulate and characterize immunological, inflammatory, and respiratory responses of asthma [72, 89, 121, 127, 128]. In the case of a chronic asthmatic mouse model, the overall objective is for the molecular stimuli which establish the model of asthma to be expressed physiologically and measured as airway hyper-responsiveness, quantified in terms of lung resistance and dynamic compliance.

3.3. Selection of criteria

Many criteria exist for defining an acceptable animal model of asthma. Core criteria for consideration are:

- Immunological and respiratory sensitivity mediated by IgE and/or IgG to the antigen that results in bronchoconstriction
- An increase in airway resistance
- Chronic inflammation of the airways, with an associated increase of eosinophils and cytokines

- Non-specific hyper-responsiveness
- Excessive production of mucus, supplemented by goblet-cell metaplasia and enlargement of the submucosal glands
- Airway tissue remodelling, including thickening of the collagen and smooth muscle layers [71, 129-131].

As mentioned, no single animal model provides all of these criteria. Fortunately, a variety of models have been developed in order to study the individual features of asthma.

The design of a sensitization protocol to develop an animal model has to take into account technical details such as the type of allergen, use of adjuvants and the method of administration of the allergen. Common types of allergens used are OVA and House Dust Mite as well as custom made allergen mixes. OVA is the most popular antigen as it is readily available and the animal can be easily prevented from any prior exposure through the environment [124, 125]. Adjuvant such as Alum, heat killed *bordetella pertussis* and ricin are used to improve the immunological response against the allergen. Among the adjuvants alum is most commonly used as it promotes and improves the response against the allergen, but has the inconvenience of inducing an immunologic response by itself [132]. The allergen can be administrated by different methods, among them are intraperitoneal (i.p.) injection; subcutaneous injection and aerosolization. The choice of protocol of sensitization will depend on the features of asthma that need to be present in the model.

3.4. Asthmatic models

Asthmatic models are referred to as either acute or chronic in an effort to represent and replicate features of acute or chronic human asthma. In animal models the terms are also indicative of the duration of allergen exposure (sensitization) and the maintenance of the disease state after sensitization has ended. Acute asthma in a murine model has multiple interpretations which can also overlap with chronic models' insights. While acute characteristics are interpreted as being less advanced physiologically and immunologically than chronic asthma characteristics, acute subjects still present (milder) asthmatic consequences of lung resistance and dynamic compliance that are also associated with longer exposures to allergens. Indeed, since the allergen exposure is for shorter durations in acute models, an acute model can even be described as a (short-exposure) chronic asthmatic state. Throughout the discussions of this work, any reference to acute models of asthma are deemed equivalent to also being a short-term chronic model.

3.4.1. Chronic model

The long-term chronic asthma model in this study is established in mice by using a 12-week protocol. Where short-term asthma protocols sensitize mice for 3-6 weeks, a chronic asthma model protocol typically requires 2-3 months [124-131, 134-137].

The desired symptoms of chronic asthma obtained from Goplen's protocol [135] are:

- Airway tissue hypertrophy and hyperplasia
- Inflammatory response, with increased eosinophils, mast cells, and molecular markers, and
- Airway hyper-responsiveness [135].

Despite the generation of desired symptoms for study, there are still disadvantages associated with chronic asthma models. In particular, there are differences in the inflammatory physiology between mice and human respiratory systems. Additionally, the maintenance of chronic characteristics in mice is not well known. The lesions which develop due to allergen exposure, and overall airway tissue remodelling are not well-known subjects. There is also uncertainty regarding how long the timeline of AHR remains after the final sensitization and associated rest period.

The chronic asthma model of this study is based on other long term protocols where the duration of the sensitization is more than 2 months [124-131, 134-137]. The features of asthma obtained from these protocols are:

- Allergic inflammation characterised by eosinophilic influx into the airway mucosa [138-143] and
- AHR [138-143].

In addition, some chronic asthmatic models present:

- Airway remodelling with goblet cell hyperplasia, epithelial hypertrophy, and either subepithelial or peribronchiolar fibrosis [133, 135, 138, 144].

Chronic asthma models are designed to ensure that key characteristics of asthma are maintained for longer periods of time after the final allergen challenge [135, 145, 146]. Long-term sensitization protocols are also instituted to support the persistence of AHR and respiratory system inflammation, which vary depending on the protocols utilized for asthma sensitization [130, 131]. Acute asthma models have shown that long-term allergen sensitization may result in some degree of tolerance [135], but this remains undefined in chronic models to date.

A key reason for the importance of the chronic model presented in this study is to introduce a different (more severe) asthmatic state to the therapeutic tests involving applied pressure oscillations. Previous IBTec studies in an acute model have yielded interesting results for the therapies tested [13]. It is therefore of great value to identify similarities and differences between acute and chronic asthmatic states that receive similar therapies of applied pressure oscillations. There are potential limitations in only assessing IBTec's initial results of applied therapies to short-exposure chronic asthma. Progression through the disease state, and physiological as well as inflammatory response changes, associated with long-exposure chronic asthma, also require pulmonary assessments rather than estimated outcomes which result from a solitary asthmatic state's generalizations.

3.5. Sensitization for a chronic asthmatic mouse model

Sensitization protocols for establishing a chronic asthmatic state require longer time periods than those protocols used with acute asthma models. A longer protocol has been associated with maintaining key features of asthma after the completion of the sensitization [124, 125, 131]. In addition to a longer protocol, the chronic model allergens are used without an adjuvant. This serves two purposes: utilizing common allergens that are associated with asthma, and elimination of the adjuvant from consideration as a cause of the sensitized state. Two stages of allergen exposure are used during sensitization for the chronic state of this study's model, the first is an i.p. injection and the second is inhalation of the nebulised allergen, based on the model presented by Goplen et al. [135].

The Balb/c strain of inbred mice was chosen for this study, as it is reactive to allergens, and demonstrates airway hyperresponsiveness in preference to other strains [150-153].

Balb/c mice aged from 8-16 weeks are used in the study, with females noted as being more reactive to allergen exposure than males [156, 157].

3.5.1. Experimental groups

Two groups of mice were used in this study. The control (healthy) group and the sensitized (chronic) group were prepared for pulmonary parameter assessments.

a) Control (Healthy) Group

The Control (Healthy) Group received only 0.9 % Saline solution during the sensitization protocol. As with the Sensitized (Chronic) Group, the healthy group was under observation for general weight, behaviour, and health status. The healthy group received injections and nebulizations of 0.9 % Saline solution, free from the allergen mix. Table 3.1 presents the details for the protocol illustrated in Fig. 3.1.

Table 3.1: Details of sensitization protocol for control group.

Protocol details	
Mice	BALB/c; Female; 8-16 Weeks old
Allergen	None
Solvent	0.9 % Saline
Anaesthetic	Ketamine (40 µg) and Xylazine (10 µg)/g weight
Challenge	ACh (10 ⁻⁴ M)
Via of Administration	Intraperitoneal (i.p.) and Inhalation (Inh)
Sensitization (Fig. 3.5)	<p>Week</p> <p>1 Day 1&2, i.p. injection of saline, weight and health checks</p> <p>2 Day 1&2, nebulized saline, general weight and health checks</p> <p>3 Day 1&2, nebulized saline, general weight and health checks</p> <p>4 Day 1&2, nebulized saline, general weight and health checks</p> <p>5 Day 1&2, nebulized saline, general weight and health checks</p> <p>6 Day 1&2, nebulized saline, general weight and health checks</p> <p>7 Day 1&2, nebulized saline, general weight and health checks</p> <p>8 Day 1&2, nebulized saline, general weight and health checks</p> <p>9-12 Rest period following control sensitization</p> <p>13-16 Experimental protocols</p>

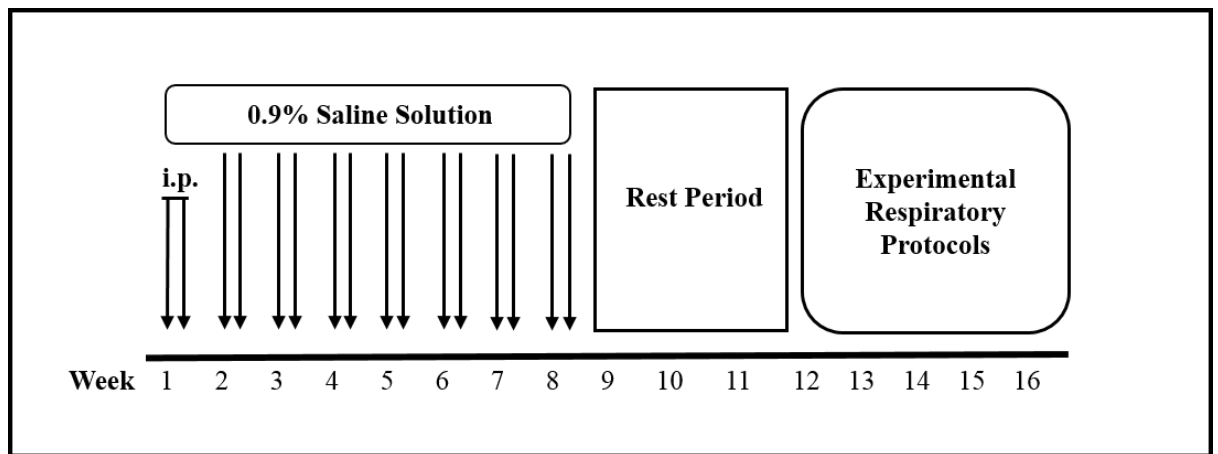


Figure 3.1: Control protocol for healthy mice. Days 1 and 2 of week 1 introduce 0.9 % saline solution via i.p. injection, and all other days introduce nebulized saline. General weight, behavior, and health of the mice was checked on the days of protocol control sensitizations as well as on days without manipulations.

b) *Chronic asthmatic model*

This model is a long-term sensitization protocol, requiring eight weeks of sensitization prior to three weeks of rest and then initiation of experiments. A mixture of three allergens, obtained from Greer Labs (Lenoir, NC, USA), was prepared in 0.9 % saline solution in order to sensitize the subjects: Dust mite (*D. farinae*, 0.3 $\mu\text{g}/\mu\text{l}$), Ragweed pollen (*A. artimissifolia*, 3.3 $\mu\text{g}/\mu\text{l}$), and Aspergillus mold (*A. fumigatus*, 0.3 $\mu\text{g}/\mu\text{l}$). The allergen mix was administered via intraperitoneal injection on the first two days of sensitization, followed by nebulisation for the remaining time points of the protocol. The objective of the chronic model was to observe the long-term response of ASM to the allergen mix, as measured primarily by lung resistance and dynamic compliance, but also with an evaluation of inflammatory and immune response markers. Table 3.2 presents the details for the sensitization protocol illustrated in Fig. 3.2.

Table 3.2: Details of sensitization protocol for asthmatic group.

Protocol details	
Mice	BALB/c; Female; 8-16 Weeks old
Allergen	DRA mix (Dust mite, Ragweed, Aspergillus)
Solvent	0.9 % Saline solution
Anesthetic	Ketamine (40 µg) and Xylazine (10 µg)/g weight
Challenge	ACh (10 ⁻⁴ M)
Via of Administration	Intraperitoneal (i.p.) and Inhalation (inh.)
Sensitization (Fig. 3.6)	<p>Week</p> <p>1 Day 1&2, i.p. injection of DRA mix, weight and health checks</p> <p>2 Day 1&2, nebulized DRA mix, general weight and health checks</p> <p>3 Day 1&2, nebulized DRA mix, general weight and health checks</p> <p>4 Day 1&2, nebulized DRA mix, general weight and health checks</p> <p>5 Day 1&2, nebulized DRA mix, general weight and health checks</p> <p>6 Day 1&2, nebulized DRA mix, general weight and health checks</p> <p>7 Day 1&2, nebulized DRA mix, general weight and health checks</p> <p>8 Day 1&2, nebulized DRA mix, general weight and health checks</p> <p>9-12 Rest period following DRA mix sensitization</p> <p>13-16 Experimental protocols begin</p>

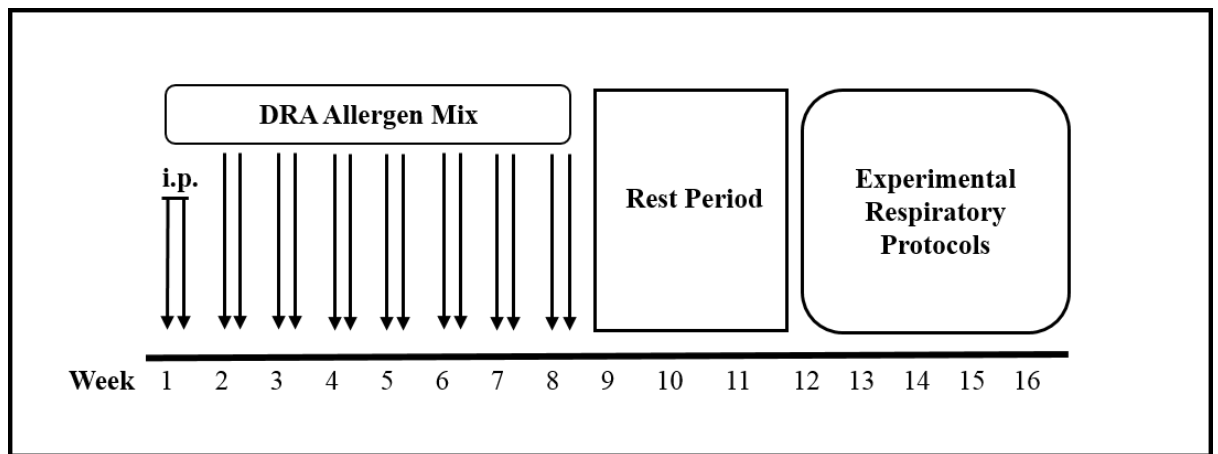


Figure 3.2. Sensitization protocol for chronic asthmatic mice. Days 1 and 2 of week 1 introduce the DRA allergen mix in 0.9% saline solution via i.p. injection, and all other days introduce nebulized DRA allergen mix. General weight, behavior, and health of the mice was checked on the days of protocol chronic sensitizations as well as on days without manipulations.

3.6. Selected techniques to evaluate the model

The chronic asthmatic model will be evaluated for successful sensitization using multiple techniques. Airway hyperresponsiveness (bronchoconstriction) will be determined by testing lung resistance, R_L , and dynamic compliance, C_{dyn} , using IBTEC's plethysmography equipment. A device under development by IBTEC, which delivers oscillations to live spontaneously breathing mice, will be used in coordination with the plethysmography set-up. Respiratory tidal flow volumes and pulmonary pressure data generated in the experiments will be sent directly to a National Instruments LabVIEW program (NI-DAQ7/LabVIEW6) which was developed for this purpose. Data analysis of the respiratory parameters tested will be used to confirm the chronic sensitization. ELISA measurement of total IgE levels, and bronchoalveolar lavage to assess changes in airway white cell presence, are used as additional confirmation of the chronic state. Combining both mechanical and chemical detection parameters will provide conclusions to assess the sensitization achieved by the protocol.

3.6.1. Airway hyper-responsiveness/ pneumotachography

Evaluation of AHR is carried out by measuring the induced bronchoconstriction in both control and sensitized animals. Anaesthetized, tracheotomized mice are placed on a thermoregulated blanket, and tracheal and oesophageal cannulas are inserted into upper respiratory and digestive tracts. Fig. 3.5 is a scheme of AHR measurement devices used to induce and measure bronchoconstriction (see Chapt. IV), as well as an indication of the devices' placements in relation to the test animal's physiology.

Lung resistance and dynamic compliance are considered to be the most significant ways to evaluate bronchoconstriction in murine airway models of this type. Through the use of this technique we expect to evaluate AHR in both healthy and asthmatic mice by collecting the flow and pressure data detected by the cannulas. AHR is determined by performing an invasive protocol to calculate pulmonary resistance and dynamic compliance from upper pulmonary regions (see Section 2.6) in anaesthetized, spontaneously breathing mice. Resistance and compliance are measured following a challenge of nebulized (aerosolized) ACh. All AHR protocols were approved by the University of Auckland Code of Ethical Conduct (AEC) (Appendix A), and performed in accordance with the Animal Welfare Act 1999.

Mice are anaesthetized with i.p. injections of ketamine (40 µg/g) and xylazine (10 µg/g). If required during the protocol, additional anaesthetic is provided to ensure minimal discomfort to the animal. Anaesthesia is achieved by assessment of the loss of a righting reflex, as well as the loss of the pinch toe reflex. Mice are then placed in a supine position on a prepared surface for tracheotomy and clearance of surrounding tissue, preparatory for the insertion of the tracheal cannula (Fig. 3.3, protocol detailed in Chapt. IV).

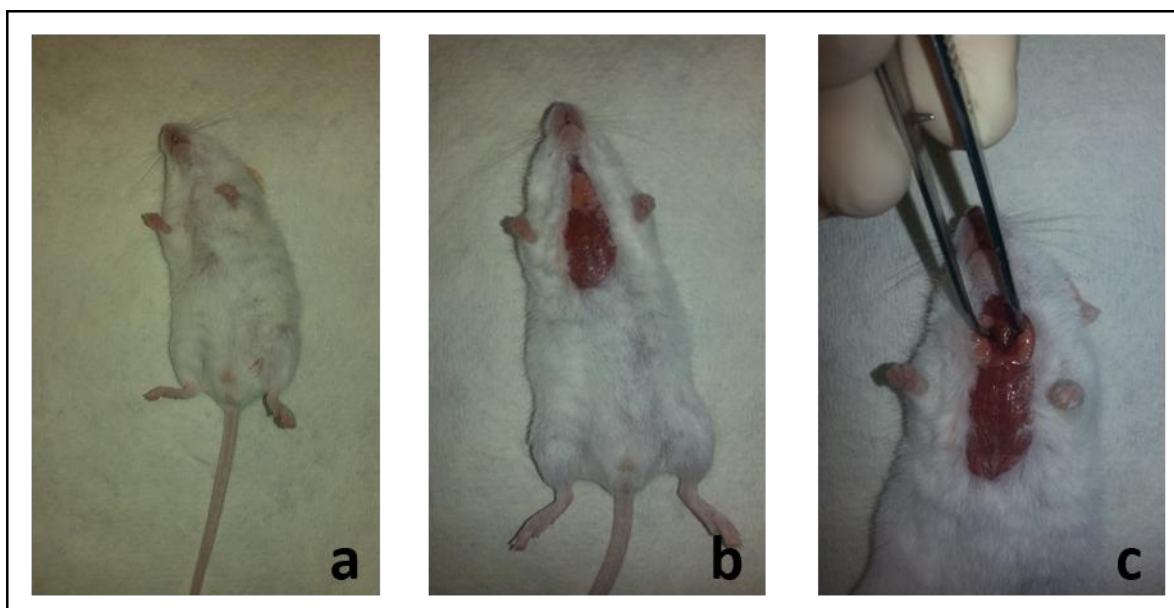


Figure 3.3. Positioning of mouse for tracheotomy and insertion of tracheal cannula. Following anaesthesia, the subject is placed in a supine position (a) and tissues are cleared from the airway (b, c) preparatory to tracheotomy and placement of the tracheal cannula.

The trachea is perforated with a small surgical cut to create a hole between adjacent tracheal rings, approximately 3 or 4 rings below the larynx. The cannula is placed within the lumen of the trachea towards the bronchi and secured with silk thread (Fig. 3.4(a)). The mouse is placed on a thermoregulated (37°C) blanket, and the tracheal cannula, connected directly to a pneumotachograph, is in turn connected to a differential pressure transducer. The tidal flow is measured in this way.

Transpulmonary pressure is measured by inserting a water-filled tube through the mouth of the mouse and down the oesophagus to the level of the mid thorax (Fig. 3.4(b)). This oesophageal tube is coupled to a pressure transducer, which generates analogue signals. The signals are digitalized and used in the assessment of respiratory parameters.

Doses of 0.9 % (normal) saline, or specific concentrations of ACh (as the bronchoconstrictor) or Isoproterenol (ISO; the bronchodilator) are administered to the mouse through the system's nebulizer, which aerosolizes the solutions and carries the

aerosol to the spontaneously breathing mouse via a tube which terminates at the pneumotachometer. Five (5) ml of test solution is placed in the nebulizer tank for use at appropriate times in the protocols (Fig. 3.5).

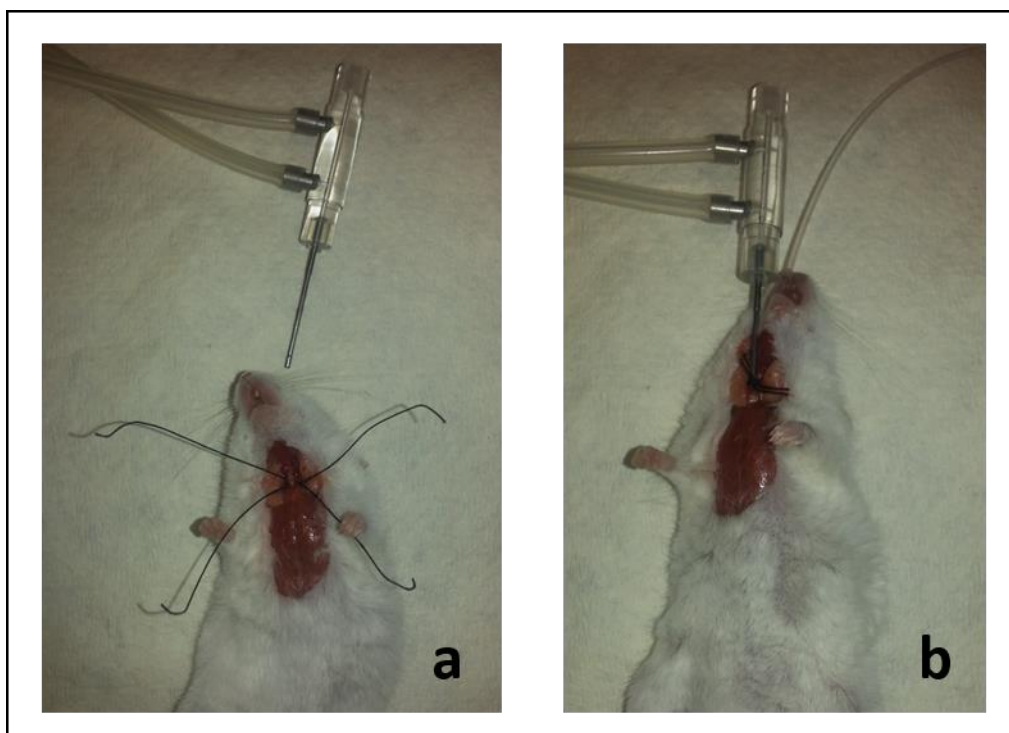


Figure 3.4. Insertions of the tracheal cannula and oesophageal catheter. Following anaesthesia and tissue clearance from the airway, silk threads are placed (a) to secure the tracheal cannula within the trachea (b). The oesophageal catheter is also positioned within the oesophagus (b).

Dose-response testing of ACh (10^{-6} to 10^{-2} M) and ISO (10^{-8} to 10^{-3} M) was carried out in order to determine optimal doses for use in testing of control and chronic mice. Pulmonary parameters were recorded during the entire protocol. Nebulization of normal saline solution for 2 min was followed by 1-min rest. ACh nebulization for 1 min was followed by a 1-min rest. A normal saline challenge for 2 min was followed by a 2-min rest. ACh 10^{-4} M was determined to be the optimal dose for the protocol, and ISO optimization was then carried out.

ISO optimization used the same protocol for ACh dose-response determination, with the addition of an ISO step prior to the final normal saline nebulization step described above. Pulmonary parameters were recorded during the entire protocol. Nebulization of normal saline solution for 2 min was followed by a 1-min rest. ACh (10^{-4} M) nebulization for 1 min was followed by a 1-min rest. ISO nebulization for 1 min was followed by a 2-min rest. A normal saline challenge for 2 min was followed by a 2-min rest before beginning the next ISO test. ISO 10^{-6} M was determined to be the optimal dose for the protocol.

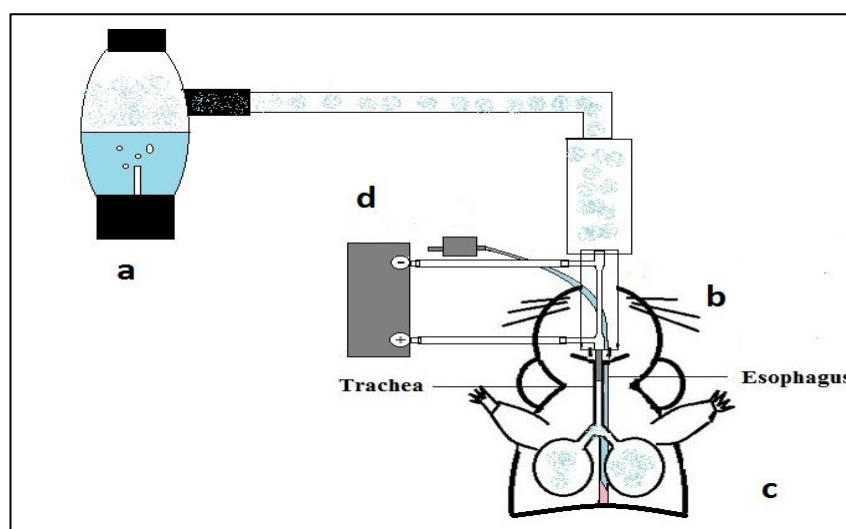


Figure 3.5. Representation of system carrying aerosol drug from nebulizer to mouse. a) Nebulizer with its solution chamber for nebulization of drugs (normal saline, ACh, ISO); b) pneumotachograph and pressure differential ports; c) mouse; d) pressure transducer receiving input from pneumotachograph.

3.6.2. *Physiochemical evaluations*

Mechanical assessments of pulmonary functions are also supported by physiochemical evaluations of the airways. In establishing an asthmatic model, the sensitization of the mice, and their airway hyper-responsiveness, can be further evaluated using physiochemical techniques for immune response, cellular number changes, and immune-specific cell population changes. Enzyme-Linked Immunosorbent Assays (ELISAs) are used to measure levels of immunoglobulins in serum samples drawn from control and

sensitized animals. Bronchoalveolar lavage (BAL) samples are used to qualify the change in amounts of cells found in the airways, particularly white cells, as a means of evaluating sensitization in the asthmatic model [140].

a) *Total IgE determination*

ELISAs are performed as a common biochemical technique to determine levels of antibodies present in collected fluids [147-153]. In asthmatic individuals, higher levels of IgE and IgG are commonly observed [125, 126, 131, 135]. As mentioned, in asthmatic models the levels of IgE and IgG antibodies are increased, reflecting an increased immune response associated with the disease. In order to support establishment of an asthmatic model, the levels of total IgE antibodies were tested using a direct sandwich Enzyme Linked Immunosorbent Assay (ELISA) method. Sera from sensitized samples was diluted 100-fold for measurement within the standard curve. Total IgE levels were determined in duplicate.

Following the experimental protocols, blood samples were taken from healthy and sensitized subjects via cardiac punctures. Coagulation and centrifugation steps were carried out to prepare serum. Samples were stored at -80°C. IgE levels of control and sensitized sera were quantified using total IgE ELISA from Labtech (division of md biosciences) and evaluated. Sera from sensitized samples was diluted 100-fold in order to measure within the range of the standard curve.

b) *Presence of white cells*

Bronchoalveolar lavage (BAL) is performed to obtain a sample of terminal airway (alveolar) cells. A small volume of physiologically buffered (normal saline) fluid is injected into the lungs and withdrawn for analysis of cell counts and cytology.

Comparative analysis of total numbers of cells as well as specific cellular types is useful for characterization of immunologic and inflammatory states at the alveolar level [154, 155]. Particular attention is paid to the presence of atypical cellularity (significant increases in white cells for example), indicating a pathological state in the airways. In order to account for the small respiratory system volume of mice, a 1-ml syringe is used for the infusion steps. Multiple, consecutive lavage steps are carried out in order to isolate samples of white cells. Collected cells are counted in a hemacytometer, or Neubauer chamber.

Lungs are cannulated in situ and washed with 1 ml of normal saline (NaCl 0.9 %) several times before collecting a representative sample of the airways. The solution collected from the lungs is placed into a cell chamber and observed at 40X for the presence of white blood cells. Quantitative white cell presence was catalogued and categorized as percentages of the total cell counts taken.

3.7. Assessment of long-exposure chronic asthma sensitization

Assessment of the long-exposure sensitization protocol is presented in this section. Results from chemical and physiological tests are provided as evidence of the model's effectiveness to elicit immune and airway hyperresponsiveness. Dose responses of healthy and sensitized subjects to ACh and ISO also determine the best concentrations for induction and treatment of bronchoconstriction as baseline values in the study. Indicators of bronchoconstriction are interpreted in support of an established long-exposure chronic asthma model for use in the testing of therapeutic applied pressure oscillations.

3.7.1. Lung resistance indicates chronic bronchoconstriction

Lung resistance was measured as a response to ACh concentrations to determine the extent of bronchoconstriction achieved by the model's protocol. Selection of a single concentration (10^{-4} M) for all subsequent administrations to healthy and sensitized subjects was made from the tested range (Fig. 3.6).

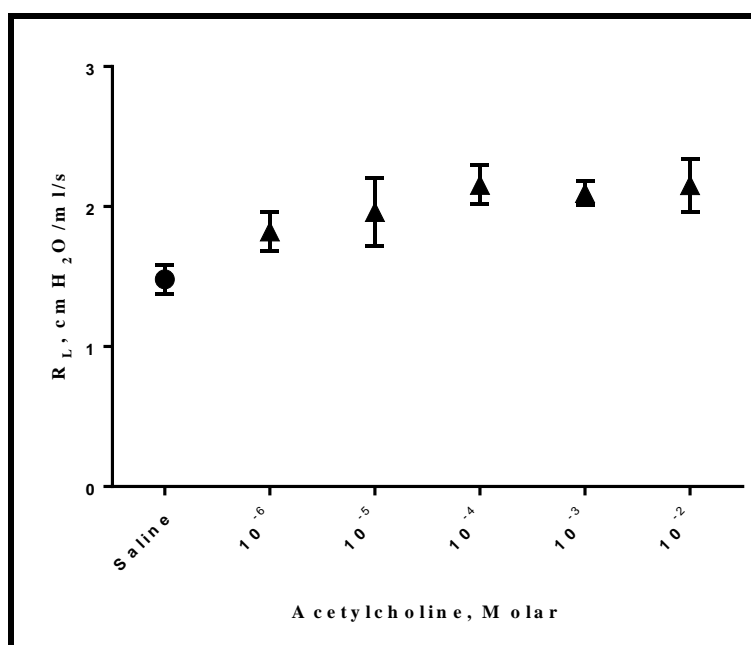


Figure 3.6. Lung resistance in response to aerosolised ACh. Increasing doses of ACh from 10^{-6} to 10^{-2} M were administered, and lung resistance was measured in order to determine the optimal dose for the experimental protocols. ACh 10^{-4} M was selected as the lowest concentration with greatest resistance in sensitized mice. (●, Saline; ▲, ACh; n=5.)

Lung resistance was also measured as a response to ISO concentrations to determine the extent of bronchorelaxation achieved by the model's protocol. Following treatment with 10^{-4} M ACh, selection of a single ISO concentration (10^{-6} M) for all subsequent administrations to healthy and sensitized subjects was made from the tested range (Fig. 3.7).

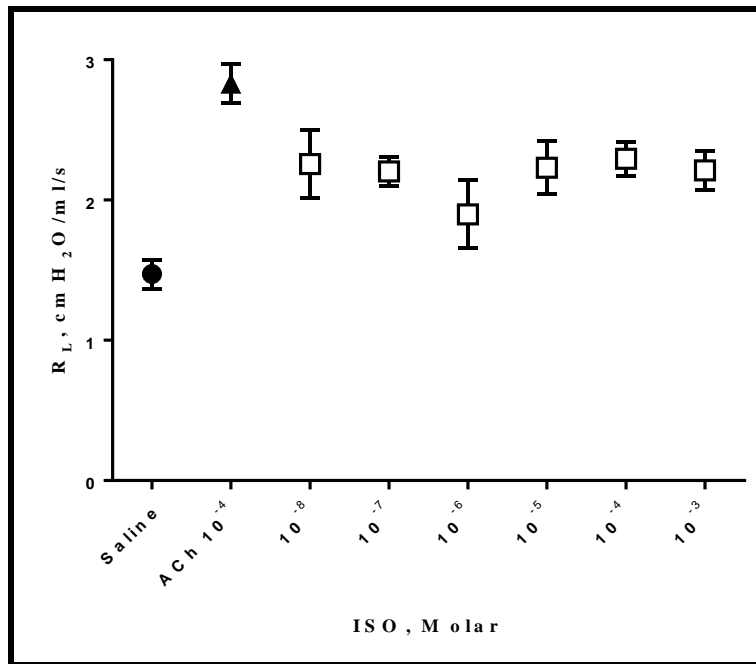


Figure 3.7. Lung resistance in response to aerosolised ISO following treatment with ACh (10^{-4} M). Increasing doses of ISO from 10^{-8} to 10^{-3} M were administered, and lung resistance was measured in order to determine the optimal dose for the experimental protocols. ISO 10^{-6} M was selected as the lowest concentration of bronchorelaxant with greatest reduction in ACh-mediated resistance in sensitized mice. (●, Saline; ▲, ACh; □, ISO concentrations; n=5.)

3.7.2. Total IgE and chronic immunoresponse

The standard curve for the ELISA assessment of IgE consists of values from 13 ng/ml to 2000 ng/ml (Fig. 3.8). Optical density (OD) values for healthy and sensitized samples were converted to ng/ml based on the equation of the standard curve. The healthy OD = 0.173 gives a total IgE of 87.9 ng/ml, and (100-fold dilution) sensitized OD = 0.254 is equivalent to total IgE of 18.7 μ g/ml.

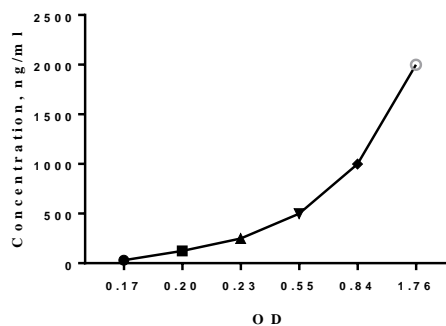


Figure 3.8. Standard curve for total IgE. Concentrations of IgE from 13ng/ml – 2000 ng/ml were measured for OD and graphed for use in determining levels of IgE in healthy and sensitized mice. The linear equation for concentration as a function of OD is $y = 1222.9x - 124.4$, where y is the concentration of IgE in the sample, and x is the average OD of the given sample.

3.7.3. White cell presence and chronic cellularity

BAL analysis of long-term sensitized mice indicated a greater white cell presence in the lavage when compared to healthy mice. Healthy mice not only had fewer total cells present in the lavage samples, but also a lower representation of white cells. Sensitized mice BAL samples contained ~7 times the number of cells as healthy mice, and of the cells counted, 21.8% were WBC. Healthy mice BAL samples contained 5.1% WBC. The marked difference in cellularity, and specifically, the increase in white cell presence from long-term sensitized mice, is indicative of a chronic state compared to healthy mice in this study.

3.8. Summary

The first objective of this study (establishment of a chronic asthmatic model) using long-term DRA sensitization was achieved. Comparisons of asthmatic characteristics between healthy and sensitized subjects indicate markedly different responses to common stimuli. For sensitized subjects, increased AHR was demonstrated in response to ACh, and a reduced response to ISO was also observed. IgE levels were higher in the sensitized group of subjects compared to levels in the control group. Finally, BAL revealed that changes in cellularity occurred due to the sensitization, with higher white cell counts present in sensitized mice. Taken together, the assessments of these asthmatic characteristics leads to the conclusion that a chronic model was established for use in the study of pulmonary responses to applied pressure oscillations.

CHAPTER IV

Experimental investigation of the asthmatic model

4.1. Introduction

Previous acute asthmatic modelling has provided some information about ASM behaviour in both *in vivo* and *in vitro* scenarios. Due to the uncertain effects of chronic sensitization conditions on the mice in this research, the primary objective is to determine the *in vivo* response of asthmatic airways to applied pressure oscillations. The purpose then of this chapter is to describe the methodology for the *in vivo* work carried out. The chapter covers the selected methods of research, the parameters by which pulmonary function is assessed, and the logistics of the *in vivo* setup. The calibration of the oscillation device is also presented, along with a brief explanation of its use.

Several areas of research are able to benefit from the chronic asthmatic model in mice. The potential for biomedical, pharmacological, and toxicology applications of the research are available from determining the respiratory function of laboratory mice *in vivo*. The preference for mice in this type of modelling has been discussed in detail earlier (Chapters I-III). However, in summary, the established characterisations of the murine immune system and physiology relative to allergic airway disease are a strong context for conducting this research. The availability of desired inbred strains, short breeding periods, and relatively low maintenance costs are also positives.

Measurement of murine respiratory parameters for pulmonary function is demanding. The airways of mice are small and introducing a phenotypic condition which further restricts breathing functions introduces unknown challenges. Several techniques are available to measure murine lung function. Both invasive and non-invasive lung function

techniques are able to characterise the established experimental model's phenotype of chronic asthma. Determining the techniques for this project is a matter of finding the balance between invasive/non-invasive and convenient/inconvenient measurements which provide accurate, consistent data which is reproducible and physiologically applicable.

4.2. Experimental layout

Invasive and non-invasive pulmonary function techniques are used to assess *in vivo* experiments. There are both advantages and disadvantages to each category, and at times the techniques are combined for heightened accuracy in the results. This section summarizes and discusses the *in vivo* protocols selected for our experiments.

An invasive methodology was determined for this study. In order to control the data collection following the preceding manipulations of the chronic model, invasive protocols were determined to offer more reliable results over the putative results that would be gained from non-invasive techniques. The invasive protocols utilise tracheal intubation and oesophageal cannulation. This plethysmographic technique provides key measurements of respiratory parameters. Tidal volume and transpulmonary pressure, along with Peak Inspiratory Pressure (PIP) and Positive End-Expiratory Pressure (PEEP) are associated with the dynamic elasticity of the airways, and are used for the determination of C_{dyn} . Tracheal pressure and flow are associated with resistance of the airways and are used to calculate R_L . R_L and C_{dyn} are the specific parameters used in this study to evaluate bronchoconstriction and relaxation during the protocols.

The experimental layout was designed in order to allow for measurement of parameters which generate R_L and C_{dyn} values. The experimental layout (Fig. 4.1) consists of a

thermo-regulated blanket for animal positioning, and the associated measuring components of pressure transducers and amplifiers. Auxiliary systems for the measuring components are the aerosol device (a Jet Nebulizer for allergen and drug delivery) and data acquisition system (a combination of Powerlab hardware components and Labchart software). The elements of the experimental layout are explained in detail in the following sections.

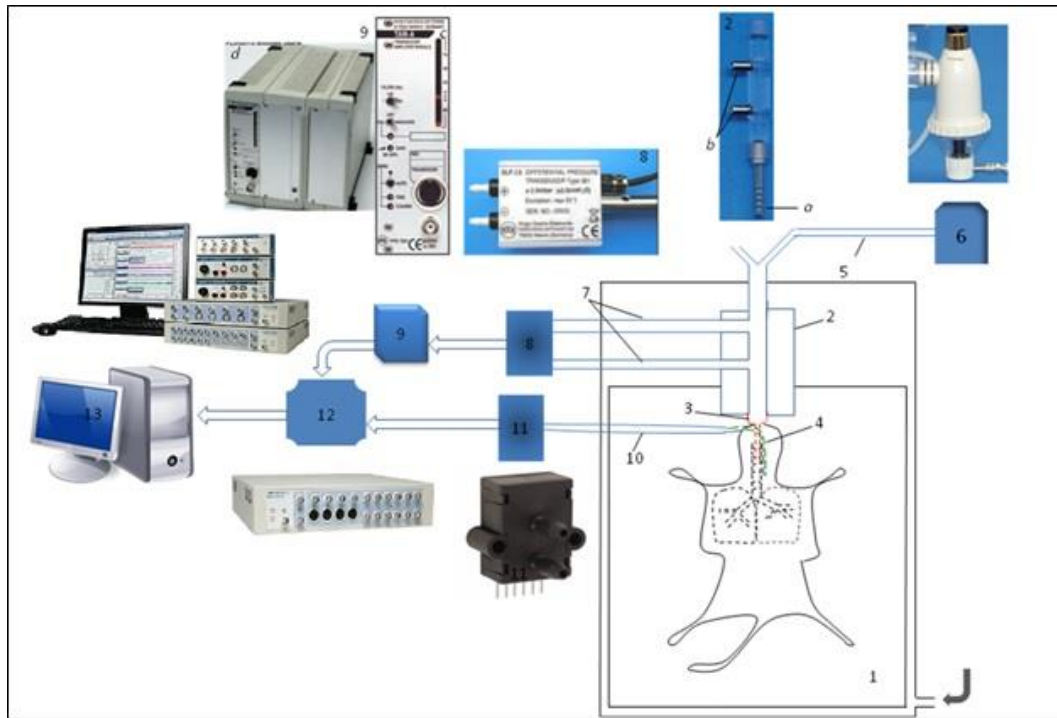


Figure 4.1. The experimental layout for respiratory parameter protocols in this study. Components and auxiliary system combinations are labelled as follows: 1) Data collection surface (with warming blanket) for animal placement during protocols; 2) Pneumotachometer; 3) Tracheal cannula; 4) Oesophageal catheter; 5) Tube supplying the nebulised solutions; 6) Nebulizer; 7) Connection tubes from pneumotachometer to transducer; 8) Differential low pressure transducer, DLP; 9) TAM-A transducer amplifier module (c) and PLUGSYS Minicase (d); 10) Connection pipe from catheter to transducer; 11) Honeywell pressure transducer; 12) 16-channel data acquisition board (Powerlab component); 13) Computer with data acquisition (Labchart software).

4.3. Animal positioning

This section details the elements of the set-up required for positioning the animal during data collection.

4.3.1 Data collection surface

The mice in this study are positioned on a rectangular Styrofoam pad (Fig. 4.2(a)) which fulfils important requirements in order to facilitate data collection. The pad is large enough to accommodate different sizes of animals from mice to rats, though in this study mice were the animal of choice. Additionally, the pad provides a surface for the thermo-regulating blanket (Fig. 4.2(b)) to be placed below the animal being studied. Finally, the pad provides an accessible space where the measurement components are not impeded from easily connecting to the experimental animal.

4.3.2 Thermo-regulated blanket

The thermo-regulated blanket is composed of the warming pad and a temperature sensor probe (Fig. 4.2(c)). The pad is directly beneath the test subject, and is connected to the temperature control unit (Fig. 4.2(d)), allowing it to be heated to a range of physiologically relevant temperatures. The temperature settings are maintained as the sensor probe monitors the mat temperature and adjusts the output temperature accordingly. For the purposes of this study, the blanket was assigned a temperature of 37°C in order to maintain a physiologically relevant temperature for the animal subjects.

4.4. Measurement components

The different measurement components of the experimental setup are used to determine T_v , Flow, T_p , and P_{tp} . PIP values are also determined by the software, based on component measurements. These individual respiratory parameters are then used to calculate R_L and C_{dyn} as defined by equations 2.1 and 2.2. The experimental elements used to obtain these parameters are: a) the pneumotachometer and tracheal cannula; b)

the oesophageal cannula; and c) two differential pressure transducers (each associated with the tracheal and oesophageal cannula respectively). The pneumotachometer and

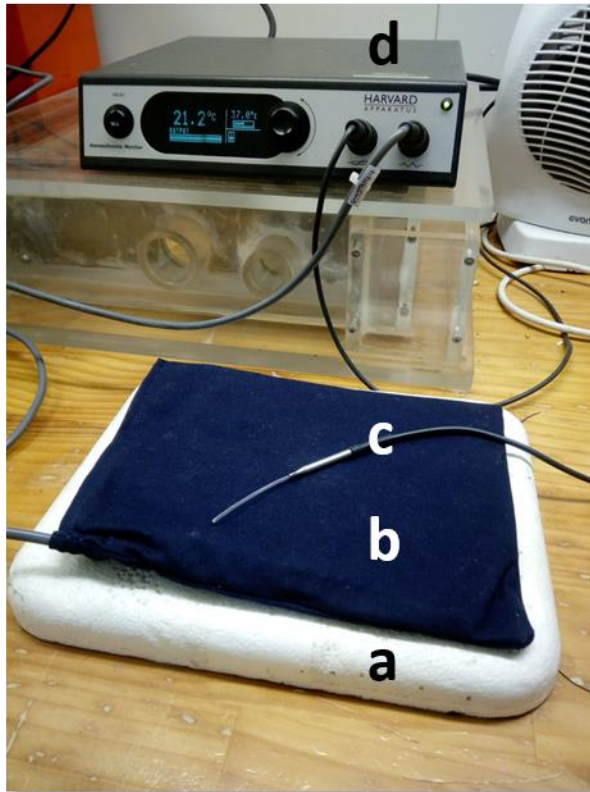


Figure 4.2. Data collection surface and thermo-regulated blanket. The data collection surface (a) is insulated from the bench below. The thermo-regulated blanket (b) lies beneath the test subject. The temperature sensor probe (c) is placed between the blanket and the test subject. Both the blanket and probe are connected to the temperature control unit (d) in order to maintain a constant temperature of 37°C.

tracheal cannula are used for measurements of T_p , PIP, V, and T_v . The oesophageal cannula is used for measurements of P_{tp} . As mentioned, T_v , PIP, and P_{tp} measurements are associated with the dynamic elasticity of the airways, and are used for the determination of C_{dyn} . Tracheal pressure and flow are associated with resistance of the airways and are used to calculate R_L .

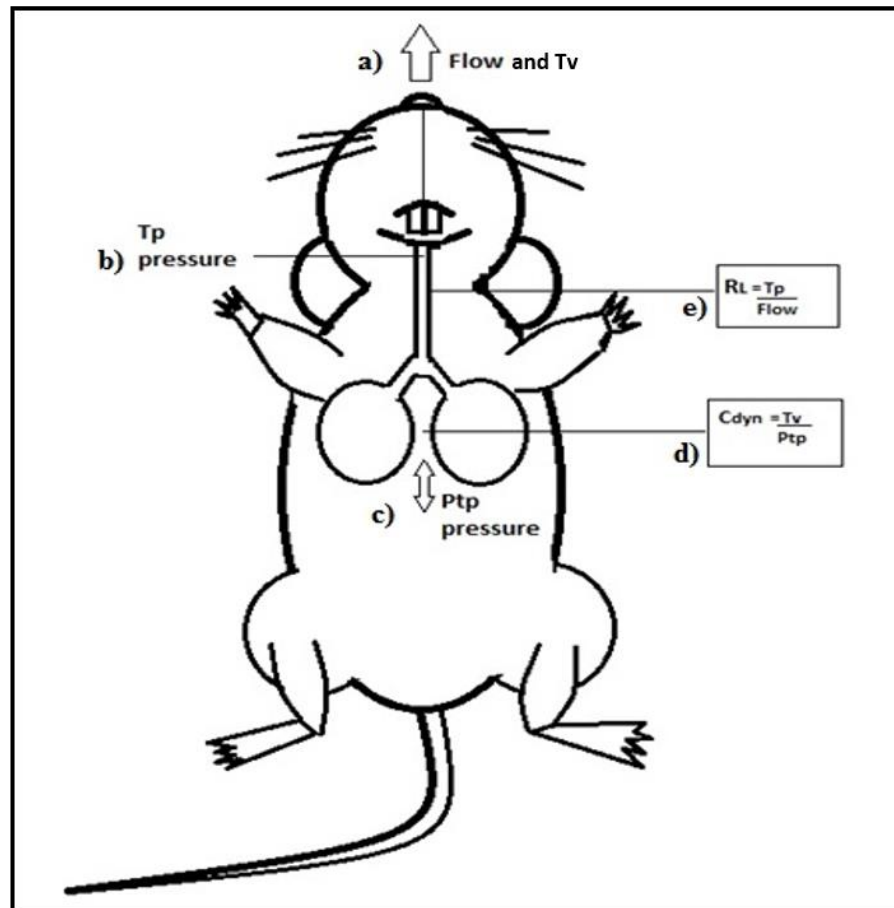


Figure 4.3. Representative map of respiratory parameter measurements. Components used to gather data for the parameters are the pneumotachometer, tracheal cannula, oesophageal cannula, and associated differential pressure transducer elements. The pneumotachometer measures flow and tidal volume (T_v) data (a) as well as tracheal pressure (b). Transpulmonary pressure, P_{tp} , (c) is measured from the oesophageal cannula's mid-thorax placement between the lungs, allowing for indirect calculation of dynamic compliance C_{dyn} . C_{dyn} is calculated from T_v and P_{tp} data (d), while lung resistance, R_L , is calculated from T_p and flow values (e).

4.4.1 Pneumotachometer and tracheal cannula

The pneumotachometer (also referred to as the pneumotachograph) and tracheal cannula allow for measurement of pressure changes critical to determining both R_L and C_{dyn} values. The tracheal cannula keeps the airway open during experimental procedures and is connected to the pneumotachometer. The pneumotachometer is connected to the DLP 2.5 differential pressure transducer, allowing for measurement of tracheal pressure changes, air flow, and tidal volume during respiration. The pneumotachograph (Fig. 4.4)

was purchased in New Zealand from Alphatech Systems who sourced the equipment from Harvard Apparatus (USA). Specifications are listed in Table 4.1.

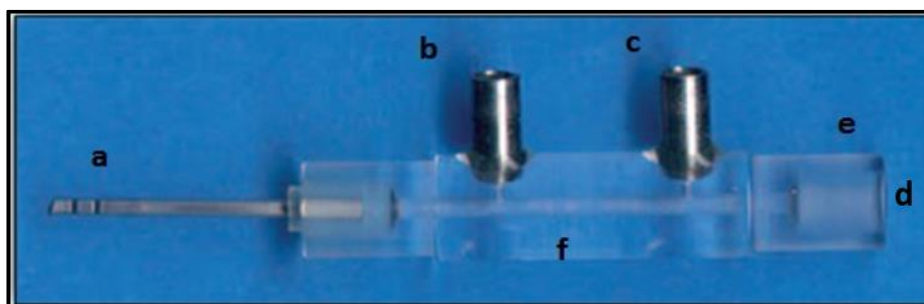


Figure 4.4. HSE-Pneumotachometer PTM Type 378/0.9 for mice and rats. The key functional areas of the component are listed as follows: a) (Murine) tracheal cannula, b) Outlet for oral-level pressure measurements, c) Outlet for atmospheric pressure measurements, d) Outlet for “airway opening”, and e) Pneumotachometer portion of the “airway” in the study; note the reduction of the tube’s diameter (resistance) relative to the airway opening the section (f). Outlets b and c are connected to the differential pressure transducer (Figure 4.5) by dedicated tubes. Aerosolized saline, ACh, and ISO, as well as SIPO treatments are introduced at the airway opening (d).

Table 4.1. Specifications for HSE-Pneumotachometer PTM Type 378/0.9, P/N 73-0981, for mice and rats. The protocol of this study is for mice, and so murine-specific information is of primary relevance. The tracheal cannula may also be changed to one appropriately sized for rats.

Specification	Mice	Rats
Nominal sensitivity	10 mmH ₂ O for 27 ml/s	10 mmH ₂ O for 10.5 ml/s
Nominal flow range	±27 ml/s	±10.5 ml/s
Flow resistance (approx.)	0.4 mmH ₂ O/ml/s	1.0 mmH ₂ O/ml/s
Dead space (approx.)	50 µl	25 µl

4.4.2 Differential low-pressure transducer

The differential low pressure (DLP) transducer (Fig. 4.5) was selected for its ability to maintain accurate readings at low pressures, such as those occurring in murine airways. Accurate low-pressure readings are essential for measuring the tracheal pressure, airflow, and tidal volume in this study. The DLP transducer was sourced from Hugo Sachs (Germany); product specifications are listed in Table 4.2.



Figure 4.5. Differential Low-Pressure Transducer DLP 2.5. The key functional areas of the component are listed as follows: a) Inlet for oral-level pressure signal, b) Inlet for atmospheric pressure signal, c) Body of the differential pressure transducer, d) Connection cable from DLP to signal amplifier. Dedicated tubes from the pneumotachometer's outlets (Figure 4.3, b and c) are connected to DLP inlets a and b respectively, allowing for measurement of low pressure signals during protocols.

Table 4.2. Specifications for the Differential Low-Pressure Transducer DLP 2.5, P/N 73-3882 from Hugo Sachs (Germany). Low pressure signals received by the DLP from the pneumotachometer require further amplification.

Specification	Value
Overpressure	$\pm 2.5 \text{ cmH}_2\text{O}$
Natural frequency	250 cmH_2O
Measuring system	Full bridge
Pressure cavity volume	120 mm^3
Excitation voltage	5VDC
Thermal zero shift	$\pm 1.5 \%$ FS (-25 to 85°C)
Sensitivity	65 to 67 $\text{mV/cmH}_2\text{O}$ at 5 V excitation
Linearity	$\pm 0.25 \%$ FS
Weight	190 g

Signal amplification of the DLP transducer's output is necessary, given the low-pressure differences measured. Amplification is achieved by using a TAM-A transducer amplifier module inside of a PLUGSYS Minicase. The amplifier module and minicase were purchased from Hugo Sachs (Germany), and are pictured in Fig. 4.6. Once amplified, the data is transmitted to Labchart software for analysis.



Figure 4.6. TAM-A transducer amplifier module and its PLUGSYS Minicase. The minicase contains the amplifier module, the power supply for the amplifier, and has a second slot available for installation of an additional transducer amplifier module. The connection cable from the DLP 2.5 (shown in Fig. 4.5(d)) locks into the 6-pin socket of the TAM-A module.

Table 4.3. Specifications for the TAM-A transducer amplifier module (P/N 73-0065) from Hugo Sachs (Germany). Signal from the DLP is amplified prior to being transmitted to the PowerLab data acquisition component.

Specifications	Description
Bridge Supply Voltage	+5 V / 50 mA max.
Transducer Input	6-pin socket with screw lock (Amphenol-Tuchel connector); differential input circuit, input impedance $10^{10} \Omega$.
Gain	Selectable Ranges by Internal Jumper: 0.2 to 10, 0.4 to 20, 1 to 50, 2 to 100, 4 to 200, 10 to 500, 20 to 1000, 100 to 5000, 200 to 10000. Fine adjustment through 10-turn trimmer.
Bridge Balance	Coarse adjustment through 10-turn trimmer, and electronic auto-zero by push button (LED for error if auto-zero is not possible)
Signal Output	<ul style="list-style-type: none"> On front panel through BNC socket, ± 10 V pulsatile filtered or mean signal output, internally selectable. Through bus connector to PLUGSYS measuring system through links, ± 10 V pulsatile filtered and mean signal voltage.
Output low-pass filter	<ul style="list-style-type: none"> Selectable by switch on front panel for pulsatile output signal: 1, 100, 300 Hz. Selectable by internal jumper for mean output signal: 0.1, 0.3 Hz.
Analog indication	TAM-A LED bar graph 20 LEDs (+13/-7) for visual check on the signal sensitivity, approximately 1 V/LED. The TAM-D module (Fig. 4.5) has a 3½-digit LED display.
Electrical calibration	Selectable by switch on front panel: <ul style="list-style-type: none"> 0 V output signal with switch in '0' position. Positive or negative calibration output voltage adjustable with 10-turn trimmer if switch is in 'CAL' position.
Power supply	+5 V through connector from PLUGSYS bus system
PLUGSYS width	2 slot units

4.4.3 Oesophageal catheter

The oesophageal catheter measures Ptp during the experimental protocols of this study. The catheter must be flexible enough to bend and slide through the oral space and oesophagus of test subjects. The catheter must also reach to the mid-thorax and detect low level pressure changes. The catheter for this study was made of PE 90 tubing (inner diameter = 3 mm, outer diameter = 5 mm) attached to a blunted 20-gauge needle (Fig. 4.7). The PE tubing (length = 120 mm) covered the blunted needle, and the tip of the tubing was bevelled (45°) and smoothed for ease of insertion into the murine oesophagus. Two oval holes (2 mm x 1 mm) were cut with a scalpel into the tubing, approximately 3 and 8 mm from the tip. The silicone tubing sleeve of the needle was connected to the oesophageal differential pressure transducer. In order to measure small changes in pressure, the catheter was filled with saline solution. Once positioned, with the tip of the cannula in the oesophagus down to the mid-thorax level, changes in the position of the column of saline are then interpreted by the pressure transducer as readings of pressure changes at the mid-thorax level.

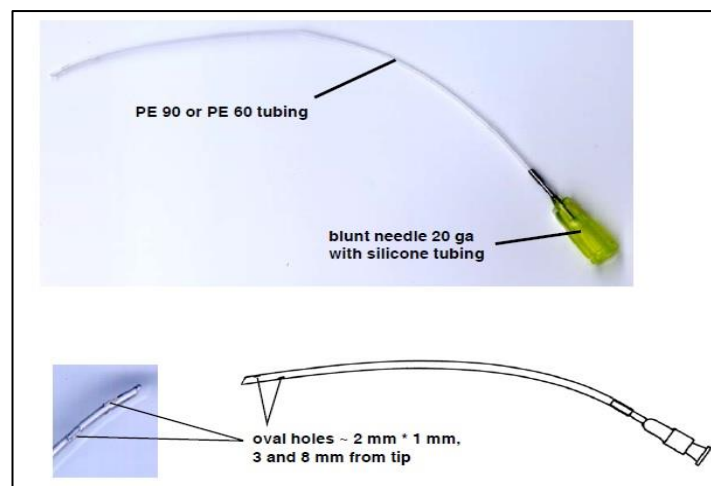


Figure 4.7. Oesophageal catheter used in measurements of transpleural pressure, Ptp. PE 90 tubing and a blunted 20-gauge needle are combined to form the framework of the catheter. Modifications of the tubing tip with oval holes allow for detection of small transpulmonary pressure changes. The catheter is loaded with saline and connected to its transducer at the needle hub. Signals from the transducer are sent to the PowerLab data acquisition component.

4.4.5 Oesophageal pressure transducer

The oesophageal pressure transducer (Fig. 4.8) was sourced from Honeywell S&C (New Zealand). The transducer is connected to the oesophageal catheter at the needle hub and interprets measurements of Ptp values from the change in position of the catheter's column of saline solution. The transducer maintains accurate readings at low pressures (± 1 psi), which is essential for measuring physiological values of pressure occurring at the mid-thorax level, between the lungs of the test subjects.

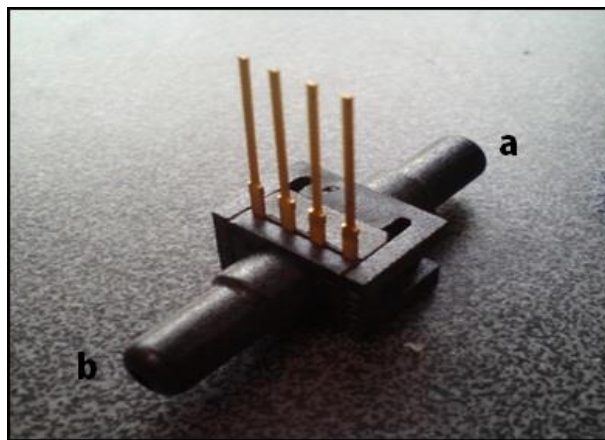


Figure 4.8. - Sensor technics model 26PC0050D6A: a) Inlet for pressure signal from mid thorax, b) inlet for pressure signal from the environment.

Table 4.4. Sensor technics pressure transducer specifications. Honeywell S&C (P/N HSCSAAN001PDAA5)

Specification	Value
Operating pressure	0-50 cmH ₂ O
Sensitivity	240 μ V/mbar
Full-Scale span - Minimum	10.5 mV
Full-Scale span - Typical	12.0 mV
Full-Scale span - Maximum	13.6 mV
Response time	1 ms
Repeatability and hysteresis	± 0.2

Together, the pneumotachometer, tracheal cannula, oesophageal catheter, and two differential low-pressure transducers are the measurement elements used in the study's

protocols. They are combined in their functions to define the plethysmograph which generates the overall data for the respiratory parameter calculations. Additionally, our in-house oscillation device works in conjunction with the plethysmograph, delivering therapeutic positive air pressures *in vivo*. This oscillation device is discussed further in (6), below.

4.4.6 PowerLab 16Ch and Labchart 7.0

The PowerLab 16/30 data acquisition system (Fig. 4.9) from ADInstruments (Australia) was used to record and process data generated from the sensory and amplification components in this study. PowerLab is suitable for research projects requiring up to 16 input channels and can record up to 400,000 samples per second for storage without interruption. PowerLab is compatible with a wide range of equipment from ADInstruments other equipment providers. Signal conditioners and transducers are most relevant to equipment required for this study, given the nature of our (low) pressure readings. The PowerLab 16/30 accommodates standard single-ended BNC coaxial cable inputs and 4 differential Pod ports. The Pod ports provide a direct connection for appropriate signal conditioners and transducers. In our study, both pressure transducers are attached to ports 1 and 7 of the system board using coaxial connectors.



Figure 4.9. ADInstruments PowerLab 16/30. Input from signal conditioners and transducers is possible with 16 available channels to select. Coaxial cable and pod ports are provided for connectors. The DLP 2.5 (tracheal pressure data source) and Honeywell transducer (oesophageal pressure data source) are connected to ports 1 and 7 of the PowerLab system board. Output of signals is sent to LabChart software for further processing.

The PowerLab 16/30 works in conjunction with the ADInstruments software, LabChart, which is user-friendly and adaptable to a range of study objectives. The role of the software in this study is to convert the signals from both pressure transducers into pressure-change data. The data is then used to calculate real time values of respiratory parameters T_p , flow, T_v , PIP, Ptp, R_L and C_{dyn} (Fig. 4.10). Calibration of the system is discussed in (7) below.

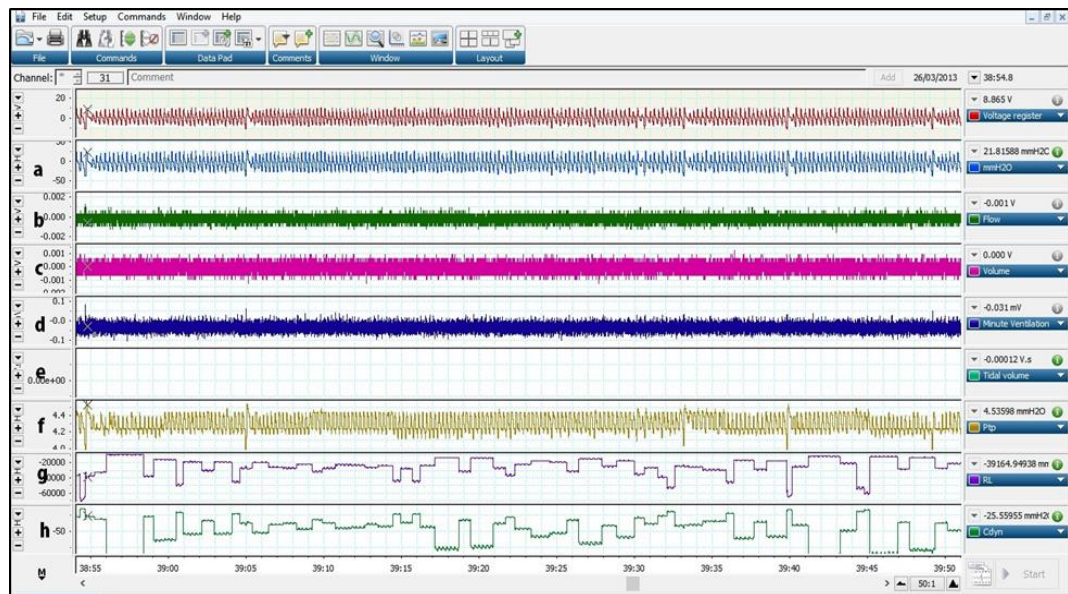


Figure 4.10. Screenshot of ADInstruments LabChart with selected real-time channel data displayed for variables as follows: a) Tracheal pressure (T_p , mmH₂O); b) Flow (ml/sec); c) Volume (ml); d) minute ventilation (ml/min); e) Tidal volume (T_v , ml); f) Transpulmonary pressure (P_{tp} , cmH₂O); g) Lung Resistance (R_L , mmH₂O/ml/s) and h) Dynamic compliance (C_{dyn} , ml/mmH₂O).

4.5. Drugs and allergen-mix delivery system

This section discusses the equipment required to deliver drugs and allergens to the healthy and sensitized animals in this study. (Drug and allergen details are presented in Chapter III.) The jet nebulizer is critical for introducing aerosolized ACh to the airways of test subjects, in order to mimic the bronchoconstriction of an asthmatic attack. The nebulizer is also required to provide relief from the ACh by providing the bronchorelaxant ISO as

needed. Additional accessories in the delivery system are also detailed to present their utility within the protocols.

4.5.1 Aerosol jet nebulizer

The aerosol jet nebulizer from Harvard Apparatus (P/N 73-1963) is used in this study to deliver the baseline saline aerosol as well as the ACh and ISO drug treatments to study animals. The nebulizer requires an operating pressure of ~1.5 bar (22 psi) and is supported by an AMPRO air brush compressor with a working range of 15-50 psi. The particles generated by the jet nebulizer (Fig. 4.11) are 10 μm or less in size, with 60 % of the particles being 2.5 μm or less (data taken from jet nebulizer datasheet).

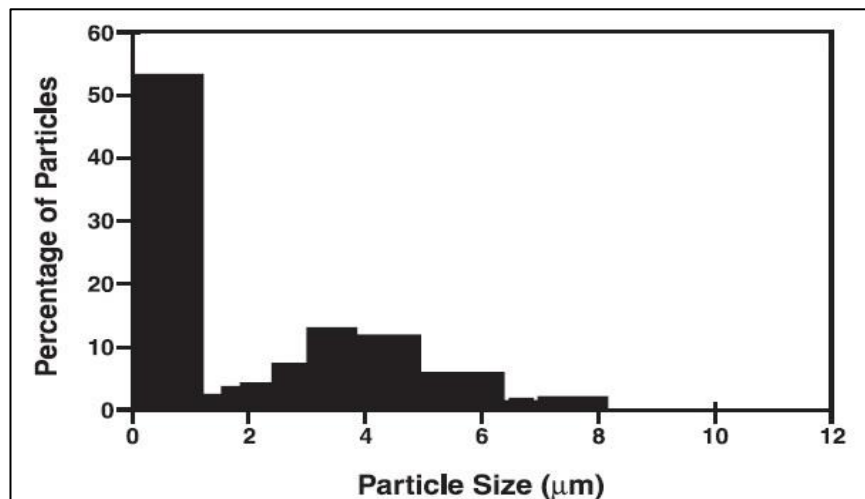


Figure 4.11. Harvard Apparatus aerosol jet nebulizer particle size chart. Distribution of particles following addition of 5 ml of 0.9 % saline solution, nebulized with inlet pressure of 1.5 bar. (Data taken from jet nebulizer datasheet.) Greater than 50 % of generated particles are less than 2 μm in size.

The nebulizer is placed above the position of the study animal during experimental protocols and is held in place by a clamp and supporting ringstand (Fig. 4.12(a)). The nebulizer receives pressurized input air from the air condenser (Fig. 4.12(b)) through support tubing and delivers aerosolized droplets to the test subjects by additional tubing. The tubing which runs from the nebulizer to the subject ends with an opening that is positioned facing the airway of the test subject. The nebulizer's tubing is flexible and is

easily positioned relative to the study animal's nostrils and the pneumotachometer's tracheal inlet.



Figure 4.12. Harvard Apparatus aerosol jet nebulizer protocol setup. The components of the nebulizer setup ensure delivery of aerosolized particles of saline, ACh, and ISO to the test subjects. Positioning of the nebulizer is above the study animals during the protocol, held in place on a ringstand by a three-prong clamp (a). The nebulizer receives pressurised air from the AMPRO air brush compressor (b) and support tubing. Nebulized products are carried from the nebulizer to the study animal in similar support tubing and positioned at the airway.

4.5.2 Pressure oscillation setup

Pressure oscillations are necessary in this study in order to assess the responses of sensitized asthmatic airways during spontaneous breathing. Common methodologies used to generate pressure oscillations on experimental animals involve electromagnetic shakers, acoustic waves generated from audio speakers, or pressure-volume changes. This study utilizes a pressure oscillation delivery system developed by IBTEc (Figs. 4.13 and 4.14), which is based on the pressure-volume generation of oscillations. Pressure-volume oscillations in the study maintain a low level of invasiveness and are focussed in a manner that minimises the dispersal of generated waves away from the study animal.

Pressure oscillations are generated from multiple assembled components, indicated in the schematic below (Fig. 4.13). A programmable waveform generator from Hewlett

Packard (a) is connected to a power amplifier (LDS PA25E, b). The amplifier is in turn connected to the protocol's oscillating shaker (Ling Dynamics System LTD, Model V203, c). The shaker is held in place by a stable base, and in combination with a 10 ml plastic (air reservoir) chamber (d), generates the volumes of pressurized air for the protocols. The air chamber has one inlet for the shaker piston (e) and one outlet for the generated pressure oscillations. Pressure oscillations are carried away from the chamber's outlet through flexible tubing to the airway of the study animal.

Together, the components generate and deliver oscillatory pressure changes as a function of the programmable waveform generator's output signal. The output signal from the waveform generator is based on selections of frequency and millivolt values which define the oscillation pressures available for study. Frequency/millivolt signals are sent to the shaker, thereby displacing the piston within its sealed plastic chamber, generating pulse waves of changing pressures.

The oscillation setup meets key requirements for establishing the basis of respiratory studies in mice. The setup generates and delivers frequency/voltage output that is physiologically relevant for volumes of air delivered. In addition to duplicating the frequency of spontaneously breathing mice, the oscillation setup allows for generation of calculated pressures for testing a range of treatments for murine airways. The tidal volume of mice is roughly 200 μl /per breathing cycle, and the current settings for the shaker's piston displacement result in a volume change of 100-200 μl . The breathing frequency of mice is close to 200 breaths/min, ~ 3.3 Hz, and the device has been tested from 3-20 Hz in conjunction with voltage amplitudes from 50 mV to 1.3 V. The combination of frequency and voltage values are responsible for establishing the pressure values delivered from the device to the murine airways.

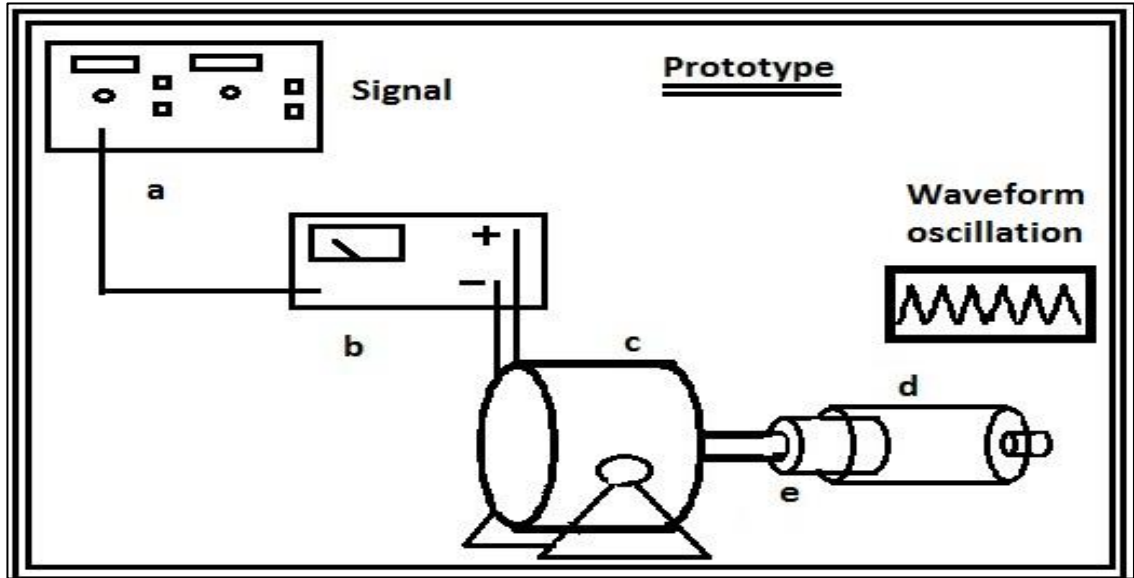


Figure 4.13. Generation of the positive pressure oscillations is accomplished by IBTec's waveform oscillator. The setup for the oscillator includes the a) waveform generator; b) Power amplifier; c) shaker; d) chamber; e) piston.

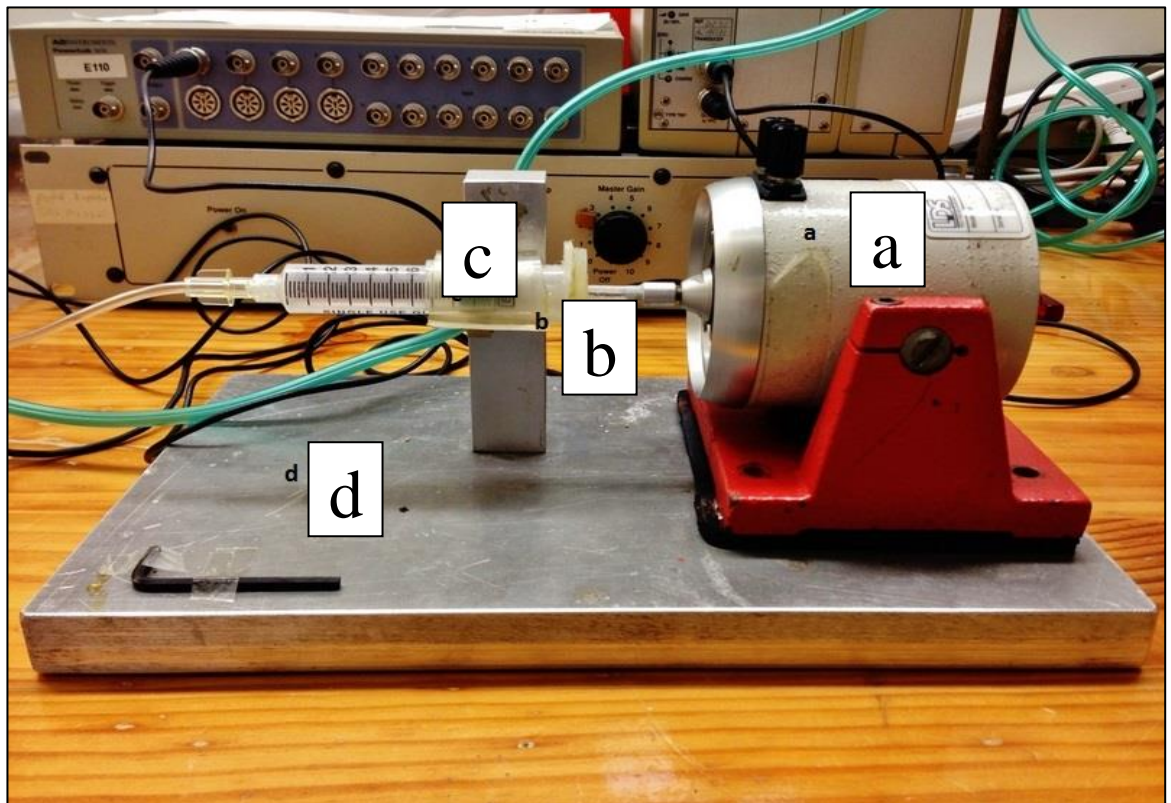


Figure 4.14. Pressure oscillation setup: a) Shaker, b) Chamber, c) Piston and d) base. Converting the input criteria of the waveform generator, the shaker produces oscillations that are then imposed as treatments on spontaneously breathing mice.

4.6. Calibration of pressure transducers and oscillation setup

This section presents the calibration and standardization of the tracheal and oesophageal pressure transducers and the pressure oscillation device.

4.6.1 Calibration of the differential low pressure (tracheal) transducer

Prior to its use in experiments, the differential low pressure (DLP 2.5, tracheal) transducer was tested and calibrated. The DLP 2.5 transducer was connected through a plastic pipe to a water manometer (Fig. 4.15) and was calibrated using nine (9) increments of 1 mmH₂O per data point. Data points, increasing sequentially from 1 mmH₂O to 9 mmH₂O, were measured a minimum of three times. The data from the calibration points was collected using LabChart, tabled, and plotted for analysis (Table 4.5 and Fig. 4.16).

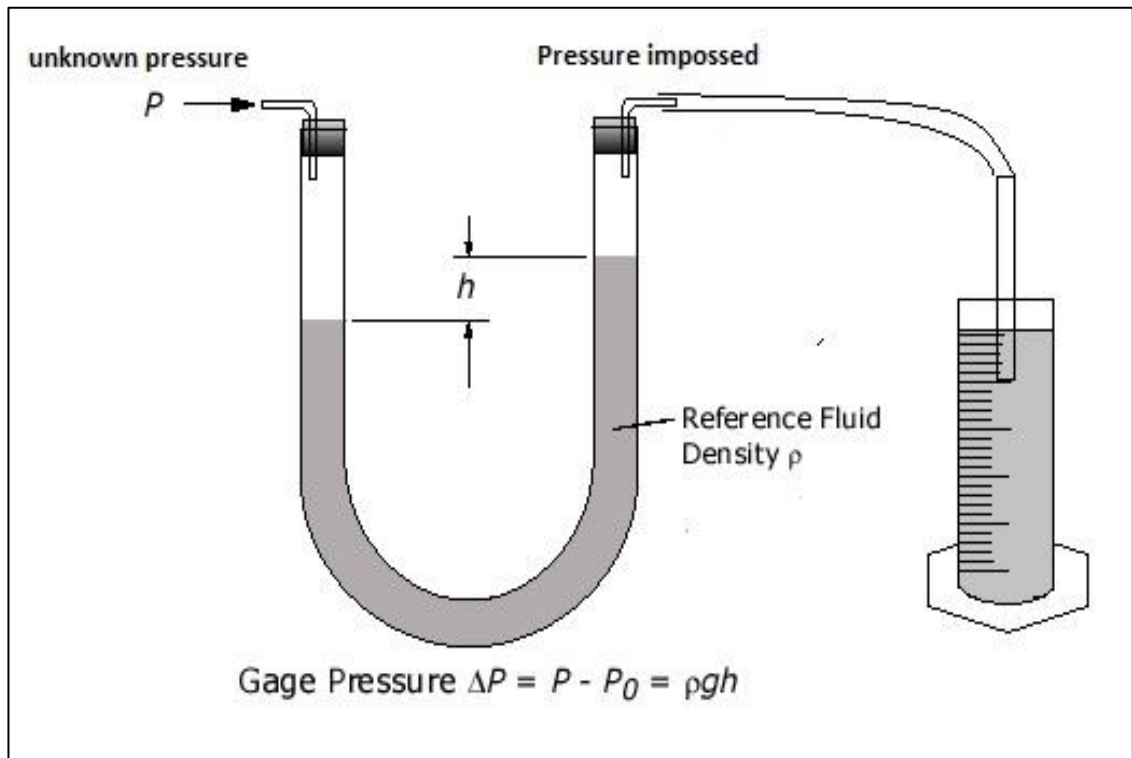


Figure 4.15. Representative diagram of the water manometer setup used for the calibration curve of the DLP 2.5 low pressure transducer. Calibration of the transducer established the voltage equivalents of known mmH₂O pressure values as indicated in Table 4.5 and Fig. 4.16.

Table 4.5. Calibration measurements of the DLP 2.5 low pressure transducer. Increments of 1 mmH₂O were equilibrated with the measured (triplicate) voltage values for use in calibrating the transducer for determining experimental *T_p* values. Mean voltage data for each increment of pressure is also shown.

DLP 2.5 Transducer, Tracheal Cannula				
Calibration point triplicate measurements, Volts				
mmH₂O	1	2	3	Mean
1	2.14	2.22	2.30	2.22
2	2.49	2.60	2.55	2.55
3	2.92	2.93	2.84	2.89
4	3.27	3.29	3.11	3.22
5	3.70	3.58	3.38	3.55
6	3.99	3.80	3.74	3.84
7	4.12	4.08	4.19	4.13
8	4.48	4.30	4.50	4.43
9	4.75	4.50	4.93	4.73

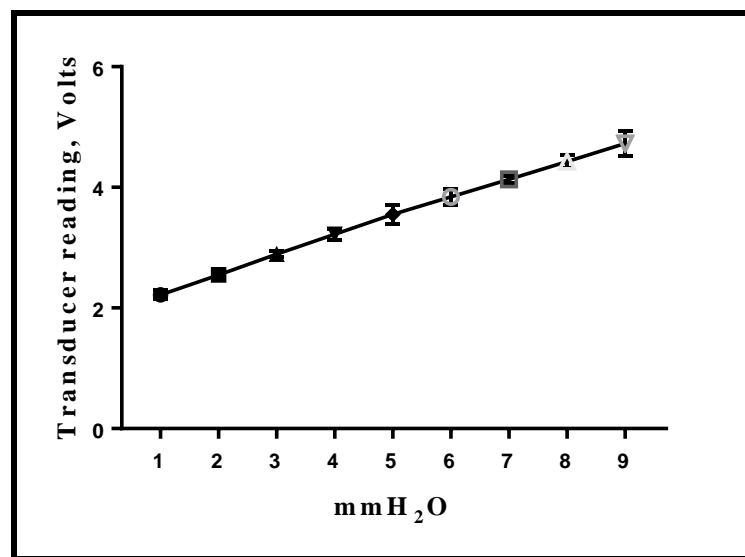


Figure 4.16. Calibration curve for the DLP 2.5 low pressure transducer. Triplicate voltage measurements of known 1mmH₂O increments of pressure are shown for a range of 1 mmH₂O to 9 mmH₂O. Calibration of the transducer was necessary to establish experimental values of *T_p* based on gathered experimental voltage data.

4.6.2 Calibration of low differential (oesophageal) pressure transducer

Prior to its use in experiments, the low differential (oesophageal/Honeywell) pressure transducer was calibrated using the same process as that used for the tracheal pressure

transducer. The data from the calibration points was collected using Labchart, tabled, and plotted for analysis (Table 4.6 and Fig. 4.17).

Table 4.6. Calibration measurements of the Honeywell (oesophageal) low pressure transducer. Increments of 1 mmH₂O were equilibrated with the measured (triplicate) voltage values for use in calibrating the transducer for determining experimental P_{tp} values. Mean voltage data for each increment of pressure is also shown.

Honeywell Transducer, Oesophageal Cannula				
Calibration points, Volts				
mmH₂O	1	2	3	Mean
1	0.005	0.005	0.004	0.005
2	0.009	0.009	0.008	0.009
3	0.013	0.012	0.012	0.012
4	0.018	0.017	0.018	0.018
5	0.022	0.023	0.022	0.022
6	0.026	0.027	0.027	0.027
7	0.032	0.032	0.031	0.032
8	0.037	0.036	0.035	0.036
9	0.041	0.040	0.040	0.040

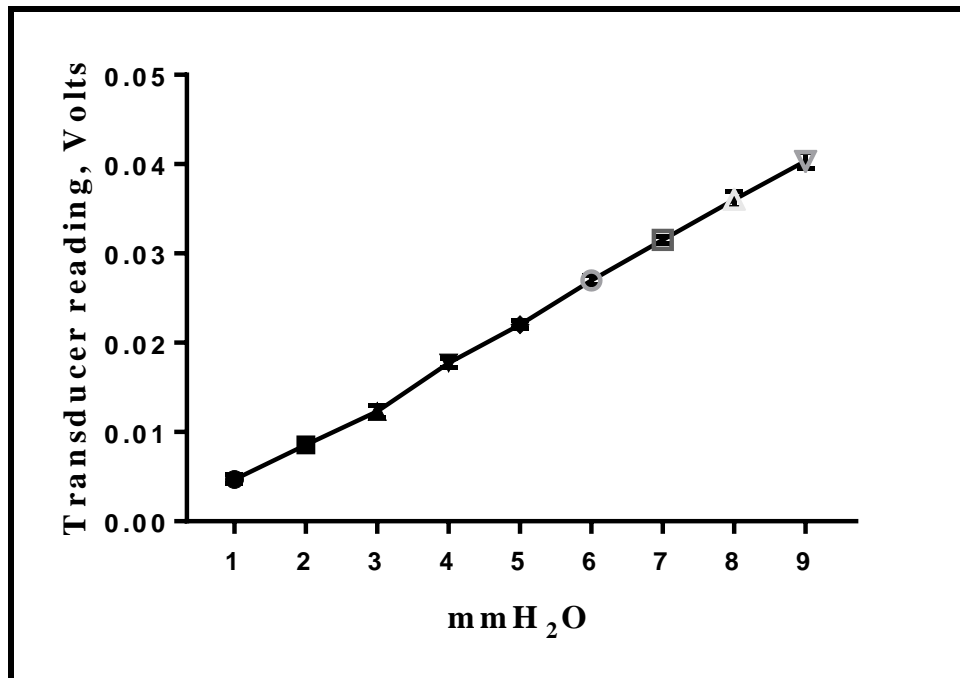


Figure 4.17. Calibration curve for the Honeywell (oesophageal) low pressure transducer. Triplicate voltage measurements of known 1 mmH₂O increments of pressure are shown for a range of 1 mmH₂O to 9 mmH₂O. Calibration of the transducer was necessary to establish experimental values of P_{tp} based on gathered experimental voltage data.

4.6.3 Calibration of oscillation setup

Prior to its use in experiments, the oscillation setup was tested and calibrated to yield pressure values (measured in cmH₂O) from gathered voltage data. Frequencies and amplitudes for the calibration pressures were selected based on previous studies carried out in an acute asthmatic murine model. Frequencies ranging from 3-20 Hz were combined with amplitude values from 50 mV to 1.3 V (Table 4.7, left column).

The Hz/mV combinations were entered into the waveform generator, and corresponding output pressures were collected as voltage readings by the Honeywell transducer using LabChart. Data from LabChart was tabled and plotted for analysis (Table 4.7 and Fig. 4.18). The frequency/voltage values established a potential pressure range of nearly 12 cmH₂O available for consideration in the study. Based on previous studies [13] in murine models utilizing pressure oscillations, a smaller set of frequency/voltage settings were selected to study a pressure range of 0.43 - 3.60 cmH₂O. This smaller range of pressures was applied to murine airways during the study as superimposed pressure oscillations over spontaneous breathing.

The pressures selected for the study correspond to the permutations of 5-20 Hz frequencies with 100-400 mV amplitudes (Fig. 4.18). Due to the number of measurements already taken from the (16) 5-20 Hz sets of selected pressures, the Hz/mV combinations generated by the 3 Hz set were not utilized in this study.

4.7. Testing superimposed pressure oscillations in vivo

Following calibration of the low-pressure transducers and the oscillation device setup, superimposed pressure oscillations were tested *in vivo* using the described plethysmography equipment. Oscillations were not used in the sensitization assessments

of Chapter III but are introduced here as treatments to achieve Chapters V and VI outcomes. SIPO protocol details are summarized below, with additional details in Appendix C.

As with the sensitization assessments (Chapt. III), anaesthetised animals, intubated with the tracheal cannula and oesophageal catheter were administered doses of normal saline (0.9 %) solution, bronchoconstrictor (ACh, 10^{-4} M), and bronchodilator (ISO, 10^{-6} M) as necessary, using the jet nebulizer. The nebulizer mist was directed to the inlet of the airway (pneumotachometer-tracheal cannula). Respiratory parameters were recorded through the entire series of control, rest, and challenge portions of the protocol as noted in Section 3.6.1.

Table 4.7. Table of pressures (cmH₂O) generated by frequency (Hz) and amplitude (mV) combinations. The Hz/mV combinations were entered into the waveform generator, and output pressures were measured by the calibrated DLP 2.5 transducer. Voltage readings were converted to physiological pressures and indicated as shown. From this range of pressures, the combination sets of 5-20 Hz and 100-400 mV were selected for the study.

Pressure, cmH₂O from frequency and amplitude combinations				
Voltage	5 Hz	10 Hz	15 Hz	20 Hz
0.05	0.32	0.07	0.06	0.13
0.06	0.42	0.35	0.08	0.18
0.07	0.45	0.43	0.26	0.19
0.08	0.57	0.50	0.33	0.33
0.09	0.65	0.59	0.40	0.40
0.10	0.76	0.68	0.43	0.43
0.20	1.63	1.51	1.05	1.05
0.30	2.61	2.40	1.67	1.68
0.40	3.60	3.34	2.35	2.31
0.50	4.66	4.28	3.03	2.96
0.60	5.53	5.10	3.67	3.57
0.70	6.67	6.16	4.40	4.29
0.80	7.55	7.02	4.97	4.84
0.90	8.49	7.89	5.64	5.48

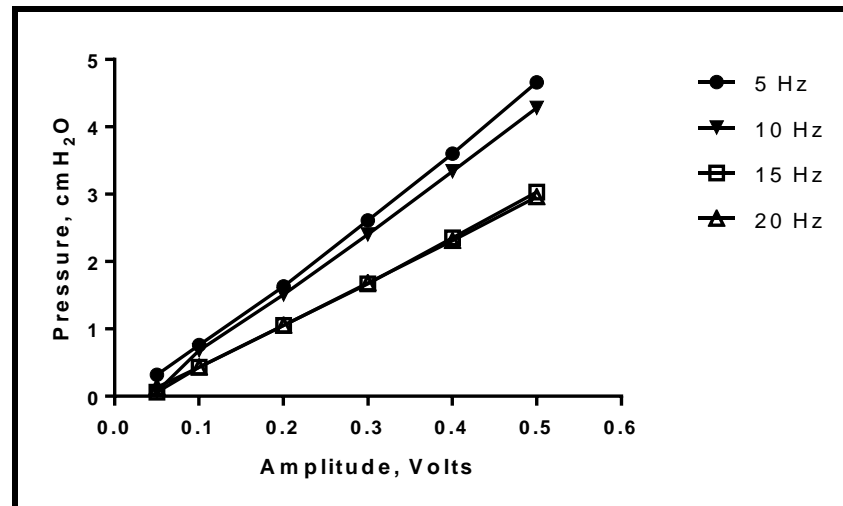


Figure 4.18. Oscillation device pressures (cmH₂O) measured by the calibrated DLP 2.5 transducer. The waveform generator's frequency and voltage permutations were measured as voltage and converted to pressure. A small range of physiologically applicable pressures were selected for use as respiratory treatments in the study. Combinations of 5-20 Hz/100-400 mV waveforms correspond with a pressure range of 0.43 – 3.60 cmH₂O.

In lieu of ISO treatments as bronchorelaxant candidates in this study, the SIPO treatment protocols include the option of administering a selected pressure for a given test condition. SIPO values are selected from the range of defined superimposed oscillations. In order to avoid potential linear effects of applied oscillatory pressures, each Hz/mV combination's corresponding cmH₂O pressure was randomized, and oscillations were applied during the study according to the determined order. Applied pressures greater than 2.4 cmH₂O were removed from the sequence of random assignments and tested as final challenges for given study animals, due to the higher pressures' potential for negative impacts on spontaneous breathing.

4.8. Summary

This chapter has detailed the devices and equipment responsible for facilitating the studies of respiratory parameters in a murine model of chronic asthma. The pressure transducers, signal amplifiers, data acquisition tools, and additional support equipment are discussed

within the context of this study. Once tested and calibrated, the devices and equipment function to determine how healthy and sensitized (chronic) airways respond *in vivo* to challenges from bronchoconstrictors, bronchodilators, and applied superimposed pressure oscillations (Chapters V and VI).

CHAPTER V

Lung resistance in healthy and chronic, sensitized mice

5.1. Introduction

The primary objective of the *in vivo* testing is to characterize the spontaneous breathing responses of healthy and chronically-sensitized airways to superimposed pressure oscillations. The *in vivo* testing of this study is carried out using the (calibrated and tested) equipment detailed in Chapter IV. Respiratory parameters are measured in spontaneously breathing study animals exposed to combinations of chemical challenges and applied mechanical pressure oscillations. Definitions for the combinations of chemical and mechanical respiratory challenges are explained, and a summary of the *in vivo* experimental methodology used to obtain values for R_L , is presented. The experimental results for healthy and sensitized (chronic asthmatic model) subjects' data along with their statistical analyses and discussion points conclude the chapter.

5.2. Method

The respiratory challenges using saline, ACh, ISO, and superimposed airway pressure applications are combined in a manner that allows for lung resistance to be measured and compared relative to an established healthy baseline condition. The combinations of chemical solutions and superimposed pressures are described in detail in the General Methods of Chapter III and further in Section 4.7 and Appendix C.

Briefly, each set of respiratory challenges is separated from any other test by a rest period, where no manipulations are carried out. Every test begins with a normal saline challenge,

a 1-min rest period, and (1-min) ACh challenge. Every test is then completed with either an ISO challenge or application of a superimposed pressure oscillation. (The order in which the ISO or oscillation challenge is applied to a given study animal is from a randomized list in order to ensure that linear progression through the applied pressures is avoided.) A 2-min rest period separates the end of one test from the start of the next test.

Testing for any subject gathers parametric values of T_p and flow, and is concluded when any of the respiratory parameters associated with calculating R_L (Eqn. 2.1) do not recover from zero (terminal) values. Results are compiled, and statistical analysis is performed.

5.2.1. Statistical analysis

GraphPad Prism 7.0™ (GraphPad) was designed for use in pharmacology- and physiology-based studies. Its initial focus groups were laboratory and clinical researchers. As such, the software is of great use in the statistical analysis of data generated in this study. By combining data organization and straightforward statistical functions, GraphPad establishes an effective platform for subsequent scientific graphing and curve fitting as means to illustrate comparative data.

The data obtained from this study was analysed with multiple statistical tools. Common statistical tests such as t-tests, nonparametric comparisons, one- and two-way ANOVA, analysis of contingency tables, and survival analysis are performed on the data by GraphPad. For the purpose of this study, due to its small sample sizes with outcomes that are not normally distributed, the use of the t-test, nonparametric comparison, and one- and two-way ANOVA applications, are all ideal for analysis. Additionally, post-analysis Dunnett testing is used for identifying differences in data obtained from the protocols utilized in this study.

The initial use of t-test, nonparametric comparison, and one- and two-way ANOVA are highlighted. The t-test is used to compare the means between two independent groups, and to identify differences. ANOVA is used to compare several (3 or more) means from different, independent groups, and to report if there are significant differences between the tested groups. The Dunnett test performs comparisons of the means from multiple treatment groups with a single control group, and determines differences that shape conclusions of the data. Initial comparisons of pulmonary responses were performed in the evaluation of the chronic model's saline, ACh, and ISO data (Chapt. III). Subsequent comparisons of pulmonary responses to ACh, ISO, and applied pressure oscillations were added to the analyses of this chapter as well as Chapters VI and VII.

The responses of pre-constricted airways to applied pharmacological treatments (ACh and ISO) or pressure oscillations were carried out according to the frequency, amplitude, or pressure status of the treatments. In other words, frequency and mV combinations define the applied pressures in this study, and were analysed either separately (as frequency- or amplitude-based functions) or as the physiological measurement of their pressure-based function. Saline, ACh, and ISO treatments are all considered equal to a condition of zero applied pressure, with 0 Hz and 0 mV as their respective superimposed frequency and amplitude components.

Frequency-based analysis of the 5 Hz group consists of all data characterized by application of 5 Hz frequency and a 100 – 400 mV amplitude component to a spontaneously breathing subject. This same pattern is also used for each of the 10-, 15-, and 20 Hz groups. Amplitude-based analysis of the 100 mV group consists of all data characterized by application of the 100 mV amplitude component along with a 5-, 10-,

15- or 20 Hz frequency setting to a spontaneously breathing mouse. This same pattern is also used for each of the 200-, 300-, and 400 mV groups. Pressure-based analysis consists of all data characterized by the application of the 16 pressures tested (ranging from 0.4 cmH₂O to 3.6 cmH₂O). As indicated, ACh and ISO treatment data are presented for comparison throughout the results and analyses. Results of the analyses are expressed as mean \pm SE for each of the R_L respiratory parameters presented.

The primary method of discussing the analysed data is in terms of frequency-based groups. Additional mention of groups determined by either amplitude- (mV) or pressure (cmH₂O)-based experimental conditions further reveals the trends of SIPO-related bronchorelaxation in a sensitized model.

5.3. Results

Experimental data points for the lung resistance respiratory parameters were recorded in real time using Labchart 7.0 software (ADInstruments). As described in Chapter IV, Labchart (in conjunction with Powerlab) measures several signals directly from channels 1-7 of the acquisition system, which are then converted to physiological values. For calculations of R_L, values of T_p and flow are used. Channels 8 and 9 of the software incorporate signal data from channels 1-7. Calculations for R_L are made using Eqn. 2.1 which utilises raw data of T_p and flow signals. Although not involved in the software's R_L calculations, another key measurement for assessing the ability to move air in and out of the lungs is the subject's respiratory rate (rr). Respiratory rate values are cited in this chapter's tables, along with pressure and flow data.

5.3.1. Raw data measurements

Summary data of healthy and sensitized groups' means for Tp, Flow and rr values are presented in Tables 5.1 – 5.4 according to Hz-generated pressure sets. Standard error values are excluded in these tables. Each table for 5 - 20 Hz-generated pressure sets also include saline, ACh, and ISO data for comparisons. Units for each measurement category are provided. Respiratory rates are presented as breaths/min (bpm). All mean values for both healthy and sensitized data are from n = 7, except for sensitized SIPO data, where n=5.

Table 5.1. Summary table of Healthy and Sensitized Groups' Tp, Flow, and respiratory rate (rr) responses from applied pressure oscillations in the 5 Hz-generated set. Data obtained from Saline, ACh, and ISO treatments are presented along with the data responses from the four physiological pressures (0.8 – 3.6 cmH₂O) that comprise the set.

5 Hz-generated Pressure Set							
Healthy Group				Sensitized Group			
	Tp, cmH ₂ O	Flow, ml/s	rr, bpm		Tp, cmH ₂ O	Flow, ml/s	rr, bpm
Saline	2.3	0.71	188	Saline	3.9	1.96	148
ACh	2.4	0.76	195	ACh	6.1	1.78	160
0.8	2.2	0.69	211	0.8	4.9	2.35	199
1.6	2.3	1.23	192	1.6	3.9	2.06	156
2.6	2.3	1.02	190	2.6	5.0	2.38	138
3.6	2.0	0.96	195	3.6	4.6	1.86	156
ISO	2.0	0.36	173	ISO	3.9	2.44	177

The 5 Hz healthy group tracheal pressures range from 2.0 cmH₂O for ISO and 400 mV treatments up to a high of 2.4 cmH₂O with ACh challenge. Flow values from 0.36 (ISO) – 1.23 (200 mV) ml/s were calculated, and the subjects' respiratory rates across the treatments are highest (211 breaths/min) for the 100 mV treatment, with the lowest rate (173 breaths/min) coming from the ISO group. Sensitized tracheal pressures range from 3.9 cmH₂O for saline, ISO and 200 mV treatments up to a high of 6.1 cmH₂O with ACh challenge. Flow values from 1.78 – 2.44 ml/s (ACh and ISO respectively) were calculated, and the subjects' respiratory rates across the treatments are highest (199

breaths/min) for the 100 mV treatment, with the lowest rate (138 breaths/min) coming from the 300 mV group.

Table 5.2. Summary table of Healthy and Sensitized Groups' tracheal pressure (Tp), Flow, and respiratory rate (rr) responses from applied pressure oscillations in the 10 Hz-generated set. Data obtained from Saline, ACh, and ISO treatments are presented along with the data response from the four physiological pressures (0.7 – 3.3 cmH₂O) that comprise the set.

10 Hz-generated Pressure Set							
Healthy Group				Sensitized Group			
	Tp, cmH ₂ O	Flow, ml/s	rr, bpm		Tp, cmH ₂ O	Flow, ml/s	rr, bpm
Saline	2.3	0.71	188	Saline	3.9	1.96	148
ACh	2.4	0.76	195	ACh	6.1	1.78	160
0.7	2.1	1.18	200	0.7	3.4	2.15	165
1.5	2.4	1.13	191	1.5	4.0	1.90	148
2.4	2.1	1.38	206	2.4	3.9	1.75	147
3.3	2.2	1.33	197	3.3	4.7	2.03	166
ISO	2.0	0.36	173	ISO	3.9	2.44	177

The 10 Hz healthy group tracheal pressures range from 2.0 cmH₂O for ISO treatments up to a high of 2.4 cmH₂O with ACh and 200 mV challenges. Flow values from 0.36 (ISO) – 1.38 (300 mV) ml/s were calculated, and the subjects' respiratory rates across the treatments are highest (206 breaths/min) for the 300 mV treatment, with the lowest rate (173 breaths/min) coming from the ISO group. Sensitized tracheal pressures range from 3.9 cmH₂O for saline, ISO and 300 mV treatments up to a high of 6.1 cmH₂O with ACh challenge. Flow values from 1.75 – 2.44 ml/s (300 mV and ISO respectively) were calculated, and the subjects' respiratory rates across the treatments are highest (177

breaths/min) for the ISO treatment, with the lowest rate (147 breaths/min) coming from the 300 mV group.

Table 5.3. Summary table of Healthy and Sensitized Groups' tracheal pressure (Tp), Flow, and respiratory rate (rr) responses from applied pressure oscillations in the 15 Hz-generated set. Data obtained from Saline, ACh, and ISO treatments are presented along with the data response from the four physiological pressures (0.4 – 2.4 cmH₂O) that comprise the set.

15 Hz-generated Pressure Set							
Healthy Group				Sensitized Group			
	Tp, cmH ₂ O	Flow, ml/s	rr, bpm		Tp, cmH ₂ O	Flow, ml/s	rr, bpm
Saline	2.3	0.71	188	Saline	3.9	1.96	148
ACh	2.4	0.76	195	ACh	6.1	1.78	160
0.4	2.2	1.10	205	0.4	5.1	2.24	177
1.1	2.4	1.27	197	1.1	3.9	1.97	144
1.7	2.1	1.28	178	1.7	3.3	2.13	169
2.4	2.1	1.43	185	2.4	3.9	1.88	157
ISO	2.0	0.36	173	ISO	3.9	2.44	177

The 15 Hz healthy group tracheal pressures range from 2.0 cmH₂O for ISO treatments up to a high of 2.4 cmH₂O with ACh and 200 mV challenges. Flow values from 0.36 (ISO) – 1.43 (400 mV) ml/s were calculated, and the subjects' respiratory rates across the treatments are highest (205 breaths/min) for the 100 mV treatment, with the lowest rate (173 breaths/min) coming from the ISO group. Sensitized tracheal pressures range from 3.9 cmH₂O for saline, 200 mV, 400 mV and ISO treatments up to a high of 6.1 cmH₂O with ACh challenge. Flow values from 1.78 – 2.44 ml/s (ACh and ISO respectively) were calculated, and the subjects' respiratory rates across the treatments are highest (177

breaths/min) for the 100 mV and ISO treatments, with the lowest rate (144 breaths/min) coming from the 200 mV group.

Table 5.4. Summary table of Healthy and Sensitized Groups' tracheal pressure (Tp), Flow, and respiratory rate (rr) responses from applied pressure oscillations, 20 Hz-generated set. Data obtained from Saline, ACh, and ISO treatments are presented along with the data response from the four physiological pressures (0.4 – 2.3 cmH₂O) that comprise the set.

20 Hz-generated Pressure Set							
Healthy Group				Sensitized Group			
	Tp, cmH ₂ O	Flow, ml/s	rr, bpm		Tp, cmH ₂ O	Flow, ml/s	rr, bpm
Saline	2.3	0.71	188	Saline	3.9	1.96	148
ACh	2.4	0.76	195	ACh	6.1	1.78	160
0.4	2.1	1.24	204	0.4	4.3	1.87	144
1.1	2.4	1.63	186	1.1	3.9	1.98	154
1.7	2.2	0.96	190	1.7	3.6	1.94	150
2.3	2.3	1.08	195	2.3	3.7	1.88	167
ISO	2.0	0.36	173	ISO	3.9	2.44	177

The 20 Hz healthy group tracheal pressures range from 2.0 cmH₂O for ISO treatments up to a high of 2.4 cmH₂O with ACh and 200 mV challenges. Flow values from 0.36 (ISO) – 1.63 (200 mV) ml/s were calculated, and the subjects' respiratory rates across the treatments are highest (204 breaths/min) for the 100 mV treatment, with the lowest rate (173 breaths/min) coming from the ISO group. Sensitized tracheal pressures range from 3.9 cmH₂O for saline, 200 mV, and ISO treatments up to a high of 6.1 cmH₂O with ACh challenge. Flow values from 1.78 (ACh) – 2.44 (ISO) ml/s (ACh and ISO respectively) were calculated, and the subjects' respiratory rates across the treatments are highest (177 breaths/min) for the ISO treatments, with the lowest rate (144 breaths/min) coming from the 100 mV group.

5.3.2. R_L measurements

Tracheal pressure and Flow data determine R_L values (Eqn. 2.1), which are relative indicators of airway bronchoconstriction or bronchorelaxation in the mouse airways. The established values of R_L for ACh challenges and ISO treatments serve as standards of bronchoconstriction and bronchorelaxation to gauge the efficacy of applied pressure oscillations across the tested healthy and sensitized mice.

Values for R_L are presented in Tables 5.5 – 5.8 in this section and are expressed as the mean \pm SE for each given condition. Tables provide the summary of experimental data from applications of ACh, ISO, and SIPO treatments in healthy and sensitized mice. SIPO values are grouped within each table according to frequency, amplitude, and the generated physiological pressure (cmH₂O) sets in order to effectively present results.

Table 5.5 contains the R_L experimental data obtained from the set of 5 Hz-derived SIPO treatments of healthy and sensitized mice. Conditions are described both as Hz/mV combinations and corresponding physiological pressures. The 5 Hz data set consists of pressures derived from 5 Hz in combination with amplitudes of 100 - 400 mV, which are equivalent to 0.8, 1.6, 2.6, and 3.6 cmH₂O respectively. Experimental results for ACh and ISO conditions are also presented as parameter references.

The 5 Hz sensitized R_L values range from 3.37 cmH₂O/ml/s for 200 mV treatments up to a high of 5.29 cmH₂O/ml/s with ACh challenge. The lowest pulmonary resistance value for sensitized subjects was achieved from the 1.6 cmH₂O SIPO set, which was also comparable to ISO treatment. Healthy group R_L values range from 1.66 cmH₂O/ml/s for ISO treatments up to a high of 2.06 cmH₂O/ml/s with ACh challenge. The lowest

pulmonary resistance value for healthy subjects was achieved from the ISO and 3.6 cmH₂O SIPO sets.

Table 5.5. 5 Hz experimental data set for R_L evaluation of sensitized and healthy subjects. 5 Hz-generated waveforms combined with indicated amplitudes produce the applied SIPO treatment (cmH₂O). Results include ACh and ISO comparison values and are presented as R_L ± SE (cmH₂O/ml/s).

	Sensitized	Healthy
Experimental condition	R _L , cmH ₂ O/ml/s	
ACh (10 ⁻⁴ M)	5.29 ± 0.42	2.06 ± 0.08
5 Hz/100 mV (0.8 cmH ₂ O)	4.14 ± 0.33	1.93 ± 0.11
5 Hz/200 mV (1.6 cmH ₂ O)	3.37 ± 0.14	1.99 ± 0.08
5 Hz/300 mV (2.6 cmH ₂ O)	4.26 ± 0.09	1.93 ± 0.08
5 Hz/400 mV (3.6 cmH ₂ O)	4.00 ± 0.24	1.71 ± 0.08
ISO (10 ⁻⁶ M)	3.46 ± 0.24	1.66 ± 0.10

Table 5.6 contains the R_L experimental data obtained from the set of 10 Hz-derived SIPO treatments of healthy and sensitized subjects. Conditions are described both as Hz/mV combinations and corresponding physiological pressures. The 10 Hz data set consists of pressures derived from 10 Hz in combination with amplitudes of 100 - 400 mV, which are equivalent to 0.7, 1.5, 2.4, and 3.3 cmH₂O respectively. Experimental results for ACh and ISO conditions are also presented.

The 10 Hz sensitized R_L values range from 2.97 cmH₂O/ml/s for 100 mV treatments up to a high of 5.29 cmH₂O/ml/s with ACh challenge. The lowest pulmonary resistance

value for sensitized subjects was achieved from the 0.7 cmH₂O SIPO set. Healthy group R_L values range from 1.66 cmH₂O/ml/s for ISO treatments (comparable to 100 and 300 mV treatments) up to a high of 2.06 cmH₂O/ml/s with ACh challenge, which is also comparable to the 1.5 and 3.3 cmH₂O SIPO sets. The lowest pulmonary resistance value for healthy subjects was achieved from the ISO, 0.7, and 2.4 cmH₂O SIPO sets.

Table 5.6. 10 Hz experimental data set for R_L evaluation of sensitized and healthy subjects. 10 Hz-generated waveforms combined with indicated amplitudes produce the applied SIPO treatment (cmH₂O). Results include ACh and ISO comparison values and are presented as R_L ± SE (cmH₂O/ml/s).

	Sensitized	Healthy
Experimental condition	R _L , cmH ₂ O/ml/s	
ACh (10 ⁻⁴ M)	5.29 ± 0.42	2.06 ± 0.08
10 Hz/100 mV (0.7 cmH ₂ O)	2.97 ± 0.04	1.83 ± 0.10
10 Hz/200 mV (1.5 cmH ₂ O)	3.51 ± 0.03	2.05 ± 0.10
10 Hz/300 mV (2.4 cmH ₂ O)	3.37 ± 0.16	1.79 ± 0.08
10 Hz/400 mV (3.3 cmH ₂ O)	4.07 ± 0.17	1.90 ± 0.05
ISO (10 ⁻⁶ M)	3.46 ± 0.24	1.66 ± 0.10

Table 5.7 contains the R_L experimental data obtained from the set of 15 Hz-derived SIPO treatments of healthy and sensitized subjects. Conditions are described both as Hz/mV combinations and corresponding physiological pressures. The 15 Hz data set consists of pressures derived from 15 Hz in combination with amplitudes of 100 - 400 mV, which are equivalent to 0.4, 1.1, 1.7, and 2.4 cmH₂O respectively. Experimental results for ACh and ISO conditions are also presented.

Table 5.7. 15 Hz experimental data set for R_L evaluation of sensitized and healthy subjects. 15 Hz-generated waveforms combined with indicated amplitudes produce the applied SIPO treatment (cmH₂O). Results include ACh and ISO comparison values and are presented as $R_L \pm SE$ (cmH₂O/ml/s).

	Sensitized	Healthy
Experimental condition	R_L , cmH ₂ O/ml/s	
ACh (10^{-4} M)	5.29 ± 0.42	2.06 ± 0.08
15 Hz/100 mV (0.4 cmH ₂ O)	4.31 ± 0.17	1.95 ± 0.06
15 Hz/200 mV (1.1 cmH ₂ O)	3.41 ± 0.30	2.03 ± 0.12
15 Hz/300 mV (1.7 cmH ₂ O)	2.72 ± 0.22	1.78 ± 0.10
15 Hz/400 mV (2.4 cmH ₂ O)	3.37 ± 0.16	1.84 ± 0.09
ISO (10^{-6} M)	3.46 ± 0.24	1.66 ± 0.10

The 15 Hz sensitized R_L values range from 2.72 cmH₂O/ml/s for 300 mV treatments up to a high of 5.29 cmH₂O/ml/s with ACh challenge. The lowest pulmonary resistance value for sensitized subjects was achieved from the 1.7 cmH₂O SIPO set. Healthy group R_L values range from a low of 1.66 cmH₂O/ml/s for ISO treatments (comparable to 300 and 400 mV treatments) up to a high of 2.06 cmH₂O/ml/s with ACh challenge, which is also comparable to the 0.4, 1.1, and 2.4 cmH₂O SIPO sets. The lowest pulmonary resistance values for healthy subjects was achieved from the ISO, 1.7, and 2.4 cmH₂O SIPO sets. The standard error calculation from 2.4 cmH₂O SIPO treatments is enough to overlap low and high R_L values in the narrow range of healthy subjects' data.

Table 5.8 contains the R_L experimental data obtained from the set of 20 Hz-derived SIPO treatments of healthy and sensitized subjects. Conditions are described both as Hz/mV combinations and corresponding physiological pressures. The 20 Hz data set consists of

pressures derived from 20 Hz in combination with amplitudes of 100 - 400 mV, which are equivalent to 0.4, 1.1, 1.7, and 2.3 cmH₂O respectively. Experimental results for ACh and ISO conditions are also presented.

Table 5.8. 20 Hz experimental data set for R_L evaluation of sensitized and healthy subjects. 20 Hz-generated waveforms combined with indicated amplitudes produce the applied SIPO treatment (cmH₂O). Results include ACh and ISO comparison values and are presented as R_L ± SE (cmH₂O/ml/s).

	Sensitized	Healthy
Experimental condition	R _L , cmH ₂ O/ml/s	
ACh (10 ⁻⁴ M)	5.29 ± 0.42	2.06 ± 0.08
20 Hz/100 mV (0.4 cmH ₂ O)	3.63 ± 0.15	1.82 ± 0.06
20 Hz/200 mV (1.1 cmH ₂ O)	3.35 ± 0.31	2.10 ± 0.12
20 Hz/300 mV (1.7 cmH ₂ O)	2.09 ± 0.07	1.89 ± 0.10
20 Hz/400 mV (2.3 cmH ₂ O)	3.19 ± 0.16	2.00 ± 0.06
ISO (10 ⁻⁶ M)	3.46 ± 0.24	1.66 ± 0.10

The 20 Hz sensitized R_L values range from 2.09 cmH₂O/ml/s for 300 mV treatments up to a high of 5.29 cmH₂O/ml/s with ACh challenge. The lowest pulmonary resistance value for sensitized subjects was achieved from the 1.7 cmH₂O SIPO set. Healthy group R_L values range from a low of 1.66 cmH₂O/ml/s for ISO treatments (comparable to 100 mV treatments) up to a high of 2.10 cmH₂O/ml/s from the 1.1 cmH₂O SIPO set, which is also comparable to ACh, 300 and 400 mV treatments. The lowest pulmonary resistance values for healthy subjects was achieved from the ISO and 0.4 cmH₂O SIPO sets.

5.4. Discussion

The means for R_L were obtained for healthy and sensitized mice treated with ACh, compared, and yielded significant differences in the diseased response to ACh. A mean R_L of 2.06 ± 0.08 and 5.29 ± 0.42 cmH₂O/ml/s for healthy and sensitized subjects respectively, indicates the R_L of sensitized mice was 157 % higher than healthy mice. Analysis showed a significant increase in the sensitized group's response to the bronchoconstrictor (p value < 0.05), providing evidence for the presence of AHR in the airways of the sensitized mice. Percent-increase values were calculated by dividing the ($n=7$) differences of sensitized and healthy R_L by the healthy R_L , and multiplying this value by 100 (Eqn. 5.2).

$$\% \text{ Increase} = 100 \times \left[\frac{R_{L,\text{sensitized}} - R_{L,\text{healthy}}}{R_{L,\text{healthy}}} \right]_{\text{ACh or ISO}} \quad (\text{Eqn. 5.2})$$

Differences in the R_L response to ISO (following ACh treatment) were also observed, with mean R_L values of 1.66 ± 0.10 and 3.46 ± 0.24 cmH₂O/ml/s for healthy and sensitized subjects respectively. Calculations of percent R_L improvement (as a result of ISO treatment) indicate that sensitized R_L decreased 35 % from its value at 5.29 cmH₂O/ml/s, while healthy R_L decreased 20 % from its peak at 2.06 cmH₂O/ml/s. ISO treatment serves as a reference for the ability of the tested airway in this model to undergo bronchorelaxation following a mimicked asthmatic attack. The range of R_L values from ACh to ISO in healthy subjects is 0.40 cmH₂O/ml/s, and in sensitized subjects, this range is greater, at 1.83 cmH₂O/ml/s. The larger range of pulmonary resistance in sensitized airways initially indicates that the airway tissue is responding to the chemical bronchorelaxant treatment (with lower R_L values) more effectively than the healthy

airway tissue. Comparison of SIPO treatments against these ACh and ISO reference values is a benchmark for efficacy of the challenges in this study.

In all cases for the study, healthy respiratory rate values are significantly higher than sensitized respiratory rate values, except for the sensitized respiratory rate associated with SIPO treatment of 5 Hz / 100 mV (0.8 cmH₂O). At this treatment there is no significance between measured healthy and sensitized respiratory rates. Unexpectedly, ACh challenge is not always responsible for the lowest respiratory rate, and ISO is not always responsible for the highest respiratory rate. Each of these reference parameters for the study are not the sole reasons for bronchoconstriction eliciting low respiratory rates or bronchorelaxation affecting higher respiratory rates. SIPO treatments are also responsible for changes in respiratory rates of healthy and sensitized mice, but due to the larger SE values in sensitized mice, the observations and measurements are not significant. Despite the initial lack of significance in the respiratory rate data however, further work in analysing the breathing cycles could lead to valuable respiratory information. For example, the lower respiratory rates (along with larger tidal volumes) in sensitized mice is evidence of the greater effort they must make to breath. This evidence in sensitized respiratory rate data indicates a change in respiratory processes to compensate for likely physical changes in the sensitized airways that are responsible for higher values of R_L measured through the study.

Application of the 5 Hz-generated SIPO waveforms resulted in significant decrease in the R_L of the sensitized airway for all treatments. The most significant decrease (36 %) was found in the 1.6 cmH₂O set, where the resistance was akin to treatment with ISO. The remaining three treatments (0.8, 2.6, and 3.6 cmH₂O) were comparable to each other, and while still significantly lower than ACh, none of the treatments was equivalent to ISO.

In healthy airways treated with the 5 Hz-generated waveforms, only the 3.6 cmH₂O set of R_L values was significantly lower than ACh; the group was also comparable to ISO, but not significantly different. Applications of 0.8, 1.6, and 2.6 cmH₂O to healthy airways were not significant improvements from R_L values associated with ACh. Figure 5.1 provides the R_L data plots of the 5 Hz-generated SIPO waveform applications, indicating the higher resistance in all sensitized groups compared to healthy groups. The trend for healthy airways to respond similarly to the ACh is also indicated. There is less effect on the magnitude of the resistance in healthy airways compared to the sensitized airways.

Application of the 10 Hz-generated SIPO waveforms also resulted in significant decrease in the R_L of the sensitized airway for all treatments, especially when using an amplitude of 100 mV. The most significant decrease (44 %) was found in the 0.7 cmH₂O set, where the resistance was significantly lower than ISO. The remaining three treatments (1.5, 2.4, and 3.3 cmH₂O) were significantly lower than ACh, with the first two groups comparable to ISO, and the 3.3 cmH₂O set still significantly higher than R_L values of ISO.

In healthy airways treated with the 10 Hz-generated waveforms, three of the treatments (0.7, 2.4, and 3.3 cmH₂O) were significantly lower than ACh; 0.7 and 2.4 cmH₂O sets were also comparable to ISO, but not significantly different. Notably, the 10 Hz / 200 mV (1.5 cmH₂O) treatment of healthy airways showed no improvement in R_L compared to ACh values. Figure 5.2 provides the R_L data plots of the 10 Hz-generated SIPO waveform applications, indicating the higher resistance in all sensitized groups compared to healthy groups, as well as the greater differences in sensitized R_L values response to SIPO treatments when compared to ACh treatment. The trend for healthy airways to respond in a closer-grouped set of R_L values is also indicated. There is less effect on the

decrease in the magnitude of the resistance in healthy airways compared to the sensitized airways.

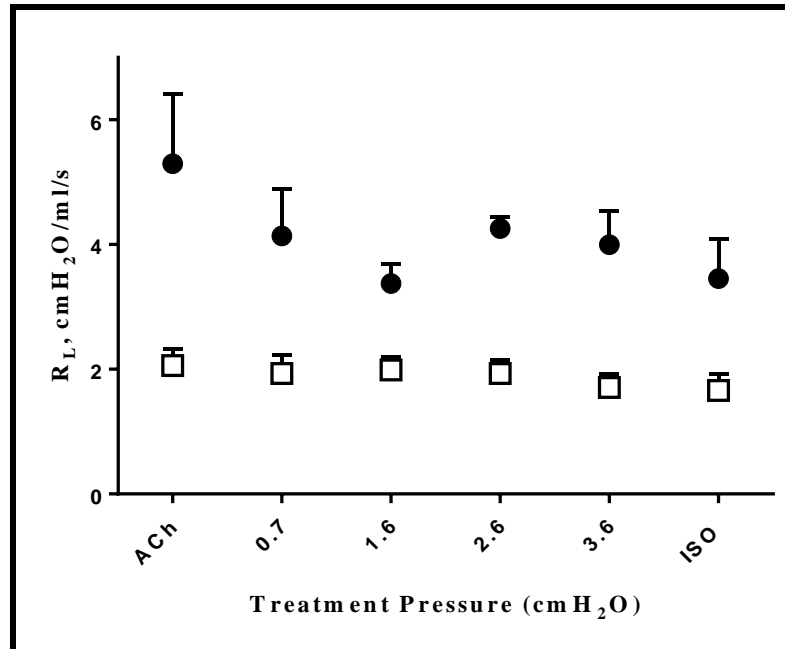


Figure 5.1. Treatment values of R_L (expressed as $\text{cmH}_2\text{O}/\text{ml/s}$) from applications of 5 Hz-generated SIPO waveform set with amplitudes in the range of 100 – 400 mV (0.8 – 3.6 cmH_2O). Experimental conditions are presented along the x-axis, with ACh and ISO as comparisons (\square = healthy; \bullet = sensitized; $n=7$ for all data points except sensitized SIPOs, $n=5$).

Application of the 15 Hz-generated SIPO waveforms resulted in significant decreases in the R_L of the sensitized airway for all treatments, especially when using an amplitude of 300 mV. The most significant decrease (48 %) was found in the 1.7 cmH_2O set, where the resistance was significantly lower than ISO. The remaining three treatments (0.4, 1.1, and 2.4 cmH_2O) were significantly lower than ACh, with the initial group (0.4 cmH_2O) having the smallest percentage (18 %) of improved R_L below ACh values. Both 1.1 and 2.4 cmH_2O sets were statistically comparable to each other and to ISO, but not significantly better than ISO.

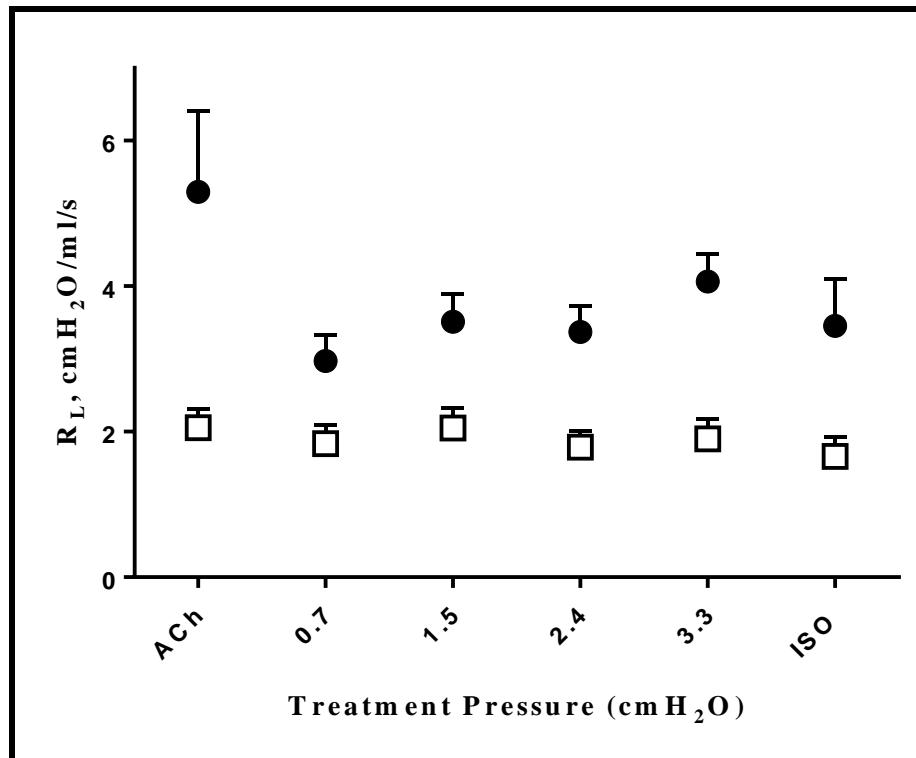


Figure 5.2. Treatment values of R_L (expressed as $\text{cmH}_2\text{O}/\text{ml/s}$) from applications of 10 Hz-generated SIPO waveform set with amplitudes in the range of 100 – 400 mV (0.7 – 3.3 cmH_2O). Experimental conditions are presented along the x-axis, with ACh and ISO as comparisons (\square = healthy; \bullet = sensitized; $n=7$ for all data points except sensitized SIPOs, $n=5$).

In healthy airways treated with the 15 Hz-generated waveforms, two of the treatments (amplitudes of 300 and 400 mV) had significantly lower R_L values than ACh; these 1.7 and 2.4 cmH_2O treatments were comparable to ISO, without significant differences in their resistance values. Notably, two of the treatments, 15 Hz/100 mV (0.4 cmH_2O) and 15 Hz/200 mV (1.1 cmH_2O) had no significant relaxation below ACh treatment R_L values. Figure 5.3 provides the R_L data plots of the 15 Hz-generated SIPO waveform applications, indicating the higher resistance in all sensitized groups compared to healthy groups, as well as the greater differences in sensitized R_L values' responses to SIPO treatments when compared to ACh treatment. The trend for healthy airways to respond in a closer-grouped set of R_L values is also evident. There is less effect on the decrease in the magnitude of the resistance in healthy airways compared to the sensitized airways.

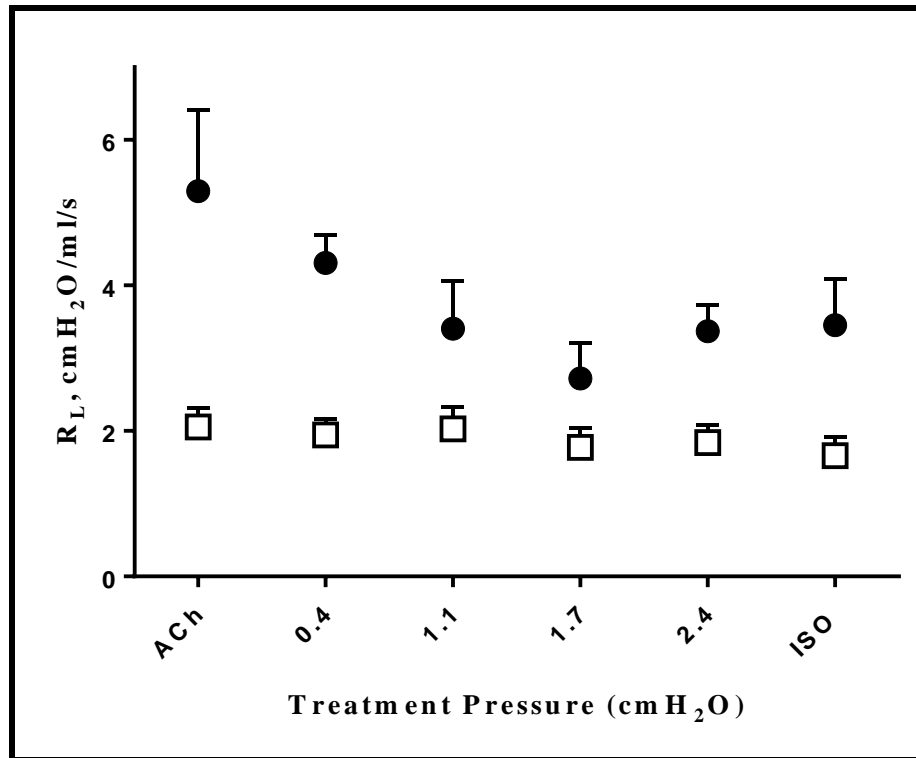


Figure 5.3. Treatment values of R_L (expressed as $\text{cmH}_2\text{O}/\text{ml/s}$) from applications of 15 Hz-generated SIPO waveform set with amplitudes in the range of 100 – 400 mV (0.4 – 2.4 cmH_2O). Experimental conditions are presented along the x-axis, with ACh and ISO as comparisons (\square = healthy; \bullet = sensitized; $n=7$ for all data points except sensitized SIPOs, $n=5$).

Application of the 20 Hz-generated SIPO waveforms resulted in significant decreases in the R_L of the sensitized airway for all treatments, and the group also contains the greatest relaxation values (the 300 mV set) from among all of the 19 distinct treatments in the study. SIPO treatments defined by 20 Hz/300mV (1.7 cmH_2O) had a mean $R_L = 2.09$ $\text{cmH}_2\text{O}/\text{ml/s}$, equivalent to a 60 % reduction in R_L values of ACh treatment. The remaining three treatments (0.4, 1.1, and 2.3 cmH_2O) had significantly lower R_L values than ACh, with all sets' R_L values comparable to ISO, though none of them are significantly different from the reference treatment. Of note, 0.4 and 2.3 cmH_2O sets are significantly different from each other in the sensitized airway tests, with the lower SIPO

application resulting in a 31 % decrease of R_L compared to the ACh value, and the latter of the two sets eliciting a 40 % decrease.

In healthy airways treated with the 20 Hz-generated waveforms, only a single treatment (amplitude of 100 mV) had a significantly lower R_L than ACh; the 0.4 cmH₂O set was also slightly less effective at lowering the airway resistance than ISO (12 % versus 19 %). Three of the treatments to healthy airways, 20 Hz/200 mV (1.1 cmH₂O), 20 Hz/300 mV (1.7 cmH₂O), and 20 Hz/400 mV (2.3 cmH₂O) had no significant relaxation below R_L values of ACh treatment. In fact, the response of the airways to 1.1 cmH₂O was non-significantly greater than the R_L of ACh treatment. Figure 5.4 provides the R_L data plots of the 20 Hz-generated SIPO waveform applications, indicating the higher resistance in all sensitized groups compared to healthy groups, as well as the greater differences in sensitized R_L values' responses to SIPO treatments when compared to ACh treatment. The trend for healthy airways to respond in a closer-grouped set of R_L values is also evident. There is less effect on the decrease in the magnitude of the resistance in healthy airways compared to the sensitized airways.

Results discussed in this chapter indicate that airways from sensitized mice are significantly more reactive to ACh (10^{-4} M) bronchoconstrictor treatment (as shown in higher R_L values) than those airways tested in healthy mice. This reactivity is a main feature associated with human asthma, and is known as airway hyper-responsiveness [51, 89, 102, 103]. Additionally, applications of superimposed pressure waves over spontaneous breathing have a bronchorelaxant effect in sensitized mice, more so in fact than in healthy mice. This relaxant effect is manifest in the significant decrease of R_L in all 16 SIPO treatments of sensitized mice compared to the ACh treatment, whereas

healthy mice respond (following ACh treatment) with significant reduction in R_L in 7 of the 16 SIPO treatments.

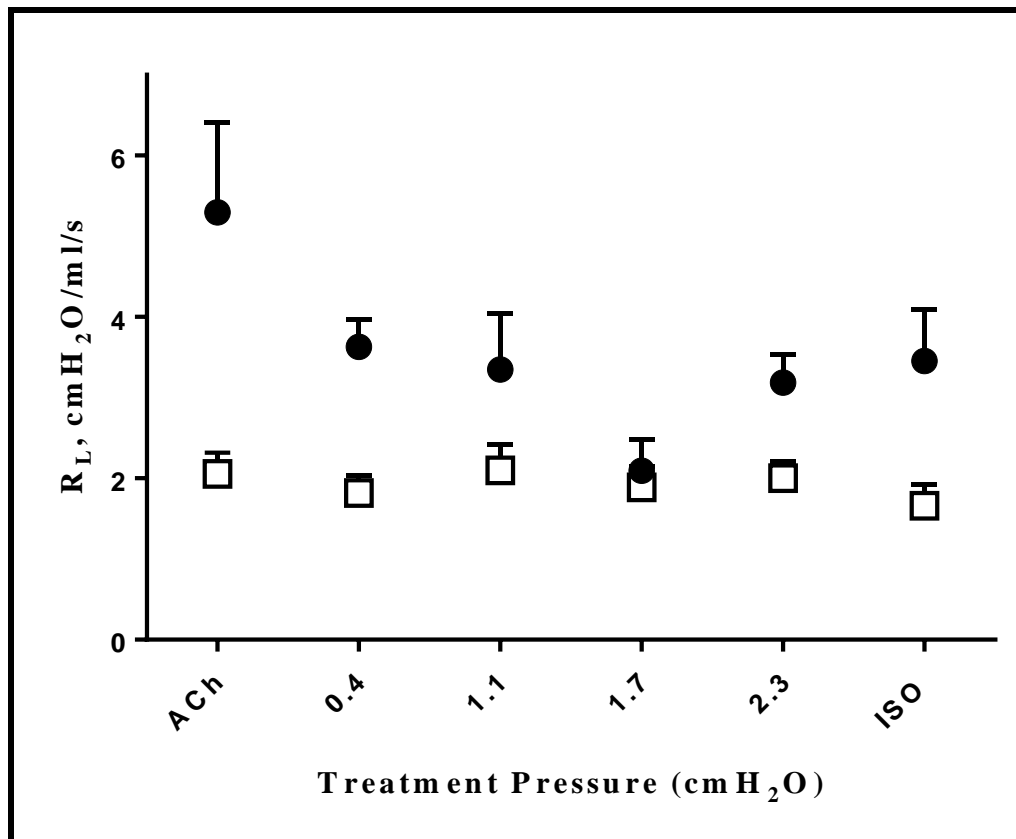


Figure 5.4. Treatment values of R_L (expressed as $\text{cmH}_2\text{O}/\text{ml/s}$) from applications of 20 Hz-generated SIPO waveform set with amplitudes in the range of 100 – 400 mV (0.4 – 2.3 cmH_2O). Experimental conditions are presented along the x-axis, with ACh and ISO as comparisons (\square = healthy; \bullet = sensitized; $n=7$ for all data points except sensitized SIPOs, $n=5$).

In treatments applied to sensitized mice, 11 are comparable to/better than ISO at relaxing the airways following ACh treatment. Of these 11 SIPO values, 3 have significantly lower R_L than ISO. In treatments of healthy mice, 6 SIPO values elicit comparable R_L values to ISO, and none of these are significantly lower than the chemical bronchorelaxant. A general trend is observed for the effectiveness of applied pressure oscillations when viewing the analyses in the context of frequency, amplitude, or physiological pressure (cmH_2O) sets across the sensitized data. The most significant (and consistent) reductions of R_L occur at the applied treatment pressure of approximately 1.7

cmH₂O. All other SIPO applications in sensitized mice, greater than (and less than) the 1.7 cmH₂O data set do not reduce R_L with the same effect. This trend does not occur in data for healthy mice. Within the healthy groups treated with the same SIPO values, there are different trends in the R_L values' outcomes.

Healthy subjects treated with ACh respond best (present greatest bronchorelaxation) when SIPO treatment values are not 1.7 cmH₂O. In fact, healthy mice treated with 1.5, 1.6, and 1.7 cmH₂O (from 5-, 10-, and 20 Hz-generated groups) responded with statistically equivalent R_L values relative to ACh treatment, which is contrary to the observed effect in sensitized airways. (The healthy mouse treatment using the SIPO value generated from 15 Hz / 300 mV (1.7 cmH₂O) was the exception to the trend, with lower R_L than the ACh treatment.) In healthy mice, the greatest number of significant reductions occurs at the higher and lower applied pressure oscillations: 0.4, 0.7, 2.4, and 3.6 cmH₂O are all associated with greater benefits to the airways following ACh treatment.

5.5. Summary

The results presented in this chapter are a partial fulfilment of this study's objective to assess the respiratory parameters of healthy and sensitized mice in a chronic model of asthma. Analysis of R_L values obtained for ACh, ISO, and SIPO treatments has indicated the presence (and treatment-dependent decrease) of AHR in sensitized mice as well as changes in respiratory responses in the airways of healthy mice. Applications of bronchorelaxant methods in the form of SIPO treatments improve respiratory conditions

of both healthy and sensitized mice in terms of decreasing pulmonary resistance caused by ACh exposure. Greater numbers of statistically significant decreases in R_L are found in sensitized mice compared to healthy mice. Both healthy and sensitized mice respond most favourably to SIPO sets from distinct ranges of pressures, indicating that diseased and healthy airways respond to similar treatments in different fashions. Stated another way, the response of airway tissues' pulmonary resistance to SIPO treatments has at least a partial dependence on the state of health or disease in the mouse.

CHAPTER VI

Dynamic compliance in healthy and chronic sensitized mice

6.1. Introduction

In keeping with the study's primary objective of investigating the effects of pressure oscillations on measured bronchoconstrictive parameters, this chapter builds on the R_L analyses of Chapter V, and initially summarizes the *in vivo* experimental methodology to obtain values for C_{dyn} . Notably, the parameters for both R_L and C_{dyn} are measured at the same time, and so while the overall methodology remains largely constant, there are raw data differences which emerge for C_{dyn} calculations compared to R_L . Rather than place the narrative for all resistance and compliance in a single chapter, separation of the two diagnostic markers allows for greater clarity in the presentation of two simultaneously observed events. Combinations of chemical challenges and applied pressure oscillations are briefly reviewed for their parts in obtaining values for C_{dyn} . Spontaneous breathing responses of healthy and chronically-sensitized airways to superimposed pressure oscillations are measured using the equipment detailed in Chapter IV. Finally, the experimental results for healthy and sensitized mouse data along with their statistical analyses and discussion points conclude the chapter.

6.2. Method

The respiratory challenges using saline, ACh, ISO, and superimposed airway pressure applications which were previously described for R_L measurements also measure raw data points which calculate values of C_{dyn} . The treatments provide data sets relative to an established healthy baseline condition. As with R_L methodology, the combinations of

chemical solutions and superimposed pressures are described in detail in the General Methods of Chapter III and further in Section 4.7 and Appendix C.

Briefly, each set of respiratory challenges is separated from any other test by a rest period, where no manipulations are carried out. Every test begins with a normal saline challenge, a 1-min rest period, and (1-min) ACh challenge. Every test is then completed with either an ISO challenge or application of a superimposed pressure oscillation. (The order in which the ISO or oscillation challenge is applied to a given study animal is from a randomized list in order to ensure that linear progression through the applied pressures is avoided.) A 2-min rest period separates the end of one test from the start of the next test. Testing for any subject gathers parametric values of T_v and P_{tp} , and is concluded when any of the respiratory parameters associated with calculating C_{dyn} (Eqn. 2.2) do not recover from zero (terminal) values.

6.2.1 *Statistical analysis*

As mentioned in Chapter V (R_L results), GraphPad is the ideal platform for analysis of results in this study and is also utilized for this chapter's C_{dyn} results. Descriptions of the software tools, reasons for comparisons of data sets, and descriptions of analysis groups are as previously represented in Section 5.4. Also consistent with Chapter V, ACh and ISO treatment data are presented for comparison throughout the results and analyses. Results of the analyses are expressed as mean \pm SE for each of the C_{dyn} respiratory parameters presented. The primary method of discussing the analysed data is in terms of frequency-based groups. Additional mention of groups determined by either amplitude- or pressure-based experimental conditions further reveals the trends of SIPO-related bronchorelaxation in this sensitized model.

6.3. Results

Experimental data points for the dynamic compliance respiratory parameters were recorded in real time using Labchart 7.0 software. As described in Chapter IV, Labchart (in conjunction with Powerlab) measures several signals directly from channels 1-7 of the acquisition system, which are then converted to physiological values. For calculations of C_{dyn} , values of T_v and P_{tp} are used. Channels 8 and 9 of the software incorporate signal data from channels 1-7. Calculations for C_{dyn} are made in the software by using the equation (Eqn. 2.2) that utilises raw data of T_v and P_{tp} signals. Respiratory rate values are again cited in this chapter's tables, along with tidal volume and applicable pressure data. Additional indirect calculations of C_{dyn} (as per Eqn. 6.1) were carried out independent of the automated internal software signal processing, using the values for T_v and selected pressure readings.

$$C_{dyn} = \frac{T_v}{(PIP-PEEP)} \quad (\text{Eqn. 6.1})$$

The preferred C_{dyn} calculation of Eqn. 6.1 utilizes the PIP value, measured in real-time with the Labchart/Powerlab setup, as well as PEEP values. These two pressure terms are preferred over the transpulmonary pressure for calculating values of C_{dyn} in order to more accurately represent the work required to overcome airway resistance in the breathing process. PEEP measures are defined by the applied oscillation pressures of each experimental condition, and together with PIP values from the software, were substituted into the C_{dyn} equation as applicable, in lieu of P_{tp} signal values.

6.3.1 Raw data measurements

Summary data tables of healthy and sensitized subjects' means for T_v , (PIP-PEEP), and respiratory rate values are presented below according to Hz-generated pressure sets.

Standard error values are excluded in these tables. Tables for 5, 10, 15, and 20 Hz-generated pressure sets also include saline, ACh, and ISO data for comparisons. Units for each measurement category are provided. Respiratory rates are measured as breaths/min. All mean values for healthy and sensitized data are from $n = 7$, except for sensitized SIPO data, where $n = 5$.

The 5 Hz healthy group tidal volumes range from 0.12 ml for ISO up to a high of 0.38 ml at SIPO treatment of 1.6 cmH₂O. (PIP – PEEP) values from 2.71 (ISO) – 3.32 (ACh) cmH₂O were calculated, and the subjects’ respiratory rates across the treatments are highest (211 breaths/min) for the 100 mV treatment, with the lowest rate (173 breaths/min) coming from the ISO group. Sensitized tidal volumes range from 0.67 ml for ACh treatments up to a high of 1.04 ml at SIPO treatment of 2.6 cmH₂O. Sensitized (PIP – PEEP) values from 8.22 (ACh) – 5.43 (200 mV) cmH₂O were calculated, and the subjects’ respiratory rates across the treatments are highest (199 breaths/min) for the 100 mV treatment, with the lowest rate (138 breaths/min) coming from the 300 mV group.

Table 6.1. Summary table of Healthy and Sensitized Groups’ tidal volume (Tv), (PIP – PEEP), and respiratory rate (rr) responses from applied pressure oscillations in the 5 Hz-generated set. Data obtained from Saline, ACh, and ISO treatments are presented along with the data responses from the four physiological pressures (0.8 – 3.6 cmH₂O) that comprise the set.

5 Hz-generated Pressure Set							
Healthy Group				Sensitized Group			
	Tv, ml	(PIP-PEEP), cmH ₂ O	rr, bpm		Tv, ml	(PIP-PEEP), cmH ₂ O	rr, bpm
Saline	0.23	3.22	188	Saline	0.79	5.45	148
ACh	0.23	3.32	196	ACh	0.67	8.22	160
0.8	0.20	3.14	211	0.8	0.71	7.02	199
1.6	0.38	3.27	192	1.6	0.80	5.43	156
2.6	0.32	3.13	190	2.6	1.04	7.11	138
3.6	0.30	2.79	195	3.6	0.72	6.34	156
ISO	0.12	2.71	173	ISO	0.83	5.53	177

The 10 Hz healthy group tidal volumes range from 0.12 ml for ISO up to a high of 0.41 ml at SIPO treatment of 3.3 cmH₂O. (PIP – PEEP) values from 2.71 (ISO) – 3.37 (200 mV) cmH₂O were calculated, and the subjects’ respiratory rates across the treatments are highest (206 breaths/min) for the 300 mV treatment, with the lowest rate (173 breaths/min) coming from the ISO group. Sensitized tidal volumes range from 0.67 ml for ACh treatments up to a high of 0.83 ml (ISO). Sensitized (PIP – PEEP) values from 8.22 (ACh) – 5.47 (300 mV) cmH₂O were calculated, and the subjects’ respiratory rates across the treatments are highest (177 breaths/min) for the ISO treatment, with the two lowest rates (148 and 147 breaths/min) coming from the 200 and 300 mV groups respectively.

Table 6.2. Summary table of Healthy and Sensitized Groups’ tidal volume (Tv), (PIP – PEEP), and respiratory rate (rr) responses from applied pressure oscillations in the 10 Hz-generated set. Data obtained from Saline, ACh, and ISO treatments are presented along with the data responses from the four physiological pressures (0.7 – 3.3 cmH₂O) that comprise the set.

10 Hz-generated Pressure Set							
Healthy Group				Sensitized Group			
	Tv, ml	(PIP-PEEP), cmH ₂ O	rr, bpm		Tv, ml	(PIP-PEEP), cmH ₂ O	rr, bpm
Saline	0.23	3.22	188	Saline	0.79	5.45	148
ACh	0.23	3.32	195	ACh	0.67	8.22	160
0.7	0.35	3.00	200	0.7	0.78	4.76	165
1.5	0.35	3.37	191	1.5	0.77	5.52	148
2.4	0.40	2.96	206	2.4	0.72	5.47	147
3.3	0.41	3.06	197	3.3	0.74	6.60	166
ISO	0.12	2.71	173	ISO	0.83	5.53	177

The 15 Hz healthy group tidal volumes range from 0.12 ml for ISO up to a high of 0.46 ml at SIPO treatment of 2.4 cmH₂O. (PIP – PEEP) values from 2.71 (ISO) – 3.32 (ACh)

cmH₂O were calculated, and the subjects' respiratory rates across the treatments are highest (205 breaths/min) for the 100 mV treatment, with the lowest rate (173 breaths/min) coming from the ISO group. Sensitized tidal volumes range from 0.67 ml for ACh treatments up to a high of 0.83 ml (ISO). The 200 mV treatment set was also comparable to this Tv with a volume of 0.82 ml. Sensitized (PIP – PEEP) values from 8.22 (ACh) – 4.47 (300 mV) cmH₂O were calculated, and the subjects' respiratory rates across the treatments are highest (177 breaths/min) for the 100 mV and ISO treatments, with the lowest rate (144 breaths/min) coming from the 200 mV group.

Table 6.3. Summary table of Healthy and Sensitized Groups' tidal volume (Tv), (PIP – PEEP), and respiratory rate (rr) responses from applied pressure oscillations in the 15 Hz-generated set. Data obtained from Saline, ACh, and ISO treatments are presented along with the data responses from the four physiological pressures (0.4 – 2.4 cmH₂O) that comprise the set.

15 Hz-generated Pressure Set							
Healthy Group				Sensitized Group			
	Tv, ml	(PIP-PEEP), cmH ₂ O	rr, bpm		Tv, ml	(PIP-PEEP), cmH ₂ O	rr, bpm
Saline	0.23	3.22	188	Saline	0.79	5.45	148
ACh	0.23	3.32	195	ACh	0.67	8.22	160
0.4	0.32	3.14	205	0.4	0.76	7.24	177
1.1	0.39	3.27	197	1.1	0.82	5.26	144
1.7	0.43	2.86	178	1.7	0.76	4.47	169
2.4	0.46	2.96	185	2.4	0.72	5.47	157
ISO	0.12	2.71	173	ISO	0.83	5.53	177

The 15 Hz healthy group tidal volumes range from 0.12 ml for ISO up to a high of 0.46 ml at SIPO treatment of 2.4 cmH₂O. (PIP – PEEP) values from 2.71 (ISO) – 3.32 (ACh) cmH₂O were calculated, and the subjects' respiratory rates across the treatments are highest (205 breaths/min) for the 100 mV treatment, with the lowest rate (173

breaths/min) coming from the ISO group. Sensitized tidal volumes range from 0.67 ml for ACh treatments up to a high of 0.83 ml (ISO). The 200 mV treatment set was also comparable to this Tv with a volume of 0.82 ml. Sensitized (PIP – PEEP) values from 8.22 (ACh) – 4.47 (300 mV) cmH₂O were calculated, and the subjects’ respiratory rates across the treatments are highest (177 breaths/min) for the 100 mV and ISO treatments, with the lowest rate (144 breaths/min) coming from the 200 mV group.

Table 6.4. Summary table of Healthy and Sensitized Groups’ tidal volume (Tv), (PIP – PEEP), and respiratory rate (rr) responses from applied pressure oscillations in the 20 Hz-generated set. Data obtained from Saline, ACh, and ISO treatments are presented along with the data responses from the four physiological pressures (0.4 – 2.3 cmH₂O) that comprise the set.

20 Hz-generated Pressure Set							
Healthy Group				Sensitized Group			
	Tv, ml	(PIP-PEEP), cmH ₂ O	rr, bpm		Tv, ml	(PIP-PEEP), cmH ₂ O	rr, bpm
Saline	0.23	3.22	188	Saline	0.79	5.45	148
ACh	0.23	3.32	195	ACh	0.67	8.22	160
0.4	0.36	2.94	204	0.4	0.78	5.90	144
1.1	0.53	3.39	186	1.1	0.78	5.35	154
1.7	0.30	3.10	190	1.7	0.78	5.08	150
2.3	0.33	3.25	195	2.3	0.68	5.11	167
ISO	0.12	2.71	173	ISO	0.83	5.53	177

The 20 Hz healthy group tidal volumes range from 0.12 ml for ISO up to a high of 0.53 ml (200 mV) where the SIPO treatment is 2.4 cmH₂O. (PIP – PEEP) values from 2.71 (ISO) – 3.39 (200 mV) cmH₂O were calculated, and the subjects’ respiratory rates across the treatments are highest (204 breaths/min) for the 100 mV treatment, with the lowest rate (173 breaths/min) coming from the ISO group. Sensitized tidal volumes range from 0.67 ml for ACh treatments (along with a comparable 0.68ml (400 mV treatment)) up to

a high of 0.83 ml (ISO). Sensitized (PIP – PEEP) values from 8.22 (ACh) – 5.08 (300 mV) cmH₂O were calculated, and the subjects' respiratory rates across the treatments are highest (177 breaths/min) for the 100 mV and ISO treatments, with the lowest rate (144 breaths/min) coming from the 100 mV group.

6.3.2. *C_{dyn} measurements*

C_{dyn} values are relative indicators of airway tissue facilitating the process of breathing. The dynamic compliance of the airway is critical to inspirations and expirations of the spontaneously breathing subjects in this study and is indicative of the ability of pulmonary tissue to move volumes of air in response to applied pressures. The established values of C_{dyn} for ACh challenges and ISO treatments serve as standards of bronchoconstriction and bronchorelaxation to gauge the efficacy of applied pressure oscillations across the range of tested healthy and sensitized subjects.

The raw data from Tables 6.1 – 6.4 are the values used for calculating C_{dyn} information for this study. C_{dyn} values are presented in Tables 6.5 – 6.8 in this section and are expressed as the mean \pm SE for each given condition. Units of measurement for the raw data and for C_{dyn} are expressed differently once the quotient from Eqn. 6.1 is calculated. Units change from ml/cmH₂O in raw data to μ l/mmH₂O for C_{dyn} , as changing the orders of magnitude removes leading zeros from the data points. Tables provide the summary of experimental data from applications of ACh, ISO, and SIPO treatments in healthy and sensitized mice. SIPO values are grouped within each table according to frequency, amplitude, and the generated physiological pressure (cmH₂O) sets in order to effectively present results.

Table 6.5 contains the C_{dyn} experimental data obtained from the set of 5 Hz-derived SIPO treatments of healthy and sensitized subjects. Conditions are described both as Hz/mV

combinations and corresponding physiological pressures. The 5Hz data set consists of pressures derived from 5 Hz in combination with amplitudes of 100 - 400 mV, which are equivalent to 0.8, 1.6, 2.6, and 3.6 cmH₂O respectively. Experimental results for ACh and ISO conditions are also presented.

Table 6.5. 5 Hz experimental data set for C_{dyn} evaluation of sensitized and healthy mice. 5 Hz-generated waveforms combined with indicated amplitudes produce the applied SIPO treatment (cmH₂O). Results include ACh and ISO comparison values and are presented as C_{dyn} ± SE (μl/mmH₂O).

	Sensitized	Healthy
Experimental condition	C _{dyn} ± SE, μl/mmH ₂ O	
ACh (10 ⁻⁴ M)	6.5 ± 0.6	15.2 ± 0.6
5 Hz/100 mV (0.8 cmH ₂ O)	7.4 ± 0.5	16.3 ± 1.0
5 Hz/200 mV (1.6 cmH ₂ O)	9.4 ± 0.4	15.5 ± 0.7
5 Hz/300 mV (2.6 cmH ₂ O)	7.0 ± 0.1	16.2 ± 0.7
5 Hz/400 mV (3.6 cmH ₂ O)	8.2 ± 0.6	18.2 ± 1.0
ISO (10 ⁻⁶ M)	9.5 ± 0.8	18.9 ± 1.2

The 5 Hz sensitized C_{dyn} values range from 6.5 μl/mmH₂O for ACh challenges up to a high of 9.5 μl/mmH₂O with ISO treatment. The 200 mV (1.6 cmH₂O) treatment is also comparable to ISO. Healthy group C_{dyn} values range from 15.2 μl/mmH₂O for ACh challenge up to a high of 18.9 μl/mmH₂O with ISO treatments.

Table 6.6 contains the C_{dyn} experimental data obtained from the set of 10 Hz-derived SIPO treatments of healthy and sensitized mice. Conditions are described both as Hz/mV

combinations and corresponding physiological pressures. The 10 Hz data set consists of pressures derived from 10 Hz in combination with amplitudes of 100 - 400 mV, which are equivalent to 0.7, 1.5, 2.4, and 3.3 cmH₂O respectively. Experimental results for ACh and ISO conditions are also presented.

Table 6.6 10Hz experimental data set for C_{dyn} evaluation of sensitized and healthy mice. 10 Hz-generated waveforms combined with indicated amplitudes produce the applied SIPO treatment (cmH₂O). Results include ACh and ISO comparison values, and are presented as C_{dyn} ± SE (µl/mmH₂O).

	Sensitized	Healthy
Experimental condition	C _{dyn} ± SE, µl/mmH ₂ O	
ACh (10 ⁻⁴ M)	6.5 ± 0.6	15.2 ± 0.6
10 Hz/100 mV (0.7 cmH ₂ O)	10.5 ± 0.2	17.0 ± 1.0
10 Hz/200 mV (1.5 cmH ₂ O)	9.1 ± 0.2	15.1 ± 0.8
10 Hz/300 mV (2.4 cmH ₂ O)	9.2 ± 0.3	17.3 ± 1.1
10 Hz/400 mV (3.3 cmH ₂ O)	7.7 ± 0.3	16.4 ± 0.6
ISO (10 ⁻⁶ M)	9.5 ± 0.8	18.9 ± 1.2

The 10 Hz sensitized C_{dyn} values range from 6.5 µl/mmH₂O for ACh challenges up to a high of 10.5 µl/mmH₂O with 100 mV (0.7 cmH₂O) treatment. Healthy group C_{dyn} values range from 15.1 µl/mmH₂O for the 200 mV treatment (the ACh challenge is statistically equivalent at 15.2 µl/mmH₂O) up to a high of 18.9 µl/mmH₂O with ISO treatments.

Table 6.7 contains the C_{dyn} experimental data obtained from the set of 15 Hz-derived SIPO treatments of healthy and sensitized mice. Conditions are described both as Hz/mV

combinations and corresponding physiological pressures. The 15 Hz data set consists of pressures derived from 15 Hz in combination with amplitudes of 100 - 400 mV, which are equivalent to 0.4, 1.1, 1.7, and 2.4 cmH₂O respectively. Experimental results for ACh and ISO conditions are also presented.

Table 6.7. 15 Hz experimental data set for C_{dyn} evaluation of sensitized and healthy mice. 15 Hz-generated waveforms combined with indicated amplitudes produce the applied SIPO treatment (cmH₂O). Results include ACh and ISO comparison values and are presented as C_{dyn} ± SE (μl/mmH₂O).

	Sensitized	Healthy
Experimental condition	C _{dyn} ± SE, μl/mmH ₂ O	
ACh (10 ⁻⁴ M)	6.5 ± 0.6	15.2 ± 0.6
15 Hz/100 mV (0.4 cmH ₂ O)	7.0 ± 0.3	16.1 ± 0.6
15 Hz/200 mV (1.1 cmH ₂ O)	10.3 ± 1.2	15.6 ± 0.9
15 Hz/300 mV (1.7 cmH ₂ O)	11.7 ± 0.9	17.9 ± 1.1
15 Hz/400 mV (2.4 cmH ₂ O)	9.2 ± 0.3	17.2 ± 0.9
ISO (10 ⁻⁶ M)	9.5 ± 0.8	18.9 ± 1.2

The 15 Hz sensitized C_{dyn} values range from 6.5 μl/mmH₂O for ACh challenges up to a high of 11.7 μl/mmH₂O with 300 mV treatment (1.7 cmH₂O). Healthy group C_{dyn} values range from 15.2 μl/mmH₂O for the ACh challenge up to a high of 18.9 μl/mmH₂O with ISO treatments.

Table 6.8 contains the C_{dyn} experimental data obtained from the set of 20 Hz-derived SIPO treatments of healthy and sensitized mice. Conditions are described both as Hz/mV combinations and corresponding physiological pressures. The 20 Hz data set consists of pressures derived from 20 Hz in combination with amplitudes of 100 - 400 mV, which are equivalent to 0.4, 1.1, 1.7, and 2.3 cmH₂O respectively. Experimental results for ACh and ISO conditions are also presented.

Table 6.8. 20 Hz experimental data set for C_{dyn} evaluation of sensitized and healthy mice. 20 Hz-generated waveforms combined with indicated amplitudes produce the applied SIPO treatment (cmH₂O). Results include ACh and ISO comparison values and are presented as $C_{dyn} \pm SE$ ($\mu\text{l}/\text{mmH}_2\text{O}$).

	Sensitized	Healthy
Experimental condition	$C_{dyn} \pm SE, \mu\text{l}/\text{mmH}_2\text{O}$	
ACh (10^{-4} M)	6.5 ± 0.6	15.2 ± 0.6
20 Hz/100 mV (0.4 cmH ₂ O)	8.6 ± 0.3	17.2 ± 0.7
20 Hz/200 mV (1.1 cmH ₂ O)	10.0 ± 0.8	15.1 ± 0.9
20 Hz/300 mV (1.7 cmH ₂ O)	14.9 ± 0.6	16.4 ± 0.9
20 Hz/400 mV (2.3 cmH ₂ O)	10.0 ± 0.5	15.5 ± 0.6
ISO (10^{-6} M)	9.5 ± 0.8	18.9 ± 1.2

The 20 Hz sensitized C_{dyn} values range from 6.5 $\mu\text{l}/\text{mmH}_2\text{O}$ for ACh challenges up to a high of 14.9 $\mu\text{l}/\text{mmH}_2\text{O}$ with 300 mV treatment (1.7 cmH₂O). Healthy group C_{dyn} values range from 15.1 $\mu\text{l}/\text{mmH}_2\text{O}$ for the 200 mV treatment (the ACh challenge is statistically equivalent at 15.2 $\mu\text{l}/\text{mmH}_2\text{O}$) up to a high of 18.9 $\mu\text{l}/\text{mmH}_2\text{O}$ with ISO treatments.

6.4. Discussion

The means for C_{dyn} were obtained for healthy and sensitized mice treated with ACh, compared, and yielded significant differences in the diseased response to ACh. Mean C_{dyn} values of 15.2 ± 0.6 and 6.5 ± 0.6 $\mu\text{l}/\text{mmH}_2\text{O}$ for healthy and sensitized mice respectively, indicates the C_{dyn} of healthy mice was 134 % higher than chronic mice. Percent-increase values were calculated by dividing the (n=7) differences of sensitized and healthy C_{dyn} by the healthy C_{dyn} , and multiplying this value by 100 (Eqn. 6.2). Analysis showed a significant difference in the sensitized group's response to the bronchoconstrictor compared to healthy mice (p-value < 0.05), providing additional evidence for the presence of AHR in the airways of the sensitized mice. Differences in the C_{dyn} responses to ISO were also observed. Following ACh challenge of healthy and sensitized mice, ISO treatment resulted in means of 18.9 ± 1.2 and 9.5 ± 0.8 $\mu\text{l}/\text{mmH}_2\text{O}$ respectively, with healthy values 99 % greater than sensitized values (using Eqn. 6.2). Again, analysis confirms that there is a significantly greater C_{dyn} value for the healthy group, and a significant deficiency in the C_{dyn} of the sensitized group (p-value < 0.05).

$$\% \text{ Increase} = 100 \times \left[\frac{C_{dyn,healthy} - C_{dyn,sensitized}}{C_{dyn,sensitized}} \right]_{ACh \text{ or } ISO} \quad (\text{Eqn. 6.2})$$

Individual analysis of ISO treatment values following ACh challenge in either the healthy or sensitized groups provides addition insights regarding the effects of the chemical bronchorelaxant. The improvement of healthy C_{dyn} values following ISO treatment was 24.3 % (15.2 up to 18.9 $\mu\text{l}/\text{mmH}_2\text{O}$) greater than the ACh value, and the improvement of sensitized C_{dyn} following ISO was 46.1 % (6.5 up to 9.5 $\mu\text{l}/\text{mmH}_2\text{O}$). While the

magnitude of the dynamic compliance was greater with healthy mice, their tissue response to the ISO treatment was not half as great as experienced by sensitized tissues.

As mentioned in the discussion of Section 5.5, ISO treatment serves as a reference for the ability of the tested (healthy or sensitized) airway in this model to undergo bronchorelaxation following a mimicked asthmatic attack. The range of C_{dyn} values from ACh to ISO in healthy mice is $3.7 \mu\text{l}/\text{mmH}_2\text{O}$, and in sensitized mice, this range is less, at $3.0 \mu\text{l}/\text{mmH}_2\text{O}$. The smaller range of dynamic compliance in sensitized airways initially indicates that the airway tissue is unable to respond to the chemical bronchorelaxant treatment as well as the healthy airway tissue. Comparison of SIPO treatments against these ACh and ISO reference values therefore serves as a benchmark for the efficacy of the challenges in this study to elicit bronchorelaxant responses in measured respiratory cycles.

From Chapter V, it is appropriate to restate relevant respiratory rate information. All healthy respiratory rate values are significantly higher than sensitized respiratory rate values, except for the sensitized respiratory rate associated with SIPO treatment of 5 Hz/100 mV ($0.8 \text{ cmH}_2\text{O}$). At this treatment there is no significance between measured healthy and sensitized respiratory rates. Bronchoconstriction due to ACh challenge is not always responsible for the lowest respiratory rate, and bronchorelaxation as a result of ISO treatment is not always responsible for the highest respiratory rate. Each of the ACh and ISO reference parameters for the study are not the sole reasons for eliciting the high and low respiratory rates. SIPO treatments are also responsible for changes in respiratory rates of healthy and sensitized mice, but due to the larger SE values in sensitized mice, the observations and measurements are not significant. Further analysis of the breathing cycles could lead to valuable respiratory information despite the limitations of current

significance in the data sets. For example, the lower respiratory rates and larger tidal volumes in sensitized mice correlates well with the smaller range of C_{dyn} values ($3.0 \mu\text{l}/\text{mmH}_2\text{O}$ compared to the $3.7 \mu\text{l}/\text{mmH}_2\text{O}$ of healthy mice). The model supports a conclusion that sensitized mice exert greater effort to breath. This evidence in sensitized respiratory rate data indicates a change in respiratory processes to compensate for likely physical changes in the sensitized airways which are in turn responsible for lower values of C_{dyn} measured through the study.

Application of the 5 Hz-generated SIPO waveforms resulted in 2 of 4 treatments having a significant increase in the C_{dyn} of the sensitized airways. The most significant increase (45 %) was found in the 200 mV ($1.6 \text{ cmH}_2\text{O}$) set, where the dynamic compliance was statistically equivalent to treatment with ISO. The 400 mV ($3.6 \text{ cmH}_2\text{O}$) set increased C_{dyn} by 26 % compared to ACh, while the remaining two treatments (0.8 and $2.6 \text{ cmH}_2\text{O}$) were comparable to each other and to ACh challenge, indicating no benefit towards offsetting the mimicked asthma attack from the standpoint of compliant airways.

In healthy airways treated with the 5 Hz-generated waveforms, only the 400 mV ($3.6 \text{ cmH}_2\text{O}$) set of C_{dyn} values was significantly higher than ACh; the set was also comparable to ISO, but not significantly higher. Applications of 0.8 , 1.6 , and $2.6 \text{ cmH}_2\text{O}$ to healthy airways were not significant improvements from C_{dyn} values associated with ACh, indicating that the three other amplitudes ($100 - 300 \text{ mV}$) tested in the set were ineffective at overcoming the ACh-induced bronchoconstriction. Figure 6.1 provides the C_{dyn} data plots of the 5 Hz-generated SIPO waveform applications, indicating the lower dynamic compliance in all sensitized groups compared to healthy groups. While both healthy and sensitized data trend upward with increasing applied pressure treatment, a notable difference between the two states of wellness exists at $1.6 \text{ cmH}_2\text{O}$, where the sensitized

mice benefit with greater compliance from the treatment and healthy mice have lower compliance, closest in fact, to the ACh challenge values for this group.

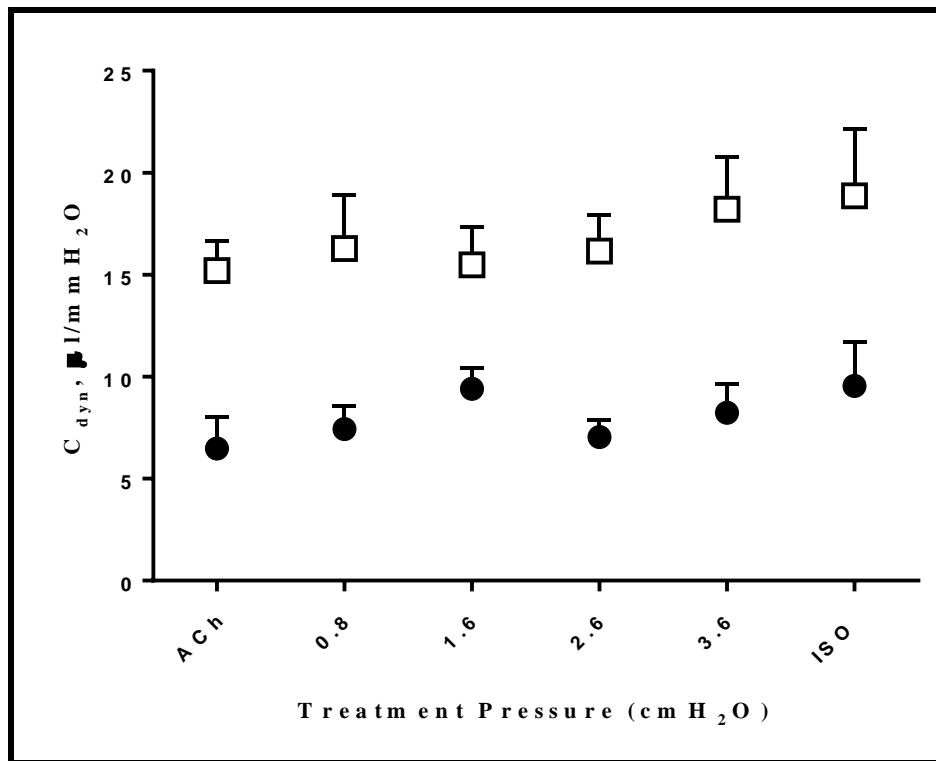


Figure 6.1 Treatment values of C_{dyn} (expressed as $\mu\text{l}/\text{mmH}_2\text{O}$) from applications of 5 Hz-generated SIPO waveform set with amplitudes in the range of 100 – 400 mV (0.8 – 3.6 cmH_2O). Experimental conditions are presented along the x-axis, with ACh and ISO as comparisons (\square = healthy; \bullet = sensitized; $n=7$ for all data points except sensitized SIPOs, $n=5$).

Application of the 10 Hz-generated SIPO waveforms resulted in significant increases in all four C_{dyn} values in sensitized airway treatments, especially when using an amplitude of 100 mV. The most significant increase (61 %) was found in the 0.7 cmH_2O set, where the dynamic compliance was higher than ISO by 15 %. The remaining three treatments (200 – 400 mV) were significantly higher than ACh, with the first two groups (1.5 and 2.4 cmH_2O) comparable to ISO, and the 3.3 cmH_2O group significantly higher than C_{dyn} values of ACh, but not comparable to ISO.

In healthy airways treated with the 10 Hz-generated waveforms, two of the treatments (100 and 300 mV) were significantly higher than ACh values of C_{dyn} ; the 0.7 and 2.4 cmH₂O groups were also comparable to ISO, but not significantly different. Notably, the 1.5 and 3.3 cmH₂O treatments of healthy airways showed no improvement in C_{dyn} compared to ACh values, indicating no that no bronchorelaxant effect was gained from the waveforms. Figure 6.2 provides the C_{dyn} data plots of the 10 Hz-generated SIPO waveform applications, indicating the lower dynamic compliance in all sensitized groups compared to healthy groups. While the healthy data from SIPO treatments is essentially constant with increasing SIPO values, the sensitized data trend is downward (towards less dynamic compliance) with increasing applied pressure treatment. The healthy treatment of 1.5 cmH₂O is equivalent to ACh challenge, while the same SIPO treatment in sensitized mice results in a significant improvement of C_{dyn} above ACh values, though not greater than ISO treatment results.

Application of the 15 Hz-generated SIPO waveforms resulted in significant decreases in the C_{dyn} of the sensitized airway in 3 of the 4 treatments, particularly when using an amplitude of 300 mV. The 2nd-most significant C_{dyn} increase (80 %) of the entire study was found in these waveforms' 1.7 cmH₂O set, where the C_{dyn} was significantly higher than ISO. The remaining two treatments (200 and 400 mV) that were significantly higher than ACh were also comparable to ISO. The 100 mV (0.4 cmH₂O) group was comparable to ACh challenge, indicating no benefit in overcoming the modelled asthmatic attack.

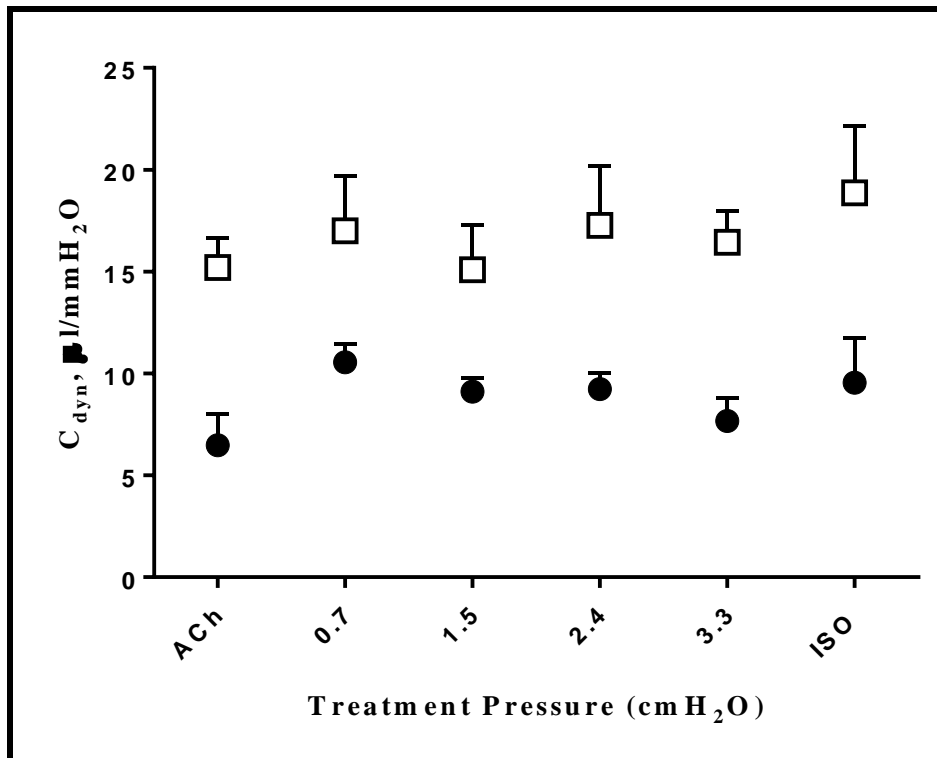


Figure 6.2 Treatment values of C_{dyn} (expressed as $\mu\text{l}/\text{mmH}_2\text{O}$) from applications of 10 Hz-generated SIPO waveform set with amplitudes in the range of 100 – 400 mV (0.7 – 3.3 cmH_2O). Experimental conditions are presented along the x-axis, with ACh and ISO as comparisons (\square = healthy; \bullet = sensitized; $n=7$ for all data points except sensitized SIPOs, $n=5$).

In healthy airways treated with the 15 Hz-generated waveforms, two of the treatments (amplitudes of 300 and 400 mV) had significantly higher C_{dyn} values than ACh; these 1.7 and 2.4 cmH_2O treatments were comparable to ISO, without significant differences in their compliance values. Notably, two of the treatments, 15 Hz/100 mV (0.4 cmH_2O) and 15 Hz/200 mV (1.1 cmH_2O) had no significant values above ACh's C_{dyn} values. Figure 6.3 provides the C_{dyn} data plots of the 15 Hz-generated SIPO waveform applications, indicating the lower dynamic compliance in all sensitized groups compared to healthy groups. Both healthy and sensitized data from SIPO treatments have upward trends in compliance values with increasing SIPO values, after initial equivalence with ACh from both 0.4 cmH_2O data sets. The healthy treatment of 1.1 cmH_2O is still equivalent to ACh challenge, but the remaining healthy and sensitized groups are all comparable to ISO in

their respective groups. The most pronounced improvements in C_{dyn} are the values in the sensitized 1.1 and 1.7 cmH₂O treatment sets.

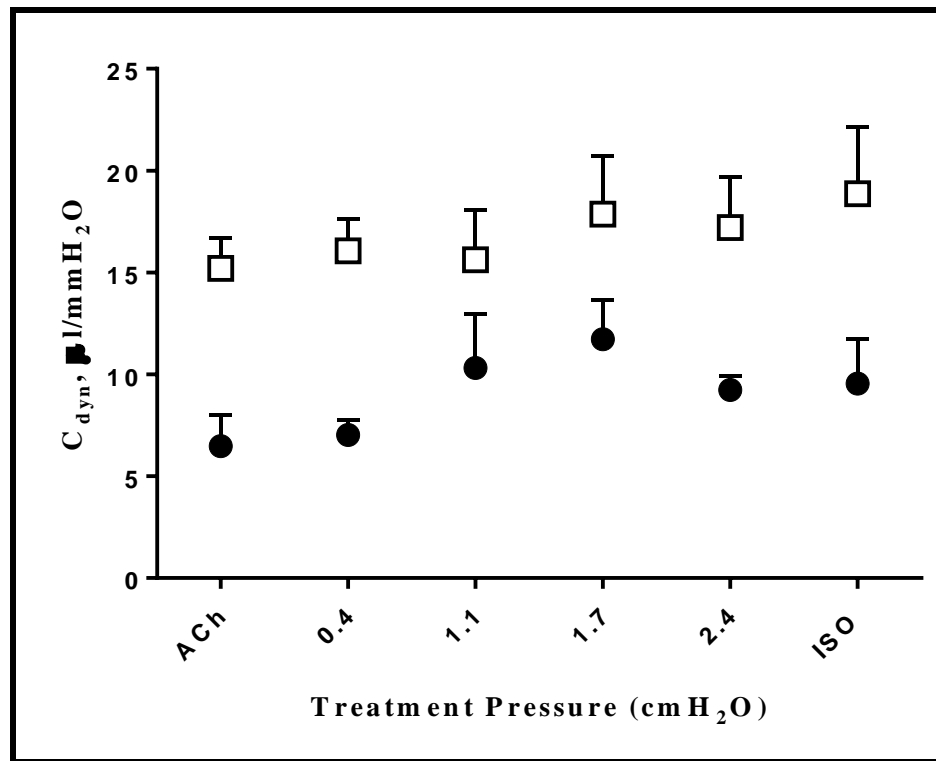


Figure 6.3 Treatment values of C_{dyn} (expressed as $\mu\text{l}/\text{mmHg}$) from applications of 15 Hz-generated SIPO waveform set with amplitudes in the range of 100 – 400 mV (0.4 – 2.4 cmH₂O). Experimental conditions are presented along the x-axis, with ACh and ISO as comparisons (\square = healthy; \bullet = sensitized; $n=7$ for all data points except sensitized SIPOs, $n=5$).

Application of the 20 Hz-generated SIPO waveforms resulted in significant increases in all of the C_{dyn} means measured for treatments of the sensitized airways. The group also contains the greatest improvement for a C_{dyn} value (129 %, in the 300 mV set) among all of the 38 (19 each for healthy and sensitized) distinct treatments in the study. The 100, 200, and 400 mV groups are all comparable to ISO values. The 0.4 cmH₂O group is the lowest of the four SIPO treatments, improving 32 % over ACh. The 1.1 and 2.3 cmH₂O groups are equivalent with each other, aside from SE values, and improve C_{dyn} by 54 % over ACh values.

In healthy airways treated with the 20 Hz-generated waveforms, only a single treatment (amplitude of 100 mV) had a significantly higher C_{dyn} than ACh; the 0.4 cmH₂O set was also comparable to ISO. Three of the treatments to healthy airways, 20 Hz/200 mV (1.1 cmH₂O), 20 Hz/300 mV (1.7 cmH₂O), and 20 Hz/400 mV (2.3 cmH₂O) had no significant improvements above C_{dyn} values of ACh challenges. Figure 6.4 provides the C_{dyn} data plots of the 20 Hz-generated SIPO waveform applications, indicating the lower resistance in all sensitized groups compared to healthy groups. While the healthy data from SIPO treatments is trending slightly downward with increasing SIPO values, the sensitized data trend is upward (towards more dynamic compliance) with increasing applied pressure treatment. Again a notable SIPO waveform for the data set is the application of 1.7 cmH₂O, where the response is equivalent to ACh challenge in healthy mice, and in sensitized mice results in the most significant improvement of C_{dyn} above ACh values for the entire study.

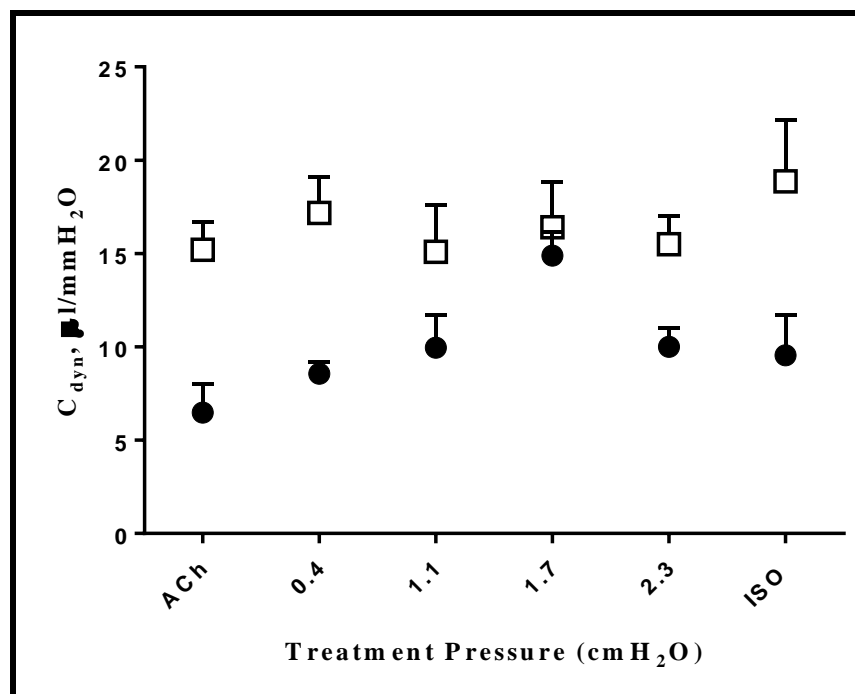


Figure 6.4. Treatment values of C_{dyn} (expressed as $\mu\text{l}/\text{mmH}_2\text{O}$) from applications of 20 Hz-generated SIPO waveform set with amplitudes in the range of 100 – 400 mV (0.4 – 2.3 cmH₂O). Experimental conditions are presented along the x-axis, with ACh and ISO as comparisons (□ = healthy; ● = sensitized; n=7 for all data points except sensitized SIPOs, n=5).

Results discussed in this chapter indicate that airways from sensitized mice are significantly more reactive to ACh (10^{-4} M) bronchoconstrictor treatment (as shown in lower C_{dyn} values) than those airways tested in healthy mice. This decrease in compliance is in line with expected structural changes resulting from the asthmatic state [57]. As mentioned in previous chapters, this reactivity is a main feature (in conjunction with pulmonary resistance) for associating this long-term sensitization model with human asthma and specifically with AHR [51, 89, 102, 103]. Additionally, applications of superimposed pressure waves over spontaneous breathing have a bronchorelaxant effect in sensitized mice, more so in fact than in healthy mice, despite the lower compliance values of the sensitized airways tested. The relaxant effect is manifest in the significant increase of C_{dyn} in 13 (81 %, from 16) SIPO treatments of sensitized mice compared to the C_{dyn} of ACh challenges. From 5 – 20 Hz waveform sets, greater airway compliance was observed in 2/4, 4/4, 3/4, and 4/4 of the SIPO values for the sets. In healthy mice the relaxant effect of applied SIPO treatments has less of a presence in the observed responses. From 5 – 20 Hz waveform sets, greater airway compliance was observed in 6 SIPO treatments: 1/4, 2/4, 2/4, and 1/4 (37 %, from 16) respectively. Despite a higher baseline of dynamic compliance, the healthy tissues did not respond to SIPO treatments with greater improvement values of dynamic compliance in the same fashion as lower-baseline values of C_{dyn} in sensitized tissues responded to identical treatments.

In treatments applied to sensitized mice, 11 are comparable to ISO at relaxing the airways following ACh treatment, and 2 are significantly better than ISO at improving the dynamic compliance of the airways. In treatments of healthy mice, 6 SIPO values elicit comparable C_{dyn} values to ISO, and none of these are significantly higher than the chemical bronchorelaxant. ISO relaxes the ASM components associated with cAMP stimulation (via β -2 receptors and their signal pathways), and it is possible that SIPO

application elicits a similar relaxation of the ASM mechanical features downstream from the initial cAMP stimulation. A general trend is observed for the effectiveness of applied pressure oscillations when viewing the analyses in the context of frequency, amplitude, or physiological pressure sets across the sensitized data. The most significant (and consistent) augmentations of C_{dyn} values occur at the applied treatment pressure of approximately 1.7 cmH₂O. All other SIPO applications in sensitized mice, greater than (and less than) the 1.7 cmH₂O data set do not increase C_{dyn} with the same effect. This trend does not occur in data for healthy mice. Within the healthy groups treated with the same SIPO values, there are different trends in the C_{dyn} values' outcomes.

Healthy mice treated with ACh respond with the best C_{dyn} values (present greatest bronchorelaxation) when SIPO treatment values are not 1.7 cmH₂O. In fact, healthy mice treated with 1.5, 1.6, and 1.7 cmH₂O (from 5-, 10-, and 20 Hz-generated groups) responded only once (15 Hz/300 mV; 1.7 cmH₂O) with statistically greater C_{dyn} values relative to ACh treatment. Not even 1.1 or 0.8 cmH₂O treatments elicited a benefit for C_{dyn} in healthy airways. This is contrary to the observed effect in sensitized airways. In healthy mice, the greatest number of significant reductions occurs at the higher and lower applied pressure oscillations: 0.4, 0.7, 2.4 (from two different frequencies), and 3.6 cmH₂O (generated from 20 Hz/100 mV, 10 Hz/100 mV, 15 Hz/400 mV, 10 Hz/300 mV, and 5 Hz/400 mV) are responsible for improved C_{dyn} values in healthy airways following ACh challenges.

6.5. Summary

The results presented in this chapter complete this study's objective to assess the respiratory parameters of healthy and sensitized mice in a long-term sensitization (chronic) model of asthma. Analysis of C_{dyn} values obtained for ACh, ISO, and SIPO

treatments has indicated the presence (and treatment-dependent decrease) of AHR in sensitized mice as well as changes in respiratory responses in the airways of healthy mice. Applications of bronchorelaxant methods in the form of SIPO treatments improve respiratory conditions of both healthy and sensitized mice though with different statistical outcomes. Greater numbers of statistically significant increases in C_{dyn} are found in sensitized mice compared to healthy subjects. Further, both healthy and sensitized mice respond most favourably to SIPO sets from distinct ranges of pressures, indicating that diseased and healthy airways respond to similar treatments in different fashions. Stated another way, the response of airway tissues to SIPO treatments has at least a partial dependence on the state of health or disease in the mice. Further analysis and discussion of this conclusion is presented in Chapter VII through deductions based on the R_L and C_{dyn} results of this modelled chronic asthma study.

CHAPTER VII

Superimposed pressure oscillation effects on asthmatic airway smooth muscle

7.1. Introduction

Chapters V and VI presented the *in vivo* results of R_L and C_{dyn} measurements, respectively, taken from healthy and sensitized mice. Trends identified in the data comparisons of the two states indicate that the chronic model was successfully established as a basis for this study. Immunoresponse and pulmonary cellularity changes support the model. Response of sensitized mice to ACh challenge demonstrate AHR greater than healthy mice. Further responses to treatment of ACh-driven bronchoconstriction indicate that ISO relief of mimicked asthma attacks is an effective reference point for assessing SIPO applications. Respiratory rates are all significantly higher in healthy compared to sensitized mice, except for a single exception of statistically comparable rates at SIPO treatments of 0.8 cmH₂O. Parameters measured to define R_L and C_{dyn} in healthy and sensitized mice respond most favourably to SIPO sets from distinct ranges of pressures, indicating that diseased and healthy airway tissues respond to similar treatments in different fashions. The state of health or disease in the murine airways is a factor in how SIPO treatments affect the key measurements of this study. Indeed, the evidence supports an interpretation that SIPO treatments affect the crossbridge cycle of ASM contraction and relaxation based on the disease state of the mice.

To further assess the impact of the findings in the chronic long-term sensitization model, previous work from IBTec's short-term (acute) asthmatic model [13] is inspected. This chapter discusses the respiratory parameters for R_L and C_{dyn} and their interpretations in greater detail by comparing chronic results with *in vivo* results from OVA-sensitized

(short-term protocol) mice. Comparison of the two sets of asthmatic states is accomplished by normalizing the data sets with a standard respiratory constant. Using the constant, a detailed analysis of super-imposed pressure oscillations, ACh, and ISO is presented for murine asthmatic models. Recommendations for future work are also discussed prior to conclusions of the thesis.

7.2. Length and pressure oscillations

The effects of length oscillations on ASM have been studied in healthy and allergen-sensitized (asthmatic) ASM. Studies in healthy tissues indicate that bronchodilation is accomplished by treatments using length oscillations similar to those in either deep inspirations [7, 8, 81, 82, 85, 155] or tidal breathing patterns [7, 10, 81-83, 97, 98, 155]. The observed effects of the oscillations in healthy tissues depend on whether the treatment occurs before or after the ASM is stimulated to contract, leading to studies focussed on treating pre-constricted ASM. Additionally, there are indications that a temporal rearrangement of ASM contractile elements results from applied length changes to the tissue [152]. Based on the observed healthy airways' responses to applied length oscillations, Fredberg et al. [9] proposed a model of crossbridge perturbation to explain the affected contractile behaviour, wherein the equilibrium of the system is disrupted by the applied oscillations. Similar defining studies for the contractile elements in asthmatic ASM are not as common as those in healthy tissue. However, previous work performed in an acute (OVA-sensitization) model of asthma [13] does provide key information which is in line with the findings of this chronic (DRA-sensitization) study as well as with studies performed in healthy airways.

Previous *in vitro* studies carried out by IBTec [11, 13] established the basis of acute *in vitro* superimposed length oscillation (SILO) studies. Findings *in vitro* were comparable

to literature descriptions of tested healthy ASM tissues, showing that pre-constricted ASM is relaxed after application of ISO alone, normal breathing oscillations alone, and ISO combined with normal breathing oscillations [7, 10, 36, 81-83, 95, 97, 98, 151]. Of interest, the *in vitro* work also indicated that there are differences in the bronchorelaxant effects of SILO across two strains of healthy mice, wherein similar applied frequencies do not share replicated effects. The preferential effects of bronchorelaxant treatments due to physiological differences in healthy tissues is also consistent with the observed differences in SIPO treatment outcomes across healthy and diseased states in tissues from the same strain of mice.

Short-term sensitized airways were tested for relaxation, and compared to healthy airway results. Both SILO and SIPO testing indicated that the bronchorelaxant effect of ISO alone, normal breathing oscillations, and their combinations was decreased in acute airways compared to healthy airways. SIPO application to intact acute airways did however demonstrate improved outcomes when the frequency remained constant and amplitude was increased.

Studies which replicate normal breathing conditions (those found in deep inspirations and tidal oscillations) and apply them to healthy and asthmatic airways are the main basis for generating past and current airway responsiveness theories. Unfortunately, the use of normal breathing conditions does not induce comparable relaxation of asthmatic airway tissues when compared to healthy airway tissues. In fact, responses of asthmatic tissue can be either less than that observed in normal tissue, or there is no effect from the tidal oscillations and deep inspiration oscillations at all [7, 153]. Such findings have generated a need to identify reasons for the lack of response by the tissues, as well as drive investigations into alternative (SIPO) oscillations which *do* elicit responses in precontracted, sensitized ASM.

Previous work in our laboratory has shown that in a short-term sensitization model of asthma, there are indications of beneficial alternative oscillations that can be applied to sensitized, pre-constricted ASM in spontaneously breathing mice. Such results support the body of knowledge already collected relative to healthy tissues and the modelling of crossbridge perturbations. Current assessments of bronchodilation and bronchoconstriction in this study's chronic model of asthma further address postulates and hypotheses regarding such alternative oscillations and the contractile machinery of airway smooth muscle. Analysis of the long- and short-term models' data is able to provide a unique interpretation of the crossbridge cycle relative to healthy and two different diseased states of the treated tissues.

Effective comparisons of the disparate states of asthmatic (short-term versus long-term sensitization) and healthy airways are not immediately apparent however. This is especially the case when viewing multiple data sets from asthmatic models whose severity is developed by using distinct immune challenges to generate respiratory sensitivities. The acute model of asthma under consideration used a short-term sensitization with OVA as the allergen. This study's long-term sensitization model for asthma is achieved by using an allergen mix of DRA components. Using a basis set of respiratory parameters rather than the sensitization allergens (or durations of sensitization) as the point of commonality, it is possible to introduce a method of normalization across the states of the disease. In this context, it is possible to interpret the effects of SIPO on both acute and chronic models of asthmatic as well as healthy ASM against a single (normal) reference subject rather than a single type of data from a subject. In doing so, inferences and conclusions regarding the effects of SIPO on differing states of asthmatic disease are used for interpreting the pressure treatments on a range of health states in mice.

A set of experimentally-determined respiratory measurements in healthy (control) subjects were used to normalize the R_L and C_{dyn} data sets (Appendix F). Briefly, transformation of the data sets required average values for specific pressure and volume relationships which were taken from testing conditions of healthy subjects receiving only aerosolized saline (0.9 %). The control values were used to normalise R_L and C_{dyn} values to the respiratory parameters \check{R}_L and \check{C}_{dyn} . The use of the $\check{}$ (caron) symbol above each of the leading letters in the abbreviations for lung resistance and dynamic compliance, indicates that a transformation has occurred, and the data is then normal to the standard reference. \check{R}_L and \check{C}_{dyn} transformation data are no longer directly interpreted as pulmonary resistance and dynamic compliance, but rather as the “inverse of power” and “work,” respectively (Appendix F).

7.3. \check{R}_L in two asthmatic models

The R_L results presented in Chapter V correspond to the *in vivo* chronic asthmatic data obtained using the protocols and resources outlined in Chapters III and IV. The total lung resistance values in this chronic model are compared to their corresponding parameters in our previous acute model (Appendix D) following transformation to values of \check{R}_L . The effects of SIPO are analysed for significant differences across frequency and amplitude determinants of the applied pressure oscillations.

The airways of acute and chronic sensitized subjects are shown to be hyperresponsive to ACh compared to healthy mice. As a classic feature found in human asthma, AHR is an effect which corresponds to development of the disease, and is modelled in this study across healthy, acute, and chronic conditions. Literature also notes that development of the disease is evidenced physiologically in the airways with an increase in basal tone [26,

33, 81, 99, 101, 152, 153]; our results are consistent with this finding. It is expected then that development of the disease from healthy to chronic conditions is evidenced with greater AHR parameter values in long-term asthmatic ASM compared to short-term asthmatic ASM, as the tissues respond to a bronchoconstrictive stimulus.

Comparison of one part of the AHR parameters is accomplished by using R_L data and the respiratory constant to determine \check{R}_L values (Equation A.6) for acute and chronic data sets. \check{R}_L values then serve as relative indicators of airway bronchoconstriction or bronchorelaxation. The established values of \check{R}_L for ACh challenges and ISO treatments serve as standards to gauge the efficacy of applied pressure oscillations across the tested acute and sensitized mice.

Values for \check{R}_L are presented in Tables 7.1 – 7.4 in this section and are expressed as the mean \pm SE for each given condition. Tables provide the summary of transformed data from applications of ACh, ISO, and SIPO treatments in acute and sensitized mice. SIPO values are grouped within each table according to frequency, amplitude, and the generated physiological pressure sets in order to effectively present results.

Table 7.1 contains the \check{R}_L data obtained from the set of 5 Hz-derived SIPO treatments of acute and sensitized mice. Conditions are described both as Hz/mV combinations and corresponding physiological pressures. The 5 Hz data set consists of pressures derived from 5 Hz in combination with amplitudes of 100 - 400 mV, which are equivalent to 0.8, 1.6, 2.6, and 3.6 cmH₂O respectively. Experimental results for ACh and ISO conditions are also presented as parameter references.

The 5 Hz acute \check{R}_L values range from 0.65 ((cmH₂O·ml)/s)⁻¹ for 400 mV treatment up to a high of 0.79 ((cmH₂O·ml)/s)⁻¹ with ACh challenge. The lowest \check{R}_L value for acute

subjects was achieved from the 3.6 cmH₂O SIPO group was also comparable to 100 mV (0.8 cmH₂O) and ISO treatments. Significant differences are observed when comparing the ACh standard with three of the groups data points (0.8 and 3.6 cmH₂O, and ISO). Figure 7.1(a) illustrates the 5 Hz acute \check{R}_L values, indicating significant ($p < 0.05$) differences relevant to ACh with an asterisk (*). Chronic group \check{R}_L values range from 1.05 ((cmH₂O·ml)/s)⁻¹ for 200 mV treatments up to a high of 1.64 ((cmH₂O·ml)/s)⁻¹ with ACh challenge. The lowest \check{R}_L value for chronic mice was achieved from the 1.6 cmH₂O SIPO group and ISO treatment, which were statistically equivalent. All data for the chronic group was significantly lower than ACh ($p < 0.05$). Figure 7.1(b) illustrates the 5 Hz chronic \check{R}_L values, indicating significant ($p < 0.05$) differences relevant to ACh with an asterisk (*).

Table 7.1 Sensitized \check{R}_L from the 5 Hz-derived pressure set. 5 Hz-generated waveforms combined with indicated amplitudes produce the applied SIPO treatment (cmH₂O). Transformed results include ACh and ISO comparison values, and are presented as $\check{R}_L \pm SE$ [(cmH₂O·ml)/s]⁻¹.

	OVA-Sensitized (Acute)	DRA-Sensitized (Chronic)
Experimental condition	$\check{R}_L \pm SE$ [(cmH ₂ O·ml)/s] ⁻¹	
ACh (10 ⁻⁴ M)	0.79 ± 0.03	1.64 ± 0.13
5 Hz/100 mV (0.8 cmH ₂ O)	0.66 ± 0.02	1.28 ± 0.10
5 Hz/200 mV (1.6 cmH ₂ O)	0.70 ± 0.04	1.05 ± 0.04
5 Hz/300 mV (2.6 cmH ₂ O)	0.73 ± 0.05	1.32 ± 0.03
5 Hz/400 mV (3.6 cmH ₂ O)	0.65 ± 0.02	1.24 ± 0.08
ISO (10 ⁻⁶ M)	0.66 ± 0.03	1.07 ± 0.08

The differences in the magnitudes of acute and chronic data are apparent when viewed in the context of normalised data (Fig. 7.1(c)), and indicate that physiological responses to SIPO treatments differ based on the health/disease status of the same mouse strain. This conclusion is further supported with comparing the percent change in \check{R}_L values (against ACh challenge as the reference) for acute and chronic mice in this 5 Hz SIPO treatment group (Fig. 7.1(d)). There are clear differences in the change in responses of short- and long-term asthmatic mice, based on all of the applied SIPO, and their modelled disease state.

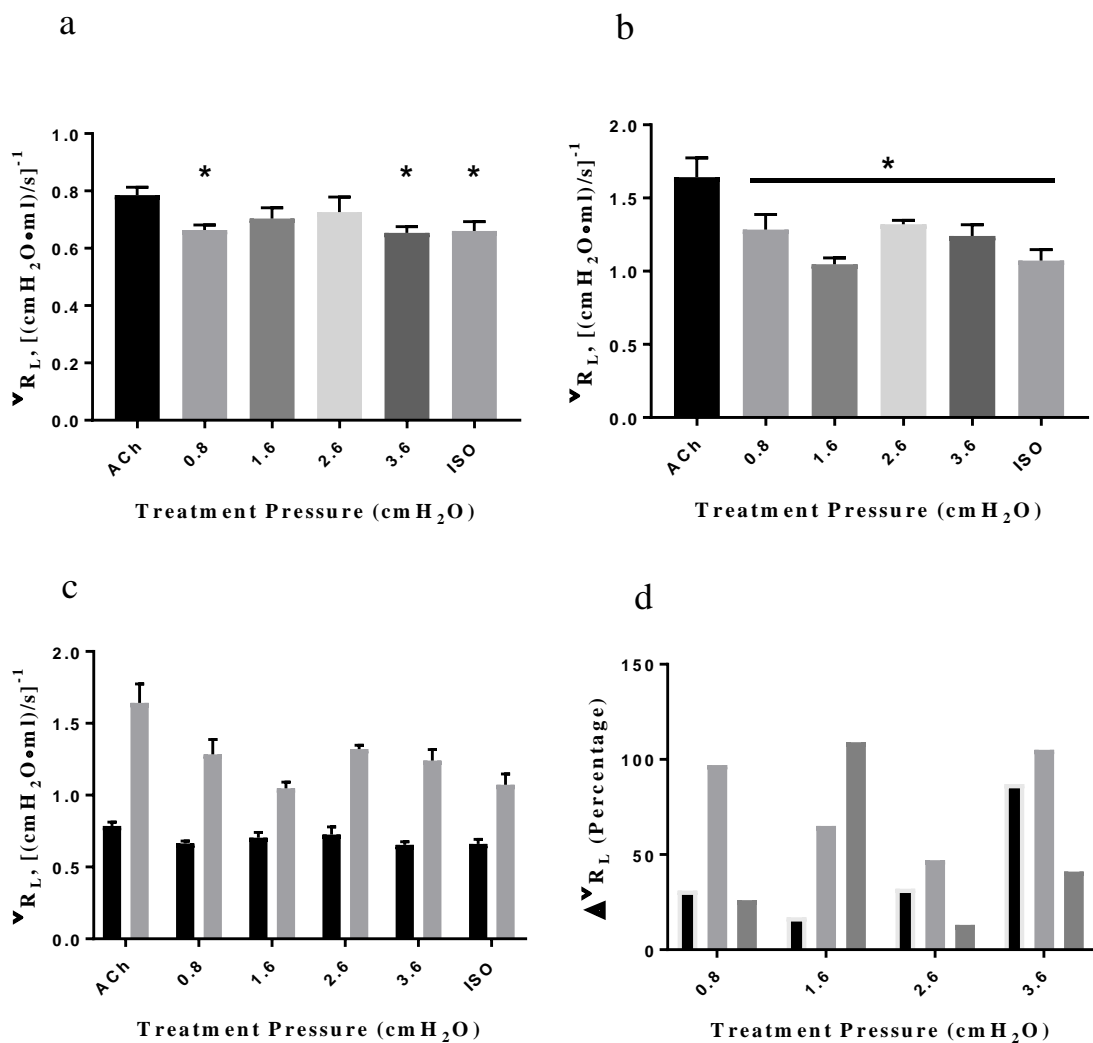


Figure 7.1. Transformations of 5 Hz R_L values to \check{R}_L . Acute (a) and Chronic (b) groups with SIPO amplitudes of 100 – 400 mV (0.8, 1.6, 2.6, and 3.6 cmH₂O) are presented (n=7, except for chronic SIPO, n = 5). (c) Magnitudes of acute (black) and chronic (grey) \check{R}_L values; and (d) percent change in \check{R}_L (compared to ACh) of acute (light grey) and chronic (dark grey) values; healthy changes are indicated (black) for comparison.

Table 7.2 contains the \check{R}_L data obtained from the set of 10 Hz-derived SIPO treatments of acute and sensitized subjects. Conditions are described both as Hz/mV combinations and corresponding physiological pressures. The 10 Hz data set consists of pressures derived from 10 Hz in combination with amplitudes of 100 - 400 mV, which are equivalent to 0.7, 1.5, 2.4, and 3.3 cmH₂O respectively. Experimental results for ACh and ISO conditions are also presented as parameter references.

Table 7.2 Sensitized \check{R}_L from the 10 Hz-derived pressure set. 10 Hz-generated waveforms combined with indicated amplitudes produce the applied SIPO treatment (cmH₂O). Transformed results include ACh and ISO comparison values, and are presented as $\check{R}_L \pm SE$ [(cmH₂O·ml)/s]⁻¹.

	OVA-Sensitized (Acute)	DRA-Sensitized (Chronic)
Experimental condition	$\check{R}_L \pm SE$ [(cmH ₂ O·ml)/s] ⁻¹	
ACh (10 ⁻⁴ M)	0.79 ± 0.03	1.64 ± 0.13
10 Hz/100 mV (0.7 cmH ₂ O)	0.66 ± 0.05	0.92 ± 0.01
10 Hz/200 mV (1.5 cmH ₂ O)	0.63 ± 0.03	1.09 ± 0.01
10 Hz/300 mV (2.4 cmH ₂ O)	0.66 ± 0.05	1.05 ± 0.05
10 Hz/400 mV (3.3 cmH ₂ O)	0.64 ± 0.04	1.26 ± 0.05
ISO (10 ⁻⁶ M)	0.66 ± 0.03	1.07 ± 0.08

The 10 Hz acute \check{R}_L values range from 0.63 ((cmH₂O·ml)/s)⁻¹ for 200 mV treatment up to a high of 0.79 ((cmH₂O·ml)/s)⁻¹ with ACh challenge. The lowest \check{R}_L value for acute mice was achieved from the 1.5 cmH₂O SIPO group, but in fact all values other than ACh are statistically comparable. Significant differences are observed when comparing the ACh standard against the entire set. Figure 7.2(a) illustrates the 10 Hz acute \check{R}_L values, indicating significant ($p < 0.05$) differences relevant to ACh with an asterisk (*). Chronic group \check{R}_L values range from 0.92 ((cmH₂O·ml)/s)⁻¹ for 100 mV treatments up to a high of

1.64 ((cmH₂O·ml)/s)⁻¹ with ACh challenge. The lowest \check{R}_L value for chronic mice was achieved from the 0.7 cmH₂O SIPO group, with all data for the chronic group significantly lower than ACh ($p < 0.05$). Fig. 7.2(b) illustrates the 10 Hz chronic \check{R}_L values, indicating significant ($p < 0.05$) differences relevant to ACh with an asterisk (*).

The differences in the magnitudes of acute and chronic 10 Hz groups are apparent when viewed in the context of normalised data (Fig. 7.2(c)), and indicate that physiological responses to SIPO treatments differ based on the health/disease status of the same mouse strain. This conclusion is further supported with comparing the percent change in \check{R}_L values for acute and chronic subjects in this 10 Hz SIPO treatment group (Fig. 7.2(d)). There are clear differences in the change in responses of short- and long-term asthmatic mice, based on the applied SIPO (except for 2.4 cmH₂O), and their modelled disease state.

Table 7.3 contains the \check{R}_L data obtained from the set of 15 Hz-derived SIPO treatments of acute and sensitized subjects. Conditions are described both as Hz/mV combinations and corresponding physiological pressures. The 15 Hz data set consists of pressures derived from 15 Hz in combination with amplitudes of 100 - 400 mV, which are equivalent to 0.4, 1.1, 1.7, and 2.4 cmH₂O respectively. Experimental results for ACh and ISO conditions are also presented as parameter references.

The 15 Hz acute \check{R}_L values range from 0.64 ((cmH₂O·ml)/s)⁻¹ for 200 mV treatment up to a high of 0.79 ((cmH₂O·ml)/s)⁻¹ with ACh challenge. The lowest \check{R}_L value for acute mice was achieved from the 1.1 cmH₂O SIPO group, but it is not significantly different from other SIPO values for the group. No significant differences are observed when comparing the ACh standard with the group's SIPO or ISO data points. Figure 7.3(a) illustrates the 15 Hz acute \check{R}_L values, indicating the lack of significant ($p > 0.05$) differences relevant to

ACh. The chronic group \check{R}_L values range from 0.85 ((cmH₂O·ml)/s)⁻¹ for 300 mV treatments up to a high of 1.64 ((cmH₂O·ml)/s)⁻¹ with ACh challenge. The lowest \check{R}_L value for chronic mice was achieved from the 1.7 cmH₂O SIPO group. All data for the chronic group except for the 0.4 cmH₂O treatment was significantly lower than ACh ($p < 0.05$). Fig. 7.3(b) illustrates the 15 Hz chronic \check{R}_L values, indicating significant ($p < 0.05$) differences relevant to ACh with an asterisk (*).

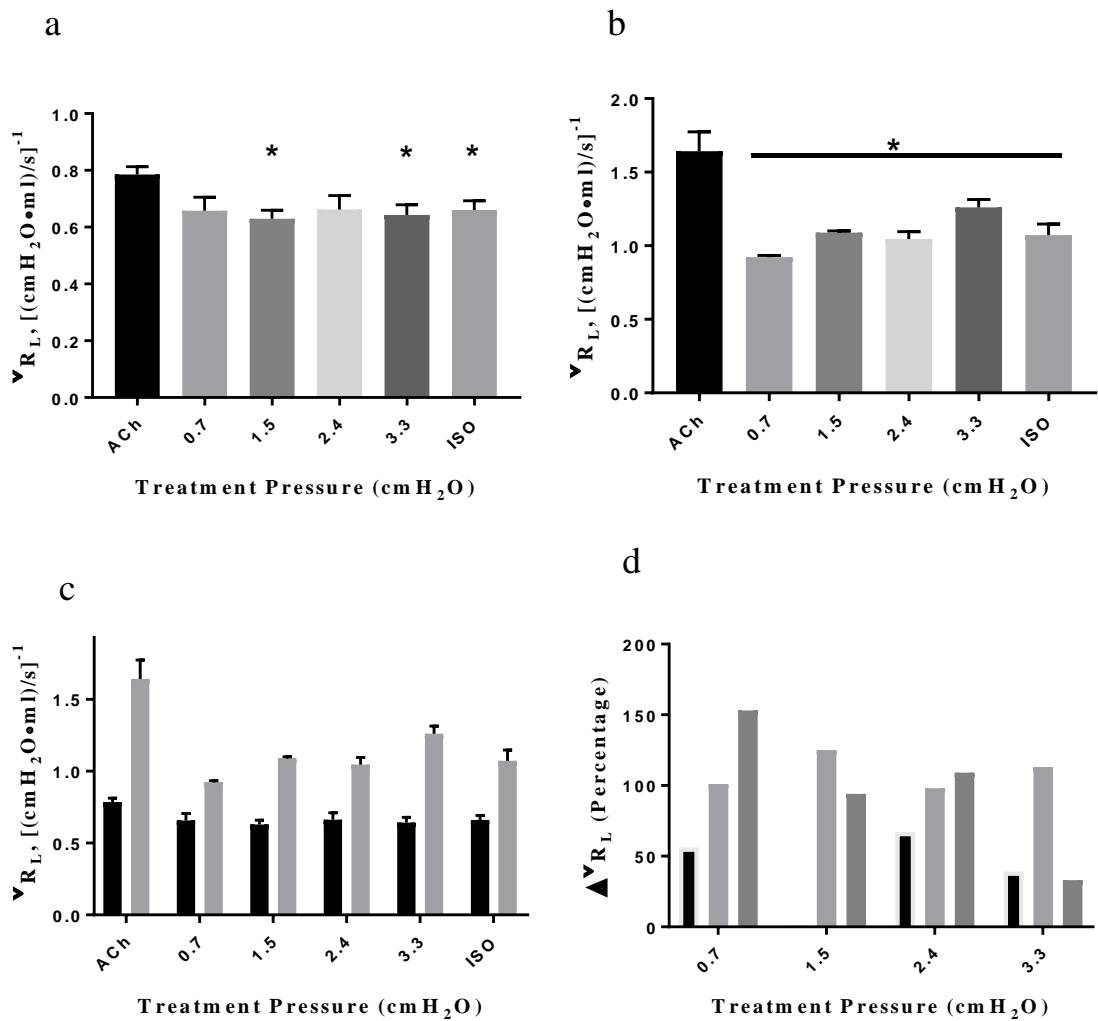


Figure 7.2. Transformations of 10 Hz R_L values to \check{R}_L . Acute (a) and Chronic (b) groups with SIPO amplitudes of 100 – 400 mV (0.7, 1.5, 2.4, and 3.3 cmH₂O) are presented ($n=7$, except for chronic SIPO, $n = 5$). (c) Magnitudes of acute (black) and chronic (grey) \check{R}_L values; and (d) percent change in \check{R}_L (compared to ACh) of acute (light grey) and chronic (dark grey) values; healthy changes are indicated (black) for comparison.

Table 7.3 Sensitized \check{R}_L data from the 15 Hz-derived pressure set. 15 Hz-generated waveforms combined with indicated amplitudes produce the applied SIPO treatment (cmH₂O). Transformed results include ACh and ISO comparison values, and are presented as $\check{R}_L \pm SE$ [(cmH₂O·ml)/s]⁻¹.

	OVA-Sensitized (Acute)	DRA-Sensitized (Chronic)
Experimental condition	$\check{R}_L \pm SE$ [(cmH ₂ O·ml)/s] ⁻¹	
ACh (10 ⁻⁴ M)	0.79 ± 0.03	1.64 ± 0.13
15 Hz/100 mV (0.4 cmH ₂ O)	0.69 ± 0.04	1.34 ± 0.05
15 Hz/200 mV (1.1 cmH ₂ O)	0.64 ± 0.03	1.06 ± 0.09
15 Hz/300 mV (1.7 cmH ₂ O)	0.68 ± 0.03	0.85 ± 0.07
15 Hz/400 mV (2.4 cmH ₂ O)	0.72 ± 0.06	1.05 ± 0.05
ISO (10 ⁻⁶ M)	0.66 ± 0.03	1.07 ± 0.08

The differences in the magnitudes of acute and chronic data are apparent when viewed in the context of normalised data (Fig. 7.3(c)), and indicate that physiological responses to SIPO treatments differ based on the health/disease status of the same mouse strain. This conclusion is further supported with comparing the percent change in \check{R}_L values for acute and chronic mice in this 15 Hz SIPO treatment group (Fig. 7.3(d)). There are clear differences in the change in responses of short- and long-term asthmatic mice, based on the applied SIPO in this group (except for the 1.1 cmH₂O set), and their modelled disease state.

Table 7.4 contains the \check{R}_L data obtained from the set of 20 Hz-derived SIPO treatments of acute and sensitized subjects. Conditions are described both as Hz/mV combinations and corresponding physiological pressures. The 20 Hz data set consists of pressures derived from 20 Hz in combination with amplitudes of 100 - 400 mV, which are equivalent to 0.4, 1.1, 1.7, and 2.3 cmH₂O respectively. Experimental results for ACh and ISO conditions are also presented as parameter references.

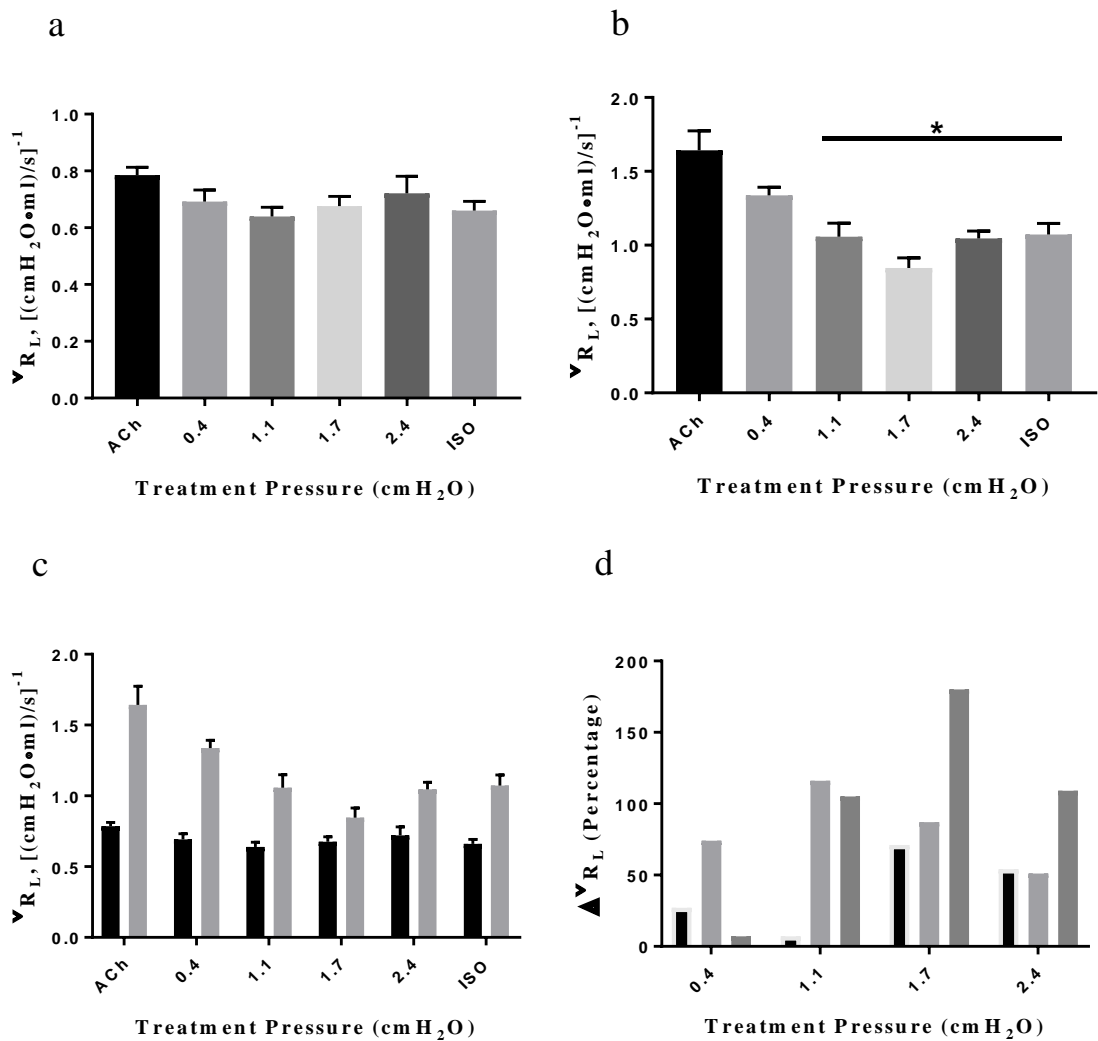


Figure 7.3. Transformations of 15 Hz R_L values to \check{R}_L . Acute (a) and Chronic (b) groups with SIPO amplitudes of 100 – 400 mV (0.4, 1.1, 1.7, and 2.4 cmH₂O) are presented ($n=7$, except for chronic SIPO, $n = 5$). (c) Magnitudes of acute (black) and chronic (grey) \check{R}_L values; and (d) percent change in \check{R}_L (compared to ACh) of acute (light grey) and chronic (dark grey) values; healthy changes are indicated (black) for comparison.

The 20 Hz acute \check{R}_L values range from 0.66 ((cmH₂O·ml)/s)⁻¹ for ISO treatment up to a high of 0.85 ((cmH₂O·ml)/s)⁻¹ with the 300 mV treatment. The lowest \check{R}_L value for acute subjects treated with ISO was also comparable to 400 mV (2.3 cmH₂O) treatments. No significant differences are observed when comparing the ACh standard with the group's data points, though notably, the 1.7 cmH₂O treatment is great than ACh. Figure 7.4(a) illustrates the 20 Hz acute \check{R}_L values, indicating no significant ($p > 0.05$) differences relevant to ACh with an asterisk. Chronic group \check{R}_L values range from 0.65 ((cmH₂O·ml)/s)⁻¹ for 300 mV treatments up to a high of 1.64 ((cmH₂O·ml)/s)⁻¹ with ACh challenge. The lowest \check{R}_L value for chronic mice was achieved from the 1.7 cmH₂O SIPO group. All data for the chronic group was significantly lower than ACh ($p < 0.05$). Fig. 7.3(b) illustrates the 20 Hz chronic \check{R}_L values, indicating significant differences relevant to ACh with an asterisk (*).

Table 7.4 Sensitized \check{R}_L and data from the 20 Hz-derived pressure set. 20 Hz-generated waveforms combined with indicated amplitudes produce the applied SIPO treatment (cmH₂O). Transformed results include ACh and ISO comparison values, and are presented as $\check{R}_L \pm SE$ [(cmH₂O·ml)/s]⁻¹.

	OVA-Sensitized (Acute)	DRA-Sensitized (Chronic)
Experimental condition	$\check{R}_L \pm SE$ [(cmH ₂ O·ml)/s] ⁻¹	
ACh (10 ⁻⁴ M)	0.79 ± 0.03	1.64 ± 0.13
20 Hz/100 mV (0.4 cmH ₂ O)	0.71 ± 0.03	1.13 ± 0.05
20 Hz/200 mV (1.1 cmH ₂ O)	0.73 ± 0.05	1.04 ± 0.10
20 Hz/300 mV (1.7 cmH ₂ O)	0.85 ± 0.06	0.65 ± 0.02
20 Hz/400 mV (2.3 cmH ₂ O)	0.67 ± 0.05	0.99 ± 0.05
ISO (10 ⁻⁶ M)	0.66 ± 0.03	1.07 ± 0.08

The differences in the magnitudes of acute and chronic data are apparent when viewed in the context of normalised data (Fig. 7.4(c)), and indicate that physiological responses to SIPO treatments differ based on the health/disease status of the same mouse strain. This conclusion is further supported with comparing the percent change in \check{R}_L values for acute and chronic subjects in this 20 Hz SIPO treatment group (Fig. 7.4(d)). There are clear differences in the change in responses of short- and long-term asthmatic mice, based on the applied SIPOs of 1.1 and 1.7 cmH₂O, and their modelled disease state.

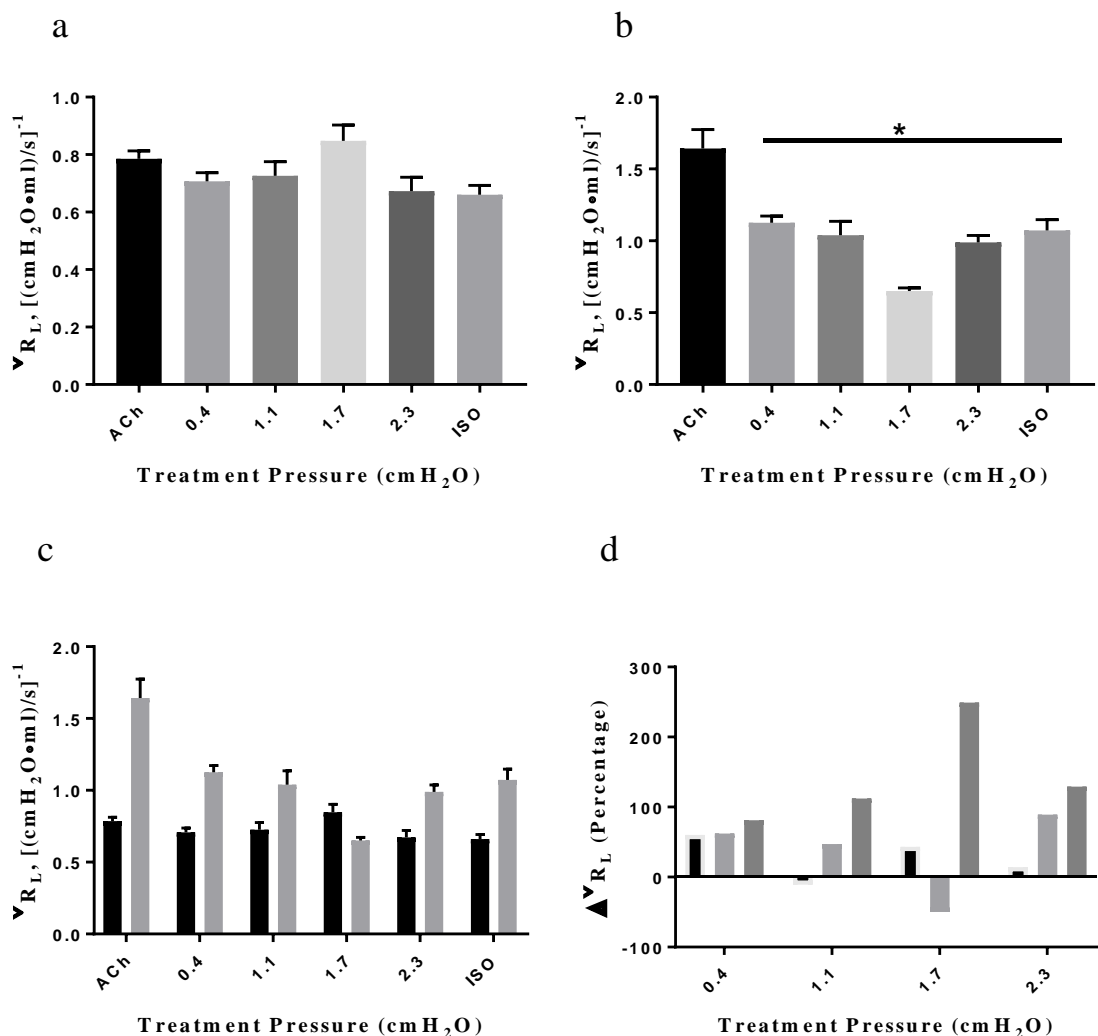


Figure 7.4. Transformations of 20 Hz R_L values to \check{R}_L . Acute (a) and Chronic (b) groups with SIPO amplitudes of 100 – 400 mV (0.4, 1.1, 1.7, and 2.3 cmH₂O) are presented ($n=7$, except for chronic SIPO, $n=5$). (c) Magnitudes of acute (black) and chronic (grey) \check{R}_L values; and (d) percent change in \check{R}_L (compared to ACh) of acute (light grey) and chronic (dark grey) values; healthy changes are indicated (black) for comparison.

7.4. \check{C}_{dyn} in two asthmatic models

The C_{dyn} results presented in Chapter VI correspond to the *in vivo* chronic asthmatic data obtained using the protocols and resources outlined in Chapters III and IV. The total dynamic compliance values in this chronic model are compared to their corresponding parameters in our previous acute model (Appendix D) following transformation to values of \check{C}_{dyn} . The effects of SIPO are analysed for significant differences across frequency and amplitude determinants of the applied pressure oscillations.

As noted in the discussion relative to R_L (and \check{R}_L), hyperresponsive airways are a classic feature found in human asthma. This study uses values of C_{dyn} across healthy, acute, and chronic conditions to further evaluate AHR. Development of the disease, as modelled in healthy to chronic mice, is expected to present AHR parameter values in long-term asthmatic ASM that are more severe when compared to short-term asthmatic ASM, as the tissues respond to a bronchorelaxant stimulus.

Comparison of the complementary elements of the AHR parameters is accomplished by using C_{dyn} data and the respiratory constant to determine \check{C}_{dyn} values (Equation A.7) for this study's data sets. \check{C}_{dyn} values are relative indicators of airway bronchoconstriction or bronchorelaxation, and gauge the efficacy of applied pressure oscillations across the tested acute and sensitized mice.

Values for \check{C}_{dyn} are presented in Tables 7.5 – 7.8 in this section and are expressed as the mean \pm SE for each given condition. Tables provide the summary of transformed data from applications of ACh, ISO, and SIPO treatments in acute and sensitized mice. SIPO values are grouped within each table according to frequency (Hz), amplitude (mV), and the generated physiological pressure (cmH₂O) sets in order to effectively present results.

Table 7.5 contains the \check{C}_{dyn} data obtained from the set of 5 Hz-derived SIPO treatments of acute and sensitized mice. Conditions are described both as Hz/mV combinations and corresponding physiological pressures. The 5 Hz data set consists of pressures derived from 5 Hz in combination with amplitudes of 100 - 400 mV, which are equivalent to 0.8, 1.6, 2.6, and 3.6 cmH₂O respectively. Experimental results for ACh and ISO conditions are also presented as parameter references.

Table 7.5. Sensitized \check{C}_{dyn} from the 5 Hz-derived pressure set. 5 Hz-generated waveforms combined with indicated amplitudes produce the applied SIPO treatment (cmH₂O). Transformed results include ACh and ISO comparison values, and are presented as $\check{C}_{dyn} \pm SE$ (cmH₂O·ml).

	OVA-Sensitized (Acute)	DRA-Sensitized (Chronic)
Experimental condition	$\check{C}_{dyn} \pm SE$ (cmH ₂ O·ml)	
ACh (10 ⁻⁴ M)	0.39 ± 0.02	0.27 ± 0.03
5 Hz/100 mV (0.8 cmH ₂ O)	0.47 ± 0.02	0.24 ± 0.02
5 Hz/200 mV (1.6 cmH ₂ O)	0.45 ± 0.03	0.30 ± 0.01
5 Hz/300 mV (2.6 cmH ₂ O)	0.44 ± 0.04	0.23 ± 0.00
5 Hz/400 mV (3.6 cmH ₂ O)	0.48 ± 0.03	0.27 ± 0.02
ISO (10 ⁻⁶ M)	0.48 ± 0.03	0.31 ± 0.03

The 5 Hz acute \check{C}_{dyn} values range from 0.39 (cmH₂O·ml) for ACh challenge up to a high of 0.48 (cmH₂O·ml) with ISO and 3.6 cmH₂O SIPO treatment. No significant differences are observed when comparing the ACh standard with the groups' data points. Figure 7.5(a) illustrates the 5 Hz acute \check{C}_{dyn} values. Chronic group \check{C}_{dyn} values range from 0.23 (cmH₂O·ml) for 300 mV treatments up to a high of 0.31 (cmH₂O·ml) with ISO treatment. The highest \check{C}_{dyn} value for chronic mice was achieved from the 1.6 cmH₂O SIPO group and ISO treatment, which were statistically equivalent as well as significantly different from ACh challenge. Figure 7.5(b) illustrates the 5 Hz chronic \check{C}_{dyn} values, indicating significant ($p < 0.05$) differences relevant to ACh with an asterisk (*).

The differences in the magnitudes of acute and chronic data are apparent when viewed in the context of normalised data (Fig. 7.5(c)), and indicate that physiological responses to SIPO treatments differ based on the health/disease status of the same mouse strain. This conclusion is further supported with comparing the percent change in \check{C}_{dyn} values for acute and chronic subjects in this 5 Hz SIPO treatment group (Fig. 7.5(d)). There are clear differences in all of the responses of short- and long-term asthmatic mice (except for the applied SIPO at 1.6 cmH₂O) and their modelled disease state.

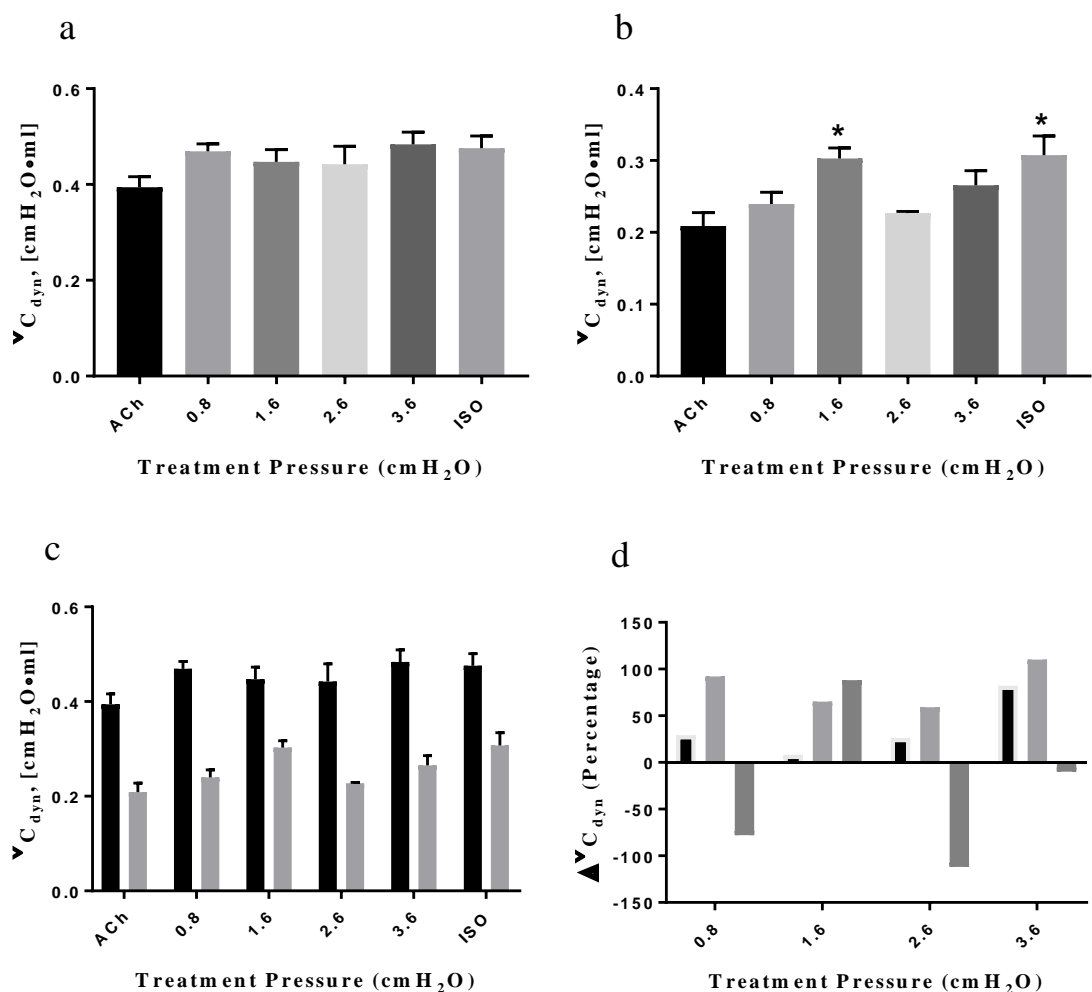


Figure 7.5. Transformations of 5 Hz C_{dyn} values to \check{C}_{dyn} . Acute (a) and Chronic (b) groups with SIPO amplitudes of 100 – 400 mV (0.8, 1.6, 2.6, and 3.6 cmH₂O) are presented ($n=7$, except for chronic SIPO, $n = 5$). (c) Magnitudes of acute (black) and chronic (grey) \check{C}_{dyn} values; and d) percent change in \check{C}_{dyn} (compared to ACh) of acute (light grey) and chronic (dark grey) values; healthy changes are indicated (black) for comparison.

Table 7.6 contains the \check{C}_{dyn} data obtained from the set of 10 Hz-derived SIPO treatments of acute and sensitized subjects. Conditions are described both as Hz/mV combinations and corresponding physiological pressures. The 10 Hz data set consists of pressures derived from 10 Hz in combination with amplitudes of 100 - 400 mV, which are equivalent to 0.7, 1.5, 2.4, and 3.3 cmH₂O respectively. Experimental results for ACh and ISO conditions are also presented as parameter references.

Table 7.6 Sensitized \check{C}_{dyn} from the 10 Hz-derived pressure set. 10 Hz-generated waveforms combined with indicated amplitudes produce the applied SIPO treatment (cmH₂O). Transformed results include ACh and ISO comparison values, and are presented as $\check{C}_{dyn} \pm SE$ (cmH₂O·ml).

	OVA-Sensitized (Acute)	DRA-Sensitized (Chronic)
Experimental condition	$\check{C}_{dyn} \pm SE$ (cmH ₂ O·ml)	
ACh (10 ⁻⁴ M)	0.39 ± 0.02	0.27 ± 0.03
10 Hz/100 mV (0.7 cmH ₂ O)	0.48 ± 0.04	0.34 ± 0.01
10 Hz/200 mV (1.5 cmH ₂ O)	0.50 ± 0.03	0.29 ± 0.01
10 Hz/300 mV (2.4 cmH ₂ O)	0.50 ± 0.06	0.30 ± 0.01
10 Hz/400 mV (3.3 cmH ₂ O)	0.51 ± 0.04	0.25 ± 0.01
ISO (10 ⁻⁶ M)	0.48 ± 0.03	0.31 ± 0.03

The 10 Hz acute \check{C}_{dyn} values range from 0.39 (cmH₂O·ml) for ACh challenge up to a high of 0.51 (cmH₂O·ml) with 400 mV treatment. All values other than ACh are statistically comparable, and no significant differences are observed when comparing the ACh standard against the entire set. Figure 7.6(a) illustrates the 10 Hz acute \check{C}_{dyn} values.

Chronic group \check{C}_{dyn} values range from 0.25 (cmH₂O·ml) for 400 mV treatments up to a high of 0.34 (cmH₂O·ml) with 100 mV treatments. Figure 7.6(b) illustrates the 10 Hz chronic \check{C}_{dyn} values, indicating significant ($p < 0.05$) differences relevant to ACh with an asterisk (*).

The differences in the magnitudes of acute and chronic 10 Hz groups are apparent when viewed in the context of normalised data (Fig. 7.6(c)), and indicate that physiological responses to SIPO treatments differ based on the health/disease status of the same mouse strain. This conclusion is further supported with comparing the percent change in \check{C}_{dyn} values for acute and chronic mice in this 10 Hz SIPO treatment group (Fig. 7.6(d)). There are clear differences in the change in responses of short- and long-term asthmatic mice, based on all applied SIPO of this group, and the two modelled disease states.

Table 7.7 contains the \check{C}_{dyn} data obtained from the set of 15 Hz-derived SIPO treatments of acute and sensitized subjects. Conditions are described both as Hz/mV combinations and corresponding physiological pressures. The 15 Hz data set consists of pressures derived from 15 Hz in combination with amplitudes of 100 - 400 mV, which are equivalent to 0.4, 1.1, 1.7, and 2.4 cmH₂O respectively. Experimental results for ACh and ISO conditions are also presented as parameter references.

The 15 Hz acute \check{C}_{dyn} values range from 0.39 (cmH₂O·ml) for ACh challenge up to a high of 0.51 (cmH₂O·ml) with 200 mV treatment. The highest \check{C}_{dyn} value for acute mice was achieved from the 1.1 cmH₂O SIPO group, but it is not significantly different from other SIPO values for the group. No significant differences are observed when comparing the ACh standard with the group's SIPO or ISO data points. Figure 7.7(a) illustrates the 15 Hz acute \check{C}_{dyn} values, indicating the lack of significant ($p > 0.05$) differences relevant to

ACh. The chronic group \check{C}_{dyn} values range from 0.23 (cmH₂O·ml) for 100 mV treatments up to a high of 0.38 (cmH₂O·ml) with 300 mV treatment. The highest \check{C}_{dyn} value for chronic mice was achieved from the 1.7 cmH₂O SIPO group. All data for the chronic group except for the 0.4 cmH₂O treatment was significantly higher than ACh ($p < 0.05$). Figure 7.7(b) illustrates the 15 Hz chronic \check{C}_{dyn} values, indicating significant ($p < 0.05$) differences relevant to ACh with an asterisk (*).

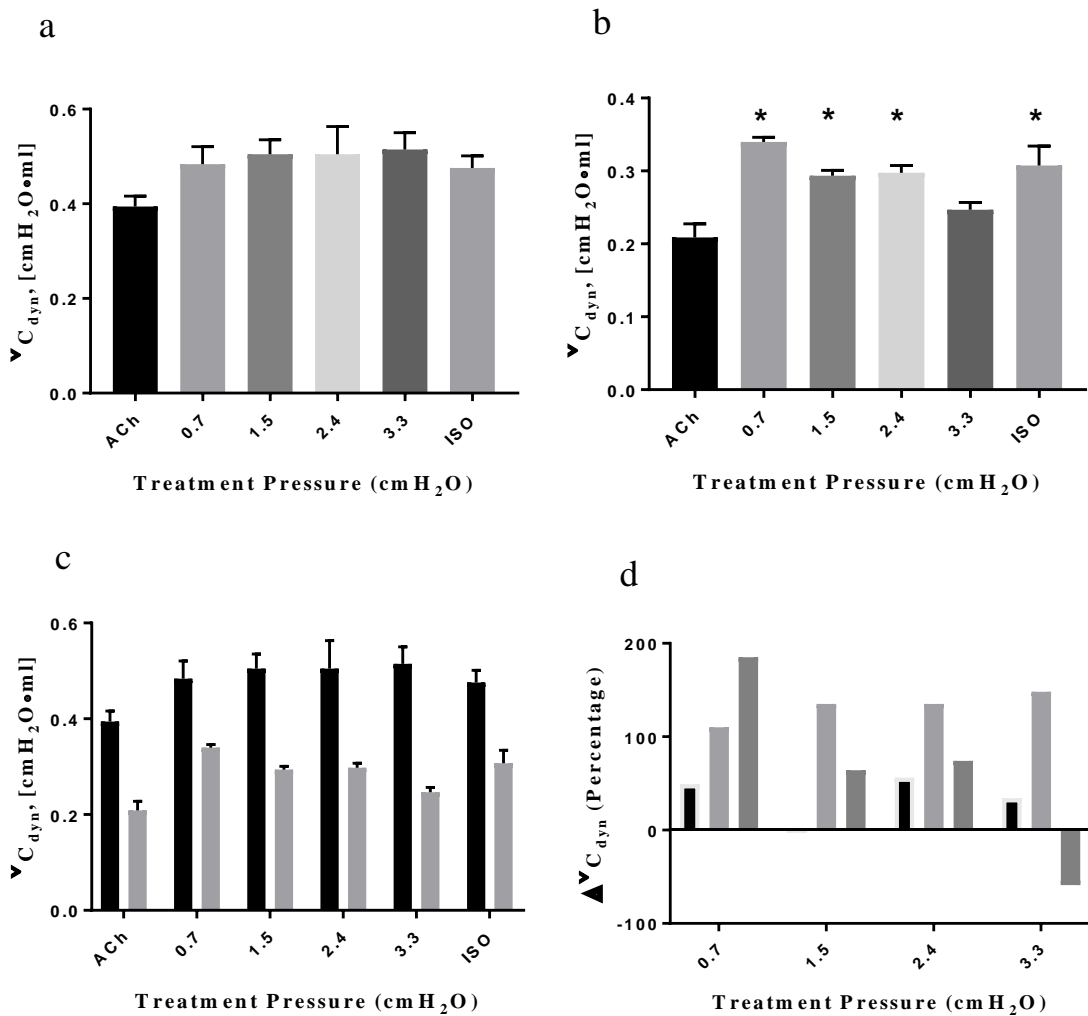


Figure 7.6. Transformations of 10 Hz C_{dyn} values to \check{C}_{dyn} . Acute (a) and Chronic (b) groups with SIPO amplitudes of 100 – 400 mV (0.7, 1.5, 2.4, and 3.3 cmH₂O) are presented ($n=7$, except for chronic SIPO, $n = 5$). (c) Magnitudes of acute (black) and chronic (grey) \check{C}_{dyn} values; and (d) percent change in \check{C}_{dyn} (compared to ACh) of acute (light grey) and chronic (dark grey) values; healthy changes are indicated (black) for comparison.

Table 7.7 Sensitized \check{C}_{dyn} data from the 15 Hz-derived pressure set. 15 Hz-generated waveforms combined with indicated amplitudes produce the applied SIPO treatment (cmH₂O). Transformed results include ACh and ISO comparison values, and are presented as $\check{C}_{dyn} \pm SE$ (cmH₂O·ml).

	OVA-Sensitized (Acute)	DRA-Sensitized (Chronic)
Experimental condition	$\check{C}_{dyn} \pm SE$ (cmH ₂ O·ml)	
ACh (10 ⁻⁴ M)	0.39 ± 0.02	0.27 ± 0.03
15 Hz/100 mV (0.4 cmH ₂ O)	0.46 ± 0.03	0.23 ± 0.01
15 Hz/200 mV (1.1 cmH ₂ O)	0.51 ± 0.04	0.33 ± 0.04
15 Hz/300 mV (1.7 cmH ₂ O)	0.47 ± 0.02	0.38 ± 0.03
15 Hz/400 mV (2.4 cmH ₂ O)	0.46 ± 0.05	0.30 ± 0.01
ISO (10 ⁻⁶ M)	0.48 ± 0.03	0.31 ± 0.03

The differences in the magnitudes of acute and chronic data are apparent when viewed in the context of normalised data (Fig. 7.7(c)), and indicate that physiological responses to SIPO treatments differ based on the health/disease status of the same mouse strain. This conclusion is further supported with comparing the percent change in \check{C}_{dyn} values for acute and chronic mice in this 15 Hz SIPO treatment group (Fig. 7.7(d)). There are clear differences in the change in responses of short- and long-term asthmatic mice, based on the applied SIPOs of 0.4 and 1.7 cmH₂O, and their modelled disease state.

Table 7.8 contains the \check{C}_{dyn} data obtained from the set of 20 Hz-derived SIPO treatments of acute and sensitized mice. Conditions are described both as Hz/mV combinations and

corresponding physiological pressures. The 20 Hz data set consists of pressures derived from 20 Hz in combination with amplitudes of 100 - 400 mV, which are equivalent to 0.4, 1.1, 1.7, and 2.3 cmH₂O respectively. Experimental results for ACh and ISO conditions are also presented as parameter references.

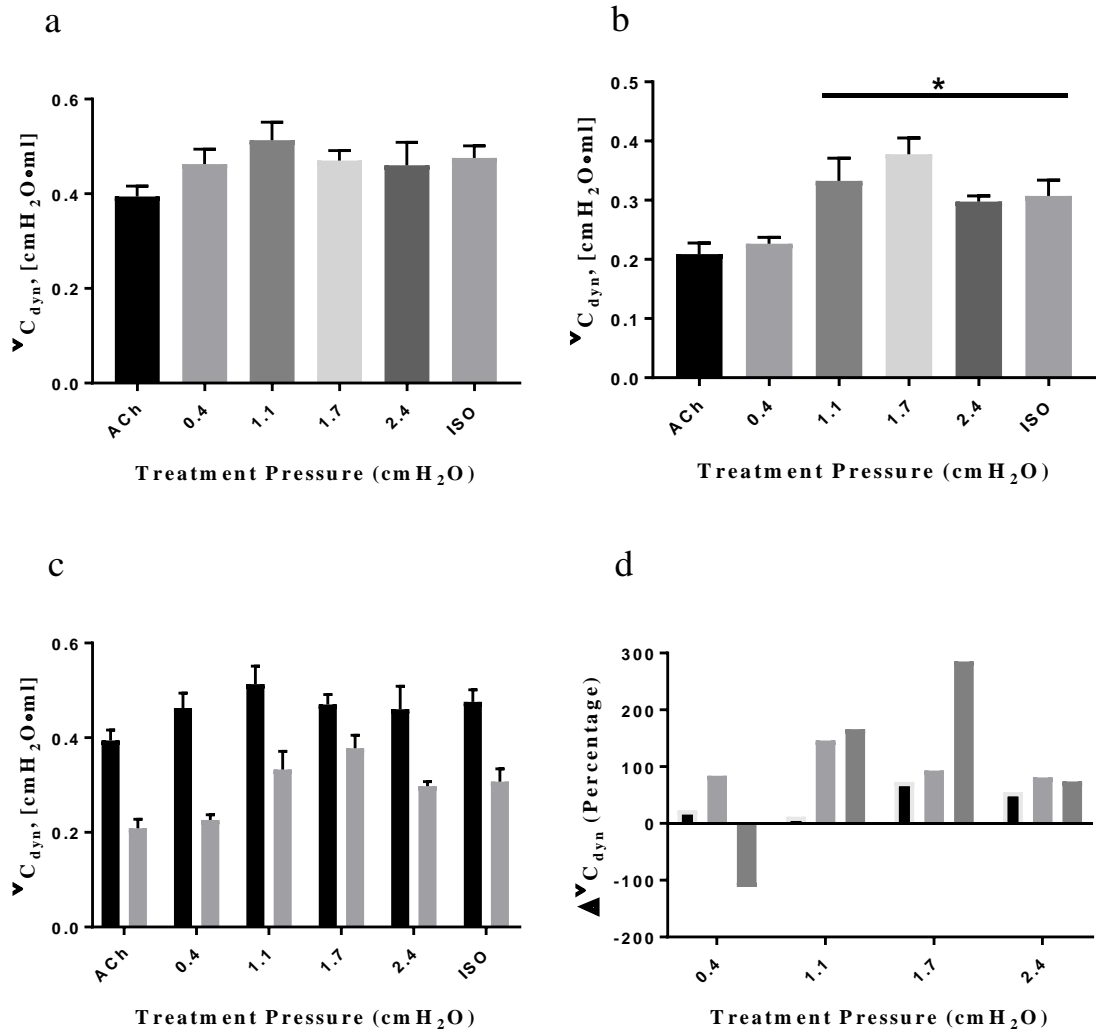


Figure 7.7. Transformations of 15 Hz C_{dyn} values to \check{C}_{dyn} . Acute (a) and Chronic (b) groups with SIPO amplitudes of 100 – 400 mV (0.4, 1.1, 1.7, and 2.4 cmH₂O) are presented ($n=7$, except for chronic SIPO, $n = 5$). (c) Magnitudes of acute (black) and chronic (grey) \check{C}_{dyn} values; and (d) percent change in \check{C}_{dyn} (compared to ACh) of acute (light grey) and chronic (dark grey) values; healthy changes are indicated (black) for comparison.

The 20 Hz acute \check{C}_{dyn} values range from 0.38 (cmH₂O·ml) for 300 mV treatment up to a high of 0.48 (cmH₂O·ml) with the 400 mV and ISO treatments. The highest \check{C}_{dyn} value

for acute mice treated with ISO was also comparable to 2.3 cmH₂O treatments. No significant differences are observed when comparing the ACh standard with the group's data points, though notably, the 1.7 cmH₂O treatment is equivalent to ACh. Figure 7.8(a) illustrates the 20 Hz acute \check{C}_{dyn} values, indicating no significant ($p > 0.05$) differences relevant to ACh. Chronic group \check{C}_{dyn} values range from 0.27 (cmH₂O·ml) for ACh challenge up to a high of 0.48 (cmH₂O·ml) with 300 mV treatment. The highest \check{C}_{dyn} value for chronic mice was achieved from the 1.7 cmH₂O SIPO group; this same group in the acute data was the lowest value of the groups' analyses. All data for the chronic group was significantly higher than ACh ($p < 0.05$). Figure 7.8(b) illustrates the 20 Hz chronic \check{C}_{dyn} values, indicating significant differences relevant to ACh with an asterisk (*).

Table 7.8 Sensitized \check{C}_{dyn} and data from the 20 Hz-derived pressure set. 20 Hz-generated waveforms combined with indicated amplitudes produce the applied SIPO treatment (cmH₂O). Transformed results include ACh and ISO comparison values, and are presented as $\check{C}_{dyn} \pm SE$ (cmH₂O·ml).

	OVA-Sensitized (Acute)	DRA-Sensitized (Chronic)
Experimental condition	$\check{C}_{dyn} \pm SE$ (cmH ₂ O·ml)	
ACh (10^{-4} M)	0.39 ± 0.02	0.27 ± 0.03
20 Hz/100 mV (0.4 cmH ₂ O)	0.46 ± 0.02	0.28 ± 0.01
20 Hz/200 mV (1.1 cmH ₂ O)	0.44 ± 0.03	0.32 ± 0.03
20 Hz/300 mV (1.7 cmH ₂ O)	0.38 ± 0.02	0.48 ± 0.02
20 Hz/400 mV (2.3 cmH ₂ O)	0.48 ± 0.03	0.32 ± 0.01
ISO (10^{-6} M)	0.48 ± 0.03	0.31 ± 0.03

The differences in the magnitudes of acute and chronic data are apparent when viewed in the context of normalised data (Fig. 7.8(c)), and indicate that physiological responses to SIPO treatments differ based on the health/disease status of the same mouse strain. This conclusion is further supported with comparing the percent change in \check{C}_{dyn} values for acute and chronic subjects in this 20 Hz SIPO treatment group (Fig. 7.8(d)). There is a clear difference in the change in responses of short- and long-term asthmatic mice, based on the applied SIPO of 1.7 cmH₂O, and their modelled disease state.

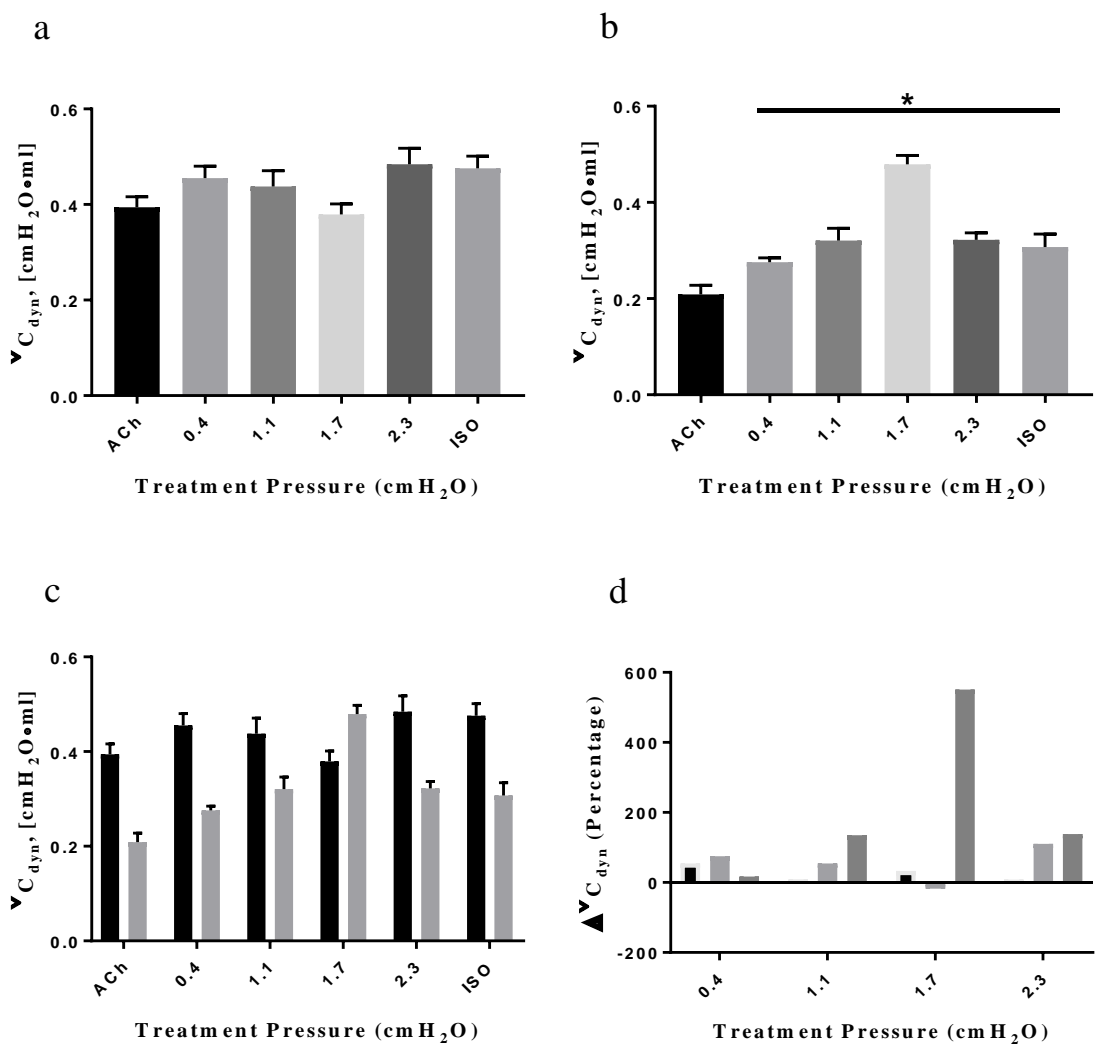


Figure 7.8. Transformations of 20 Hz C_{dyn} values to \check{C}_{dyn} . Acute (a) and Chronic (b) groups with SIPO amplitudes of 100 – 400 mV (0.4, 1.1, 1.7, and 2.3 cmH₂O) are presented ($n=7$, except for chronic SIPO, $n = 5$). (c) Magnitudes of acute (black) and chronic (grey) \check{C}_{dyn} values; and (d) percent change in \check{C}_{dyn} (compared to ACh) of acute (light grey) and chronic (dark grey) values; healthy changes are indicated (black) for comparison.

7.5. Discussion

Our studies show that two separate states of asthmatic airways respond differently across a similar range of applied SIPO treatments. As mentioned (Chapt. II), the observed responses of the airways are likely due to changes in the basal tone, rearrangement of internal cellular structures, as well as overall change to the cellular composition of ASM [26, 33, 81, 99, 101, 152, 153].

While healthy tissues (*in vitro* and *in vivo*) are influenced by mechanically applied (physiological value-based) TO and DI oscillations, resulting in effective relaxation of the tissues tested, this is not the case for asthmatic tissues. The applied oscillations' effects are believed to act on mechanical structures rather than chemical pathways. The mechanical structures involved in contraction, and relevant to this discussion, are the actin and myosin elements of the crossbridge. Given that the identity of the crossbridge is maintained regardless of healthy or diseased states, it is therefore plausible that crossbridge activity changes with the state of the disease. Evidence for this differential tissue response is found in application of similar oscillations to differing states of healthy and sensitized ASM. Adaptation of ASM over the course of disease progression is a valid characterization of changes to chemical and mechanical ASM identities. In fact, the adaptability of the tissues is consistent with the proposed conclusions of this comparison between healthy, acute and chronic asthma models. The observed effects of SIPO in a single strain of mice, across different disease states, allows for the assumption that the crossbridge remains the same in terms of components, but changes in its functional capabilities to effect force over the distance of its structures.

The results of this study are presented with the view that the crossbridge cycle of ASM is a periodic function determined by the state of health/disease of the system. The periodic

cycle can be disrupted by specific interference patterns based on combinations of applied frequencies and amplitudes.

The basal tone of the tissue is viewed as a physiological result of this periodic function of actinomyosin interactions within the cellular framework. Changes in the rate of crossbridge cycling are then expected to change the basal tone of the tissue, and are expected to influence the degree of AHR to external challenges – ACh in this study, for example. Relaxation of pre-contracted ASM due to applied SIPO can then be viewed as a disruption to the intrinsic disease-state cycling of the actinomyosin crossbridge. Rates of myosin attachment and detachment are perturbed, in line with Fredberg's proposals. The consistency of the theory is found in the fact that in healthy tissues, the perturbation of the crossbridge is possible with TO and DI applications [16, 83, 7, 78], while in acute or chronic asthmatic ASM, with a cycling rate expected to be different from the healthy rate, the successful "healthy" interference pattern from similar applications does not occur because the template cycle is no longer present in the crossbridge of diseased tissues.

Tidal breathing and deep inspirations are the basis for theories of healthy ASM reactivity to applied oscillations. Efforts to relax pre-constricted tissue with these traditional oscillation patterns are effective in healthy samples and subjects [7, 9, 10, 16, 21, 33, 82, 83, 95, 97, 99, 156], yet asthmatic tissues do not respond in kind [7, 153]. Testing similar oscillation patterns across different states of healthy and asthmatic conditions has resulted in the development of models which portray changes in structural components of ASM as adaptations characteristic of a diseased state [26, 33, 81, 99, 101, 152, 153]. The initial theories of healthy tissue functionality (in the context of their response to applied oscillations) have been maintained in striving to understand the observations from testing both short- and long-term sensitization conditions in asthmatic models. Along with the traditional oscillations, which mimic physiological patterns, alternative non-

physiological values for the applied oscillations have been investigated against healthy and asthmatic mice [9, 82, 83, 97, 101]. Additionally, superimposed pressure oscillations which overlay the natural breathing patterns have been tested against healthy and asthmatic mice [9].

This study has focussed on modelling DRA-sensitized (long-term, chronic) asthmatic airways' responses to SIPO applications and analyzing the results with established short-term asthmatic modelling in our laboratory. Analysis of the collected respiratory parameters' data indicates results consistent with a model of crossbridge perturbation. Further comparison of the chronic data with our laboratory's acute results also serves to augment the current body of knowledge relative to interference patterns applied to pre-constricted ASM. Based on data normalisation, inferences also arise from this study regarding significant differences in power and work performed by short- and long-term asthmatic tissues, depending on the applied SIPO treatments.

7.6. *Future work*

This study presents a novel long-term sensitization model for murine asthma. Further novelty is found in the observed effects of applied SIPO treatments to the modelled mice. The results of experimental investigations elucidate the perturbation of crossbridge cycling as a result of superimposed oscillations acting on the inherent contractile behaviour of pre-contracted ASM in sensitized airways. Comparison of the dynamic conditions across healthy and chronic disease states indicates that there is a significant effect observed *in vitro* based on applied pressures. This study has addressed a long-term sensitization model of asthma, and compared the observed effects against a short-term sensitization model, thereby assessing a broader spectrum of application for the SIPO

treatments. Additional studies are needed to investigate the effect of SIPO on chronic states, given the pronounced (and differing) effects of specific SIPO treatments at different states of the modelled disease.

With future goals of alleviating a dependence on asthma medications, it is imperative to build an understanding of the optimal applications that alleviate AHR characteristics, and support a return to normal breathing patterns. Future work in this area involves a refinement of SIPO treatments to ascertain their observed range of effective pressures identified in this study. Additionally, a combination of SIPO treatments with and without bronchorelaxant medications will expand knowledge relative to the mechanical and chemical components of ASM contraction and relaxation responses.

7.7. Conclusions

The objectives of the study were to develop a long-term model of asthma, experimentally investigate the effect of SIPO in sensitized airways, and quantify the response of these airways to the range of applied oscillations. Once the long-term sensitization model was analysed, its conclusions along with findings in our earlier acute asthmatic model were assessed for effects of SIPO in asthmatic disease. A detailed literature review regarding ASM and asthma research (Chapt. II) preceded the stated objectives, all of which were achieved. Chapter III presented asthma models, selection criteria and sensitization protocols, as well as successful assessment of this study's long-term asthmatic model in mice. Chapter IV detailed the mechanical and chemical techniques, and equipment as well as calibrations and experimental protocols for the *in vitro* testing. Chapter V presented all the lung resistance results and analyses, followed by Chapter VI with its dynamic compliance results and analyses. Finally, Chapter VII compared two established

models of chronic asthma in mice, and discusses the effects of SIPO on the study's murine airways.

Results from this study build on the theory that length oscillations of ASM during contraction have an effect on the interaction of actin and myosin, characterized as a disruption of the actinomyosin crossbridge [9, 10, 82, 83, 97]. SILO studies indicate that there are effective frequency or amplitude values which are effective on sensitized airways. Oscillations of pre-constricted sensitized airways are therefore interpreted as being capable of inducing relaxation, in line with the hypothesis that the main components of the crossbridge (actin, myosin and the actinomyosin crossbridge) do not change, yet can be disrupted or perturbed.

Changes in ASM occur as a result of asthma development. Length adaptation, change in the basal tone, and rearrangement of cellular structures are expected to present different responses of tissue to a practical range of applied SIPO values. Indeed, comparisons of healthy, short-term, and long-term sensitization model responses indicate that this is the case for establishing a return to normal breathing patterns. The results of this study continue to add to the understanding of asthmatic airway responses to SIPO treatments. Furthermore, there is a refinement to previous observations in our short-term model, in that the application of oscillations is not only a means for inducing ASM length changes: SIPO applications vary in their ability to improve the work of the asthmatic airway based on the state of disease, as seen in the long-term sensitization treatment responses.

REFERENCES

1. Asthma and Respiratory Foundation of New Zealand, The burden of asthma in New Zealand. 2001, Adis International Ltd: Auckland, New Zealand.
2. Eder, W., Ege, M. J., & von Mutius, E. (2006). The asthma epidemic. *New England Journal of Medicine*, 355(21), 2226-2235.
3. (WHO) World Health Organization. Asthma. (2011). Fact Sheet No 307. [cited 2013 5/8/13]; Available from: <http://www.who.int/mediacentre/factsheets/fs307/en/>.
4. Green, R. H., Brightling, C. E., Pavord, I. D., & Wardlaw, A. J. (2003). Management of asthma in adults: current therapy and future directions. *Postgraduate Medical Journal*, 79(2), 259-267.
5. Rizzo, M. C. V., & Solé, D. (2006). Inhaled corticosteroids in the treatment of respiratory allergy: safety vs. efficacy. *Jornal de Pediatria*, 82(5), S198-S205.
6. Pearce, N., & Hensley, M. J. (1998). Epidemiologic studies of beta agonists and asthma deaths. *Epidemiologic reviews*, 20(2), 173-186.
7. Walters, E. H., Gibson, P. G., Lasserson, T. J., & Walters, J. A. (2007). Long-acting beta2-agonists for chronic asthma in adults and children where background therapy contains varied or no inhaled corticosteroid. *The Cochrane Library*.
8. Al-Jumaily, A., & Alizad, A. (Eds.). (2008). *Biomedical Applications of Vibration and Acoustics in Therapy, Bioeffects and Modeling* (pp. 215-244). ASME Press.
9. Bateman, E. D., Hurd, S. S., Barnes, P. J., Bousquet, J., Drazen, J. M., FitzGerald, M., ... & Pizzichini, E. (2008). Global strategy for asthma management and prevention: GINA executive summary. *European Respiratory Journal*, 31(1), 143-178.
10. Al-Jumaily, A. M., Roos, K. L. T., Bessaguet, S., & Jo-Avila, M. (2017). Prestretched airway smooth muscle response to length oscillation. *Physiological reports*, 5(2).
11. Al-Jumaily, A. M., Mbikou, P., & Redey, P. R. (2012). Effect of length oscillations on airway smooth muscle reactivity and cross-bridge cycling. *American Journal of Physiology-Lung Cellular and Molecular Physiology*, 303(4), L286-L294.

12. Al-Jumaily, A. M., Mathur, M., & Cairns, S. (2015). Combination of isoproterenol and length oscillations in relaxing porcine airway smooth muscles. *Biomaterials and Biomechanics in Bioengineering*, 2(4), 225-235.
13. Jo-Avila, M., Al-Jumaily, A. M., & Lu, J. (2014). Relaxant effect of superimposed length oscillation on sensitized airway smooth muscle. *American Journal of Physiology-Lung Cellular and Molecular Physiology*, 308(5), L479-L484.
14. An, S. S., Bai, T. R., Bates, J. H. T., Black, J. L., Brown, R. H., Brusasco, V., ... & Fabry, B. (2007). Airway smooth muscle dynamics: a common pathway of airway obstruction in asthma. *European Respiratory Journal*, 29(5), 834-860.
15. Fredberg, J. J. (2001). Airway obstruction in asthma: does the response to a deep inspiration matter?. *Respiratory research*, 2(5), 273.
16. Fredberg, J. J., Inouye, D. S., Mijailovich, S. M., & Butler, J. P. (1999). Perturbed equilibrium of myosin binding in airway smooth muscle and its implications in bronchospasm. *American journal of respiratory and critical care medicine*, 159(3), 959-967.
17. Gump, A., Haughney, L., & Fredberg, J. (2001). Relaxation of activated airway smooth muscle: relative potency of isoproterenol vs. tidal stretch. *Journal of applied physiology*, 90(6), 2306-2310.
18. Mijailovich, S. M., Butler, J. P., & Fredberg, J. J. (2000). Perturbed equilibria of myosin binding in airway smooth muscle: bond-length distributions, mechanics, and ATP metabolism. *Biophysical Journal*, 79(5), 2667-2681.
19. (NZGG) New Zealand Guidelines Group. (2002). The diagnosis and treatment of adult asthma. In NZGG (Eds.), *Best Practice Evidence-based Guideline*. Wellington, New Zealand: Author.
20. Masoli, M., Fabian, D., Holt, S., & Beasley, R. (2004). Global burden of asthma. GINA (Global Initiative for Asthma), p122.
21. Holt, S., & Beasley, R. (2002). The burden of asthma in New Zealand. 2002, Wellington.
22. Guyton, A., & Hall, J. (2006). Medical Physiology, in Textbook of Medical Physiology, E. Sanders, Editor. Elsevier Inc.: Philadelphia.
23. Marieb, E. N., & Marieb, S. J. (2008). *Human anatomy and physiology laboratory manual*. Pearson/Benjamin Cummings: San Francisco, CA.
24. Wikipedia. (2008). Respiratory system. [cited 2010; Available from: http://commons.wikimedia.org/wiki/File:Respiratory_system_complete_en.svg.

25. Berne, R. M., & Levy, M. N. (2008). *Physiology* (6th ed.). Mosby: Maryland Heights, Missouri.
26. Lee, J. Y., Lim, K. M., Kim, S. Y., Bae, O. N., Noh, J. Y., Chung, S. M., ... Chung, J. H. (2010). Vascular Smooth Muscle Dysfunction and Remodeling Induced by Ginsenoside Rg3, a Bioactive Component of Ginseng. *Toxicological Sciences*, 17(2), 505-514.
27. Leonardi, R. & Alemanni, M. (2011). The management of erectile dysfunction: innovations and future perspectives. *Arch Ital Urol Androl.*, 83(1), 60-62.
28. Whorwell, P. J., Lupton, E. W., Erduran, D., & Wilson, K. (1986). Bladder smooth muscle dysfunction in patients with irritable bowel syndrome. *Gut*, 27(9), 1014-1017.
29. Seow, C. Y., & Paré, P. D. (2007). Ultrastructural basis of airway smooth muscle. *Canadian Journal of Physiology and Pharmacology*, 85, 659-665.
30. Zhang, J., Herrera, A. M., Paré, P. D., & Seow, C. Y. (2010). Dense-body aggregates as plastic structures supporting tension in smooth muscle cells. *American Journal of Physiology-Lung Cellular and Molecular Physiology*, 299(5), L631-L638.
31. Léguillette, R., & Lauzon, A. M. (2008). Molecular mechanics of smooth muscle contractile proteins in airway hyperresponsiveness and asthma. *Proceedings of the American Thoracic Society*, 5(1), 40-46.
32. Gunst, S. J., & Tang, D. D. (2000). The contractile apparatus and mechanical properties of airway smooth muscle. *European Respiratory Journal*, 15(3), 600-616.
33. Huxley, A. F., & Niedergerke, R. (1954). Structural changes in muscle during contraction; interference microscopy of living muscle fibres. *Nature*, 173, 971-973.
34. Huxley, H. E., & Hanson, J. (1954). Changes in the cross-striations of muscle during contraction and stretch and their structural interpretation. *Nature*, 173, 973-976.
35. Hai, C. M., & Murphy, R. A. (1988). Cross-bridge phosphorylation and regulation of latch state in smooth muscle. *American Journal of Physiology: Cell Physiology*, 254(1), C99-106.

36. Hai, C. M., & Murphy, R. A. (1988). Regulation of shortening velocity by cross-bridge phosphorylation in smooth muscle. *American Journal of Physiology-Cell Physiology*, 255(1), C86-C94.
37. Mitchell, R. W., Seow, C. Y., Burdyga, T., Maass-Moreno, R., Pratusевич, V. R., Ragozzino, J., & Ford, L. E. (2001). Relationship between myosin phosphorylation and contractile capability of canine airway smooth muscle. *Journal of applied physiology*, 90(6), 2460-2465.
38. Henry, P. J., & Goldie, R. G. (1990). β 1-Adrenoceptors mediate smooth muscle relaxation in mouse isolated trachea. *British journal of pharmacology*, 99(1), 131-135.
39. Mulvihill, D. P., & Hyams, J. S. (2001). Shedding a little light on light chains. *Nature cell biology*, 3(1), E10.
40. Vibert, P., Craig, R., & Lehman, W. (1993). Three-dimensional reconstruction of caldesmon-containing smooth muscle thin filaments. *The Journal of cell biology*, 123(2), 313-321.
41. Ansari, S., Alahyan, M., Marston, S. B., & Mohammed, E. M. (2008). Role of Caldesmon in the Ca^{2+} Regulation of Smooth Muscle Thin Filaments EVIDENCE FOR A COOPERATIVE SWITCHING MECHANISM. *Journal of biological chemistry*, 283(1), 47-56.
42. Burridge, K., & Chrzanowska-Wodnicka, M. (1996). Focal adhesions, contractility, and signaling. *Annual review of cell and developmental biology*, 12(1), 463-519.
43. MCGREGOR, A., Blanchard, A. D., Rowe, A. J., & Critchley, D. R. (1994). Identification of the vinculin-binding site in the cytoskeletal protein alpha-actinin. *Biochemical Journal*, 301(Pt 1), 225.
44. Wang, L., Chitano, P., & Murphy, T. M. (2005). A maturational model for the study of airway smooth muscle adaptation to mechanical oscillation. *Canadian journal of physiology and pharmacology*, 83(10), 817-824.
45. Takemura, M., Gomi, H., Colucci-Guyon, E., & Itohara, S. (2002). Protective role of phosphorylation in turnover of glial fibrillary acidic protein in mice. *Journal of Neuroscience*, 22(16), 6972-6979.
46. Gunst, S. J., Tang, D. D., & Saez, A. O. (2003). Cytoskeletal remodeling of the airway smooth muscle cell: a mechanism for adaptation to mechanical forces in the lung. *Respiratory physiology & neurobiology*, 137(2-3), 151-168.

47. Veigel, C., Molloy, J. E., Schmitz, S., & Kendrick-Jones, J. (2003). Load-dependent kinetics of force production by smooth muscle myosin measured with optical tweezers. *Nature cell biology*, 5(11), 980.
48. Mehta, D., & Gunst, S. J. (1999). Actin polymerization stimulated by contractile activation regulates force development in canine tracheal smooth muscle. *The Journal of physiology*, 519(3), 829-840.
49. Fredberg, J. J., & Silveira, P. S. (2005). Smooth muscle length adaptation and actin filament length: a network model of the cytoskeletal dysregulation. *Canadian journal of physiology and pharmacology*, 83(10), 923-931.
50. Fabry, B., & Fredberg, J. J. (2003). Remodeling of the airway smooth muscle cell: are we built of glass?. *Respiratory physiology & neurobiology*, 137(2-3), 109-124.
51. Draeger, A., Amos, W. B., Ikebe, M., & Small, J. V. (1990). The cytoskeletal and contractile apparatus of smooth muscle: contraction bands and segmentation of the contractile elements. *The Journal of cell biology*, 111(6), 2463-2473.
52. Bossé, Y., Sobieszek, A., Pare, P. D., & Seow, C. Y. (2008). Length adaptation of airway smooth muscle. *Proceedings of the American Thoracic Society*, 5(1), 62-67.
53. Kuo, K. H., Herrera, A. M., & Seow, C. Y. (2003). Ultrastructure of airway smooth muscle. *Respiratory physiology & neurobiology*, 137(2-3), 197-208.
54. Herrera, A. M., Martinez, E. C., & Seow, C. Y. (2004). Electron microscopic study of actin polymerization in airway smooth muscle. *American Journal of Physiology-Lung Cellular and Molecular Physiology*, 286(6), L1161-L1168.
55. Smolensky, A. V., Ragozzino, J., Gilbert, S. H., Seow, C. Y., & Ford, L. E. (2005). Length-dependent filament formation assessed from birefringence increases during activation of porcine tracheal muscle. *The Journal of physiology*, 563(2), 517-527.
56. O'byrne, P. M., & Inman, M. D. (2003). Airway hyperresponsiveness. *Chest*, 123(3), 411S-416S.
57. Bentley, J. K., & Hershenson, M. B. (2008). Airway smooth muscle growth in asthma: proliferation, hypertrophy, and migration. *Proceedings of the American Thoracic Society*, 5(1), 89-96.

58. Giembycz, M. A., & Newton, R. (2006). Beyond the dogma: novel β 2-adrenoceptor signalling in the airways. *European Respiratory Journal*, 27(6), 1286-1306.
59. Angus, R., Reagon, R., & Cheesbrough, A. (2005). Short-acting β 2-agonist and oral corticosteroid use in asthma patients prescribed either concurrent beclomethasone and long-acting β 2-agonist or salmeterol/fluticasone propionate combination. *International journal of clinical practice*, 59(2), 156-162.
60. Prenner, B. M. (2008). Role of long-acting β 2-adrenergic agonists in asthma management based on updated asthma guidelines. *Current opinion in pulmonary medicine*, 14(1), 57-63.
61. McHugh, P., Aitcheson, F., Duncan, B., & Houghton, F. (2003). Buteyko Breathing Technique for asthma: an effective intervention. *The New Zealand Medical Journal (Online)*, 116(1187).
62. Bowler, S. D., Green, A., & Mitchell, C. A. (1998). Buteyko breathing techniques in asthma: a blinded randomised controlled trial. *Medical journal of Australia*, 169, 575-578.
63. Alkhalil, M., Schulman, E. S., & Getsy, J. (2008). Obstructive sleep apnea syndrome and asthma: the role of continuous positive airway pressure treatment. *Annals of Allergy, Asthma & Immunology*, 101(4), 350-357.
64. Bonekat, H. W., & Hardin, K. A. (2003). Severe upper airway obstruction during sleep. *Clinical reviews in allergy & immunology*, 25(2), 191-210.
65. Lafond, C., Series, F., & Lemiere, C. (2007). Impact of CPAP on asthmatic patients with obstructive sleep apnoea. *European Respiratory Journal*, 29(2), 307-311.
66. Castro, M., Musani, A. I., Mayse, M. L., & Shargill, N. S. (2010). Bronchial thermoplasty: a novel technique in the treatment of severe asthma. *Therapeutic advances in respiratory disease*, 4(2), 101-116.
67. Castro, M., & Cox, G. (2010). Bronchial thermoplasty in developing countries: is it really worth it?. *American journal of respiratory and critical care medicine*, 182(5), 719-719.
68. Rubin, A. S., & Cardoso, P. F. (2010). Bronchial thermoplasty in asthma. *Journal Brasileiro de Pneumologia*, 36(4), 506-512.
69. Homer, R. J., & Elias, J. A. (2005). Airway remodeling in asthma: therapeutic implications of mechanisms. *Physiology*, 20(1), 28-35.

70. Gupta, S., Siddiqui, S., Haldar, P., Entwisle, J. J., Mawby, D., Wardlaw, A. J., ... & Brightling, C. E. (2010). Quantitative analysis of high-resolution computed tomography scans in severe asthma subphenotypes. *Thorax*, *65*(9), 775-781.
71. Benayoun, L., Druilhe, A., Dombret, M. C., Aubier, M., & Pretolani, M. (2003). Airway structural alterations selectively associated with severe asthma. *American journal of respiratory and critical care medicine*, *167*(10), 1360-1368.
72. Jeffery, P. K. (2001). Remodeling in asthma and chronic obstructive lung disease. *American journal of respiratory and critical care medicine*, *164*(supplement_2), S28-S38.
73. Elias, J. A., Lee, C. G., Zheng, T., Ma, B., Homer, R. J., & Zhu, Z. (2003). New insights into the pathogenesis of asthma. *The Journal of clinical investigation*, *111*(3), 291-297.
74. Ijpma, G., Al-Jumaily, A. M., Cairns, S. P., & Sieck, G. C. (2010). Logarithmic superposition of force response with rapid length changes in relaxed porcine airway smooth muscle. *American Journal of Physiology-Lung Cellular and Molecular Physiology*, *299*(6), L898-L904.
75. Raqeeb, A., Solomon, D., Paré, P. D., & Seow, C. Y. (2010). Length oscillation mimicking periodic individual deep inspirations during tidal breathing attenuates force recovery and adaptation in airway smooth muscle. *Journal of Applied Physiology*, *109*(5), 1476-1482.
76. Fredberg, J. J., Inouye, D., Miller, B., Nathan, M., Raboudi, S. H., ... Shore, S. A. (1997). Airway smooth muscle, tidal stretches, and dynamically determined contractile states. *American journal of respiratory and critical care medicine*, *156*(6), 1752-1759.
77. Ansell, T. K., McFawn, P. K., Noble, P. B., West, A. R., Fernandes, L., & Mitchell, H. W. (2009). Potent bronchodilation and reduced stiffness by relaxant stimuli under dynamic conditions. *European respiratory journal*, *33*(4), 844-851.
78. Hughes, J. M., Hoppin Jr, F. G., & Mead, J. (1972). Effect of lung inflation on bronchial length and diameter in excised lungs. *Journal of Applied Physiology*, *32*(1), 25-35.
79. Noble, P. B., McFawn, P. K., & Mitchell, H. W. (2007). Responsiveness of the isolated airway during simulated deep inspirations: effect of airway smooth muscle stiffness and strain. *Journal of Applied Physiology*, *103*(3), 787-795.

80. Wang, L., & Paré, P. D. (2003). Deep inspiration and airway smooth muscle adaptation to length change. *Respiratory physiology & neurobiology*, 137(2-3), 169-178.
81. Gunst, S. J., & Wu, M. F. (2001). Plasticity in Skeletal, Cardiac, and Smooth Muscle-Selected Contribution: Plasticity of airway smooth muscle stiffness and extensibility: Role of length-adaptive mechanisms. *Journal of Applied Physiology*, 90(2), 741-749.
82. Skloot, G., Permutt, S., & Togias, A. (1995). Airway hyperresponsiveness in asthma: a problem of limited smooth muscle relaxation with inspiration. *The Journal of clinical investigation*, 96(5), 2393-2403.
83. Burns, G. P., & Gibson, G. J. (1998). Airway hyperresponsiveness in asthma: not just a problem of smooth muscle relaxation with inspiration. *American journal of respiratory and critical care medicine*, 158(1), 203-206.
84. Shen, X., Gunst, S. J., & Tepper, R. S. (1997). Effect of tidal volume and frequency on airway responsiveness in mechanically ventilated rabbits. *Journal of Applied Physiology*, 83(4), 1202-1208.
85. Dowell, M. L., Lakser, O. J., Gerthoffer, W. T., Fredberg, J. J., Stelmack, G. L., Halayko, A. J., ... & Mitchell, R. W. (2005). Latrunculin B increases force fluctuation-induced relengthening of ACh-contracted, isotonicly shortened canine tracheal smooth muscle. *Journal of applied physiology*, 98(2), 489-497.
86. Fredberg, J. J. (2002). Airway narrowing in asthma: does speed kill?. *American Journal of Physiology-Lung Cellular and Molecular Physiology*, 283(6), L1179-L1180.
87. Turner, D. J., Noble, P. B., Lucas, M. P., & Mitchell, H. W. (2002). Decreased airway narrowing and smooth muscle contraction in hyperresponsive pigs. *Journal of Applied Physiology*, 93(4), 1296-1300.
88. Mitchell, R. W., Dowell, M. L., Solway, J., & Lakser, O. J. (2008). Force Fluctuation-induced Relengthening of Acetylcholine-contracted Airway Smooth Muscle. *Proceedings of the American Thoracic Society*, 5(1), 68-72.
89. Ali, F., Chin, L., Paré, P. D., & Seow, C. Y. (2007). Mechanism of partial adaptation in airway smooth muscle after a step change in length. *Journal of applied physiology*, 103(2), 569-577.

90. Chin, L. Y., Bossé, Y., Pascoe, C., Hackett, T. L., Seow, C. Y., & Paré, P. D. (2012). Mechanical properties of asthmatic airway smooth muscle. *European Respiratory Journal*, *40*(1), 45-54.
91. Pascoe, C. D., Seow, C. Y., Paré, P. D., & Bossé, Y. (2012). Decrease of airway smooth muscle contractility induced by simulated breathing maneuvers is not simply proportional to strain. *Journal of applied physiology*, *114*(3), 335-343.
92. LaPrad, A. S., West, A. R., Noble, P. B., Lutchen, K. R., & Mitchell, H. W. (2008). Maintenance of airway caliber in isolated airways by deep inspiration and tidal strains. *Journal of applied physiology*, *105*(2), 479-485.
93. LaPrad, A. S., Szabo, T. L., Suki, B., & Lutchen, K. R. (2010). Tidal stretches do not modulate responsiveness of intact airways in vitro. *Journal of applied physiology*, *109*(2), 295-304.
94. Oostveen, E., Zwart, A., Peslin, R., & Duvivier, C. (1992). Respiratory transfer impedance and derived mechanical properties of conscious rats. *Journal of applied physiology*, *73*(4), 1598-1607.
95. Cojocaru, A., Irvin, C. G., Haverkamp, H. C., & Bates, J. H. (2008). Computational assessment of airway wall stiffness in vivo in allergically inflamed mouse models of asthma. *Journal of applied physiology*, *104*(6), 1601-1610.
96. Cazzola, M., Page, C. P., Rogliani, P., & Matera, M. G. (2013). β_2 -agonist therapy in lung disease. *American journal of respiratory and critical care medicine*, *187*(7), 690-696.
97. Dahl, R. (2006). Systemic side effects of inhaled corticosteroids in patients with asthma. *Respiratory medicine*, *100*(8), 1307-1317.
98. Guo, M., Pascual, R. M., Wang, S., Fontana, M. F., Valancius, C. A., Panettieri, R. A., ... & Penn, R. B. (2005). Cytokines regulate β_2 -adrenergic receptor responsiveness in airway smooth muscle via multiple PKA-and EP2 receptor-dependent mechanisms. *Biochemistry*, *44*(42), 13771-13782.
99. Mitchell, H. W. (1984). Pharmacological studies into cyclo-oxygenase, lipoxygenase and phospholipase in smooth muscle contraction in the isolated trachea. *British journal of pharmacology*, *82*(3), 549-555.
100. Mehta, D., Wu, M. F., & Gunst, S. J. (1996). Role of contractile protein activation in the length-dependent modulation of tracheal smooth muscle force. *Am J Physiol Cell Physiol*, *270*(1), C243-252.

101. Shen, X., Wu, M. F., Tepper, R. S., & Gunst, S. J. (1997). Mechanisms for the mechanical response of airway smooth muscle to length oscillation. *Journal of Applied Physiology*, 83(3), 731-738.
102. Gosens, R., Zaagsma, J., Meurs, H., & Halayko, A. J. (2006). Muscarinic receptor signaling in the pathophysiology of asthma and COPD. *Respiratory Research*, 7, 73.
103. Knox, A. J., & Tattersfield, A. (1995). Airway smooth muscle relaxation. *Thorax*, 50(8), 894-901.
104. Hall, I. P. (2000). Second messengers, ion channels and pharmacology of airway smooth muscle. *Eur Respir J*, 15(6), 1120-1127.
105. Obara, K., & de Lanerolle, P. (1989). Isoproterenol attenuates myosin phosphorylation and contraction of tracheal muscle. *Journal of Applied Physiology*, 66(5), 2017-2022.
106. Takuwa, Y., Takuwa, N., & Rasmussen, H. (1988). The effects of isoproterenol on intracellular calcium concentration. *Journal of Biological Chemistry*, 263(2), 762-768.
107. Kumar, S. D., Emery, M. J., Atkins, N. D., Danta, I., Wanner, A. (1998). Airway mucosal blood flow in bronchial asthma. *American Journal of Respiratory and Critical Care Medicine*, 158, 153 - 156.
108. Salvato, G. (2001). Quantitative and morphological analysis of the vascular bed in bronchial biopsy specimens from asthmatic and non-asthmatic subjects. *Thorax*, 56, 902-906.
109. Broide, D. (2004). Immunomodulation and reversal of airway remodeling in asthma. *Current Opinion in Allergy and Clinical Immunology*, 4(6), 529 - 532.
110. Akers, I. A., Parsons, M., Hollenberg, M. D., Sanjar, S., Laurent, G. J., & McAnulty, R. J. (2000). Mast cell tryptase stimulates human lung fibroblast proliferation via protease-activated receptor-2. *American Journal of Physiology*, 278, L193 - L201.
111. Choe, M. M., Sporn, P. H. S., & Swartz, M. A. (2006). Extracellular matrix remodelling by dynamic strain in a three-dimensional tissue-engineered human airway wall model. *American Journal of Respiratory Cell and Molecular Biology*. 35, 306-313.

112. Martin, J.G., Duguet, A., & Eidelman, D. H. (2000). The contribution of airway smooth muscle to airway narrowing and airway hyperresponsiveness in disease. *European Respiratory Journal*, 6(16), 349-354.
113. James, A. L., Bai, T. R., Mauad, T., Abramson, M. J., Dolhnikoff, M., McKay, K. O., ... Green, F. H. (2009). Airway smooth muscle thickness in asthma is related to severity but not duration of asthma. *European Respiratory Journal*, 9(34), 1040-1045.
114. Hessel, E. M., Zwart, A., Oostveen, E., Van Oosterhout, A. J. M., Blyth, D. I., & Nijkamp, F. P. (1995). Repeated measurement of respiratory function and bronchoconstriction in unanesthetized mice. *Journal of Applied Physiology*, 79(5), 1711-1716.
115. Gunst, S. J. (1983). Contractile force of canine airway smooth muscle during cyclical length changes. *Journal of Applied Physiology*, 55(3), 759-769.
116. Galluccio, S. T., Rai, S., & Sharley, P. (2008). An unexpected ending: brain death following acute severe asthma. *Critical Care and Resuscitation*, 3(10), 235-238.
117. Du, Y., & Al-Jumaily, A. M. (2004). Respiratory smooth muscle relaxation using vibrations. *The Journal of the Acoustical Society of America*, 116(4), 2559.
118. Pathology, C. F. G. (2013). Respiratory system. Available from: <http://ctrngenpath.net/static/atlas/mousehistology/Windows/respiratory/diagrams.html>.
119. Glaab, T., Taube, C., Braun, A., & Mitzner, W. (2007). Review: Invasive and noninvasive methods for studying pulmonary function in mice. *Respiratory Research*, 8, 63.
120. Glaab, T., Mitzner, W., Braun, A., Ernst, H., Korolewitz, R., Hohlfeld, J. M., ... Hoymann, H. (2004). Repetitive measurements of pulmonary mechanics to inhaled cholinergic challenge in spontaneously breathing mice. *Journal of Applied Physiology*, 97, 1104 - 1111.
121. Kanehiro, A., Takeda, K., Joetham, A., Tomkinson, A., Ikemura, T., Irvin, C. G., & Gelfand, E. W. (2000). Timing of administration of anti-VLA-4 differentiates airway hyperresponsiveness in the central and peripheral airways in mice. *American Journal of Respiratory Critical Care Medicine*, 3(162), 1132-1139.
122. Kanehiro, A., Ikemura, T., & Makela, M. J. (2001). Inhibition of Phosphodiesterase 4 Attenuates Airway Hyperresponsiveness and Airway

- Inflammation in a Model of Secondary Allergen Challenge. *American Journal of Respiratory and Critical Care Medicine*, 163, 173-184.
123. Hoymaan, H. (2006). New developments in lung function measurements in rodents. *Experimental and Toxicologic Pathology*, 57(S2), 5-11.
 124. Zosky, G. R., & Sly, P. D. (2007). Animal models of asthma. *Clinical and Experimental Allergy*, 37, 973-988.
 125. Bates, J. H. T., Rincon, M., & Irvin, C. G. (2009). Animal models of asthma. *American Journal of Physiology Lung Cellular and Molecular Physiology*, 297, L401–L410.
 126. Bice, D. E., & Seagrave, J. C. (2000). Animal Models of Asthma: Potential Usefulness for Studying Health Effects of Inhaled Particles. *Inhalation Toxicology*, 12, 829 - 862.
 127. Epstein, M. M. (2006). Are mouse models of allergic asthma useful for testing novel therapeutics? *Experimental and Toxicologic Pathology*. 57(S2), 41-44.
 128. Plopper, C. G., & Hyde, D. M. (2008). The non-human primate as a model for studying COPD and asthma. *Pulmonary Pharmacology & Therapeutics*, 21, 755-766.
 129. Karol, M. H. (1994). Animal models of occupational asthma. *European Respiratory Journal*, 7(3), 555-568.
 130. Ulrich, K., Hincks, J. S., Walsh, R., Wetterstrand, E. M., Fidock, M. D., Sreckovic, S., ... Evans, S. M. (2008). Anti-inflammatory modulation of chronic airway inflammation in the murine house dust mite model. *Pulmonary Pharmacology & Therapeutics*, 21(4), 637-647.
 131. Kumar, R. K., & Foster, P. S. (2001). Murine model of chronic human asthma. *Immunology and Cell Biology*, 79, 141-144.
 132. Kumar, R. K. & Foster, P. S. (2002). Modeling Allergic Asthma in Mice Pitfalls and Opportunities. *Am. J. Respir. Cell Mol. Biol.*, 27, 267-272.
 133. Blyth, D. I., Wharton, T. F., Pedrick, M. S., Savage, T. J., Sanjar, S. (2000). Airway subepithelial fibrosis in a murine model of atopic asthma: suppression by dexamethasone or anti-interleukin-5 antibody. *Am. J. Respir. Cell Mol. Biol.*, 23(2), 241-246.
 134. Fernandez-Rodriguez, S., Ford, W. R., Broadley, K. J., & Kidd, E. J. (2008). Establishing the phenotype in novel acute and chronic murine models of allergic asthma. *International Immunopharmacology*, 8(5), 756-763.

135. Goplen, N., Karim, M. Z., Liang, Q., Gorska, M. M., Rozario, S., Guo, L., & Alam, R. (2009). Combined sensitization of mice to extracts of dust mite, ragweed, and *Aspergillus* species breaks through tolerance and establishes chronic features of asthma. *J Allergy Clin Immunol.*, *123*(4), 925-932.
136. Moir, L. M., Lee, S.-Y., Eynott, P. R., McVicker, C. G., Ward, J. P. T., Chung, K. F., & Hirst, S. J. J. (2003). Repeated allergen inhalation induces phenotypic modulation of smooth muscle in bronchioles of sensitized rats. *Am Jour Phys Lung Cell and Mol Physiology*, *284*, L148-L159.
137. Nials, A. T., & Uddin, S. (2008). Mouse models of allergic asthma: acute and chronic allergen challenge. *Disease Models & Mechanisms*. *1*, 213-220.
138. Janssen, E. M., van Oosterhout, A. J. M., Nijkamp, F. P., van Eden, W., & Wauben, M. H. M. (2000). The efficacy of immunotherapy in an experimental murine model of allergic asthma is related to the strength and site of T cell activation during immunotherapy. *J Immunol.*, *165*(12), 7207-7214.
139. Tomkinson, A., Duez, C., Cieslewicz, G., Pratt, J. C., Joetham, A., Shanafelt, ... Gelfand, E. W. (2001). A murine IL-4 receptor antagonist that inhibits IL-4- and IL-13-induced responses prevents antigen-induced airway eosinophilia and airway hyperresponsiveness. *J Immunol.*, *166*(9), 5792-5800.
140. Johnson, J. R., Fattouh, R., Swirski, F. K., Gajewska, B. U., Coyle, A. J., Gutierrez-Ramos, J. C., ... Jordana, M. (2004). Continuous exposure to house dust mite elicits chronic airway inflammation and structural remodeling. *Am J Respir Crit Care Med.*, *169*(3), 378-385.
141. Ricciardolo, F. L. M., Di Stefanoz, A., van Krieken, J. H. J. M., Sontz, J. K., van Schadewijk, A., Rabe, K. F., ... Mauad, T. (2003). Proliferation and inflammation in bronchial epithelium after allergen in atopic asthmatics. *Clinical and Experimental Allergy*, *33*, 905-911.
142. Choi, I. S., Lin, X.-H., Koh, Y.-A., Koh, Y. I., & Lee, H.-C. (2005). Strain-dependent suppressive effects of BCG vaccination on asthmatic reactions in BALB/c mice. *Ann Allergy Asthma Immunol.*, *95*(6), 571-578.
143. Choi, I. W., Sun-Kim, Kim, Y. S., Ko, H. M., Im, S. Y., Kim, J. H., ... Lee, H. K. (2005). TNF-alpha induces the late-phase airway hyperresponsiveness and airway inflammation through cytosolic phospholipase A(2) activation. *J Allergy Clin Immunol.*, *116*(3), 537-543.

144. Leigh, R., Ellis, R., Wattie, J. N., Hirota, J. A., Mattaei, K. I., Foster, P. S., ... Inman, M. D. (2002). Dysfunction and Remodeling of the Mouse Airway Persist after Resolution of Acute Allergen-Induced Airway Inflammation. *Am. J. Respir. Cell Mol. Biol.*, 27, 526-535.
145. Temelkovski, J., Hogan, S. P., Shepherd, D. P., Foster, P. S., & Kumar, R. K. (1998). An improved murine model of asthma: selective airway inflammation, epithelial lesions and increased methacholine responsiveness following chronic exposure to aerosolised allergen. *Thorax*, 53(10), 849 - 856.
146. Lloyd, C. M., & Robinson, D. S. (2007). Allergen-induced airway remodelling. *European Respiratory Journal*, 29, 1020-1032.
147. Balsley, M. A., Malesevic, M., Stemmy, E. J., Gigley, J., Jurjus, R. A., Herzog, D., ... & Constant, S. L. (2010). A cell-impermeable cyclosporine A derivative reduces pathology in a mouse model of allergic lung inflammation. *Journal of Immunology*, 185(12), 7663-7670.
148. Carr, V. M., Robinson, A. M., & Kern, R. C. (2012). Tissue-specific effects of allergic rhinitis in mouse nasal epithelia. *Chemical Senses*, 37(7), 655-668.
149. Vanoirbeek, J. A., Tarkowski, M., De Vooght, V., Nemery, B., & Hoet, P. H. (2009). Immunological determinants in a mouse model of chemical-induced asthma after multiple exposures. *Scandinavian Journal of Immunology*, 70(1), 25-33.
150. Choi, I. S., Lin, X. H., Koh, Y. A., Koh, Y. I., & Lee, H. C. (2005). Strain-dependent suppressive effects of BCG vaccination on asthmatic reactions in BALB/c mice. *Annals of Allergy, Asthma & Immunology*, 95(6), 571-578.
151. Brewer, J. P., Kisselgof, A. B., & Martin, T. R. (1999). Genetic variability in pulmonary physiological, cellular, and antibody responses to antigen in mice. *American Journal of Respiratory and Critical Care Medicine*, 160(4), 1150 - 1156.
152. Kelada, S. N., Wilson, M. S., Tavarez, U., Kubalanza, K., Borate, B., Whitehead, G. S., ... & Brass, D. M. (2011). Strain-dependent genomic factors affect allergen-induced airway hyperresponsiveness in mice. *American journal of respiratory cell and molecular biology*, 45(4), 817-824.
153. Wang, W., Zhu, Z., Zhu, B., & Ma, Z. (2011). Peroxisome proliferator-activated receptor- γ agonist induces regulatory T cells in a murine model of allergic rhinitis. *Otolaryngology Head and Neck Surgery*, 144(4), 506-513.

154. Welker, L., Jörres, R. A., Costabel, U., & Magnussen, H. (2004). Predictive value of BAL cell differentials in the diagnosis of interstitial lung diseases. *European Respiratory Journal*, *24*, 1000-1006.
155. Siddiqui, S., Morris, J., Avery, N., Wyand, S., Rood, D., & Silbart, L. K. (2008). Pulmonary eosinophilia correlates with allergen deposition to the lower respiratory tract in a mouse model of asthma. *Clinical and Experimental Allergy*, *38*(8), 1381-1390.
156. Melgert, B. N., Postmaw, D. S., Kuipers, I., Geerlings, M., Luinge, M. A., van der Strate, B. W. A., ... Hylkema, M. N. (2005). Female mice are more susceptible to the development of allergic airway inflammation than male mice. *Clin Exp Allergy*, *35*, 1496-1503.
157. Takeda, M., Tanabe, M., Ito, W., Ueki, S., Konno, Y., Chihara, M., ... Chihara, J. (2013). Gender difference in allergic airway remodelling and immunoglobulin production in mouse model of asthma. *Respirology*, *18*, 797-806. doi: 10.1111/resp.12078

APPENDIX

Appendix A. Ethical approval

Ethical approval for animal studies was approved by (and obtained from) the Animal Ethics Committee (AEC) located at the University of Auckland. The image of the ethical approval and expiry dates are presented below for the project entitled “Investigation of the combined effects of mechanical oscillations and bronchodilators on the smooth muscle of normal and sensitized mice airways” (AEC No 1409).



This was electronically generated on behalf of Fiona Cheal.

Appendix B. Institutional Drug Administration Order (IDAO)

The IDAO for AEC No 1409 is presented below. Ketamine and xylazine were utilized as anaesthetics for the mice in the study.

Institutional Drug Administration Order	
This form applies to use of AEC approved prescription medicines (human or animal) and/or medicines for the direct management of the animals, such as anaesthetics, analgesics and prophylactic antibiotics.	
AEC OFFICE USE ONLY	
IDAO no.	001409/1
Replaces IDAO no.	
AEC approval commencement date	15/10/2014
AEC/IDAO approval end date	15/10/2017
Cancellation date if replaced	
Replaced by IDAO no.	
Reason for issue of IDAO (excessive detail is not required or expected)	
Summary of aim of trial: This project aims to develop an animal model of asthma in order to investigate a non medicinal therapy against this disease. The current pharmacological treatment against asthma has many side effects and only relieves but does not definitely cure the patients. The airways are the maintarget of all the medicinal and non medicinal therapies against the majority of respiratory diseases. Many studies have demonstrated that mechanical oscillations have a relaxant and protector effect on the airway smooth muscle in healthy animals. our purpose is to extend this research to a pathological case in which we will study the effect of mechanical oscillations combined (or not) with pharmaceutical drugs (bronchodilator and bronchoconstrictor) on airways reactivity. The ultimate objective is to develop a new non medicinal therapy which can replace or at least reduce the use of medicines and hence avoid their side effects in asthma treatment and many other respiratory diseases associated with airway hyper-constriction.	
Reason for involvement of medicines: A ketamine/xylazine mixture will be used for anaesthesia to prevent pain and stress in the animals at some points of the experimental protocols.	
ANIMALS	
Species/Breed	Mouse BALB/c
Gender	Male and Female
Age	8-16 weeks
Weight	18-25g
Method of identification	electronic identification
Number	144
Reproductive status	Non pregnant
MEDICINES INFORMATION	
Name (trade or generic)	Ketamine and Xylazine
Active ingredient	Ketamine and Xylazine
Strength	Ketamine 100mg/ml and Xylazine 20mg/ml
Formula type	Injectable
Prescription Status	Restricted Veterinary Medicine
Is the medicine a controlled drug?	Yes
Product Type	Anaesthetic
ADMINISTRATION DETAILS	
Preparation (if required)	Mix Ketamine 20ul, Xylazine 25ul, and normal saline 445ul. Solutions are mixed in eppendorf tube using a pipette.
Dosage (e.g. mg/Kg)	
Dose (e.g. mL/Kg)	10ul per gm mouse body weight
Frequency of dosing	Other (please detail) Once, but in the event the mouse requires anaesthesia for more than 45-60min, a second dose may be given at this time
Site	intraperitoneal
Equipment	syringe and 28G needle
Technique used	manual restraint of mouse, scruffed with head slightly

Appendix C. Protocols for imposed treatments

Anaesthetised and intubated animals were administered combinations of chemical solutions and superimposed pressures as described in the sections below. Measurements from the imposed respiratory treatments were taken with equipment detailed in Chapter IV.

A.C.1. Normal saline (0.9%) solution.

A normal saline (0.9%) solution is used to establish baseline respiratory conditions for the plethysmographic readings.

- A 1-minute dose of saline is administered using the jet nebulizer.
- The nebulizer is switched off for 1 minute. The saline solution is removed from the nebulizer tank.
- No additional manipulations or testing is carried out, but the respiratory parameters are measured during the transition time from one testing condition to the next.

A.C.2. Acetylcholine (ACh, $10^{-4}M$) solution.

ACh is used as the study's bronchoconstrictor agent in order to mimic an asthmatic attack.

- A 1-minute dose of ACh ($10^{-4}M$) is administered using the jet nebulizer.
- The nebulizer is shut off. The nebulizer tank is emptied, then rinsed twice with 5ml volumes of normal saline prior to addition of either ISO or normal saline to the tank.
- Respiratory parameters continue to be measured through the entire process.
- Following the ACh challenge, either ISO or superimposed pressure oscillations are applied to the study animal with minimal delay between applications.

A.C.3. Isoproterenol (ISO, $10^{-6}M$) solution.

ISO is used as the study's bronchodilator standard against the effects of an ACh-induced (mimicked) asthma attack. ISO also serves as a comparison for the effectiveness of applied pressure oscillations. If ISO is the selected treatment, the protocol continues with the following steps, otherwise the protocol continues with SIPO applications as described in A.C.4.

- A 1-minute dose of ISO ($10^{-6} M$) is administered using the jet nebulizer.
- The nebulizer is shut off. The nebulizer tank is emptied, then rinsed twice with 5ml volumes of normal saline prior to addition of normal saline to the tank.
- Respiratory parameters continue to be measured through the entire process.
- A 2-minute rest period (no testing or manipulations are carried out) separates the series of events which measure a unit of respiratory parameters in the study from the next unit of testing. Testing is repeated, starting with the saline challenge, rest, and ACh steps.

A.C.4. Superimposed pressure oscillations (SIPO).

SIPO are used as treatments in this study to potentially overcome the effects of ACh on healthy and sensitized subjects' respiratory parameters. Oscillations ideally act as bronchodilators [10-13]. The 16 pressures tested in this study range from 0.4 cmH₂O to 3.6 cmH₂O, and are generated by frequency/amplitude (Hz/mV) pairs programmed into the waveform generator discussed in Chapter IV. The oscillations' Hz/mV pairs are 5Hz with amplitudes of 100, 200, 300 and 400 mV, 10 Hz with the same amplitudes, and 15 and 20Hz, also with the same amplitudes.

- Following the ACh challenge, a 1-minute SIPO treatment is applied to the test subject. The tip of the tube which transmits the generated pressure wave from the

shaker is placed at the opening of the pneumotachometer (the subject's airway opening).

- After 1 minute the applied oscillation is removed from the airway.
- Respiratory parameters continue to be measured through the entire process for values of bronchorelaxation or bronchoconstriction.
- A 2-minute rest period (no testing or manipulations are carried out) separates the series of events which measure a unit of respiratory parameters in the study from the next unit of testing. Testing units are repeated by starting at the saline challenge/rest/ACh steps and adding either ISO or an applied pressure oscillation to the test.

Appendix D. Acute asthma sensitization protocol

Previous SIPO studies in acute asthmatic mice were performed [13], and analysed for implications of R_L and C_{dyn} findings relative to established literature findings. The data from these parameters is immediately relevant to constructing a model for the effects of SIPO alongside this study's chronic asthmatic model. A summary of the acute sensitization protocols is presented in this section in Tables A.D.1 and A.D.2.

Table A.D.1: Details of sensitization protocol for (acute) control group.

Protocol details	
Mice	BALB/c; Female; 8-12 Weeks old
Allergen	None
Adjuvant	None
Anesthetic	Ketamine and Xylazine
Challenge	Ach (10^{-2} M)
Via of Administration	None
Sensitization	Days 0 Control of weight and general health. 7 Control of weight and general health. 14 Control of weight and general health. 24 Control of weight and general health. 28 Control of weight and general health. 32 Control of weight and general health. 33 Experimental protocol

Table A.D.2: Details of sensitization protocol for (acute) asthmatic group.

Protocol details	
Mice	BALB/c; Female; 8-12 Weeks old
Allergen	OVA
Adjuvant	Alum (Aluminum hydroxide)
Anesthetic	Ketamine and Xylazine
Challenge	Ach (10^{-2} M)
Via of Administration	Intraperitoneal (i.p.) and Inhalation (inh.)
Sensitization	Days 0 Injection of OVA at 10 μ g diluted sodium chloride 0.9% (saline) + 1mg aluminum hydroxide mixture (i.p.). 7 Injection of OVA at 10 μ g diluted sodium chloride 0.9% (saline) + 1mg aluminum hydroxide mixture (i.p.). 14 Injection of OVA at 10 μ g diluted sodium chloride 0.9% (saline) + 1mg aluminum hydroxide mixture (i.p.). 24 Aerial nebulization of Ova at 5% diluted in saline through the airways for 20 mi 28 Aerial nebulization of Ova at 5% diluted in saline through the airways for 20 mi 32 Aerial nebulization of Ova at 5% diluted in saline through the airways for 20 mi. 33 Experimental protocol

Appendix E. GraphPad Prism 7.0™ screenshot

GraphPad is used to process test data and determine statistical significance of key comparisons in this study. Primary concerns are notably the effect of ACh and ISO against the spontaneously breathing subject, and the effect of various SIPO values on improving respiratory parameters. An example of analyses is presented in this section.

The screenshot displays the GraphPad Prism 7.0 interface with a statistical analysis table. The table is titled 'Two-way ANOVA' and 'Multiple comparisons'. The following table represents the data shown in the screenshot:

Row	Comparison	Mean Diff	95.00% CI of diff	Significant?	Summary	Adjusted P Value	A-?		
1	Number of families								
2	Number of comparisons per family								
3	Alpha								
4									
5	Dunnett's multiple comparisons test	Mean Diff	95.00% CI of diff	Significant?	Summary	Adjusted P Value	A-?		
6									
7	ACh vs. 0.4 cmH2O	-0.04221	-0.09696 to 0.01153	No	ns	0.1581	B		
8	ACh vs. 0.7 cmH2O	-0.06084	-0.1347 to -0.027	Yes	***	0.0008	C		
9	ACh vs. 1.2 cmH2O	-0.1068	-0.155 to -0.05868	Yes	****	0.0001	D		
10	ACh vs. 1.7 cmH2O	-0.178	-0.2262 to -0.1299	Yes	****	0.0001	E		
11	ACh vs. 2.4 cmH2O	-0.09596	-0.1451 to -0.0468	Yes	****	0.0001	F		
12	ACh vs. 3.2 cmH2O	0.03356	0.00972 to 0.06106	No	ns	0.1502	G		
13	ACh vs. ISO	-0.09682	-0.1468 to -0.05046	Yes	****	0.0001	H		
14									
15									
16	Test details	Mean 1	Mean 2	Mean Diff	SE of diff	n1	n2	q	DF
17									
18	ACh vs. 0.4 cmH2O	0.2088	0.251	-0.04221	0.02036	21	14	2.073	146
19	ACh vs. 0.7 cmH2O	0.2088	0.2896	-0.08084	0.02036	21	14	3.971	146
20	ACh vs. 1.2 cmH2O	0.2088	0.3156	-0.1068	0.01821	21	21	5.967	146
21	ACh vs. 1.7 cmH2O	0.2088	0.3868	-0.178	0.01821	21	21	9.775	146
22	ACh vs. 2.4 cmH2O	0.2088	0.3057	-0.09596	0.01821	21	21	5.324	146
23	ACh vs. 3.2 cmH2O	0.2088	0.2443	0.03356	0.01821	21	21	2.063	146
24	ACh vs. ISO	0.2088	0.3074	-0.09682	0.01821	21	21	5.415	146
25									
26									
27									
28									
29									
30									
31									
32									
33									
34									
35									
36									
37									

Appendix F: Normalization of R_L and C_{dyn} values.

The respiratory constant in this study is based on the understanding that dynamic compliance is a representation of the work accomplished against total resistance to airflow into the lungs. The respiratory work in this study is measured by pressure and volume changes, as noted in the equations for C_{dyn} . Work can be alternatively described by the general relationship of pressure multiplied by volume, one of which must be changing in order to account for the performance of work.

$$Work = Pressure \cdot Volume \quad (\text{Eqn. A.1})$$

From this equation, work per breath is written as

$$\frac{Work}{br} = \frac{P \cdot V}{br} \quad (\text{Eqn. A.2})$$

The work accomplished per (n) breath is equivalent to the dynamic compliance (C_{dyn} , written as σ) multiplied by a proportionality constant, B , and is expressed as

$$\frac{Work}{n} = \frac{P \cdot V}{n} = B \cdot \sigma \quad (\text{Eqn. A.3})$$

Rearrangement of terms yields the equation for calculating the respiratory constant of this study.

$$B = \frac{P \cdot V}{n \cdot \sigma} \quad (\text{Eqn. A.4})$$

The mean values for P , V , and σ from healthy, saline-aerosol testing conditions (i.e. application of 0 Hz/0 mV, or PEEP = 0.0 cmH₂O), in $n = 1$ breath, are substituted into

the equation to calculate the standard respiratory constant. Pressure values are taken from inhalation data ($P_{ave} = 2.26 \text{ cmH}_2\text{O}$). The volume is calculated from tidal volume data ($TV_{ave} = 0.23 \text{ ml}$). Mean C_{dyn} values are themselves functions of tidal volume and peak inspiratory pressure, and the average ($PIP-PEEP$) = $1.46 \text{ cmH}_2\text{O}$. The value of the constant for this study is $B_{src}^\circ = 3.222 [\text{cmH}_2\text{O}]^2 \cdot \text{br}^{-1}$. To distinguish the value of the constant at the given standard respiratory measures, it is written as B_{src}° . The degree symbol is used to denote that standard P, V, and σ conditions in this study are used in the calculation of the constant.

$$B_{src}^\circ = \frac{P_{ave}^\circ \cdot (Tv)_{ave}^\circ}{n \cdot \sigma_{ave}^\circ} \quad (\text{Eqn. A.5})$$

In order to account for the multi-variable baseline conditions, healthy and sensitized R_L and C_{dyn} respiratory parameters were normalized with B_{src}° by division and multiplication, respectively. To illustrate, using the basis units of R_L ($\text{cmH}_2\text{O}/\text{ml}/\text{s}$), the resulting normalized parameter units for transformation of any of the study's data sets, $[X]_{ave}^\psi$ are indicated below. (X in this case represents either of the untransformed parameters (R_L or C_{dyn}), and ψ represents any one of the 19 (saline, ACh, ISO, or SIPO) treatments in the study that is being normalized.)

R_L units are transformed to \check{R}_L units by the standard respiratory constant, where the caron symbol ($\check{\cdot}$) represents a transformed parameter. Transformation of R_L units occurs in the following manner:

$$\frac{[R_L]_{ave}^\psi}{B_{src}^\circ} = \frac{\text{cmH}_2\text{O} \cdot \text{br}}{\text{ml} \cdot \text{s}^{-1} \cdot [\text{cmH}_2\text{O}]^2} = \frac{\text{br} \cdot \text{s}}{\text{cmH}_2\text{O} \cdot \text{ml}} = \left[\frac{\text{cmH}_2\text{O} \cdot \text{ml}}{\text{br} \cdot \text{s}} \right]^{-1} \rightarrow \left[\frac{\text{Power}}{\text{br}} \right]^{-1} = \check{R}_L \quad (\text{Eqn. A.6})$$

Once transformed, the \check{R}_L measurements are defined by (inverse) units of pressure and flow, $[(\text{cmH}_2\text{O}\cdot\text{ml})/\text{s}]^{-1}$. The units of the transformed data are consistent with presenting results in terms of “the inverse of Power per breath” where $\text{cmH}_2\text{O}\cdot\text{ml}$ are units for Work. Normalized values from all \check{R}_L experimental conditions are directly comparable to each other; they are ratios of the untransformed R_L value and the respiratory standard. Transformed \check{R}_L data were analysed for significance of measured changes using the described statistical methods. In the context of data analysis, trends observed in the analyses of \check{R}_L are representative of the inverse of Power; the lower the value of \check{R}_L , the greater the relative Power per breath. This further elaborates on the trends in the untransformed R_L data for total lung resistance: higher resistance being marked by lower values of power from the respiratory system tissues’ efforts for optimal breathing functions.

C_{dyn} units are transformed to \check{C}_{dyn} units by multiplication of the study’s constant accordingly. The same indication of transformation (use of the caron) is above the parameter symbol. Transformation of C_{dyn} units occurs in the following manner:

$$B_{\text{src}}^{\circ} \cdot \sigma_{\text{ave}}^{\psi} = \frac{[\text{cmH}_2\text{O}]^2 \cdot \text{ml}}{\text{br} \cdot \text{cmH}_2\text{O}} = \frac{\text{cmH}_2\text{O} \cdot \text{ml}}{\text{br}} \rightarrow \frac{\text{Work}}{\text{br}} = \check{C}_{\text{dyn}} \quad (\text{Eqn. A.7})$$

Once transformed, the \check{C}_{dyn} measurements are defined by units of pressure and volume, $[\text{cmH}_2\text{O}\cdot\text{ml}]$. The units of the transformed data are consistent with presenting results in terms of “Work per breath”. Normalized \check{C}_{dyn} data are directly comparable to each other; they are proportions of the untransformed C_{dyn} value and the respiratory standard. Transformed \check{C}_{dyn} data were analysed for significance of measured values using the described statistical methods (Chapters V and VI). In the context of data analysis, trends

observed in the \check{C}_{dyn} analyses are representative of the relative Work per breath. These calculations are consistent with the implications of dynamic compliance information provided by the untransformed C_{dyn} data: greater dynamic compliance affords the ability to perform greater work in the airways.

The transformed data from \check{R}_L and \check{C}_{dyn} allows for novel interpretations of crossbridge perturbations within the context of mechanically applied pressure oscillations. Manifestation of the crossbridge perturbation as a result of SIPO application is evident in the changes to values of Work and Power that arise from dynamic compliance and total resistance parameters, respectively.

Appendix G: Summary data tables

Data groups of Transformed R_L and C_{dyn} values to \check{R}_L and \check{C}_{dyn} respectively. Figures A.G.1-4 consist of acute and chronic \check{R}_L data; figures A.G.5-8 consist of acute and chronic \check{C}_{dyn} data. The tables are organized according to each frequency group from 5 - 20 Hz, with associated pressure values indicated.

Table A.G.1. Sensitized \check{R}_L from the 5 Hz-derived pressure set. 5 Hz-generated waveforms combined with indicated amplitudes produce the applied SIPO treatment (cmH₂O). Transformed results include ACh and ISO comparison values, and are presented as $\check{R}_L \pm SE$ [(cmH₂O·ml)/s]⁻¹.

	OVA-Sensitized (Acute)	DRA-Sensitized (Chronic)
Experimental condition	$\check{R}_L \pm SE$ [(cmH ₂ O·ml)/s] ⁻¹	
ACh (10 ⁻⁴ M)	0.79 ± 0.03	1.64 ± 0.13
5 Hz/100 mV (0.8 cmH ₂ O)	0.66 ± 0.02	1.28 ± 0.10
5 Hz/200 mV (1.6 cmH ₂ O)	0.70 ± 0.04	1.05 ± 0.04
5 Hz/300 mV (2.6 cmH ₂ O)	0.73 ± 0.05	1.32 ± 0.03
5 Hz/400 mV (3.6 cmH ₂ O)	0.65 ± 0.02	1.24 ± 0.08
ISO (10 ⁻⁶ M)	0.66 ± 0.03	1.07 ± 0.08

Table A.G.2. Sensitized \check{R}_L from the 10 Hz-derived pressure set. 10 Hz-generated waveforms combined with indicated amplitudes produce the applied SIPO treatment (cmH₂O). Transformed results include ACh and ISO comparison values, and are presented as $\check{R}_L \pm SE$ [(cmH₂O·ml)/s]⁻¹.

	OVA-Sensitized (Acute)	DRA-Sensitized (Chronic)
Experimental condition	$\check{R}_L \pm SE$ [(cmH ₂ O·ml)/s] ⁻¹	
ACh (10 ⁻⁴ M)	0.79 ± 0.03	1.64 ± 0.13
10 Hz/100 mV (0.7 cmH ₂ O)	0.66 ± 0.05	0.92 ± 0.01
10 Hz/200 mV (1.5 cmH ₂ O)	0.63 ± 0.03	1.09 ± 0.01
10 Hz/300 mV (2.4 cmH ₂ O)	0.66 ± 0.05	1.05 ± 0.05
10 Hz/400 mV (3.3 cmH ₂ O)	0.64 ± 0.04	1.26 ± 0.05
ISO (10 ⁻⁶ M)	0.66 ± 0.03	1.07 ± 0.08

Table A.G.3. Sensitized \check{R}_L data from the 15 Hz-derived pressure set. 15 Hz-generated waveforms combined with indicated amplitudes produce the applied SIPO treatment (cmH₂O). Transformed results include ACh and ISO comparison values, and are presented as $\check{R}_L \pm SE$ [(cmH₂O·ml)/s]⁻¹.

	OVA-Sensitized (Acute)	DRA-Sensitized (Chronic)
Experimental condition	$\check{R}_L \pm SE$ [(cmH ₂ O·ml)/s] ⁻¹	
ACh (10 ⁻⁴ M)	0.79 ± 0.03	1.64 ± 0.13
15 Hz/100 mV (0.4 cmH ₂ O)	0.69 ± 0.04	1.34 ± 0.05
15 Hz/200 mV (1.1 cmH ₂ O)	0.64 ± 0.03	1.06 ± 0.09
15 Hz/300 mV (1.7 cmH ₂ O)	0.68 ± 0.03	0.85 ± 0.07
15 Hz/400 mV (2.4 cmH ₂ O)	0.72 ± 0.06	1.05 ± 0.05
ISO (10 ⁻⁶ M)	0.66 ± 0.03	1.07 ± 0.08

Table A.G.4. Sensitized \check{R}_L and data from the 20 Hz-derived pressure set. 20 Hz-generated waveforms combined with indicated amplitudes produce the applied SIPO treatment (cmH₂O). Transformed results include ACh and ISO comparison values, and are presented as $\check{R}_L \pm SE$ [(cmH₂O·ml)/s]⁻¹.

	OVA-Sensitized (Acute)	DRA-Sensitized (Chronic)
Experimental condition	$\check{R}_L \pm SE$ [(cmH ₂ O·ml)/s] ⁻¹	
ACh (10 ⁻⁴ M)	0.79 ± 0.03	1.64 ± 0.13
20 Hz/100 mV (0.4 cmH ₂ O)	0.71 ± 0.03	1.13 ± 0.05
20 Hz/200 mV (1.1 cmH ₂ O)	0.73 ± 0.05	1.04 ± 0.10
20 Hz/300 mV (1.7 cmH ₂ O)	0.85 ± 0.06	0.65 ± 0.02
20 Hz/400 mV (2.3 cmH ₂ O)	0.67 ± 0.05	0.99 ± 0.05
ISO (10 ⁻⁶ M)	0.66 ± 0.03	1.07 ± 0.08

Table A.G.5. Sensitized \check{C}_{dyn} data from the 5 Hz-derived pressure set. 5 Hz-generated waveforms combined with indicated amplitudes produce the applied SIPO treatment (cmH₂O). Transformed results include ACh and ISO comparison values, and are presented as $\check{C}_{dyn} \pm SE$ [cmH₂O·ml].

	OVA-Sensitized (Acute)	DRA-Sensitized (Chronic)
Experimental condition	$\check{C}_{dyn} \pm SE$ [cmH ₂ O·ml]	
ACh (10 ⁻⁴ M)	0.39 ± 0.02	0.21 ± 0.02
5 Hz/100 mV (0.8 cmH ₂ O)	0.47 ± 0.02	0.24 ± 0.02
5 Hz/200 mV (1.6 cmH ₂ O)	0.45 ± 0.03	0.30 ± 0.01
5 Hz/300 mV (2.6 cmH ₂ O)	0.44 ± 0.04	0.23 ± 0.00
5 Hz/400 mV (3.6 cmH ₂ O)	0.48 ± 0.03	0.27 ± 0.02
ISO (10 ⁻⁶ M)	0.48 ± 0.03	0.31 ± 0.03

Table A.G.6. Sensitized \check{C}_{dyn} data from the 10 Hz-derived pressure set. 10 Hz-generated waveforms combined with indicated amplitudes produce the applied SIPO treatment (cmH₂O). Transformed results include ACh and ISO comparison values, and are presented as $\check{C}_{dyn} \pm SE$ [cmH₂O·ml].

	OVA-Sensitized (Acute)	DRA-Sensitized (Chronic)
Experimental condition	$\check{C}_{dyn} \pm SE$ [cmH ₂ O·ml]	
ACh (10 ⁻⁴ M)	0.39 ± 0.02	0.21 ± 0.02
10 Hz/100 mV (0.7 cmH ₂ O)	0.48 ± 0.04	0.34 ± 0.01
10 Hz/200 mV (1.5 cmH ₂ O)	0.50 ± 0.03	0.29 ± 0.01
10 Hz/300 mV (2.4 cmH ₂ O)	0.50 ± 0.06	0.30 ± 0.01
10 Hz/400 mV (3.3 cmH ₂ O)	0.51 ± 0.04	0.25 ± 0.01
ISO (10 ⁻⁶ M)	0.48 ± 0.03	0.31 ± 0.03

Table A.G.7. Sensitized \check{C}_{dyn} data from the 15 Hz-derived pressure set. 15 Hz-generated waveforms combined with indicated amplitudes produce the applied SIPO treatment (cmH₂O). Transformed results include ACh and ISO comparison values, and are presented as $\check{C}_{dyn} \pm SE$ [cmH₂O·ml].

	OVA-Sensitized (Acute)	DRA-Sensitized (Chronic)
Experimental condition	$\check{C}_{dyn} \pm SE$ [cmH ₂ O·ml]	
ACh (10 ⁻⁴ M)	0.39 ± 0.02	0.21 ± 0.02
15 Hz/100 mV (0.4 cmH ₂ O)	0.46 ± 0.03	0.23 ± 0.01
15 Hz/200 mV (1.1 cmH ₂ O)	0.51 ± 0.04	0.33 ± 0.04
15 Hz/300 mV (1.7 cmH ₂ O)	0.47 ± 0.02	0.38 ± 0.03
15 Hz/400 mV (2.4 cmH ₂ O)	0.46 ± 0.05	0.30 ± 0.01
ISO (10 ⁻⁶ M)	0.48 ± 0.03	0.31 ± 0.03

Table A.G.8. Sensitized \check{C}_{dyn} data from the 20 Hz-derived pressure set. 20 Hz-generated waveforms combined with indicated amplitudes produce the applied SIPO treatment (cmH₂O). Transformed results include ACh and ISO comparison values, and are presented as $\check{C}_{dyn} \pm SE$ [cmH₂O·ml].

	OVA-Sensitized (Acute)	DRA-Sensitized (Chronic)
Experimental condition	$\check{C}_{dyn} \pm SE$ [cmH ₂ O·ml]	
ACh (10 ⁻⁴ M)	0.39 ± 0.02	0.21 ± 0.02
20 Hz/100 mV (0.4 cmH ₂ O)	0.46 ± 0.02	0.28 ± 0.01
20 Hz/200 mV (1.1 cmH ₂ O)	0.44 ± 0.03	0.32 ± 0.03
20 Hz/300 mV (1.7 cmH ₂ O)	0.38 ± 0.02	0.48 ± 0.02
20 Hz/400 mV (2.3 cmH ₂ O)	0.48 ± 0.03	0.32 ± 0.01
ISO (10 ⁻⁶ M)	0.48 ± 0.03	0.31 ± 0.03

